144834

14897-6007-RU-00

(NASA-CR-144834) DESIGN STUDY LANDSAT FOLLOW-ON MISSION UNIQUE COMMUNICATIONS SYSTEM (TRW Defense and Space Systems Group) 210 p HC A10/MF A01 CSCL 17B

N77-14294

Unclas
G3/32 58356

DESIGN STUDY LANDSAT FOLLOW-ON MISSION UNIQUE COMMUNICATIONS SYSTEM

August 1976

Contract No. NAS5-21188

Prepared for

NASA GODDARD SPACE FLIGHT CENTER
Greenbelt, Maryland 20771

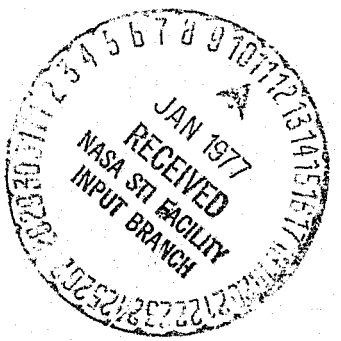

By

TRW
DEFENSE AND SPACE SYSTEMS GROUP

ONE SPACE PARK • REDONDO BEACH, CALIFORNIA 90278

CONTENTS

CONTENTS (Continued)

ILLUSTRATIONS

ILLUSTRATIONS (Continued)

ILLUSTRATIONS (Continued)

ILLUSTRATIONS (Continued)

ILLUSTRATIONS (Continued)

TABLES

TABLES (Continued)

1. INTRODUCTION

TRW Defense and Space Systems has performed a series of Application Studies for NASA Goddard Space Flight Center under contract NAS5-21188. These studies related to spacecraft subsystem design, performance evaluation, and system tradeoffs.

The study activity documented in this report focuses on the two mission-unique Ku-band data links for the LANDSAT Follow-on (LF/O) Mission:

- The LF/O spacecraft to TDRSS link for the transmission of thematic mapper (TM) and multispectral scanner (MSS) data
- The LF/O spacecraft to STDN and other direct access users link for the transmission of TM data.

The primary objective was to conduct conceptual design studies defining a recommended best approach to the implementation of the LF/O communication system. This included requirements definition, link analysis, subsystem and hardware tradeoffs, conceptual selection, hardware definition, and identification of required new technology. A further objective was to provide ROM cost estimates of the recommended communication system including both recurring and nonrecurring costs. The study was conducted over the period March 1976 to August 1976.

The LANDSAT Follow-on Mission, presently in the planning stage, will utilize the NASA Multi-Mission Modular Spacecraft (MMS). This spacecraft operates in a 705 km altitude 9:30 AM (descending mode) orbit. The payload consists of a thematic mapper and multispectral scanner.

The study (per coordination with GSFC) assumes a thematic mapper data rate of 120 Mbps and a multispectral scanner data rate of 15 Mbps. The recommended communication design, however, is insensitive to data rate. The rates may be increased in accordance with the link budget margins, or decreased greatly with no adverse performance effects.

The communication subsystem is configured as follows. One portion is contained in a mission-unique "wideband module" attached to the LF/O spacecraft (generally referred to in this report as simply the LF/O). The second portion is a mast-mounted mechanically-steerable antenna and associated electronics (RF compartment) utilized for the TDRSS link. A deployable astromast-type boom was assumed. The mast, steerable antenna gimbal drive, and associated drive electronics designs are not a part of this study.

The study results are summarized in Section 2. Section 3 presents the LF/O to TDRSS link study results. Sections 3.1 and 3.2 contain the major system level tradeoffs while Sections 3.3 through Section 3.10 discuss hardware implementation tradeoffs and present detailed descriptions of recommended designs. Section 3.11 provides an analysis of TDRSS link performance.

In a parallel fashion, Section 4 presents the LF/O to STDN/direct access link study results. Of particular interest are the shaped beam antenna pattern requirements analysis and the proposed antenna implementation discussed in Section 4.4.

A detailed equipment layout and mechanical/thermal design of the RF compartment (equipment mounted on back of parabolic dish) are presented in Section 3.9, while the layout in the wideband module is given in Section 5.

Section 6 discusses new technology and our conclusion that no new technology is required for the recommended system.

Finally, Section 7 provides a detailed cost estimate of the recommended system.

2. SUMMARY

The recommended LF/O communication system is a simple, low risk design, requiring no new or exotic technology. An extensive series of system and hardware implementation level tradeoff studies were conducted in the process of arriving at the design.

The system is shown in the functional block diagram of Figure 2-1. The mission-unique wideband module contains the STDN/direct access Ku-band transmitter, a portion of the TDRSS Ku-band autotrack receiver, and shared components (frequency source unit, digital interface unit No. 1, power converter, and RIU).

The RF compartment houses the TDRSS link transmitter and autotrack receiver front-end. The steerable antenna is attached to the RF compartment structure, thus providing direct low loss waveguide interconnection to the receiver front end and transmitter. The RF compartment and associated gimbal-drive assembly are mounted to a deployable "Astromast" type boom. All RF interconnections between the RF compartment and wide-band module are at S-band frequencies or lower so that flexible coaxial cable can be utilized along the boom without incurring excessive signal attenuation.

The TM and MSS data streams for the TDRSS transmitter are conditioned in digital interface unit No. 1 and routed to digital interface unit No. 2. Unit No. 2 provides mode control. In the normal mode, the TM (120 Mbps) and MSS (15 Mbps) data are fed to the two inputs of an unbalanced QPSK modulator, yielding a 135 Mbps composite data signal fed to the 20-watt TWTA for transmission via the antenna center feed to TDRSS. An acquisition horn is provided for initial acquisition of the LF/O by the TDRSS. In the two alternate transmission modes, TM data only, or MSS data only, is fed to both modulator inputs, thus providing full RF power to the single mode selected. Four-to-one power sharing is used in the normal mode (TM + MSS).

In order to point the antenna accurately at the TDRSS for data transmission, an autotrack system is used to track the TDRSS forward link Ku-band PN signal. A 4-horn tracking feed and comparator provide error signals which are biphase modulated, and coupled to the center-horn received signal, thus providing an amplitude modulated single channel. After amplification and downconversion in the receiver front end, the signal is sent down the mast to the wideband module and is further amplified in the autotrack receiver, square-law detected, demultiplexed, and fed to the gimbal drives.

For acquisition, LF/O signal transmission and antenna pointing are initialized by the S-band command and data handling subsystem or by preprogrammed commands issued by the on-board computer (NSSC). Transmission to the TDRSS is normally via the steerable 6-foot parabolic dish for initial acquisition. A widebeam horn is provided as a backup mode. The TDRSS acquires and autotracks the LF/O signal and transmits a signal beacon to the LF/O. The LF/O then detects signal present and reverts to the autotrack mode. Open loop LF/O dish pointing is estimated to be accurate enough to acquire the

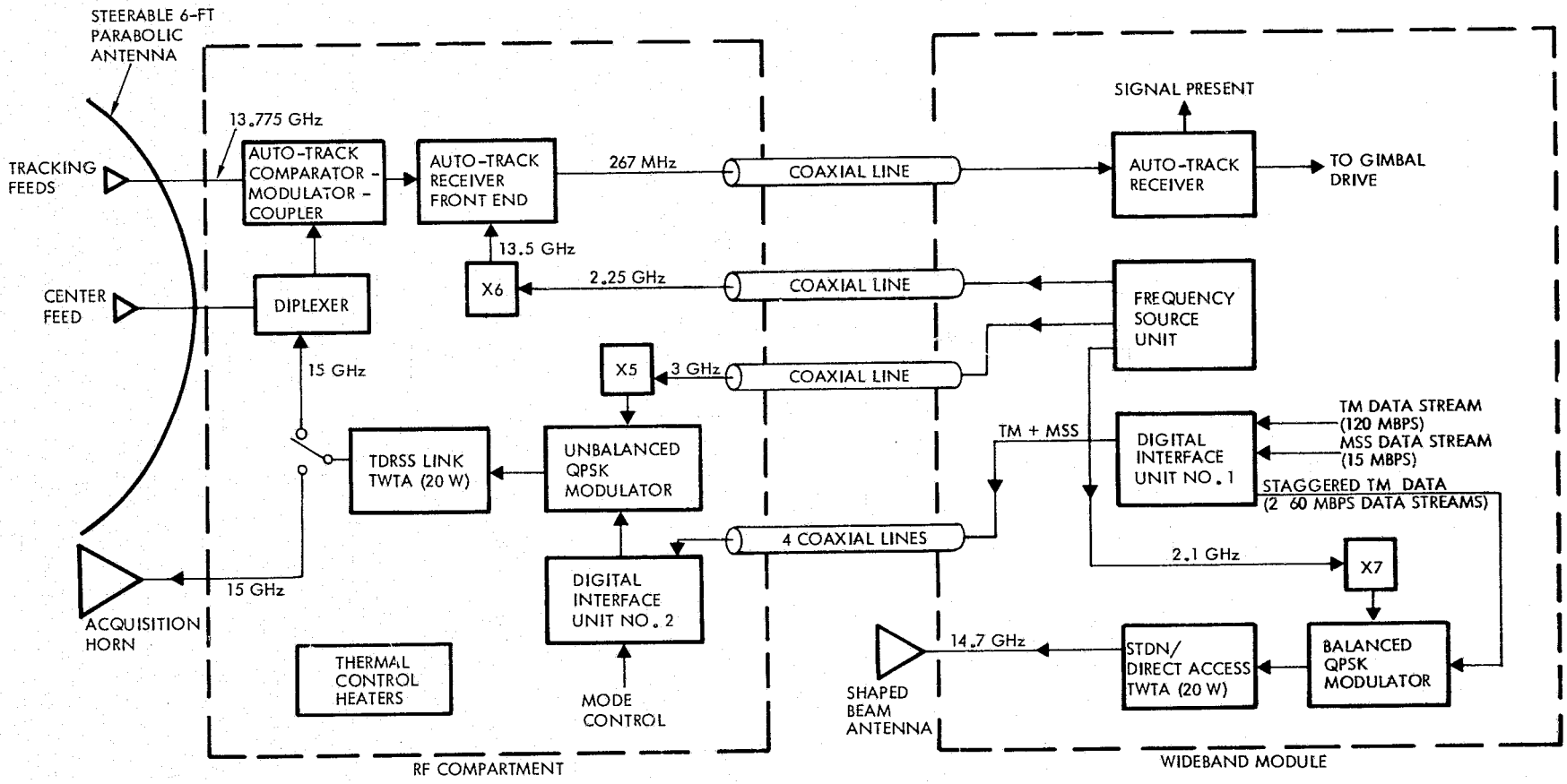

Figure 2-1. LF/O Recommended System

TDRSS signal without a search pattern. The on-board computer, however, can provide a search pattern for the steerable dish if required.

For the STDN/direct access transmitter, digital interface unit No. 1 "splits" the 120 Mbps TM data into two 60 Mbps data streams which are staggered (1/2 bit) and fed to the two inputs of a balanced QPSK modulator. The output is filtered and amplified in a 20-watt TWT for transmission via a shaped beam 18-inch dish type antenna to the STDN/direct access stations. Staggered QPSK is utilized to minimize spectrum sidelobe regeneration.

A frequency source unit provides the receive local oscillator and transmitter signal sources, all of which are derived from a highly stable oven controlled crystal oscillator.

The RF compartment utilizes second surface mirrors to radiate the TWT heat during on-time and a heater to prevent excessive low temperature during extended off-time.

The system is fully redundant in all active components. The estimated weight is given in Table 2-1 and the dc power summary in Table 2-2.

Table 2-1. Communication System Weight

Item	Weight (pounds)
Rf compartment structure	9.8
RF compartment equipment	38.9
High gain antenna and feeds	21.5
Acquisition horn	2.3
	72.7 pounds
Wideband module equipment	53.2
Shaped beam antenna	3.0
	56.2 pounds*
Total weight (RF compartment and widband module)	128.9 pounds

*Does not include S-band equipment weight or WBM structure weight.

Table 2-2. DC Power Summary

Item	TDRSS Link Prime Power (watts)	STDN/DA Link Prime Power (watts)	Common Prime Power (watts)
Power converter	15[1]	8.6	
RIU			3[3]
Osc oven			1.2
TDRSS TWTA	75[1,2]		
STDN TWTA		75[2]	
	90	83.6	4.2

Notes: 1. When TDRSS link is "off" for extended period replace this power by ≈23 watts for thermal control heaters in RF compartment.

2. Assumes use of WJ/Thomson TH3554 TWT and power supply.

3. Telemetry mode.

A series of system level studies and tradeoffs were conducted prior to configuring the recommended system. The results of these studies are as follows:

Program Pointing vs Autotrack

An analysis of "open loop" pointing errors showed an estimated open loop pointing error of ≈0.53° (3σ) which would result in ≈10 dB antenna gain loss, which is clearly unacceptable. The recommended autotrack system has a pointing error of 0.05° which results in a gain loss of about 0.06 dB.

Time Multiplex vs Unbalanced QPSK Modulation

Methods to time multiplex MSS 15 Mbps data with TM 120 Mbps data were studied. Several acceptable implementations were defined. Unbalanced QPSK (UQPSK) was studied, with mode control a key issue. The selected UQPSK implementation allows for the three possible operation modes:

- MSS plus TM data is transmitted
- TM data only is transmitted
- MSS data only is transmitted.

Our conclusion is that both time multiplex and UQPSK modulation are feasible, but that UQPSK modulation is a simpler, more reliable, and less costly method to combine the MSS and TM data for the TDRSS Ku-band return link.

TDRSS Link Interference with the STDN/Direct Access Link

It was found that if the STDN/direct access link operated in the same 15 GHz band allocated for the TDRSS KSA return link, the TDRSS link antenna sidelobes radiating towards the STDN ground stations would cause excessive interference with the STDN link operation. Operation of the STDN/direct access transmitter at a different frequency (14.7 GHz) eliminates the interference.

Radio Astronomy Interference

Radio astronomy bands lie on both sides of the TDRSS allocations (at ≈14.5 GHz and at ≈15.4 GHz). A computer simulation was performed to determine the TDRSS and STDN/direct access out-of-band spectrum energy, due to spectrum regeneration in the TWT transmitters, which could cause radio astronomy interference. Interference criteria were obtained from current CCIR reports and by consultation with members of the National Radio Astronomy Observatory, Green Bank, West Virginia. It was found that the proposed design, which utilizes staggered QPSK on the STDN/direct access transmitter (thus minimizing spectrum regeneration) and sufficient TWTA output filtering on the TDRSS link transmitter, results in interference levels well below the allowable values.

Grazing Angle Performance

The closer the line-of-sight between the LF/O and the TDRSS can approach earth tangency, the smaller is the LF/O to TDRSS coverage zone of exclusion. Analysis of the several propagation effects which might bound the minimum alltitude line-of-sight was performed. The results are as follows:

- Tropospheric absorbtion — limits attitude to ≈12 km for 0.25 dB link loss
- Refractive ray bending — limits attitude to ≈28 km for beam bending to be much less than LF/O or TDRSS beamwidths
- Multipath — limits attitude to ≈40 km for a direct to multipath ratio of 30 dB and a corresponding link degradation of ≈0.25 dB (this may be overly conservative due to difficulties in defining earth roughness and the relative amount of diffuse and specular reflection).

NASA GSFC specifications (ref. 20) define allowable flux density impinging on the earth. Based on these criteria, the minimum height is 180 km for mode 3 transmission (15 Mbps MSS data).

TWTA

The most significant hardware implementation tradeoff study was selection of the recommended TWTA. There are three potential sources for a Ku-band TWTA in the 15 to 20-watt RF power range. These are:

- Hughes Electron Dynamics Division
- Watkins Johnson/Thomson-CSF
- Telefunken-AEG

A ROM bid request was solicited from the three vendors. A current TRW military program utilizes the Hughes TWTA (288H) thus providing reliability, performance, and cost data. The WJ/Thomson tube and power supply are in a funded development for a TRW program. Engineering model completion is expected in the near future. No active development is known to be in process for the Telefunken TWTA. The Hughes TWT is an outgrowth of an earlier X-band TWT, while the WJ/Thomson and Telefunken 15 GHz tubes are both based on earlier 12 GHz developments for ESA. A tradeoff comparison is given in Table 2-3. Based on reliability history, performance, development status, and cost, TRW recommends selection of the WJ/Thomson TWTA.

Table 2-3. TWTA Tradeoff Factors

	HUGHES 288H	WJ/THOMSON TH3554	TELEFUNKEN TL12022 (MOD)
RF PERFORMANCE	COMPLIANT (16-WATT OUTPUT)	COMPLIANT (20-WATT OUTPUT)	COMPLIANT (20-WATT OUTPUT)
DC PERFORMANCE	92 WATTS $\eta_{TOTAL} \approx 17.4\%$ $\eta_{TUBE} \approx 22.9\%$ $\eta_{PWR\ SUP} \approx 76\%$	75 WATTS $\eta_{TOTAL} \approx 26.7\%$ $\eta_{TUBE} \approx 33.3\%$ $\eta_{PWR\ SUP} \approx 80\%$	80 WATTS $\eta_{TOTAL} \approx 25\%$ $\eta_{TUBE} \approx 35\%$ $\eta_{PWR\ SUP} \approx 75\%$
SIZE AND WEIGHT	← SIMILAR →		
STATUS	DEVELOPED AND QUALIFIED	IN DEVELOPMENT SOME TESTING COMPLETE	PROJECTED
AVAILABILITY	QUESTIONABLE, HAVE HAD PRODUCTION PROBLEMS	UNDER CONTRACT FOR DEVELOPMENT. QUALIFIED FLIGHT MODELS MAY BE AVAILABLE BY LATE 77/EARLY 78	QUESTIONABLE, DEVELOPMENT IS UNCERTAIN
RELIABILITY	SUSPECT - HAVE HAD PROBLEMS	EXCELLENT HISTORY FOR PREDECESSORS (TH3525)	EXCELLENT HISTORY FOR PREDECESSORS (TL12022)
COST (SEE NOTE 1)	≈ $2.25 MILLION (SEE NOTE 2)	$1.26 TO 1.66 MILLION (SEE NOTE 3)	≈ $1.51 MILLION (SEE NOTE 4)

UNDESIRABLE FEATURES

NOTES

1. TOTAL PROCUREMENT COST INCUDING (AS APPLICABLE) NRE, QUALIFICATION AND 10 FLIGHT TWTA'S.
2. HUGHES DECLINED TO BID ON LANDSAT RFQ COST ESTIMATE BASED ON PROCUREMENT COSTS OF PREVIOUS HAC 288H TWT'S.
3. WATKINS JOHNSON/THOMSON CSF COST BASED ON QUOTES RECEIVED FOR THIS TWTA. UPPER PRICE INCLUDES QUALIFICATION, LOWER PRICE ASSUMES QUALIFICATION COMPLETE BY THE TIME FRAME OF LFO. QUALIFICATION OF TWTA BY EARLY 1978 SEEMS LIKELY UNDER OTHER PROGRAMS.
4. TELEFUNKEN ITEMIZED COSTS NOT AVAILABLE AT THIS TIME. ESTIMATE DERIVED FROM TELEFUNKEN ROM COST ($1.95 MILLION) FOR DEVELOPMENT OF TWTA AND DELIVERY OF 15 FLIGHT UNITS.

3. TDRSS LINK DESIGN

A detailed description of the recommended TDRSS link subsystem (transmitter and receiver) is given in Figure 3.0-1. All active components are redundant, as shown. RF interconnections prior to the TWT and subsequent to the receiver front end are coaxial cable. All connections from the TWT output and to the receiver front end inputs are immersion gold-coated aluminum WR62 waveguide.

The RF compartment is a saddle shaped compartment configured to minimize moments of inertia on the gimbal drives. It is constructed of light weight aluminum honeycomb panels with the exception of the TWTA panel which is a 0.1 inch aluminum plate intended to prevent local hot spots in the vicinity of the TWT collectors. The outer surface of the aluminum panel is covered with second surface mirrors for efficient heat radiation. For a 50% duty cycle of operation, the temperature environment is very benign — a temperature swing of ≈15°F is predicted. During extended off periods, 20 to 30 watts of thermal heater power is required to maintain a reasonable minimum temperature (≈30°F).

All RF, dc power, and signal lines required for interconnection between the RF compartment and the wideband module are contained in a cable bundle. RF signals are at S-band or lower to prevent excessive coaxial cable attenuation. A cable wrap-up arrangement is utilized in the gimbal drive assembly. The cable bundle, on the "inboard" side of the gimbals, is routed down the deployable mast to the wideband module. Thus, as presently conceived, there is direct "hardwire" interconnection between the RF compartment and the wideband module. No RF rotary joints or slip rings are employed.

The RF compartment contains the autotrack receiver front-end components and the complete TDRSS link transmitter equipment complement. The remaining portion of the receiver is housed in the wideband module.

An unmodulated Ku-band PN spread spectrum signal (3 megachips/sec) from the TDRSS is received by the steerable antenna 5-horn feed system. The four small monopulse horn feeds which surround the sum channel horn feed and the comparator network are used to form the azimuth (α) and elevation (β) difference signals. The α and β signals are proportional to the angular error between the LF/O antenna boresight and the received TDRSS signal line-of-sight. These signals are biphase modulated, time multiplexed, and added to the reference sum channel received signal with a 10 dB coupler to form the amplitude modulated autotrack signal.

The autotrack signal is downconverted to 267 MHz and routed via coaxial cable down the astro-mast type boom to the other portion of the autotrack receiver located in the wideband module. The signal is amplified by an automatic gain controlled IF amplifier prior to square-law detection. The output of the square-law detector consists of the time-multiplexed autotrack α and β signals and a low frequency dc signal which is filtered and used for signal presence indication and AGC control.

The signal presence signal is used to activate the autotrack system and it is also telemetered to the TDRSS ground station via the C&DH subsystem to indicate that the LF/O to TDRSS link has been established. The AGC control maintains a nearly constant signal level into the square-law detector.

Separation of the autotrack α and β signals is accomplished in the autotrack demodulator. The demultiplexing waveform which separates the α and β signals is identical to and synchronized to the multiplexing waveform.

The autotrack receiver, antenna, and gimbal drive system form a closed loop tracking system. The α and β error signals position the antenna, via the gimbal drive motors, in a direction which minimizes the angular error between the antenna boresight and the TDRSS signal line-of-sight.

The TDRSS link is established as follows: the LF/O to TDRSS link antenna is prepositioned towards the TDRSS and the LF/O then transmits a signal to the TDRSS. After the TDRSS acquires and autotracks the LF/O signal, it transmits a Ku-band signal beacon to the LF/O. The LF/O to TDRSS link is established after the LF/O acquires and autotracks the TDRSS forward link signal.

LF/O signal transmission and prepositioning of the steerable antenna and attached acquisition horn are initialized by commands received by the S-band C&DH subsystem or by preprogrammed commands issued by the on-board computer (NSSC).

The LF/O signal is transmitted by the steerable dish antenna or by the acquisition horn. Although the narrowbeam steerable dish antenna, with the estimated open-loop pointing accuracy, provides more than the EIRP required by the TDRSS for initial acquisition, a widebeam ($\approx$12°) acquisition horn antenna is provided as a backup.

The transmission process begins at the sensor instruments. Digital data streams from the TM (120 Mbps) and MSS (15 Mbps) instruments are routed to digital interface unit No. 1 located in the wideband module where the data streams are prepared for routing to digital interface unit No. 2 located in the RF compartment. Two pairs of coaxial cables are routed along the 20-foot boom to provide balanced line connections between the digital interface units.

Switching logic in digital interface unit No. 2 provides data transmission flexibility; i.e., TM and MSS can be transmitted simulatenously, TM only, or MSS only. The TM and MSS data inputs to the QPSK modulator I and Q channels are controlled via ground commands. The normal transmission mode is assumed to be TM (I channel) and MSS (Q channel).

Since the data rates for the TM (120 Mbps) and MSS (15 Mbps) are unequal, optimum performance of the TDRSS return links can be achieved by unbalanced (by ratio of the data rates) QPSK modulation. The signal power ratio in the I and Q channels is restricted by the TDRSS to be 4:1 or less; therefore, the I channel is designed to have 4X the power of the Q channel.

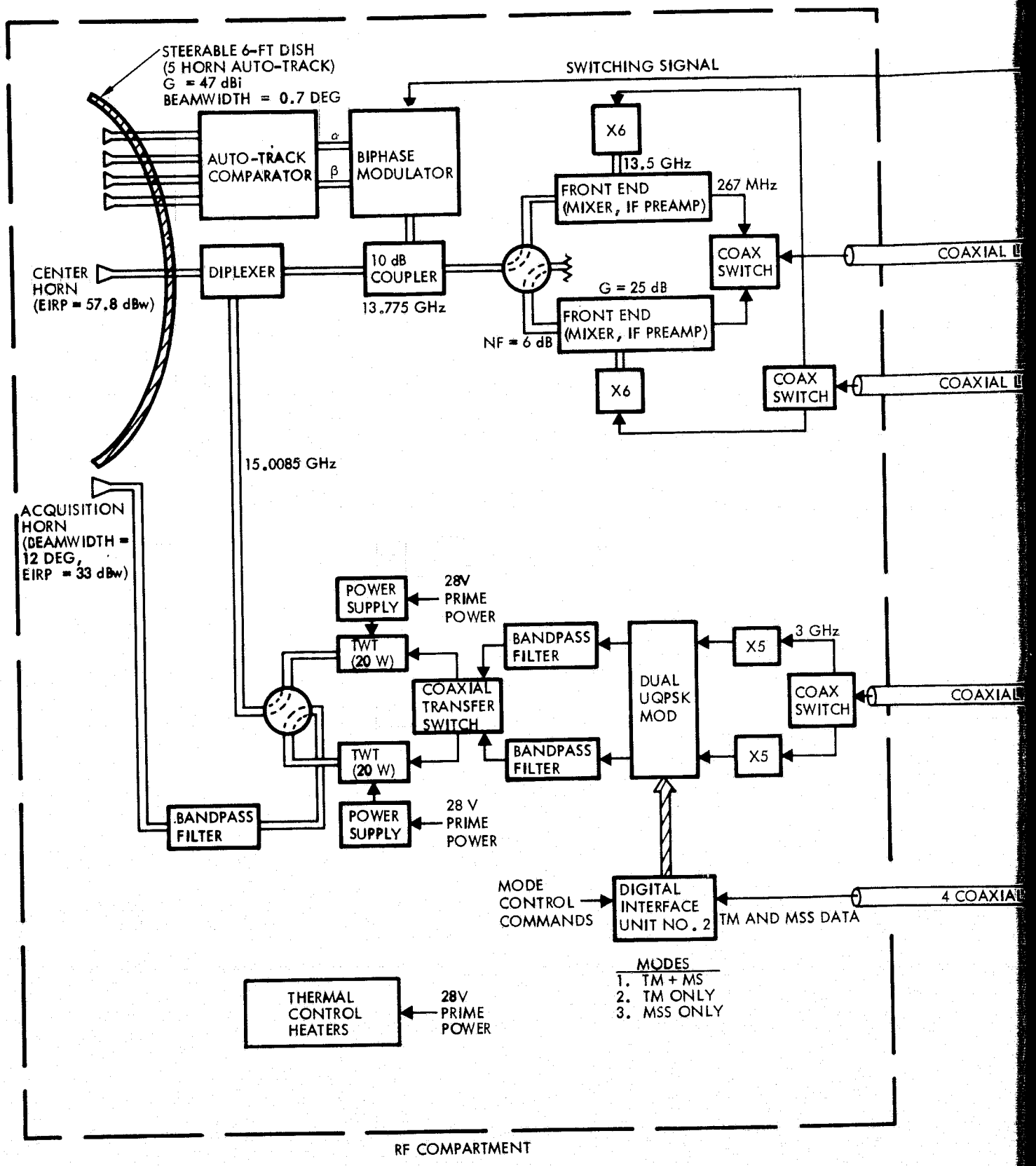

FOLDOUT FRAME /

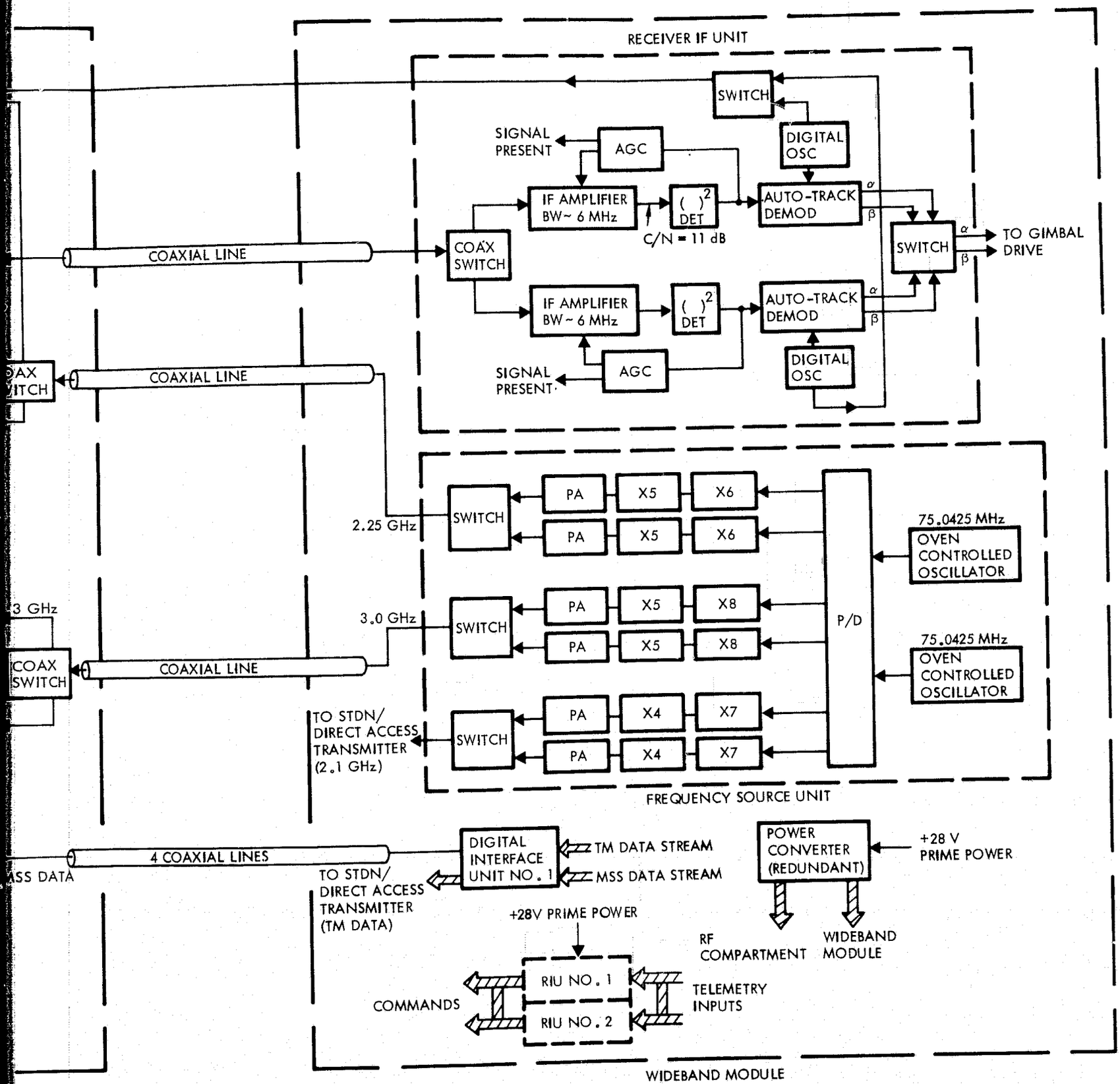

Figure 3.0-1. TDRSS Link Transmitter and Tracking Receiver

FOLDOUT FRAME 2

After the TM and MSS data QPSK modulate the 15 GHz TDRSS return link carrier, the modulated carrier is bandpass limited in a 240 MHz filter, amplified by the TWT, filtered by the diplexer, and transmitted to the TDRSS by the LF/O return link steerable antenna.

The carrier frequency is generated from a 75 MHz oven-controlled oscillator source which is multiplied to 15 GHz by a multiplier chain located in the wideband module frequency source unit and a X5 multiplier located in the RF compartment. A similar multiplier chain is used to generate the 13.5 GHz receiver local oscillator signal.

Regulated secondary power for all communications equipment except the TWTA's is provided by power converters located in the wideband module. The TWTA's have their own power converters located adjacent to the TWTA's in the RF compartment.

Redundancy management is accomplished by the remote interface units which process ground or preprogrammed commands, and accept telemetry data from the various monitoring points in the transmitter and receiver equipment.

The following sections discuss the detail performance analyses and tradeoff studies that were performed in arriving at the recommended TDRSS link subsystem design, and provide detail descriptions of the recommended hardware.

3.1 PROGRAM POINTING VS AUTOTRACK

Due to the constraint of limited TWT power, a large size LF/O antenna dish (6 feet) is required in order to achieve sufficient EIRP for the return link to the TDRSS. This results in a narrow beamwidth of about 0.7° and necessitates very accurate antenna pointing.

This section discusses the antenna pointing accuracies available from two basic antenna tracking techniques: program pointing by ground or on-board stored commands (open-loop) and autotrack (closed-loop). Detail sources of pointing error are identified for both systems and the associated errors are computed or estimated from accumulated data on current programs and tracking systems hardware.

The results show that the proposed open-loop pointing error (Rayleigh mean) is 0.663°, which corresponds to an antenna gain loss (from peak gain) of 8.2 dB for receive and 9.9 dB for transmit, and that the proposed closed-loop pointing error (Rayleigh mean) is 0.056°, which corresponds to approximately 0.1 dB antenna gain loss for both receive and transmit.

The major error source for the open-loop system comes from thermal distortion of the assumed 20 foot "Astro Mast" type of antenna boom. Since the closed-loop system can track out the pointing error caused by antenna boom distortion, as well as many of the other open loop pointing errors identified in the open loop system budget, a considerable reduction in pointing error is realized with the recommended autotrack antenna system.

3.1.1 Program Pointing Performance

Six general sources of error were found to contribute to the inaccuracies involved in open-loop pointing the LF/O Ku-band antenna at the TDRSS. These error sources, their breakdowns, and the error magnitudes are summarized in Table 3.1-1.

Spacecraft Position

The errors in the target direction arise from uncertainties in the position of the TDRSS and the LF/O. The maximum error in the TDRSS position is 61 m, assuming there is no correction immediately following each TDRSS momentum dump (ref. 1). The TDRSS orbit radius is 4.224×10^4 km and the LF/O orbit radius is 7.083×10^3 km, so the minimum distance between them is about 3.5×10^4 km. At this distance, a 61 m error is equivalent to a 10^{-4} degree line-of-sight error. An LF/O position uncertainty of 100 m (ref. 2) contributes 1.64×10^{-4} degrees error. Ref. 3 shows this uncertainty as 700 m, but the error is negligible either way. These two effects are negligible compared to the other errors shown in Table 3.1-1.

Table 3.1-1. Antenna Open Loop Pointing Error Summary

Error Source				3σ Error (degree)	
1. Spacecraft position					1.92×10^{-4}
TDRSS ephemeris, 61 m				1.0×10^{-4}	
LF/O ephemeris, 100 m				1.64×10^{-4}	
2. Spacecraft attitude					0.014
Attitude control of ACS module (gyros, star tracker and RW control errors)				0.010	
Spacecraft structural/thermal alignment (ACS to canister mount)				0.010	
3. Pointing computation and command					0.023
Computer roundoff and quantization (16 bits)				0.005	
Gimbal angle encoder (14 bits)				0.022	
4. Servo and gimballed platform errors					0.023
Servo step size (0.03 degree)				0.015	
Gimbal axes alignment (orthogonality and bearing runout)				0.017	
5. Antenna mast errors (20' Astro-mast)					0.520
Canister mounting and alignment (thermal)				0.017	
Mast deployment/repeatability					
Bending	0.1°	(3σ)	CEP	0.129	
Torsional	0.12°	(3σ)			
Thermal distortion					
Bending	0.05°	(3σ)	CEP	0.503	
Torsional	0.5°	(3σ)			
6. Antenna errors (boresight relative to mounting platform)					0.093
Antenna attachment misalignment				0.057	
Mechanical (thermal) boresight alignment				0.028	
Electrical boresight alignment				0.057	
Precomparator amplitude imbalance				0.036	
Precomparator-postcomparator phase imbalance				0.016	
Total rss error (3σ)					0.529

Spacecraft Attitude

The spacecraft alignment error is dominated by the 0.01° pointing accuracy of the spacecraft and the relative error at the canister mounting surface due to thermal and other distortions of the spacecraft itself.

Pointing Computation and Command

The computation and command error is dominated by the gimbal angle encoder error. The on-board data handling system uses 16 bits in double precision, but the payload drive encoder may well have fewer bits. The computational error, e_N, is found by letting the N bits cover a complete 360° range

$$e_N = \frac{360 \text{ deg}}{2^N} \tag{3.1}$$

The computer roundoff and quantization error is found by letting N = 16 or $e_{16} = 5.49 \times 10^{-3}$ degrees. The gimbal encoder error is $e_{14} = 0.022°$. The resultant error is 0.023°.

The gimbal, servo, and platform error capabilities were taken from ref. 4 where it was determined that the combined gimbal and steady-state servo error is 1 $\widehat{\text{min}}$ (0.017°) and the error due to gimbal step size of 0.03° is 0.015°. The total error for this category is 0.023°.

Antenna Mast Errors

The main source of pointing errors is the Astro-mast. Basically, these errors relate the total error from the canister mounting surface to the gimbal mounts. The baseline mast is assumed to be 20 feet long and 12 inches in diameter when deployed. The mounting and alignment error in the table (0.017°) is the mast mounting error. The other errors are based on information obtained from Mr. Peter Preiswerk of Astro Research. The data he provided is based on a 9-inch diameter, 40-foot long mast recently supplied to JPL. This mast has continuous epoxy longerons and is lanyard deployed. The data for the 20-foot mast was obtained by linear extrapolation; i.e., 50% of the numbers applicable to the 40-foot mast.

The LF/O assumes a canister deployed mast, but the deployment/repeatability errors are not expected to be significantly different. The 3σ numbers provided by Mr. Preiswerk assumed a standard 9-inch diameter, 20-foot long Astro-mast that is canister deployed. These numbers are given in Table 3.1-1 under item 5. The bending and torsional errors are combined and represented by a Rayleigh circular error. The maximum antenna pointing error due to the Astro-mast is 0.520°.

Antenna Errors

The antenna errors category includes all alignment errors from the antenna platform to the beam center. The 0.093° error assumes a graphite reflector and the error is compatible with that of a similar 5-foot dish currently being used on another TRW project.

The resultant rss errors for open loop pointing is 0.529°/axis or a Rayleigh mean error of 0.663°.

3.1.2 Autotrack Performance

A description of the recommended antenna autotrack system and acquisition procedure is presented. Autotrack performance is given in terms of the rss of tracking errors due to thermal noise, precomparator amplitude imbalance, precomparator and postcomparator phase imbalances, and drive step size.

The single-channel amplitude comparison autotrack system shown functionally in Figure 3.1-1 is recommended over other tracking techniques such as interferometer, self (beam)-steering, mechanical scan, conical scan, etc., because of its low risk, low cost, minimum hardware complexity, and its excellent performance in tracking the Ku-band, spread spectrum RF signal.

The 6-foot antenna assembly consists of a multiple-beam feed which is coupled to a precomparator network to provide sum and difference azimuth and elevation pattern signals. The azimuth and elevation difference signals are biphase modulated by a 1 kHz squarewave and are routed to switching circuitry where the signals are time multiplexed; i.e., half of the swtiching signal period contains the azimuth signal and the other half contains the elevation signal.

The time multiplexed signal, which contains the biphase modulated azimuth and elevation difference pattern signals, is added in-phase to the sum pattern signal by the RF coupler to form the amplitude modulated (AM) tracking signal.

The AM autotrack modulation technique was selected because the AM signal can be detected noncoherently with a simple square-law detector as opposed to the complex circuitry of coherent detection which would be required to despread and track the TDRSS forward link signal. Furthermore, there is no requirement to receive a TDRSS forward link Ku-band signal other than to use the signal as a tracking beacon.

After square-law detection, the AM signal is ac-coupled to eliminate dc signal components, filtered, and routed to the demultiplexer where the azimuth and elevation signals are separated and fed to their respective gimbal drive electronics. The servo motors with the appropriate input signals drive the antenna in the direction of peak gain reception.

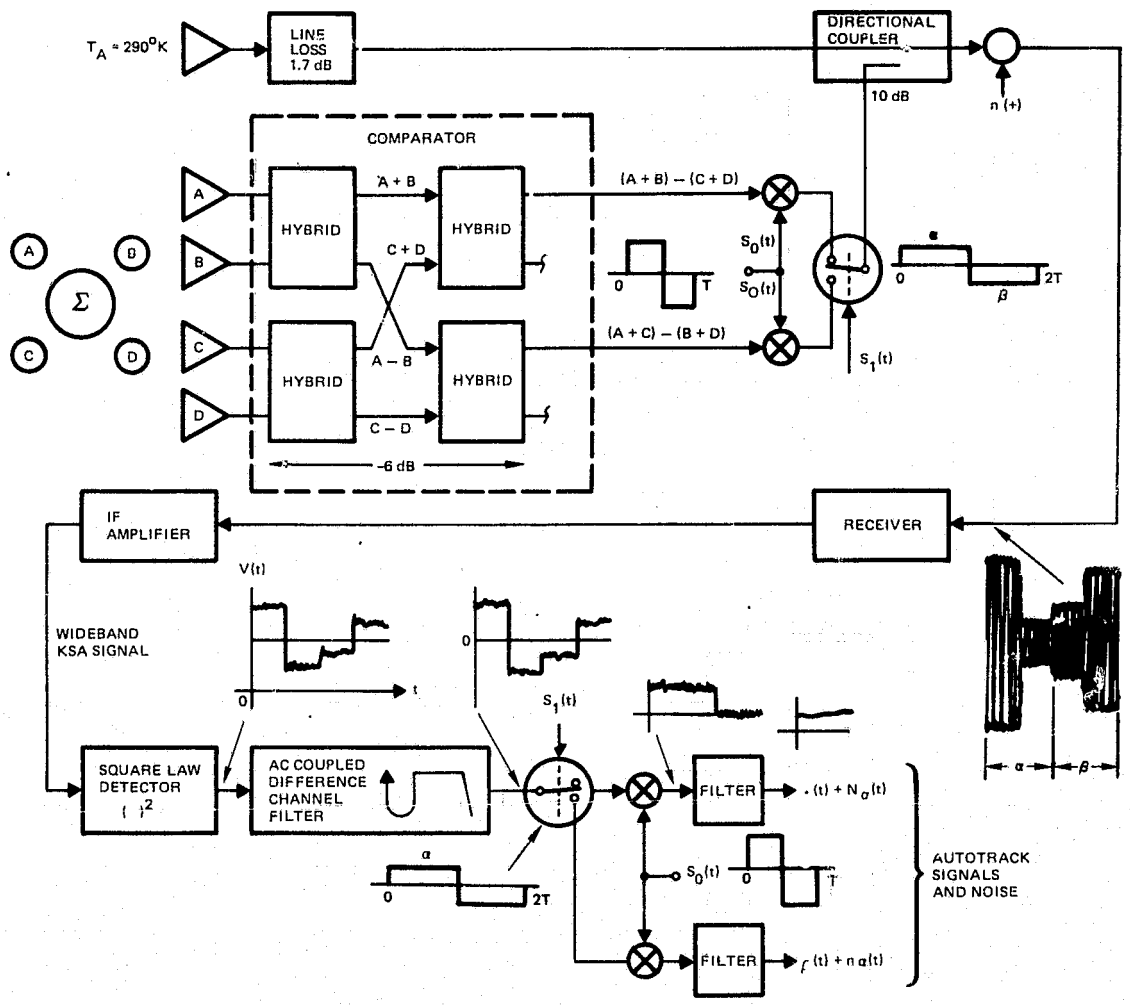

Figure 3.1-1. Antenna Autotrack Functional Block Diagram

The equipment from the antenna to the servo drive motors forms a closed loop tracking system whose effective closed-loop noise bandwidth is on the order of 2 Hz, thus providing operation with very large SNR's and correspondly small tracking errors due to receiver thermal noise. Figure 3.1-1 also shows the waveforms at selected portions of the autotrack system.

Acquisition Procedure

Acquisition procedures between the LF/O and the TDRSS are outlined in Table 3.1-2. The data was taken from the TDRSS "User Spacecraft Acquisition Procedures," P-805-1, June 1976, GSFC. For LF/O acquisition independent of the S-band TT&C link (except for initial antenna pointing programming and other tracking considerations given below), KSA acquisition sequence 2 is recommended for the LF/O mission.

Table 3.1-2. TDRSS User Spacecraft Acquisition Procedures

3.1 KSA ACQUSITION SEQUENCE NO. 1

3.1.1 An SSA return link is established with the user spacecraft using the normal SSA acquisition procedure.

3.1.2 The user spacecraft radiates a minimum S-band EIRP of +13 dBw.

3.1.3 TDRSS uses the S-band return link signal to aid antenna pointing. TDRSS radiates, within 5 seconds of user S-band turn-on and in the direction of the user spacecraft, a Ku-band +40 dBw (minimum) signal EIRP compatible with the forward link signal parameters defined in either Table 2-1 or Section 8.2.1.1 of S-805-1. The Ku-band carrier and PN clock shall include doppler compensation as scheduled.

3.1.4 The user spacecraft acquires the TDRSS Ku-band signal, begins autotracking, and begins radiating a +30 dBw (minimum) signal EIRP at Ku-band in the direction of TDRSS.

3.1.5 TDRSS then:

a. Autotracks the user Ku-band signal within 5 seconds of user turn-on (P_{acq} = 0.99 for user EIRP = +30 dBw).

b. Begins radiating normal power mode signal EIRP or high power mode signal EIRP as scheduled.

c. Either establishes return link DG 1 service and/or DG 2 service, or Shuttle Ku-band service within 5 seconds.

3.2 KSA ACQUISITION SEQUENCE NO. 2

3.2.1 An SSA forward link is established with the user spacecraft using the normal SSA acquisition procedure.

3.2.2 The user spacecraft is commanded to point its Ku-band antenna at TDRSS and to transmit in the direction of TDRSS a minimum of +30 dBw EIRP at Ku-band compatible with the return link signal parameters defined in either Table 2-2 or Section 8.2.1.2 of S-805-1.

3.2.3 TDRSS searches for the Ku-band signal and begins autotracking within 10 seconds of user turn-on (P_{acq} = 0.99 for user EIRP = +30 dBw).

3.2.4 TDRSS radiates normal power or high power EIRP at Ku-band in the direction of the user spacecraft compatible with the forward link signal parameters defined in Table 2-1 or Section 9.2.1.1 of S-805-1. The Ku-band carrier and PN clock shall include doppler compensation as scheduled.

3.2.5 The user spacecraft acquires the TDRSS Ku-band signal and begins autotracking.

3.2.6 TDRSS either establishes return link DG 1 service and/or DG 2 service within 5 seconds.

LF/O antenna tracking is accomplished as follows. Prior to coming over the horizon, the LF/O Ku-band steerable antenna is program-pointed at the TDRSS within a factor of 1.8 (open-loop pointing error) of the one-sided, half-power beamwidth (0.365°). This open-loop uncertainty does not reduce the LF/O EIRP below the minimum 30 dBW EIRP required for TDRSS Ku-band antenna acquisition and autotrack. A margin of greater than 18 dB exists.

Upon acquiring and autotracking the LF/O signal beacon, which consists of the normal composite 120 Mbps and 15 Mbps instrument signal, the TDRSS begins transmitting a spread spectrum beacon signal to the LF/O. The TDRSS beacon signal will be within 10 dB of the LF/O Ku-band high gain antenna peak. This signal level is above the threshold level which initializes autotrack.

The autotrack design provides for the inclusion of a small acquisition horn (BW $\approx$ 12°) to provide a broadbeam Ku-band beacon for initial TDRSS acquisition of the LF/O. The acquisition horn is considered as a backup acquisition aid in the event of temporary pointing anomolies (attitude control, boom distortion, etc.). Furthermore, a preprogram search routine in the communication and data handling module on-board computer provides a search raster for LF/O antenna acquisition and autotrack. This is also considered a backup mode.

Tracking Error Analysis

The autotrack error sources consist of precomparator amplitude imbalance, precomparator and postcomparator phase imbalance, drive step size, tracking loop dynamics, and the receiver system thermal noise. All the error sources except thermal noise are treated as bias errors. Thermal noise causes a circular error referenced around the bias error.

The error caused by precomparator amplitude imbalance is given (ref. 5) by

$$\sigma_{PAI} = \frac{\sqrt{2}\ \theta_m\ \Delta L}{20\ \log_{10} e}\ \text{deg} \tag{3.2}$$

where

θ_m = angle between sum and difference patterns peaks (degree)

ΔL = amplitude imbalance (dB)

For an amplitude imbalance of 0.25 dB, θ_m = 0.88°, and e = 2.71828, the error is 0.036°.

The error due to pre and postcomparator phase imbalances is given (ref. 5) by

$$\theta_{ppp} = \frac{\pi\ \sqrt{2}\ \Delta\beta}{180} \tan(\beta - Z)\ \text{deg} \tag{3.3}$$

where

$\Delta\beta$ = the precomparator differential phase imbalance

β = the average precomparator phase shift for all legs prior to the postcomparator interface

Z = the average phase shift in all legs prior to the postcomparator, reference to the sum channel

A worst case error due to phase imbalances of 0.018° results for a $\Delta\beta$ maintained within 2° and a (β-Z) maintained within 20° over thermal differentials.

The error due to drive motor step size is the same as given in the open-loop pointing error performance, 0.015°.

The error cause by the dynamics of the servo control loop is estimated to be 0.015°.

The tracking error due to thermal noise is given (ref. 6) by

$$\sigma_T = \left\{ \frac{\left(\frac{B_n}{B_{IF}}\right)}{2\,(S/N)_{IF}\,(K_A K_L)^2} \left(1 - \delta + \frac{1}{2\,(S/N)_{IF}}\right) \right\}^{1/2} \text{deg} \qquad (3.4)$$

where

B_n = close loop servo noise bandwidth ($\approx$2 Hz)

B_{IF} = IF noise bandwidth (6 MHz)

$(S/N)_{IF}$ = signal-to-noise ratio in IF noise bandwidth

1-δ = signal power loss due to signal spectrum truncation by B_{IF} (0.903 for $B_{IF} \times T = 2$; $T = \frac{1}{3 \text{ megachip/sec}}$)

K_A = antenna sensitivity gain slope ($\approx$0.79 $\frac{\text{volt/volt}}{\text{degree}}$) referenced to the sum channel antenna feed and the difference channel antenna comparator outputs

K_L = ratio of the difference channel to sum insertion loss from the K_A measurement reference point to the output of coupler

$$K_L = \frac{h_c k_c}{g_L k_\varepsilon}$$

h_c = difference channel insertion loss from comparator output to coupler (1 dB)

g_L = insertion loss from the sum antenna feed to coupler (1.2 dB)

k_c = coupler insertion loss for difference channel (10 dB)

$k_\varepsilon = \sqrt{1 - k_c^2}$ = coupler insertion loss for sum channel

The TDRSS forward link received signal link analysis is given in Section 3.11.4. The nominal IF SNR during autotrack is 11 dB and the initial acquisition worst case value is 0 dB.

The tracking error due to thermal noise for the parameter values defined in (3.4) as a function of received IF SNR is given in Figure 3.1-2.

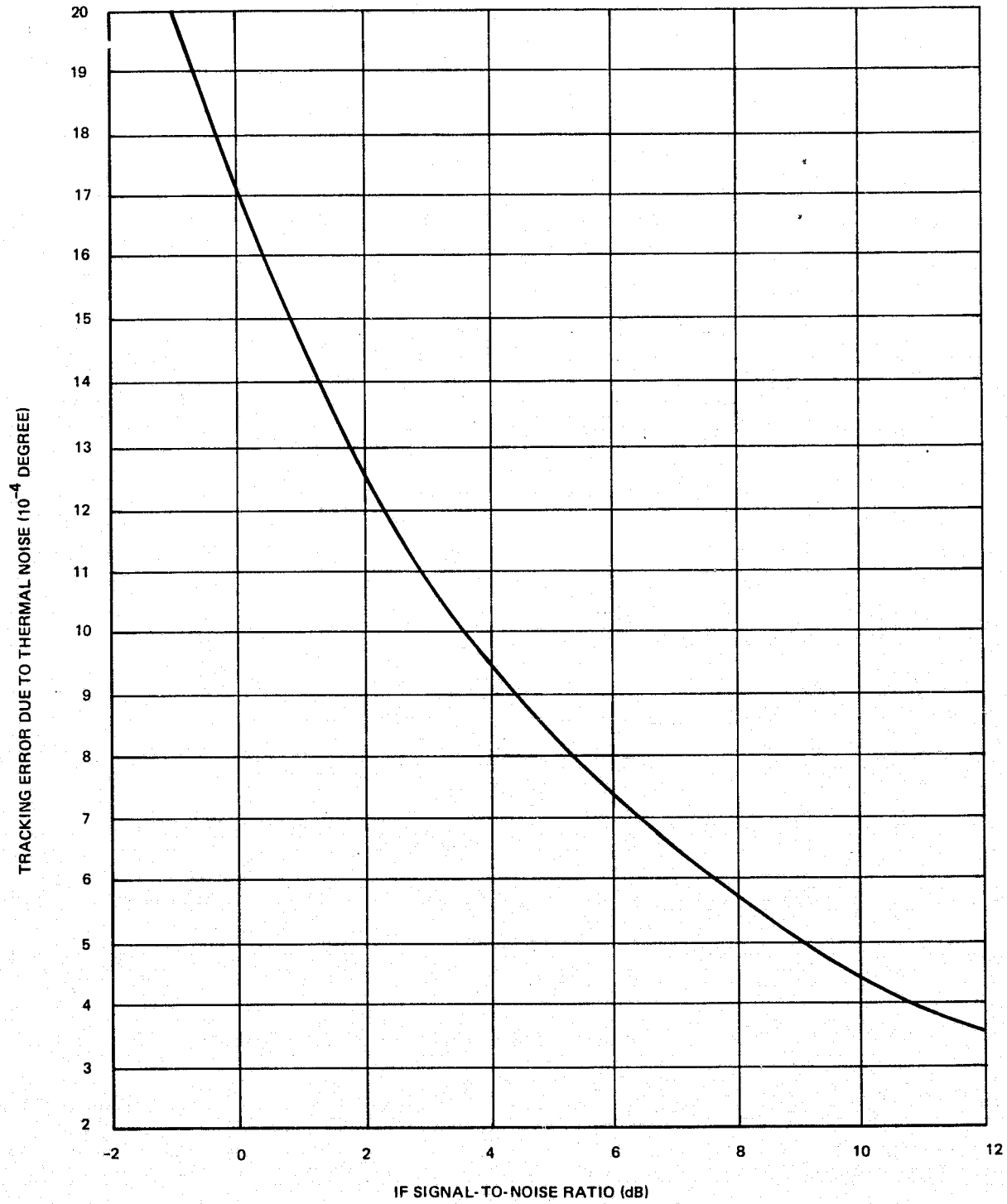

Figure 3.1-2. Antenna Tracking Error due to Thermal Noise vs IF Signal-to-Noise Ratio

The autotrack errors are summarized in Table 3.1-3. The bias and thermal noise errors are root-sum-squared and the Rayleigh mean computed. The corresponding antenna and pointing losses are computed by estimating that the sum pattern for small angles follows a Gaussian distribution. Thus, the loss relative to the sum peak gain is given by

$$P(\theta) = P\left(\theta_{3\ dB}\right)\left(\frac{\theta_\varepsilon}{\theta_{3\ dB}}\right)^2 \text{ dB} \qquad (3.5)$$

where

$P(\theta_{3\ dB}) = -3$ dB

$\theta_{3\ dB}$ = half power beamwidth (degree)

θ_ε = error (degree)

3.1.3 Conclusion

In summary, the recommended autotrack design provides excellent tracking performance. Practical limits of precomparator amplitude imbalance and precomparator and postcomparator phase imbalances do not cause appreciable contributions to the autotrack error. The errors associated with motor step size and servo loop dynamics are also minimal. The tracking error due to thermal noise is negligible at acquisition and autotrack receive signal levels.

Table 3.1-3. Autotrack Errors

Error Source	Error (degree)	Notes
Precomparator amplitude imbalance	0.036	$\theta_m = 0.88°$, $\Delta L = 0.25$ dB
Precomparator/postcomparator phase imbalances	0.018	$\Delta\beta = 2°$, $(\beta\text{-}Z)$ 20°
Drive step size	0.015	0.03° step size
Servo loop dynamics	0.015	Estimated
RSS	0.0455	
Thermal noise	0.0004	$(S/N)_{IF} = 11$ dB
RSS total	0.0455	Per axis
Circular error	0.057	Rayleigh mean
Antenna pointing loss		$= \sqrt{\pi/2}\ \sigma$
Receive	0.06 dB	3 dB beamwidth = 0.80°
Transmit	0.07 dB	3 dB beamwidth = 0.73°

3.2 TIME MULTIPLEX VS UQPSK

This section discusses communication subsystem design approaches for the simultaneous transmission of TM and MSS instrument data via the TDRSS Data Group 2 (DG2) Ku-band single access (KSA) return link, identifies potential interference between the TDRSS and STDN/direct access links, recommends methods to avoid this interference, and selects a preferred approach for combining the TM and MSS data for the TDRSS KSA return link.

One method for transmitting TM (120 Mbps) and MSS (15 Mbps) data simultaneously is the use of quadriphase-shift-key (QPSK) modulation; i.e., TM data is modulated on the QPSK modulator I channel and MSS data is modulated on the Q channel. Since the data rates are unequal, unbalanced QPSK modulation (I and Q channel powers unequal) is utilized to make efficient use of the transmitter power.

Another method is to generate a single 135 Mbps data stream by time multiplexing the TM and MSS data. The single data stream is then split into two independent data streams sequenced at half the single data stream rate. One data stream is fed to the I channel and the other to the Q channel of the modulator to form a balanced QPSK signal.

Feasible time multiplex design approaches were investigated in order to recommend a cost effective time multiplex design for use with balanced QPSK modulation. This method was then compared with the direct UQPSK method to establish a recommended TDRSS KSA communication design.

An important consideration in the tradeoff between UQPSK and time multiplexed/balanced QPSK is the potential interference between the TDRSS and the STDN/direct access transmissions. Although the signal transmitted through the main beam of the TDRSS high gain antenna does not interfere with the signal transmitted through the STDN/direct access link, there is interference from signal transmission through the antenna sidelobes. The amount of interference and the modulation for rendering the interference negligible were determined.

3.2.1 Time Multiplexing

Time multiplexing techniques to permit simultaneous transmission of the MSS and TM data on the TDRSS link were investigated. Both synchronous and asynchronous approaches were considered. The hardware implementations and their failure modes are of particular concern because of their impact on the total spacecraft mission success.

The following simplified description of the TM and MSS instrument data systems is given to clarify the multiplexing design approaches discussed below.

The MSS sensor obtains ground images in five spectral bands with a ground resolution of 79 m and multiplexes the data into a 15 Mbps wideband binary data bit stream. Included in the data stream are frame synchronization data, preamble, and scan markers

to permit ground processing of the data. The MSS data word length is 6 bits long. The data rate is controlled by a clock oscillator with a stability of $\pm 1 \times 10^{-4}$ per year. The scene scan rate is once per 73.42 msec, where the ground data requires 33 msec of the scan time, and the preamble, which is used for a filler, occupies over 20 msec of each scan period.

The TM instrument obtains its data from six or seven spectral bands with a ground resolution of 30 meters. The data word for the TM has 8 bits of resolution. The TM instrument has a data multiplexer which multiplexes the six or seven color bands and the spacecraft telemetry into a binary data stream that is sequenced at a maximum rate of 120 Mbps.

The output data rate is controlled by an unspecified clock oscillator but will probably be 1 part in 10^6 or better. The data stream contains frame sync and time code data to allow for data identification for ground processing. The ground scene data takes approximately twice as much of the total time between scans as the MSS.

Two basic multiplexing methods were considered, leading to three potential approaches. First was the addition of a box to the wideband module which would time multiplex the data stream from both the TM and the MSS. The main benefit of this approach is minimizing the impact on the two instruments.

The second basic method was to use the existing TM multiplexer which presently multiplexes six color bands and a space telemetry channel into a 120 Mbps stream. The addition of the 15 Mbps MSS data channel would increase the TM data multiplexer data rate to 135 Mbps. In this approach the MSS data stream would be handled as if it were just an additional TM data word.

Approach A. Use of TM Multiplexer – Synchronized Operation

This approach takes advantage of the fact that the TM instrument presently has a data multiplexer that is combining six or seven data channels and a spacecraft channel into a 120 Mbps digital data channel. If it is acceptable to transmit 135 Mbps on the Ku-band STDN/direct access link, a single data multiplexer can be used for the Ku-band STDN/direct access and TDRSS links. Operation of the TDRSS link at 135 Mbps and the STDN/direct access link at 120 Mbps would require two independent multiplexers in the TM instrument.

With the TM multiplexer combining the MSS data as another data channel, the TM can insert its frame sync and control words which would allow the ground processor to easily extract the MSS data stream. No additional multiplexer synchronization is required and no additional synchronization data need be entered into the data stream.

Figure 3.2-1 shows an overall functional block diagram of Approach A. The MSS normally operates in sync with the TM by means of an external clock supplied by the TM instrument. This clock frequency is 15 MHz or a multiple of 15 MHz such as 30 MHz. In

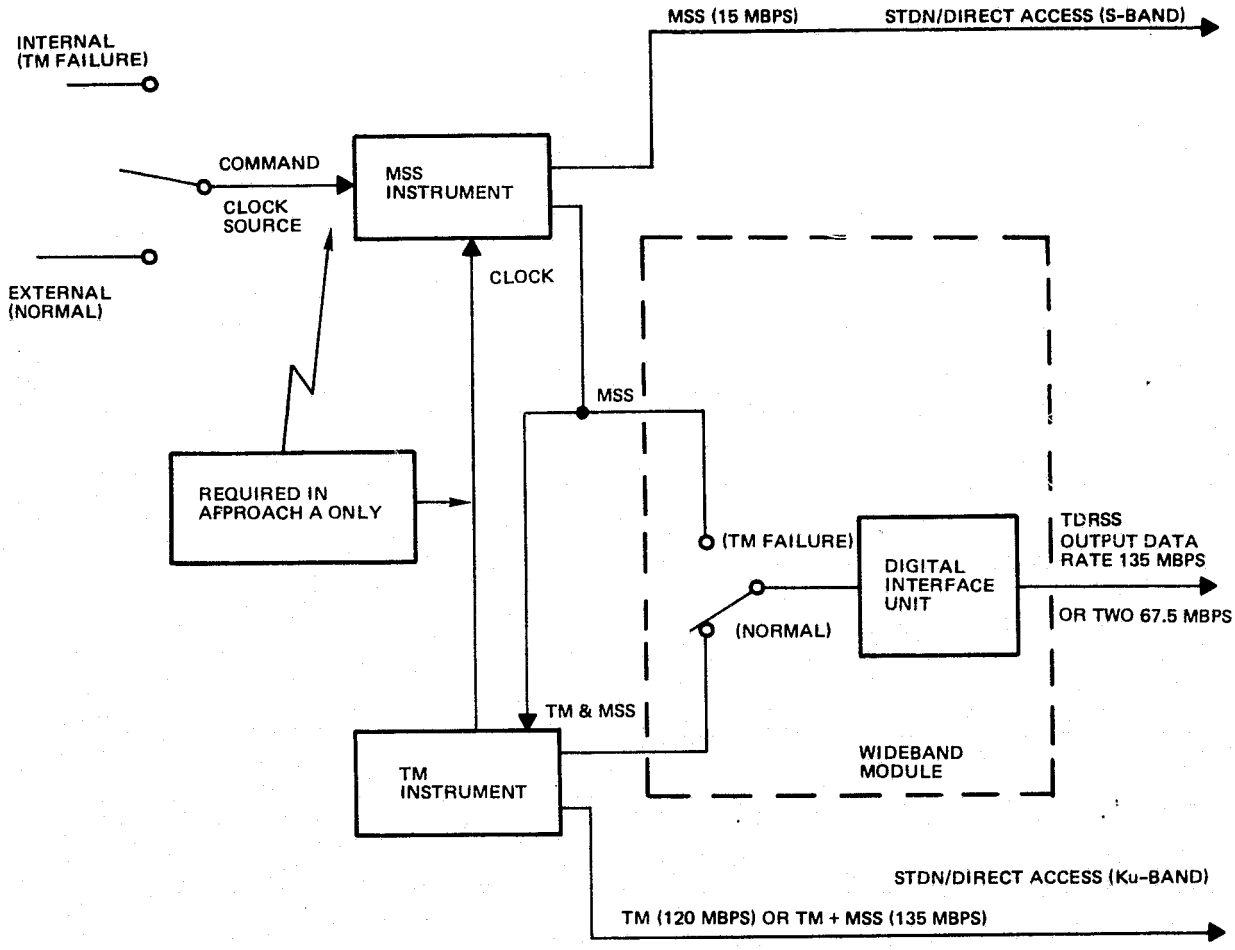

Figure 3.2-1. Time Multiplexing Digital Approaches A and B (TM Supplied Multiplexer)

the event of a TM instrument failure, the MSS is commanded back to operation on its internal clock source. The MSS output data is transmitted on the S-band STDN/direct access links and is also provided to the TM instrument for TDRSS Ku-band transmission.

The TM instrument combines the MSS data as an additional instrument data word into a 135 Mbps binary data stream for use on the TDRSS channel. This same data stream could be used for the Ku-band STDN/direct access link; however, the performance margin would be reduced by 0.5 dB ($10 \log_{10} (120/135)$). If this small link margin degradation is not acceptable, the TM instrument could contain the logic hardware for a 120 Mbps and a 135 Mbps multiplexer in order to supply both data links with the desired data rates.

If the MSS fails, the TDRSS channel operation is not impaired since the ground station would just ignore the MSS data. With a TM instrument failure, however, the TDRSS data input would be switched by command directly to the MSS instrument and the MSS switched to its internal clock. The combining of signals within the two instruments is shown in Figure 3.2-2.

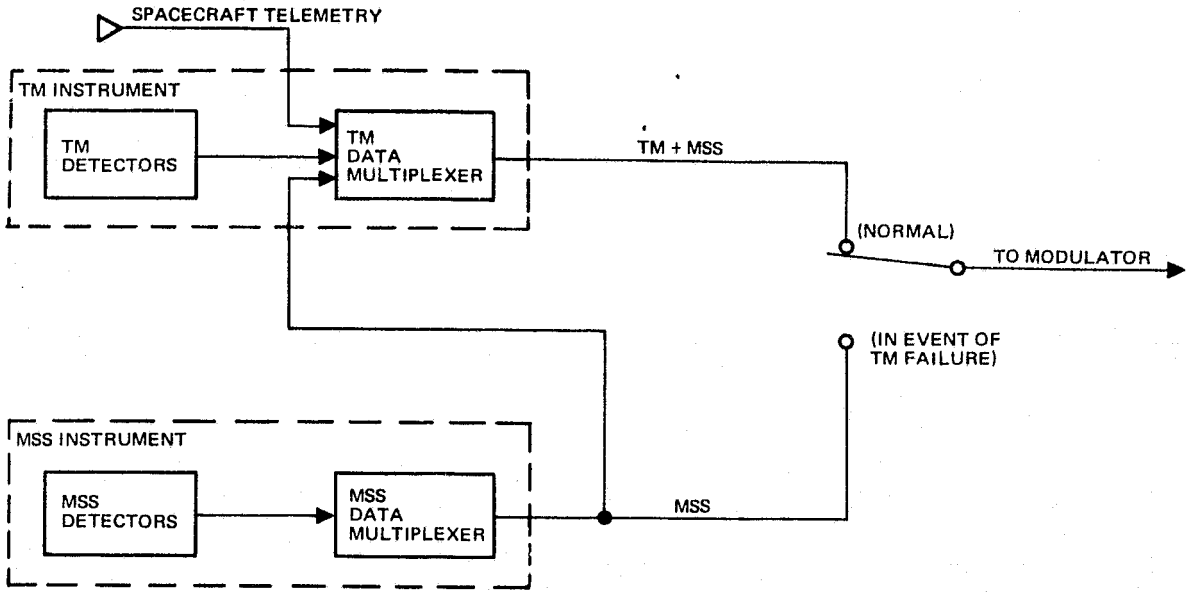

Figure 3.2-2. Time Multiplexing (TM Supplied Multiplexer)

Figure 3.2-3 shows in greater detail the changes to the TM instrument operation. It highlights the fact that the TM instrument is presently multiplexing six color channels, spacecraft telemetry, and housekeeping into a 120 Mbps data stream. Increasing the output rate to 135 Mbps allows sufficient capacity for the additional 15 Mbps MSS data. Figure 3.2-4 shows the format of the data with the MSS stream included in the TM data frame. The impact of these changes is as follows.

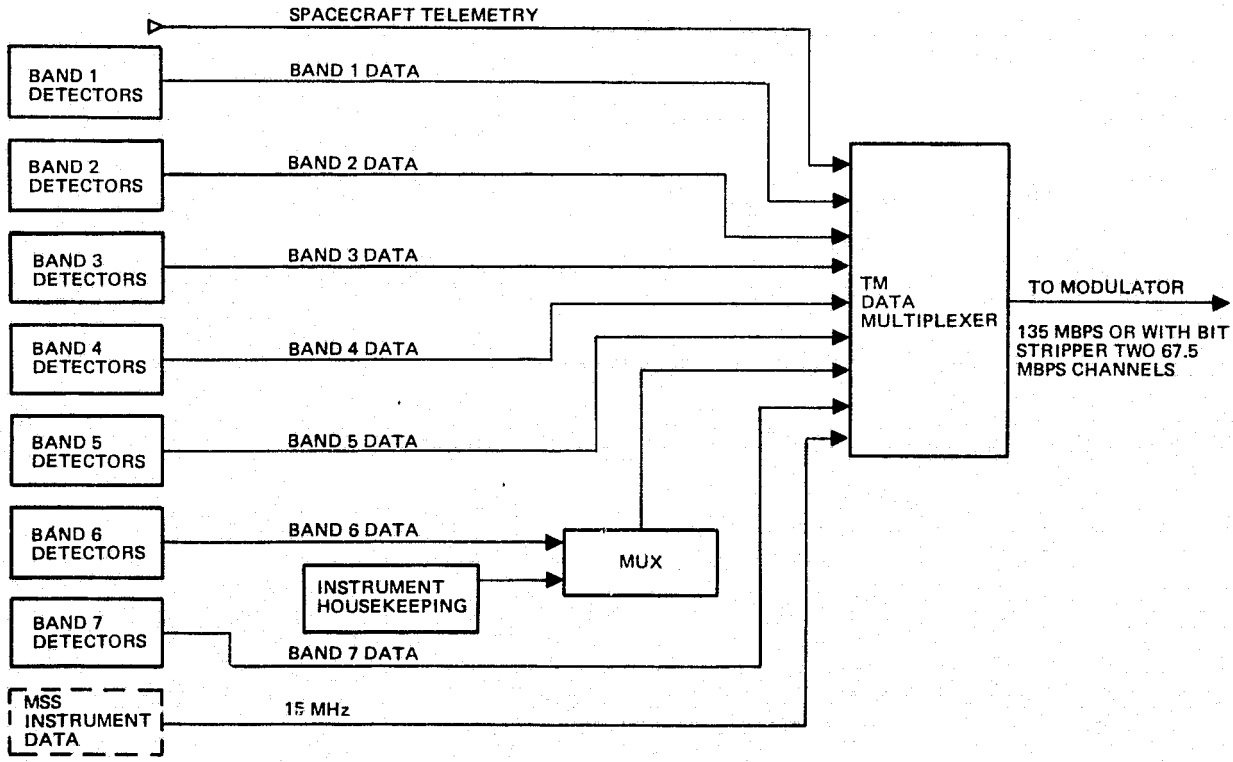

Figure 3.2-3. TM Multiplexer Details

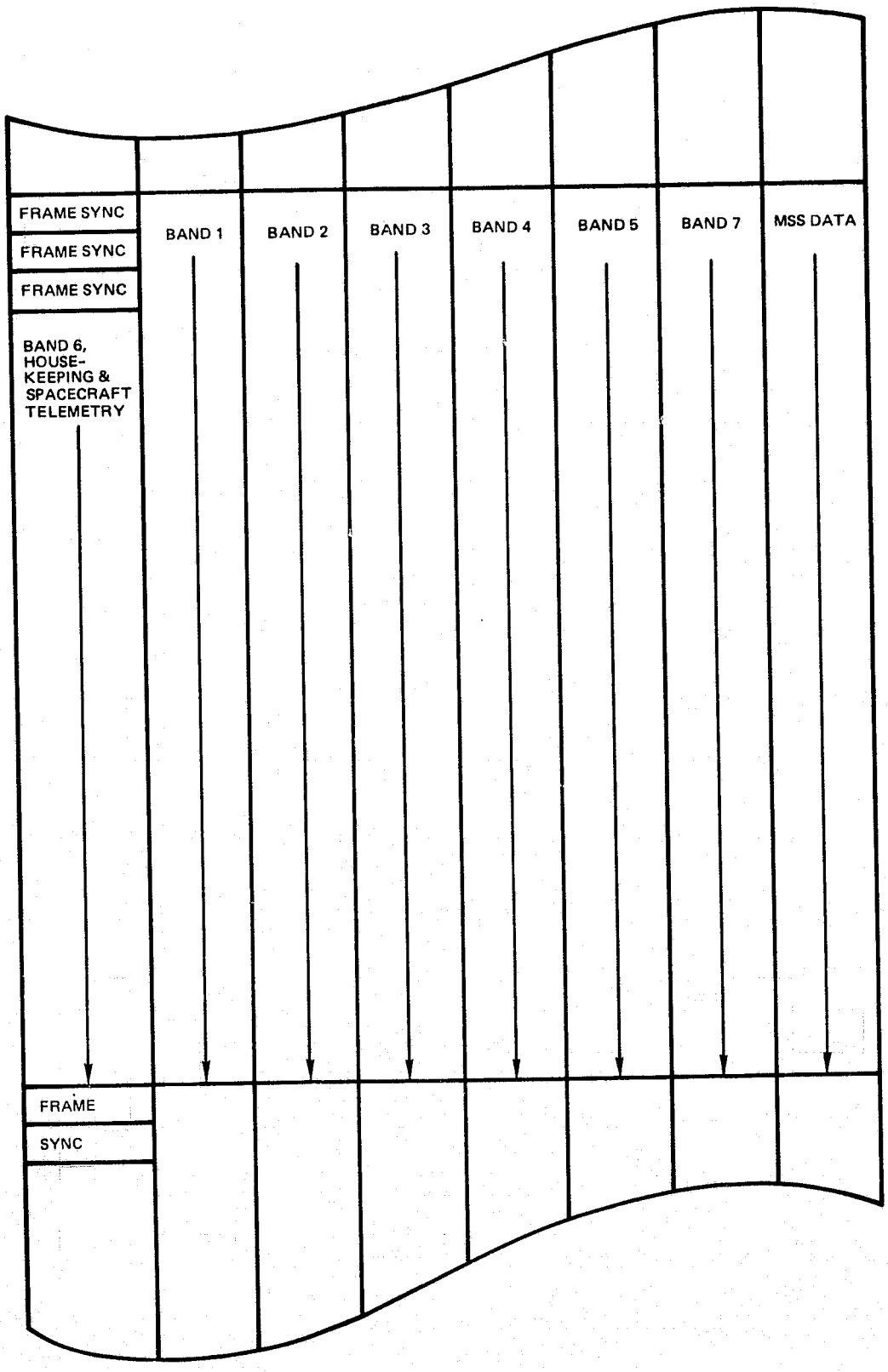

Figure 3.2-4. Data Format for TM/MSS Data (TM Supplied Multiplexer)

Instruments. Figure 3.2-5 is a detail diagram which shows the changes and additions that are made to the TM data multiplexer. There are three changes:

- An 8-bit shift register is added to accept the serial data from the MSS and to convert it into the TM word format of 8 bits. There is no relationship between the 8-bit TM word and the 6-bit MSS data word. The TM transmits the data, 8 bits at a time, in its format. Ground processing re-establishes the MSS data and the present MSS system acquires sync to the MSS 6-bit word format. The shift register operates on a MSS generated clock which is supplied by the Mapper. This synchronization prevents the MSS from generating more or less words than the accept-rate of the Mapper.

- The TM clock system is increased from 120 to 135 MHz to expand to output data capacity for the MSS data. In addition, the divide-down chain which controls the number of transmitted data words is increased. A change of 8 to 9 is shown, which is the ratio of 120 to 135 MHz.

- The output multiplexer is changed to allow for the additional word, and the output rate is increased to 135 Mbps.

The MSS impact is that it must now operate on either an external frequency or its own internal source and must also accept a ground command select signal. The MSS may also have to operate on a slightly different frequency than it presently does, but well within the picture resolution requirements; i.e., 15.00 MHz vs the present 15.06 MHz.

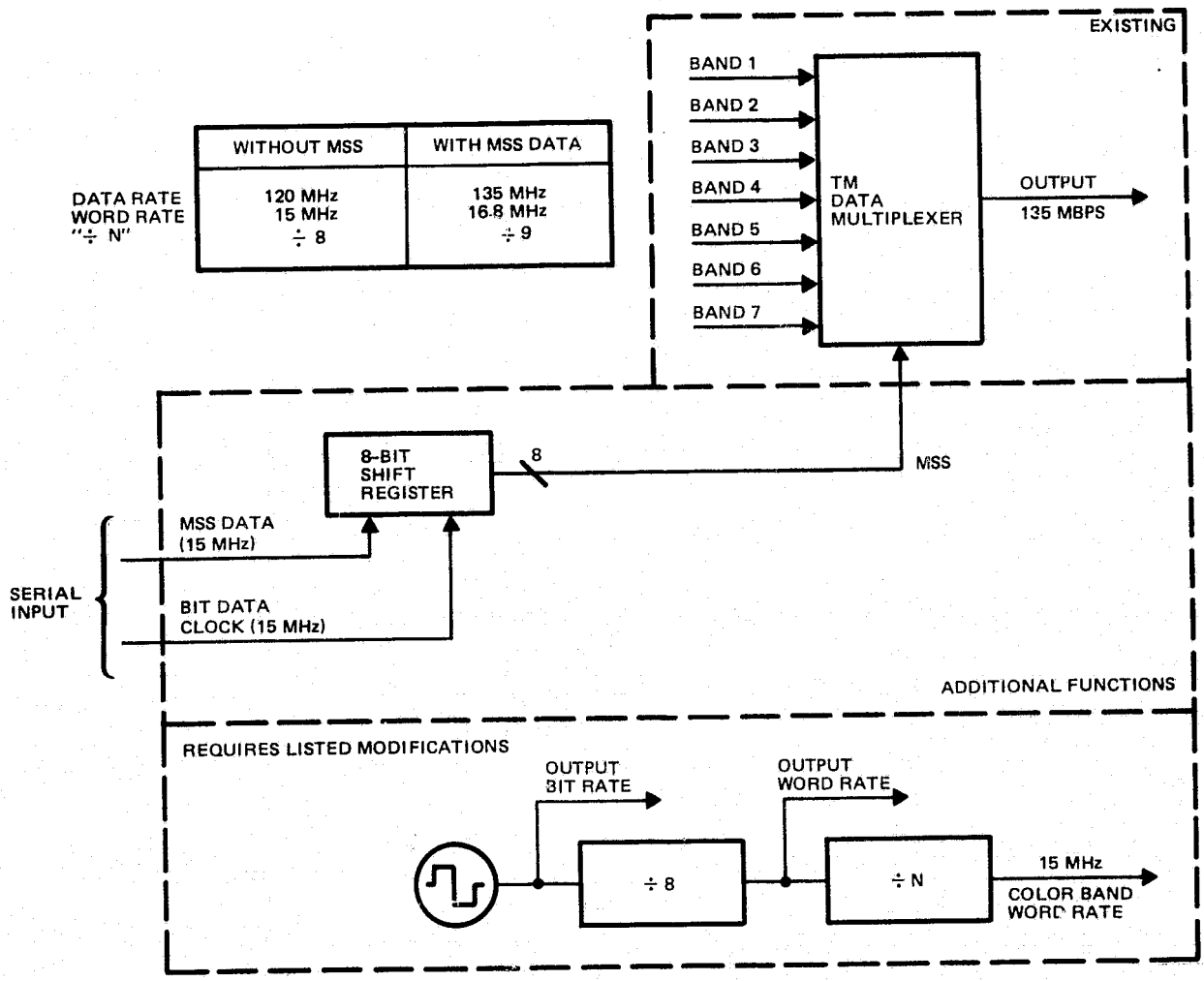

Figure 3.2-5. Changes to TM Multiplexer

Spacecraft. The spacecraft system requires the additional command capability to switch the MSS clock from internal to external. For minimum TM impact, it may be desireable to operate the Ku-band STDN/direct access links at 135 Mbps rather than 120 Mbps.

Ground Processing. There is no major impact on the ground processing. Figure 3.2-6 shows the data flow. The TM data frame allows separation of the TM color band and separation of the MSS data stream. This MSS data is then processed as in the present system.

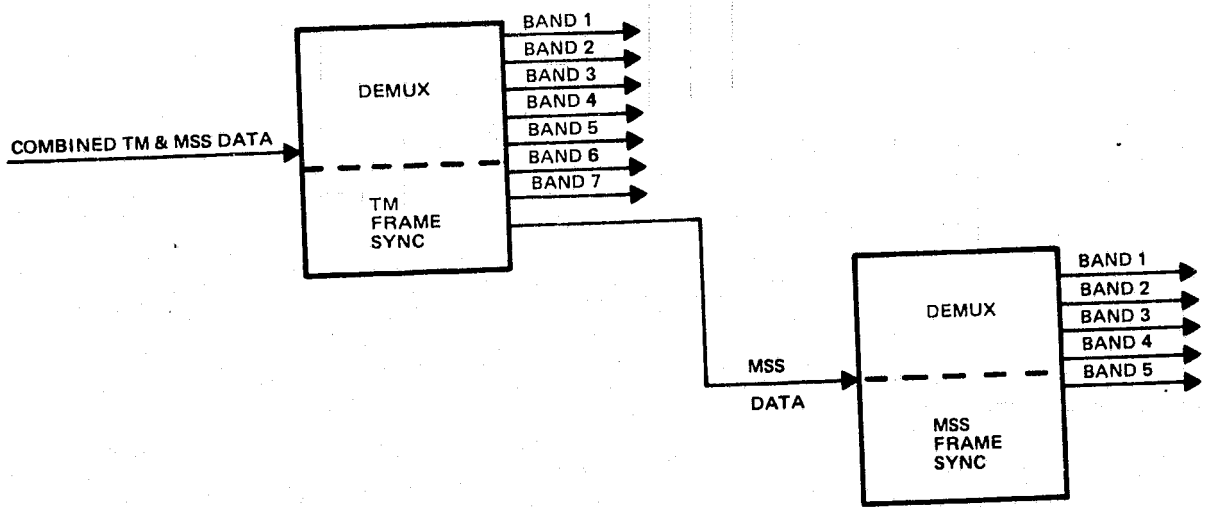

Figure 3.2-6. Ground Processing for TM/MSS Demux (TM Supplied Multiplexer)

Interactive Failure. As shown in Figure 3.2-1, two commands are required: the capability to switch the MSS to internal clock if the TM clock fails and the capability to switch the TDRSS link to MSS-only if the TM data multiplexer fails. If these two commands are exercised, the TM is completely out of the RF system and the MSS operates as in the present system.

If the MSS fails, however, no spacecraft change is required. The ground system just ignores the MSS data.

No additional hardware is placed in series with the data streams that could result in additional failure modes.

Advantages/Disadvantages. The advantages of this approach are:

- No additional multiplexer or hardware equipment boxes
- The total spacecraft instruments data systems are operated in synchronization.

The disadvantage is the change to the existing MSS requiring it to operate on an external clock and at a slightly different frequency.

Approach B. Use of TM Multiplexer — Nonsynchronized Operation

This time multiplexing approach again takes advantage of the existing multiplexer in the TM to provide a combination of TM and MSS data. It permits the MSS to operate fully independent in a nonsynchronized mode. The approach is identical to Approach A except the MSS does not operate on an external clock and the TM must provide a method to synchronize the MS data to its own data rate.

Approach B is shown in Figure 3.2-1. This approach is the same as Approach A except for the added requirement of an MSS data synchronizer in the MSS data flow as shown in Figure 3.2-7. Furthermore, this approach does not require the use of an external clock and clock select command control for the MSS. Before the detail implementation is discussed, let us consider the system implication of running a data multiplexer in a nonsynchronized manner.

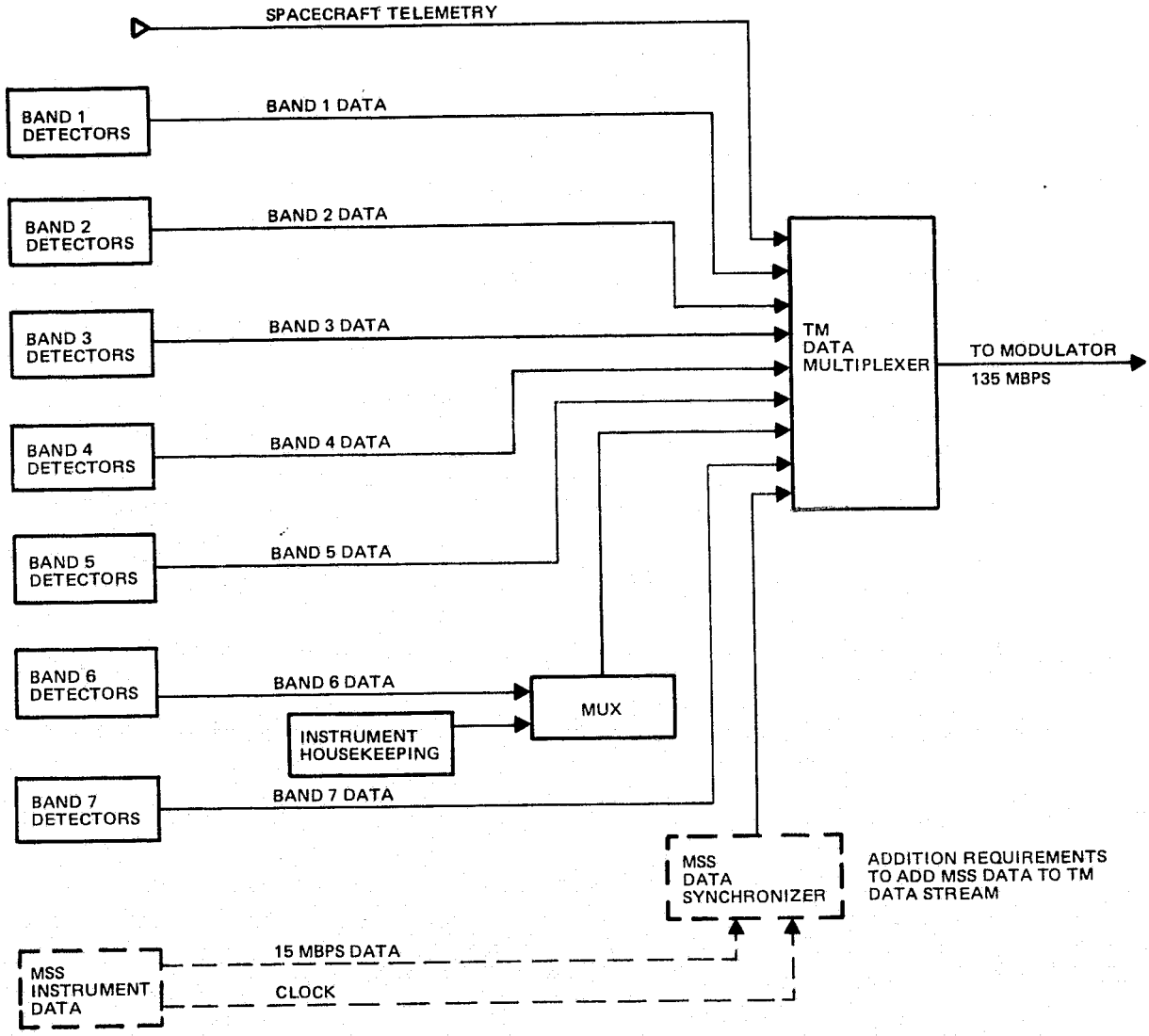

Figure 3.2-7. TM Multiplexer Details

If the MSS data system is in sync with the TM, it is producing data at exactly the same rate as the TM is accepting the data. In nonsynchronous operation, if the MSS was operating faster than the TM accept rate, data would be lost. If, however, the MSS is operating at a lower rate, filler words or bits could be inserted in the multiplexer and removed in the ground processing.

One approach to the MSS operating at a higher rate would be to buffer-store words in excess of the transmittal rate and to transmit them instead of the excessive preamble length of the present MSS data stream. This unloading of the buffer memory can only be accomplished once a scan or once every 73 msec. During the 73 msec at the 15 Mbps data rate, almost 1.1 million bits of data must be processed. Even if only the ground data was processed by the buffer memory (33 msec of data), almost a half million bits of data must be processed by the buffer before a dump or unload could be accomplished. A very small increase in the MSS data rate above the accept rate would result in a very large high speed buffer storage.

Operating the MSS at a rate slower than the accept rate is accomplished by the implementation shown in Figure 3.2-8. The implementation is the same as Approach A except for the addition of an 8-bit holding register to the MSS data stream. The 8-bit shift register assembles the MSS data into 8-bit words. When an 8-bit word has been assembled, it is transferred to the hold register. When the TM output multiplexer has read the MSS word it resets the holding register to a selected code word. This code word could be full dark or full light, or since these are used for middle and end of scan mark, full dark plus one or full light minus one may be used. If a new MSS word is assembled before the next TM readout, the code word is erased by the data. If however a new word has not been assembled, the code word will be transmitted, recognized on the ground, and removed from the MSS data stream.

The impact of these changes is as follows.

Instruments. The impact to the TM is shown in Figure 3.2-8. The addition to the hardware is the MSS data synchronizer. Additional changes are the increased clock and output data rate as described in Approach A.

This approach requires no change to the MSS design. The MSS data rate, however, must be less than the rate the TM will accept the data from the MSS.

Spacecraft. No impact.

Ground Processing. Ground processing is the same as described in Approach A with the addition of the recognition of the filler code words and their removal.

Interactive Failures. The interactive failures are as discussed in Approach A except that the MSS will only operate on its internal clock.

Advantages/Disadvantages. In addition to the advantages and disadvantages listed in Approach A, this approach has the advantage of having the MSS operate independently and nonsynchronized with the TM instrument. It, however, has the disadvantage that the MSS must operate at a slightly lower rate and that filler words must be inserted and removed from the data stream.

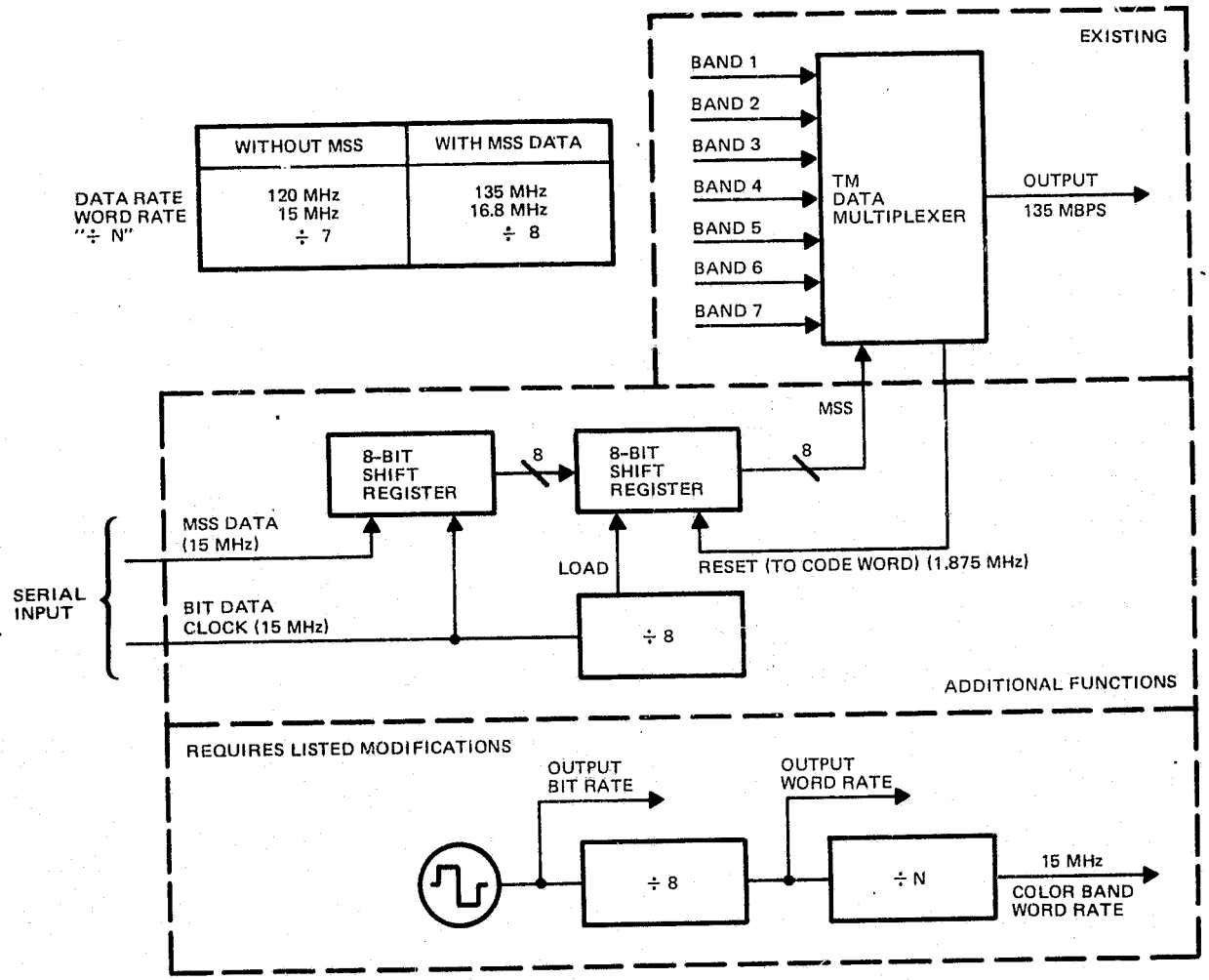

Figure 3.2-8. Additional Function Added in TM to Provide a Multiplexer if MSS has not been Synchronized

Approach C. External Multiplexer Unit

The two previous approaches modify and add hardware in the instrument and therefore add no hardware to the spacecraft communication channel. Approach C takes the opposite view point of minimizing the impact on the instruments at the cost of adding an additional unit of hardware to the spacecraft.

A simplified block diagram of Approach C is shown in Figure 3.2-9. There are no interfaces between the two instrument modules. Each instrument module independently feeds its own STDN/direct access ground link transmitter. In addition, that same data output, but with a separate output buffer, interfaces with an additional data time multiplexer. The MSS and TM data stream are multiplexed in that unit for transmission on the TDRSS data link. Figure 3.2-10 shows in greater detail the instrument data multiplexers and the additional TDRSS link multiplexer.

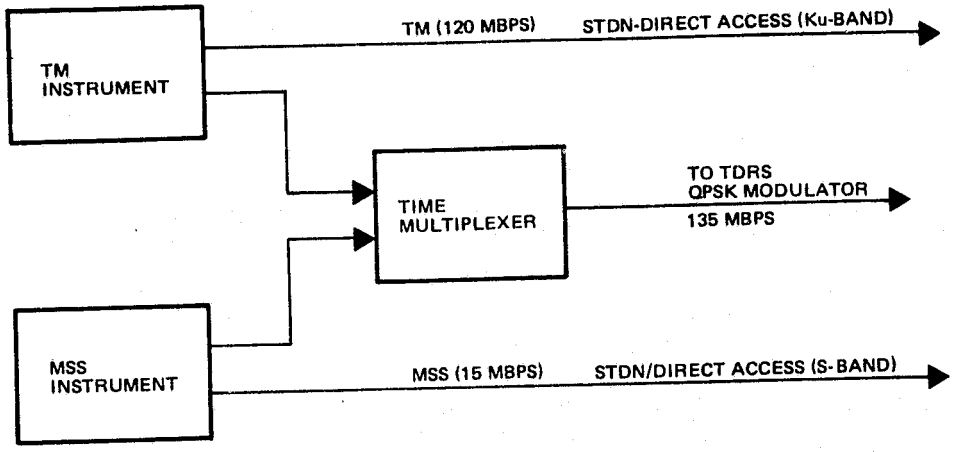

Figure 3.2-9. Approach C Separate Digital Multiplexer Box

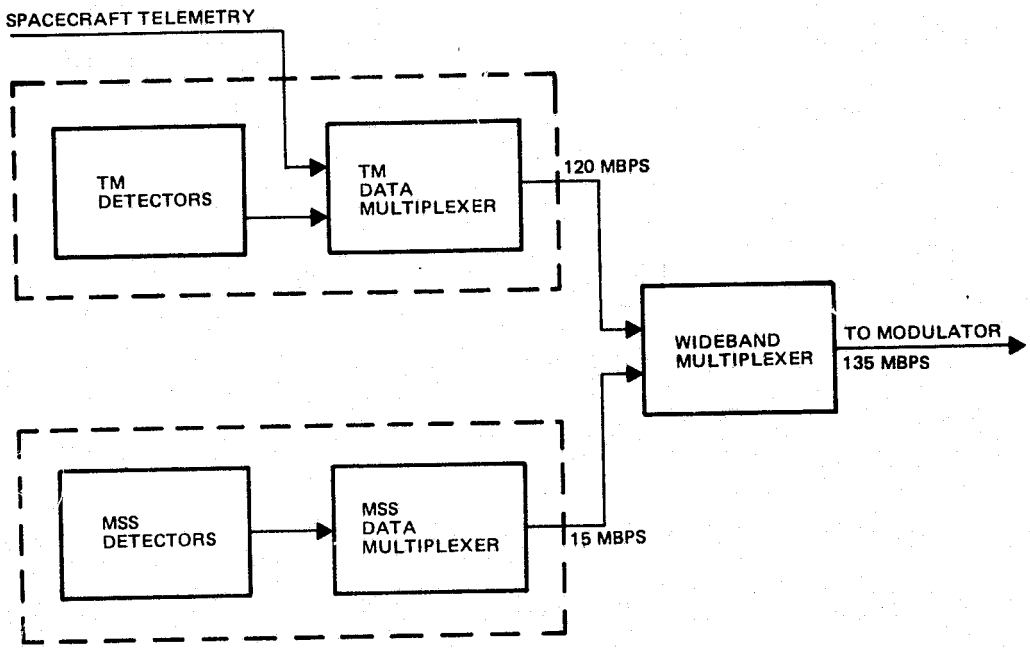

Figure 3.2-10. Approach C Separate Time Multiplexer

The details of the separate data multiplexer are shown in Figure 3.2-11. The multiplexer accepts data from the TM and the MSS at an 8 to 1 ratio using an 8-bit and a 1-bit shift register. The 8-bit TM shift register operates at 120 MHz and the 1-bit MSS shift register operates at 15 MHz. The 9 bits are then assembled in a 9-bit shift register for transmission on the TDRSS link. The output rate of this register is 135 Mbps. Shown also in Figure 3.2-11 is a bit stripping logic to prepare the data for the TDRSS link quadriphase modulator.

A synchronized clock system is shown at the bottom of Figure 3.2-11. For this system to work effectively, the MSS, TM, and the data multiplexer must operate in sync. The clock loop shown generates a 135 MHz output clock. From it, 120 MHz and 15 MHz clocks for the MSS and TM are generated. Other configurations of this system are possible such as generating the output clock and the TM clock from the MSS clock, or generating the MSS clock and the output clock from the TM clock.

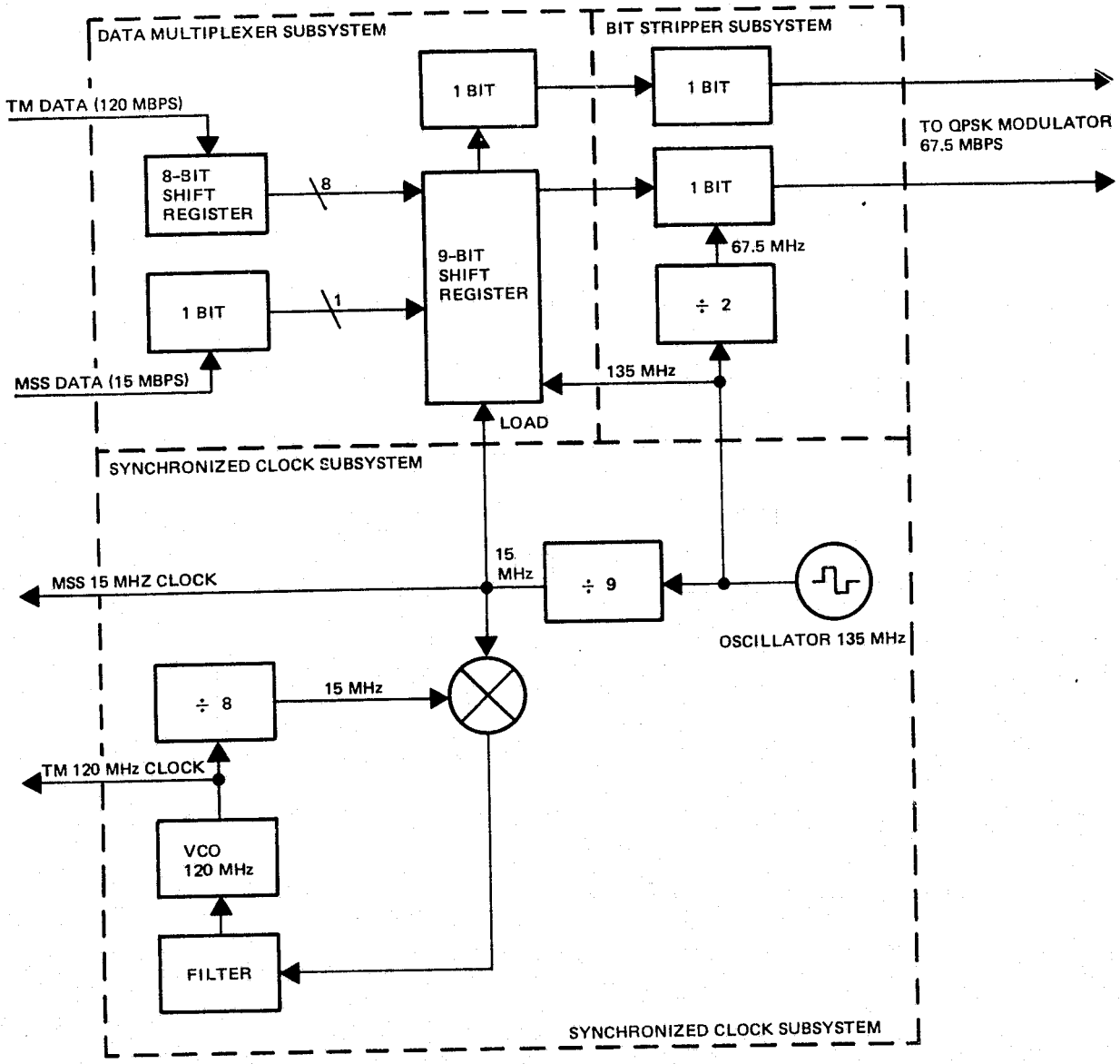

Figure 3.2-11. Separate TM and MSS Data Multiplexer

Figure 3.2-12 shows the data format for this approach. Eight bits of TM data are followed by 1 bit of MSS data and then repeated. There is no relationship between the 8-bit grouping and the word structure of the TM. However, this could be done if desirable.

The impact of these changes is as follows.

Instruments. One or both of the instrument modules (MSS or TM) must be operated on an external clock. If the TM were operated on an external clock it would also require the capability of being commanded to operate on internal clock in the event of clock generator system failure.

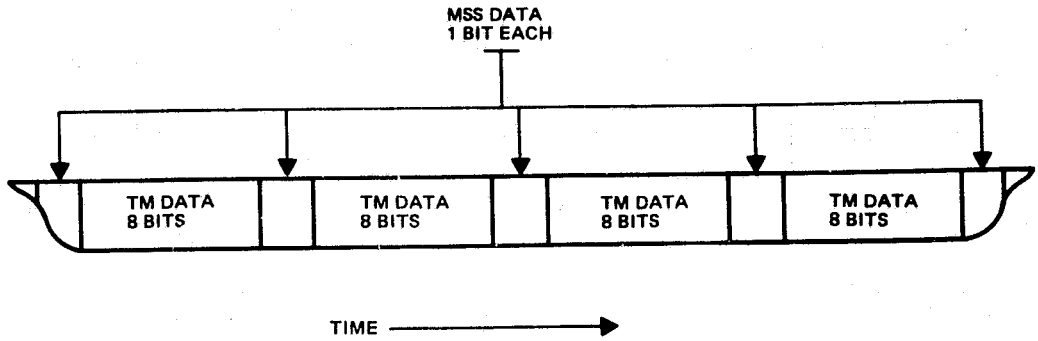

- 1 BIT OF MSS DATA FOR EVERY 8 BITS OF TM DATA
- FINAL DATA RATE 135 MHz
  FOR TM - 120 MHz
  MSS - 15 MHz

Figure 3.2-12. Data Format for TM and MSS Separate Data Multiplexer

Spacecraft. The impact to the spacecraft system is the required addition of a multiplexer unit to multiplex the TM and MSS data stream into a single data channel for the TDRSS link.

Ground Processing. In the description of Approach C, it may be noted that in the multiplexing of the two data streams, no additional frame sync information was included. This was done because the scan sequence of the two instruments is not synchronized, and it would not be desirable to preempt any data flow for frame sync purposes. The TM and MSS frame sync cannot be used directly until the two data streams are separated.

Figure 3.2-13 shows the ground processing equipment for the separation of the two data streams. This separation can be done equally well in hardware or in software. The approach takes advantage of the fact that there are only nine combinations of MSS data bit location and each can be tried until frame sync or preamble recognization is obtained in either or both of the Mapper and MSS data channels.

Interactive Failures. The failure of one instrument produces no interactive failure on the other instrument. The TDRSS link modulator can be designed to switch from the time multiplexed data stream to direct output of either instrument. The addition of the extra data multiplexer introduces an extra series failure element to the TDRSS data flow. To prevent single failure from disabling this data link, dual data multiplexers will be required. This dual redundancy approach for the multiplexer and the clock supplied to the MSS and TM will prevent failures from disabling the link.

Advantages/Disadvantages. The advantage of this approach is to minimize the impact on the TM as well as the MSS instruments by performing the data multiplexing external to either instrument. The disadvantages are the requirement of the additional hardware and the trail and error approach to the data separation in the ground processing.

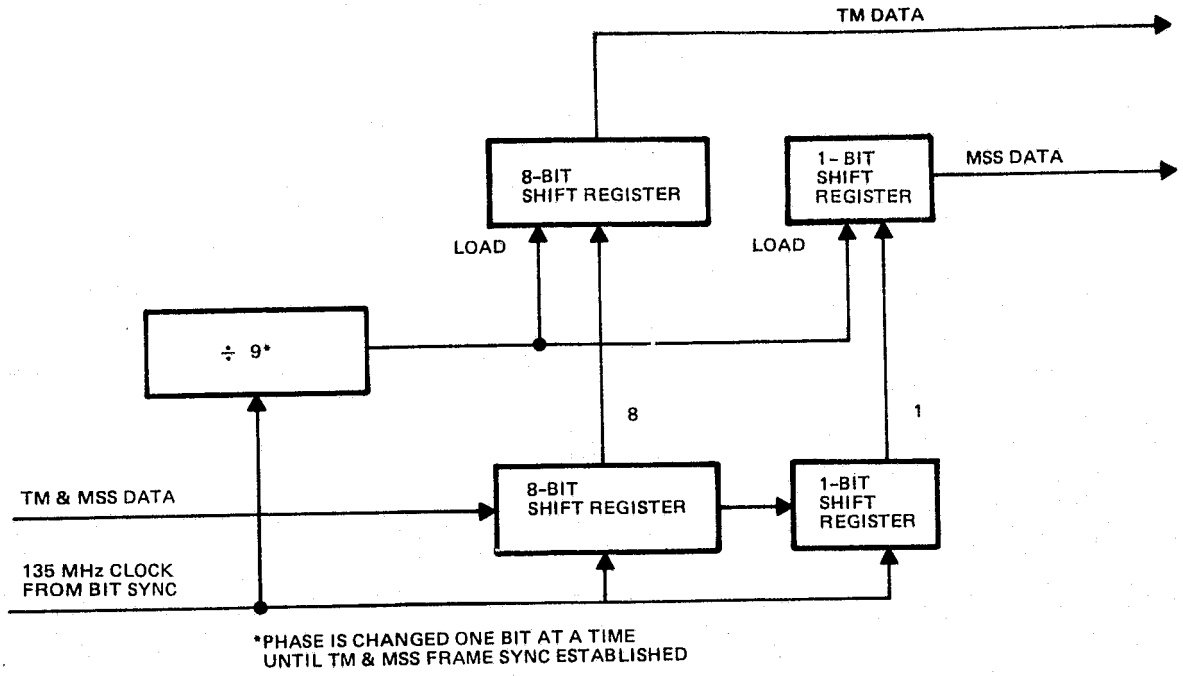

Figure 3.2-13. Ground Processing Approach for a TM/MSS Data Multiplexer (Separate Box)

Approach Comparison and Recommendations

Table 3.2-1 summarizes the three digital time multiplexing approaches, the impact on the MSS and TM instrument modules, the spacecraft, and the ground processing, the suggested approach to protect the system from a single failure which could result in a loss of the instrument data, the advantages and disadvantages, and the relative cost. All of the approaches are viable candidates.

Approach A is recommended since it introduces minimum hardware and changes to the two instruments and spacecraft systems and provides the simplest electrical interfaces when all systems are considered together; however, Approach B would be recommended if it was desirable to minimize the impact and changes to the MSS instrument. Approach C would be recommended if it was desirable to minimize the impact to both instruments at the cost of increasing the spacecraft complexity.

3.2.2 Unbalanced QPSK

The basic RF modulation technique employed by the user TDRSS KSA return link is QPSK. QPSK modulation offers the unique capability of transmitting two independent data channels over one single RF link. It also offers the capability of reducing the RF bandwidth requirements by one-half over BPSK modulation for a single data stream. Furthermore, since the data channel rates are unequal, optimum link performance, assuming equal bit error performance, can be achieved by partitioning the total transmit power for the two channels according to the ratio of the channel data rates. For example, the two independent data channel data rates for TM and MSS are 120 Mbps and

Table 3.2-1. Summary of Time Multiplexing Approaches

APPROACH	DESCRIPTION	IMPACT				FAILURE PROTECTION APPROACH	ADVANTAGES	DISADVANTAGES	RELATIVE COST
		MSS	TM	SPACECRAFT	GROUND				
A	• MULTIPLEXING OF TM & MSS PERFORMED IN TM • MSS OPERATED IN SYNCHRONISM WITH TM	• OPERATES ON TM SUPPLIED CLOCK	• COMBINES MSS DATA WITH TM SENSOR DATA • SUPPLIES DATA RATE CLOCK TO MSS • OUTPUT DATA RATE INCREASE FROM 120 TO 135 MBPS	• HARDWARE - NONE • DATA CHANNELS TDRS = 135 MBPS STDN - Ku-BAND = 135 MBPS; HOWEVER 0.5 dB LOSS DUE TO INCREASE DATA RATE OVER 120 MBPS	• SEPARATES MSS DATA FROM TM DATA BY USE OF TM FRAME SYNCH	• MSS SWITCHED OR DESIGNED TO FREE RUN ON LOSS OF TM SUPPLIED CLOCK • MSS DATA SWITCHED TO BYPASS TM AND CONNECTED TO MODULATOR IF TM FAILS	• TOTAL SPACECRAFT DATA SYSTEM IS SYNCHRONIZED • NO FILLER WORDS IN TELEMETRY • NO ADDITIONAL BOXES	• MSS REQUIRES A EXTERNAL CLOCK CAPABILITY • STDN/DIRECT ACCESS DATE RATE 135 MBPS REDUCES LINK MARGIN BY 0.5 dB	MINIMUM
B	• MULTIPLEXING OF TM & MSS PERFORMED IN TM • MSS OPERATED ASYNCHRONOUS TO TM	• MSS REQUIRED TO OPERATE AT A FREQUENCY SOME WHAT LOWER THAN TM DATA ACCEPT RATE	• COMBINES MSS DATA WITH TM SENSOR DATA • SYNCHRONIZES MSS DATA TO THE TM OUTPUT DATA STREAM	• SAME AS ABOVE	• SEPARATES MSS DATA FROM TM DATA BY USE OF TM FRAME SYNCH • REQUIRES SOME FILLER WORDS THAT ARE CODED ALL ZERO	• MSS DATA SWITCHED TO BYPASS TM AND CONNECT TO MODULATOR IF TM FAILS	• NO CHANGES OR IMPACT ON MSS • NO ADDITIONAL BOXES	• FILLER TELEMETRY WORDS MUST BE EXTRACTED IN GROUND PROCESSING • STDN/DIRECT ACCESS DATA RATE 135 MBPS REDUCES LINK MARGIN BY 0.5 dB • ADDITIONAL HARDWARE FOR TM	MEDIUM
C	• MULTIPLEXING PERFORMED IN A SEPARATE BOX • MSS, TM, AND MULTIPLEXER OPERATED IN SYCHRONISM	• OPERATES ON MULTIPLEXER SUPPLIED CLOCK	• TM OPERATES ON EXTERNAL CLOCK	• HARDWARE ADDITIONAL MULTIPLEXER BOX DATA CHANNELS TDRS = 135 MBPS STDN = Ku-BAND 120 MBPS	• SEPARATES MSS AND TM BY THE APPROACH OF 8 BITS FOR TM, 1 BIT MSS, 8 BITS FOR TM ETC. • CHANGES PHASE OF BIT SELECTION UNTIL FRAME SYNC ESTABLISHED	• REQUIRES A REDUNDANT MULTIPLEXER	• TOTAL SPACECRAFT DATA SYSTEM IS SYNCHRONIZED • MINIMAL IMPACT ON BOTH MSS AND TM	• ADDITIONAL BOX • TRIAL AND ERROR APPROACH TO DEMUX MSS DATA FROM TM DATA	HIGHEST

15 Mbps, respectively. The ratio of the data rates is 8; therefore, for optimum link design, 87.5% of the total transmitted power would be allocated to TM and 12.5% to MSS. Since the TDRSS interface requirements state that a maximum of 4:1 power split can be used in the unbalanced QPSK KSA return link, the link design allocates 80% of the total transmit power to TM and 20% of the total transmit power to MSS.

A functional diagram of the TDRSS KSA return link transmit channel is shown in Figure 3.2-14. The transmit channel consists of an RF interface unit, UQPSK modulator, power amplifier, and high gain antenna. The RF interface unit controls, via ground commands, the input data streams that are fed to the UQPSK modulator. In the normal mode of operation, TM data is routed to the modulator's I-channel input and the MSS data is routed to the modulator's Q-channel input. Should TM or MSS fail or either instrument be turned off, the nonfailed or active instrument data stream can be fed into both the I and Q channels of the modulator.

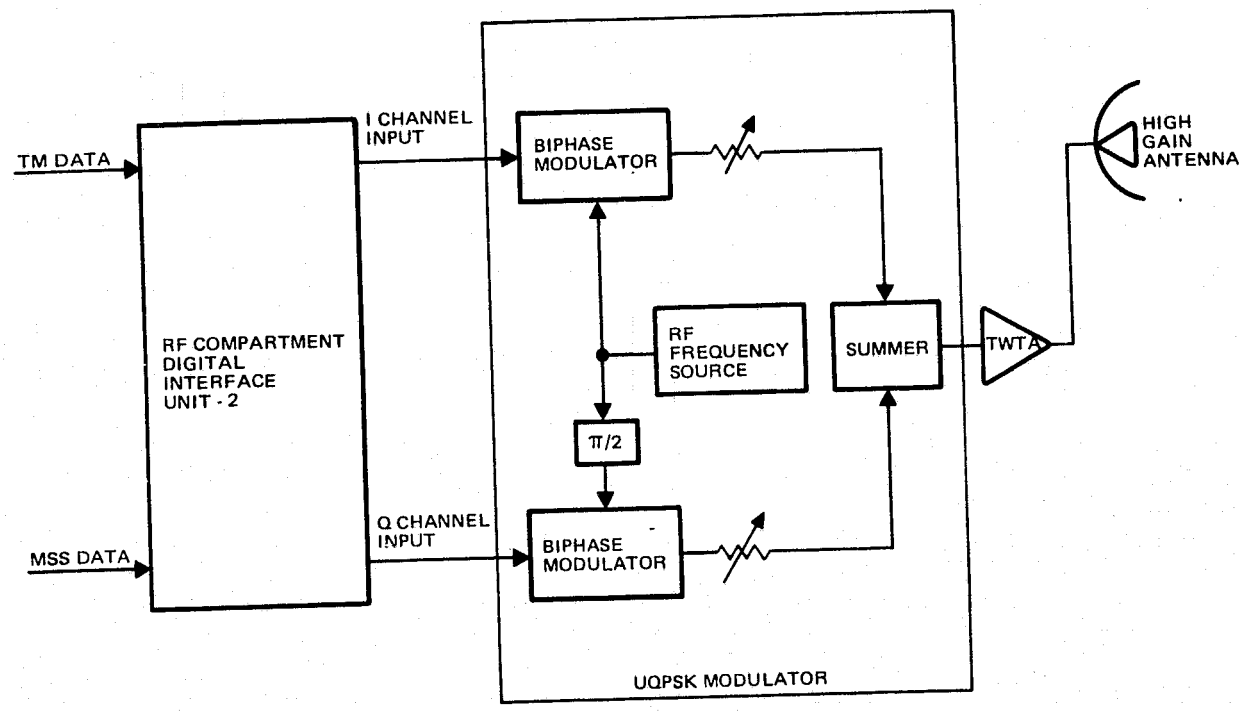

Figure 3.2-14. TDRSS KSA Transmitter

The UQPSK modulator consists of two independent biphase modulators whose reference RF carrier signals are made orthogonal to each other. The modulator I and Q-channels are adjusted by the series attenuators for a 4:1 power split. The output of the attenuators are summed to form the UQPSK modulated signal. The signal is amplified by the TWT and transmitted through the TDRSS link high gain antenna.

Figure 3.2-15 shows a functional diagram of the selected (Approach 1) RF compartment interface unit and the mode configuration control. The I_1 and Q_1 inputs are the normal operating modulator inputs. The I_2 and Q_2 inputs are routed to the redundant UQPSK modulator. Approach 1 also offers complete use of the total EIRP when identical data (TM or MSS) is fed to the modulator.

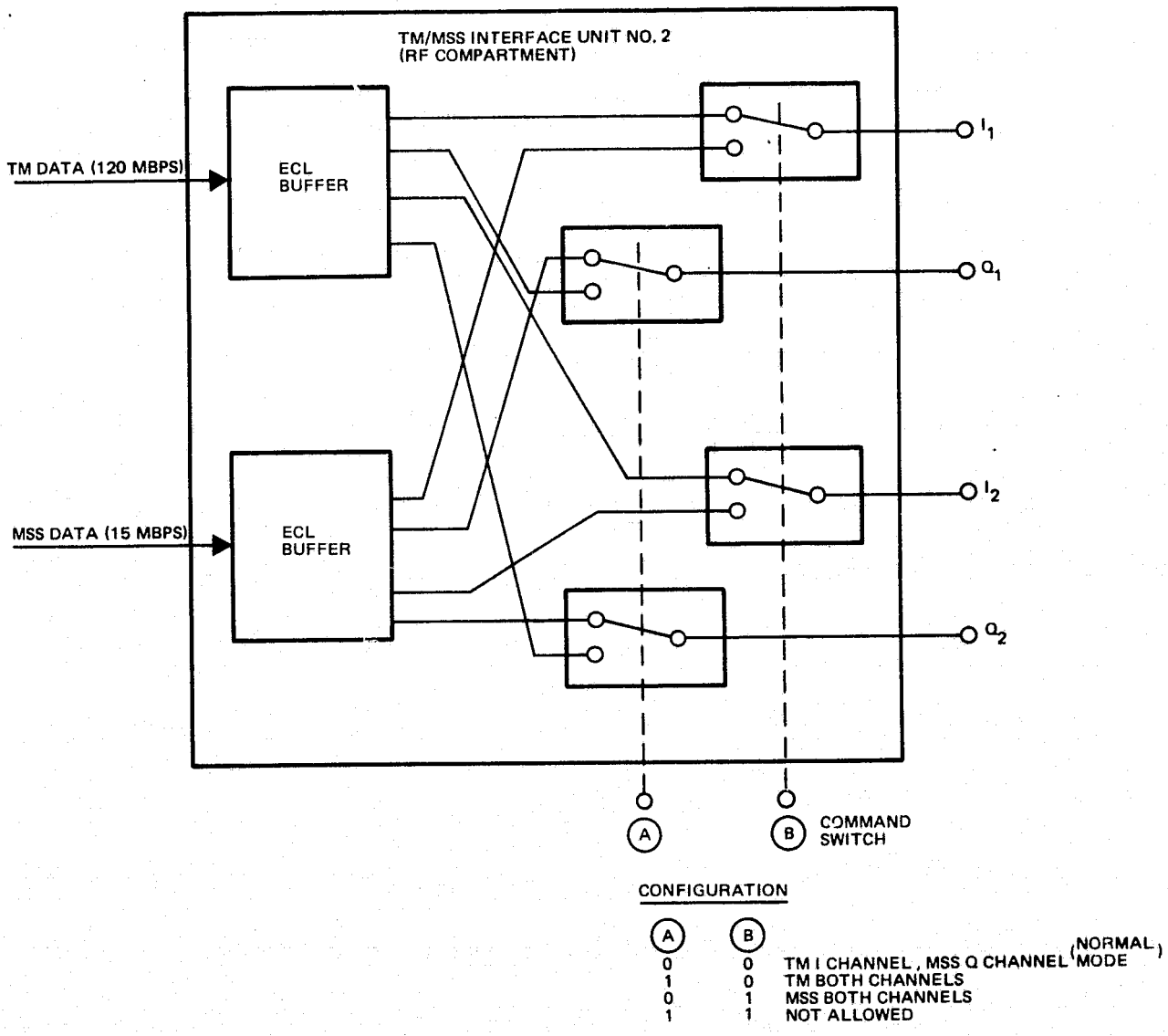

Figure 3.2-15. RF Compartment Digital Interface Unit Functional Block Diagram for Approach 1

An alternative RF interface unit is shown in Figure 3.2-16. This approach does not have the configuration mode capability-control the first approach has. Should an instrument fail or be turned off, canonical forms of biphase are transmitted as

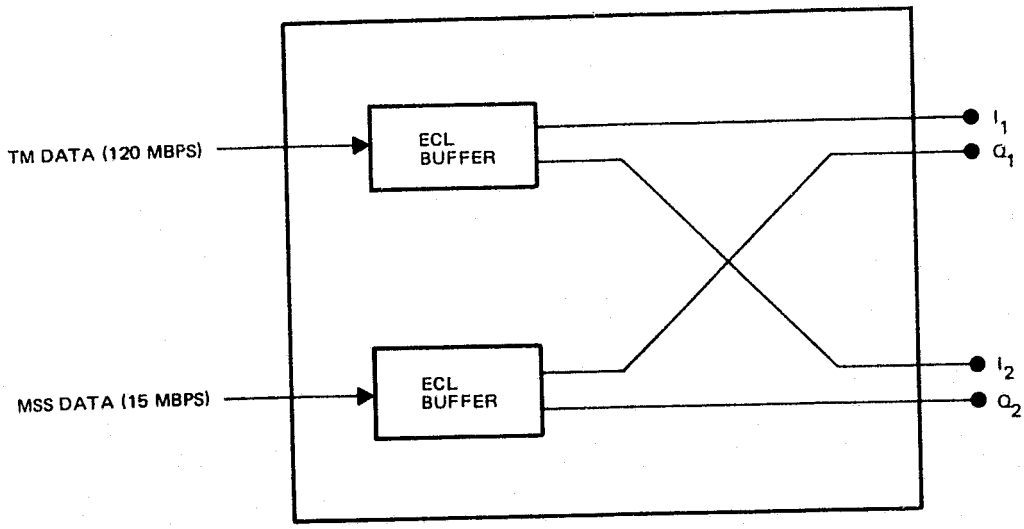

Figure 3.2-16. RF Compartment Digital Interface Unit Functional Block Diagram for Approach 2

depicted in Figures 3.2-17c and d. Figures 3.2-17b, e, and f are the signal vector space phase diagrams for Approach 1. Figure 3.2-17a depicts the signal vector space phase diagram for balanced QPSK where 00, 10, 11, and 01 are the corresponding I and Q data inputs, and 0, $\pi/2$, π, and $3\pi/2$ are the phase angles. If the TM instrument is turned off or fails while MSS is being transmitted, an unmodulated I-channel carrier is transmitted along with the MSS biphase modulated Q-channel carrier. The unmodulated carrier will produce undesirable power flux density levels when the TDRSS return signal is transmitted via a path that grazes the earth. If the reverse condition occurs, i.e., the MSS is turned off or fails while TM data is transmitted, the same undesirable flux density level condition occurs as described for the MSS on, TM off. It is concluded that Approach 2 is not desirable for failure to meet instrument failed conditions or conditions in which one instrument is turned off. The routing control circuits for either approach are not difficult to implement. Logic circuits are recommended for the routing control. Details are given in a later section.

3.2.3 Potential Interference with STDN/Direct Access Link

This section establishes that the STDN/direct access link should not operate in the same band as that occupied by the TDRSS link since sidelobe radiation from the LF/O steerable dish will cause interference in the STDN/direct access ground stations. The only alternate band (within the present TDRSS frequency plan) suitable for the STDN/direct access link is directly adjacent to the TDRSS return link band. Even with nonoverlapping bands, a potential for interference exists since the TDRSS link TWT, operating in saturation, will regenerate to some degree the $(\sin x/x)^2$ spectrum which is essentially removed at the input to the TWT by filter truncation. Hence a filter must be placed at the output of the TWT to attenuate the spectrum sidelobes falling into the STDN/direct access band. The amount of separation of the two bands (larger separation provides a larger filter guard band) is determined by the type of

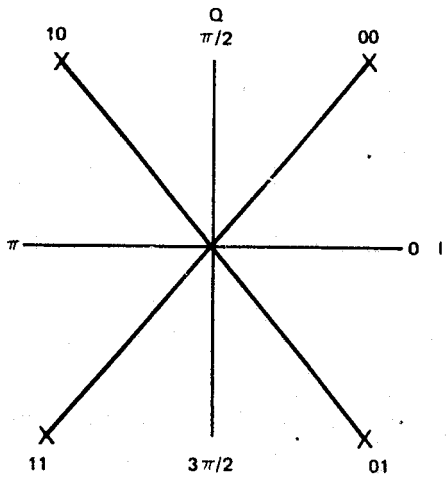

(A) BALANCED QPSK

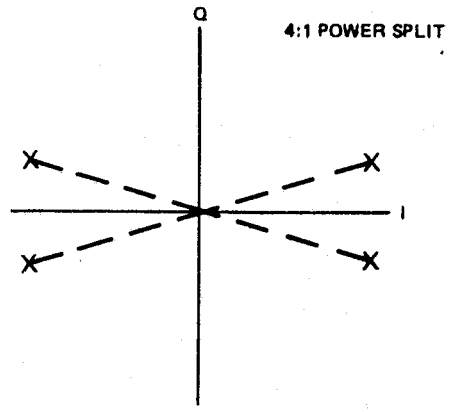

(B) UNBALANCED QPSK: 80% TM, 20% MSS

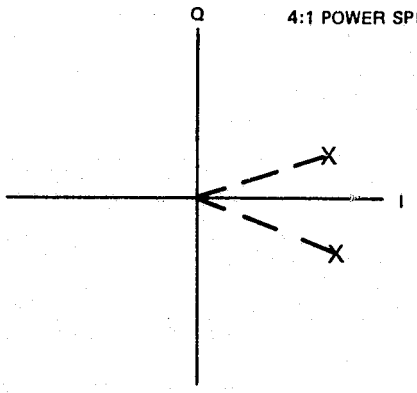

(C) UNBALANCED QPSK: 20% MSS, 80% TM (NO DATA)

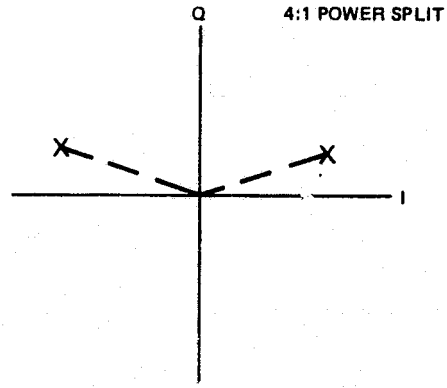

(D) UNBALANCED QPSK: 20% MSS (NO DATA), 80% TM

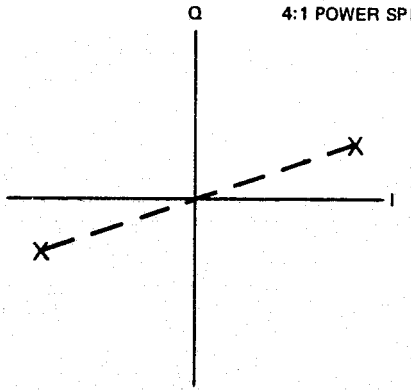

(E) UNBALANCED QPSK: IDENTICAL DATA 80% MSS 20% MSS

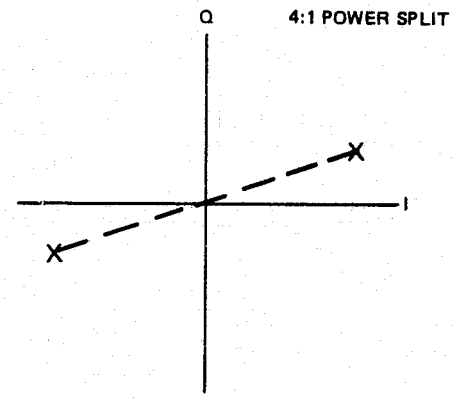

(F) UNBALANCED QPSK: IDENTICAL DATA 80% TM, 20% TM

Figure 3.2-17. Signal Vector Space for Approaches 1 and 2

modulation utilized. If both links utilize balanced QPSK modulation, the largest guard band is provided. If only the STDN/direct access link utilizes QPSK, the guard band is less. In order to utilize balanced QPSK on the TDRSS link, the TM and MSS data must be time multiplexed. This section evaluates the amount of transmit filtering required if the TDRSS link utilizes unbalanced QPSK (spectrum "sidelobes" approximately the same density as for 120 Mbps biphase modulation) in place of time multiplexed balanced QPSK. The results indicate that only modest filter attenuation is required. Hence it may be concluded that time multiplexing the TM and MSS data is not essential.

Interference When Both Links Occupy the Same Band

The STDN/direct access and TDRSS links were originally assumed to operate in the same 15 GHz band. This band (14.896 GHz to 15.121 GHz) is designated in the TDRSS User's Guide for KSA user return link. It was recognized, however, that serious degradation of the STDN/direct access link could result if sidelobe signal energy from the LF/O steerable dish antenna (TDRSS link) impinged with sufficient strength on the STDN/direct access stations. An assessment of expected antenna sidelobe levels verifies that interference results if both links operate in the same band.

The following is sufficient to demonstrate the problem. Consider the interfering TDRSS link signal to be noiselike and uniformly spread across the STDN/direct access bandwidth. Actually, the interfering signal would be coherent since the carrier frequency difference between the two links would be much less than the 120 Mbps TM bit rate present on both links.

The nominal carrier-to-noise spectral density ratio per bit rate bandwidth present in the ground station without interference is

$$C_D L/N_o\ B = 15.6\ \text{dB}\ (\text{required } E_b/N_o \text{ for } 10^{-5}\ \text{BER (12.6 dB + 3 dB margin)})$$

where

C_D = STDN/direct access link EIRP = +16.6 dBW (see Section 4.5.2)

L = space loss

The carrier-to-noise ratio with interference is

$$\frac{C_D L}{N_o B + C_T L X}$$

where

C_T = TDRSS link EIRP on boresight = +57.8 dBW (see Section 3.11.3)

X = sidelobe level in direction to ground station

For 0.1 dB degradation in ground station carrier-to-noise it is required that

$$\frac{N_o B}{C_T L X} = 16.3 \text{ dB}$$

Hence

$$\frac{C_D L}{C_T L X} = \frac{C_D}{C_T X} = 15.6 + 16.3 = 31.9 \text{ dB}$$

Note that both links experience the same nominal space loss, L. The required value of sidelobe level, X, for 0.1 dB degradation is

$$X(\text{dB}) = 31.9 + C_T - C_D$$

$$= 31.9 + 57.8 - 16.6 = 73.1 \text{ dB} \quad .$$

The required sidelobe level of approximately 73 dB is not realizable in a high aperture efficiency parabolic antenna. Radiation patterns of similar existing Ku-band antennas have been measured to verify this over a wide range of angles (see Section 3.7.3).

Selection of Alternate Band for the STDN/Direct Access Link

It is clear from the foregoing that the STDN/direct access link should operate within a nonoverlapping band separated from the TDRSS KSA return link band so as to minimize interference. Furthermore, the STDN/direct access frequency is contained (ground rule) to be within the TDRSS frequency plan. A review of the present TDRSS frequency plan as defined in the TDRSS User's Guide (see Figures 3.2-18 and 3.2-19) shows that the STDN/direct access link can be placed in the 14.6 to 14.87 GHz region (bands 5, 6, 7 region) or the 15.15 to 15.25 GHz region (band 9) without causing inter-

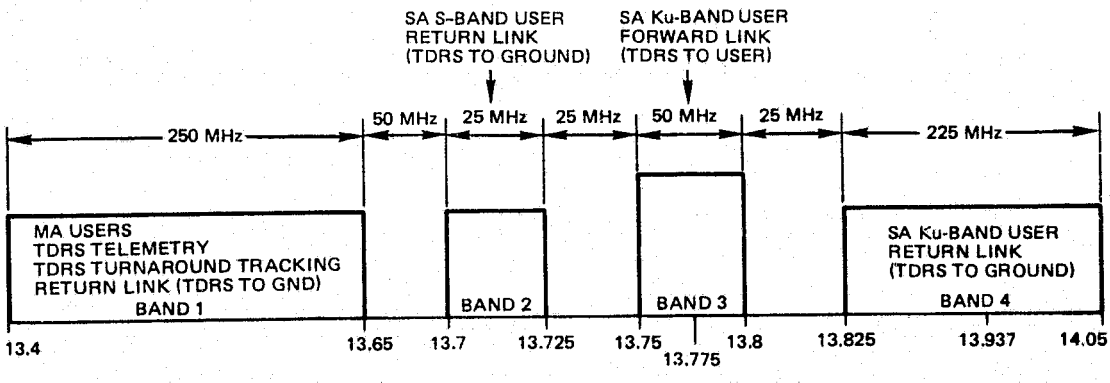

Figure 3.2-18. TDRSS Ku-Band Transmit Frequency Plan

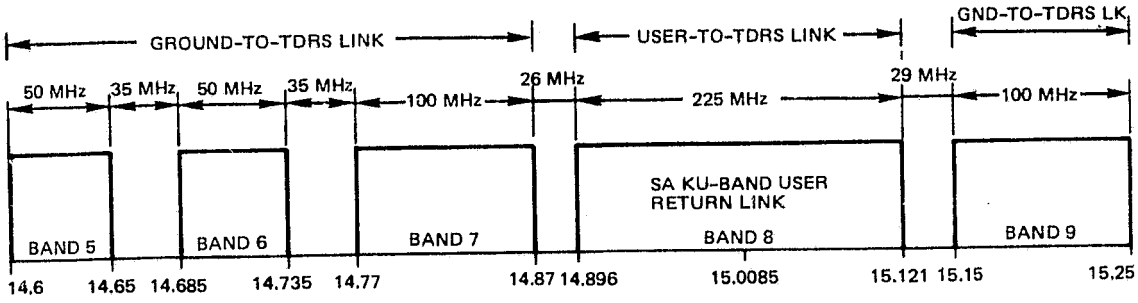

Figure 3.2-19. TDRSS Ku-Band Receiver Frequency Plan

ference with the TDRSS since these regions are allocated to TDRSS ground station transmission. However, band 9 is not preferred because of (1) higher sensitivity to weather conditions compared to the band 5, 6, and 7 region and (2) the relatively small guard band (29 MHz) from the upper edge of band 8. All TDRSS ground station receive bands (bands 1, 2, 4) are vulnerable to interference if the STDN/direct access link frequency is within these bands.

The selected frequency plan is given in Figure 3.2-20. The TDRSS link spectrum is centered in the allocated band and is assumed to occupy a bandwidth of 240 MHz, which is the main lobe bandwidth of the 120 Mbps TM data portion of the composite unbalanced QPSK signal. The STDN/direct access spectrum occupies a bandwidth of 120 MHz, which is the main lobe bandwidth of the 120 Mbps balanced QPSK signal.

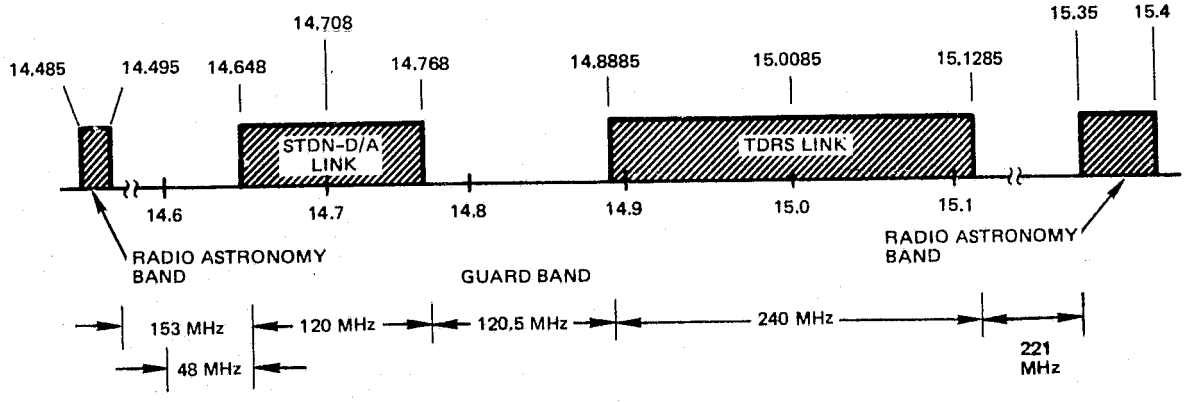

Figure 3.2-20. Selected Frequency Plan

The lower edge of the STDN/direct access band has been selected to be 48 MHz above the lower band edge of the TDRSS frequency allocation. This frequency selection simplifies the implementation of the local oscillator frequency source (see Section 3.3.2) at the expense of a reduced guard band between the two spectrums. However, as will be shown, the TDRSS link transmit filter requirement is not severe with a 120.5 MHz guard band. Of greater importance is the selection of balanced QPSK rather than biphase modulation for the STDN/direct access link. Use of biphase modulation would double the occupied bandwidth and reduce the guard band to about 48 MHz (assuming the first null of the STDN/direct access spectrum were placed at the allocated 14.6 GHz band edge).

Also shown in Figure 3.2-20 are the closest adjacent radio astronomy bands. Possible interference with these bands by the TDRSS link has also been evaluated (Section 3.2.4).

Interference Evaluation Utilizing an Alternate Frequency Band for the STDN/Direct Access Link

The worst case geometry for antenna sidelobe interference occurs when the LF/O steerable dish boresight approaches the earth grazing angle and the angle between the dish boresight and the direction to a ground station is minimum. This bounding situation is shown in Figure 3.2-21. The assumed ground station is located at the maximum coverage clear weather location determined by the LF/O STDN/direct access shaped beam coverage pattern and the associated link budget (see Sections 4.4 and 4.5). As shown, the sidelobe level approximately 3.4° off boresight will radiate towards the ground station. The envelope of sidelobes at this angle is approximately 31 dB below the peak gain (see Section 3.7.3). For all other boresight angles, the sidelobe level will be less. Note that polarization behaviour in the sidelobe region is unpredictable and varies greatly over small angles. Thus the use of orthogonal polarization between the STDN/direct access and TDRSS links will not result in appreciable rejection at the ground station.

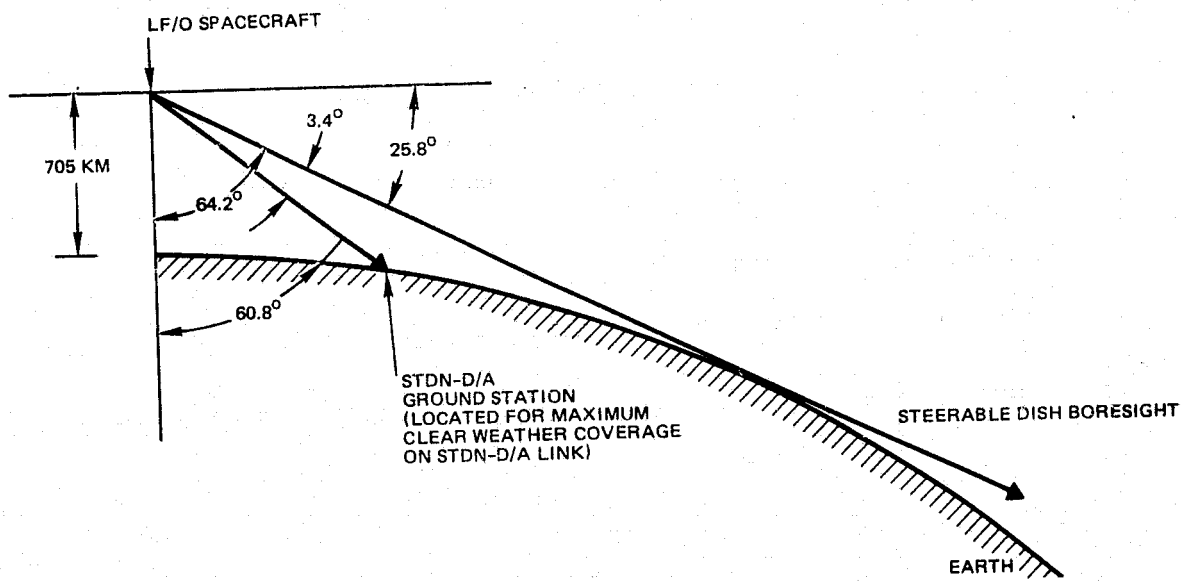

Figure 3.2-21. Worst Case Geometry for Sidelobe Level Determination

The second aspect of the interference evaluation is determination of the spectrum sidelobe amplitude of the TDRSS link signal falling into the STDN/direct access band as a result of spectrum regeneration in the TWT. If staggered QPSK were utilized for the TDRSS link, essentially no spectrum regeneration would occur. However, this modulation technique cannot be utilized without prior time multiplexing of the TM and MSS data streams. For unbalanced QPSK and biphase modulation, spectrum regeneration will occur. However, a TWT is not a true hard limiter, and the regenerated spectrum amplitude will be less than the $(\sin x/x)^2$ regeneration produced by an ideal hard limiter.

A TRW computer simulation program was utilized to determine the magnitude of regenerated spectra in a typical TWT operating at saturation. The program assumes a 5-pole Chebycheff filter with a matched bandwidth of 240 MHz at the TWT input. There are three possible modulation modes for the TDRSS link:

- Unbalanced QPSK modulation combining the 120 Mbps TM data and the 15 Mbps MSS data with a 4:1 power ratio
- TM data only – biphase (±90°) modulation
- MSS data only – biphase (±90°) modulation

The present simulation program does not accommodate unbalanced QPSK modulation. However, since the composite signal comprises a linear addition of the spectrum of a 120 Mbps biphase modulated signal and a 15 Mbps biphase modulated signal, it is reasonable to consider, separately, the spectrum regeneration for TM and MSS biphase modulation.

Note that the TWT input filter (240 MHz bandwidth) truncates the 15 Mbps MSS spectrum at about the 9th sidelobes, corresponding to the first nulls of the 120 Mbps TM spectrum (Figure 3.2-22b). If filtering is done directly at the outputs of the biphase modulators prior to summation (to allow first null filtering of the 15 Mbps spectrum, Figure 3.2-22a) rather than at the output of the summer, a possible phase matching problem occurs in maintaining a precise quadrature phase relationship between the two biphase modulation outputs.

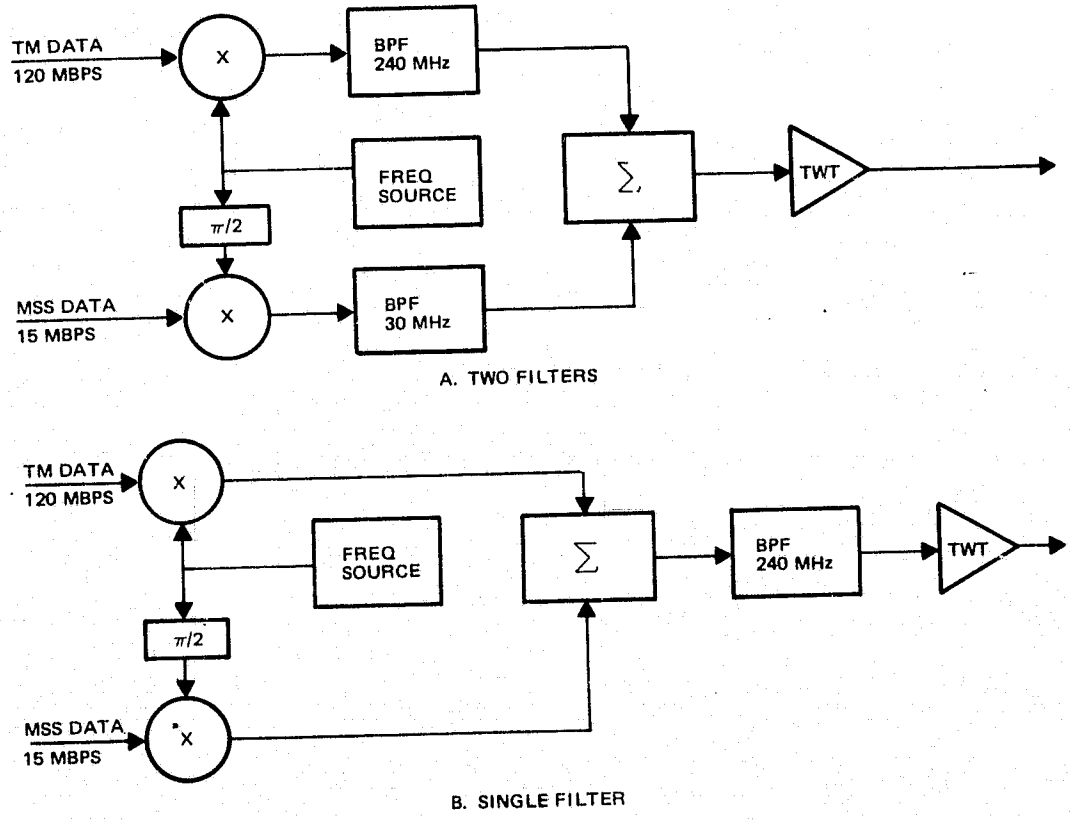

Figure 3.2-22. Input Filter Location

The results of the computer simulation are summarized in Figure 3.2-23. The MSS peak noise density, ϕ_M, is given by

$$\phi_M(dB) = ERP - B = -14.0 \text{ dBW/Hz}$$

where

ERP $\approx$ 57.8 dBW

B = 71.8 dB·Hz (15 Mbps)

The TM peak noise density, ϕ_T, is 9 dB less since the bit rate is 9 dB higher. The figure shows that the TM spectrum lobe amplitudes are larger than the MSS lobe amplitudes over the frequency range of interest. Hence, the absence of a truncation filter for the MSS spectrum does not significantly affect TWT output filter requirements.

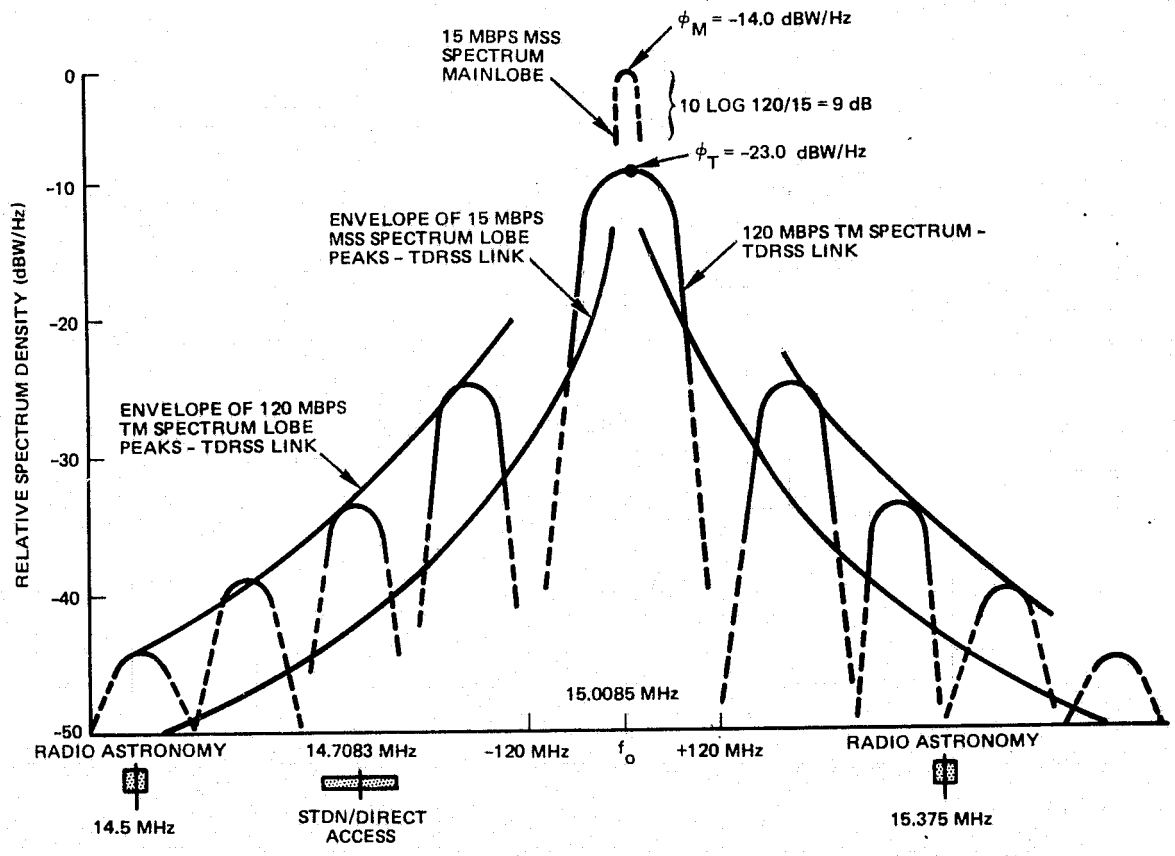

Figure 3.2-23. Spectra Magnitudes (Computer Simulation)

It was shown earlier that the required antenna sidelobe level, X, when both links occupy the same band is

$$X(dB) = 31.9 + C_T - C_D$$

For the case of nonoverlapping bands, the above relationship becomes

$$X(dB) = 31.9 + C_T - C_D - \alpha_1 - S_1$$

or

$$\alpha_1(dB) = 31.9 + C_T - C_D - X - S_1$$

where

α_1 = required output filter attenuation in STDN/direct access band

C_T = TDRSS link EIRP on boresight = +57.8 dBW

C_D = STDN/direct access link EIRP = +16.6 dBW (see Section 4.5.2)

X = worst case antenna sidelobe level $\approx$ 31 dB (see Section 3.7.3)

S_1 = relative amplitude of second TDRSS spectrum sidelobe $\approx$ 24 dB (see Figure 3.2-23).

The required filter attenuation in the STDN/direct access band is thus

$$\alpha_1 \approx 31.9 + 57.8 - 16.6 - 31 - 24$$
$$\approx 18.1 \text{ dB}$$

An additional 5-dB attenuation margin is assumed in order to account, conservatively, for uncertainties in antenna sidelobe estimation and computer simulation of spectrum sidelobe amplitudes. A 5-pole waveguide filter with the following characteristics provides the required 23 dB attenuation (see Section 3.6.1 for discussion of filter design):

TE101 rectangular waveguide (WR-62)

Chebyshev - 0.01 dB ripple

Q_u = 3900

N = 5

Matched bandwidth = 240 MHz

Passband insertion loss = 0.7 dB

3.2.4 Potential Interference with Radio Astronomy Bands

Figure 3.2-20 shows the location of the nearest adjacent radio astronomy bands. The maximum acceptable levels of interference (the threshold above which interference is considered harmful) as currently defined by the CCIR (ref. 8) are

14.5 GHz band	-219 dBW/m^2/Hz
15.375 GHz band	-232 dBW/m^2/Hz

These levels are relative to an isotropic receive antenna and are based on a 2000 second integration time with a continuous interfering source. The CCIR document requires that the allowable interfering signal must be reduced by an amount equal to the radio telescope antenna gain above the isotropic reference level. Obviously, radio astronomy antenna gains are very large, thereby imposing a severe requirement on allowable interference levels. The 100 meter radio telescope at Effelsberg, Germany (ref. 9) for example, has a gain of about 78 dB at 15 GHz. In this case, the allowable interference levels (telescope aimed at the interfering source) would be

14.5 GHz band	-297 $dBW/m^2/Hz$
15.375 GHz band	-310 $dBW/m^2/Hz$

The approximate worse case level of interference from the TDRSS link antenna sidelobes into the 15.375 GHz astronomy band is given by

$$\phi_i(dB) \approx \phi_T - S_2 - X - \alpha_2 - 10 \log (4\pi R^2)$$

where

ϕ_i = interfering signal at radio telescope ($dBW/m^2/Hz$)

ϕ_T = TDRSS link peak spectrum density, $\approx$ -23 dBW/Hz

S_2 = relative amplitude of spectrum at 15.375 GHz $\approx$ 27 dB (see Figure 3.2-23)

X = worst case antenna sidelobe level $\approx$ 31 dB (see Section 3.7.3)

α_2 = attenuation of 5 pole transmit filter in 15.375 GHz band $\approx$ 40 dB

R = 1890 km (slant range corresponding to worst case TDRSS link antenna sidelobe level)

Hence

$$\phi_i \approx -23 - 27 - 31 - 40 - 136.5 \approx -257.5 \ dBW/m^2/Hz$$

The interference level is seen to be well below the allowable levels relative to an isotropic antenna, but in excess of the levels obtained by reducing allowable interference an amount equal to the telescope main beam gain. However, a discussion with W.E. Howard III of the National Radio Astronomy Observatory, Green Bank, West Virginia indicated that revised interference criteria are being recommended. The new criteria are essentially the same as the current CCIR levels with reference to an isotropic receive antenna, but eliminate the requirement to reduce the interference level an amount equal to the main beam gain. He felt this to be a more realistic and reasonable requirement.

A different aspect of allowable interference discussed in the CCIR reference is the reduction in interference effect when the interference exists for only a fraction of the 2000 second integration time assumed in deriving the allowable interfering levels. The LF/O spacecraft would traverse a radio telescope main beam in a very short period of time. The spacecraft orbital angular velocity (705 km (380 nmi) altitude) is 0.06° per second. For an earth surface observer, the angular velocity is roughly 10 times greater (ratio of earth radius to spacecraft altitude) or ≈ 0.6° per second. In the case of the Effelsberg telescope, for example, the beamwidth is approximately 0.02°. Hence the main-beam dwell time is roughly 0.02/0.6 ≈ 1/30 second. If the radio astronomy data processing is an integration process as indicated in the CCIR reference, then the reduction in interference effect would be the ratio of interference time to integration time, or for the case of the Effelsberg telescope

$$10 \log 1/30 \times 1/2000 \approx -48 \text{ dB}$$

It is our preliminary conclusion that radio astronomy interference is not a problem for the proposed TDRSS link design. In any event, it would be a simple matter to add appropriate bandstop filtering if more detailed studies indicated such a need.

3.2.5 Recommended Method for Combining TM and MSS Data

Several factors influence the recommended choice of method for combining TM and MSS data. These include feasibility of the method, the impact on other spacecraft subsystems and ground systems, the magnitude of RF interference with the Ku-band STDN/direct access link signal caused by the Ku-band TDRSS return link signal, the associated filter requirements of the TDRSS return link and STDN/direct access link channels to minimize this interference, and the relative cost and complexity.

Both methods were found to be feasible; however, based on the time multiplex and UQPSK comparison summarized in Table 3.2-2, the UQPSK method is recommended for its minimum spacecraft and ground station impact and lower cost and complexity.

Table 3.2-2. Time Multiplex and UQPSK Comparison

Factors	Time Multiplex	UQPSK
Feasibility	Approach described in Section 3.2.1. Time multiplexing Approach A selected for comparison.	Approach described in Section 3.2.2
Impact		
Spacecraft	Instruments: TM designed to combine MSS data with TM data. MSS data clock synchronized to TM individual color band 15 MHz data clock (minor modification to MSS instrument).	No impact
RF digital interface	Slightly more complex configuration for generation of two independent data streams from single data stream for bandwidth compression.	No impact
TDRSS link modulator/ transmitter	Balanced QPSK can be used. No modification to existing QPSK hardware. Identical transmitter requirements.	Minor modification to existing QPSK hardware for UQPSK modulation. Identical transmitter requirements.
TRDSS transmit RF filter requirements for minimizing RF interference on the STDN/ direct access link	Slightly less filtering required than for the UQPSK approach.	Feasible requirements.
Ground	Additional time demultiplexing for MSS and TM separation. Not presently included in TDRSS ground station capability.	No MSS/TM time demultiplexing required.
Link performance	Optimized TM and MSS performance for the TDRSS link; however, 0.5 dB loss in Ku-band STDN/direct access link because of 135 Mbps rate.	Suboptimum TM and MSS performance due to maximum TDRSS 4:1 power split requirement; i.e., MSS margin greater than TM margin for same transmitter power.
Cost and complexity	Slightly higher overall (both spacecraft and ground).	Less overall (both spacecraft and ground).

3.3 TRANSMITTER DESIGN

The LF/O transmitter, operating at 15.0085 GHz, transmits both TM and MSS data in an unbalanced quadriphase-shift-keyed (UQPSK) modulation format. Since waveguide cannot be utilized along the deployment mast, the transmitter is located in the RF compartment.

3.3.1 Transmitter Configuration

The TDRSS link transmitter modulated the baseband digital information received from RF interface unit No. 1 onto a 15.0085 GHz carrier. The transmitter consists of an unbalanced quadriphase shift-keyed modulator and a 20-watt TWTA to provide sufficient EIRP for the TDRSS link. Since waveguide cannot be utilized along the deployable mast, the transmitter cannot be located in the wideband module. Location in the RF compartment necessitates the minimization of size and weight.

UQPSK modulation was selected for the TDRSS link on the basis of the tradeoffs presented in Section 3.2. UQPSK modulation allows a fixed carrier power to be divided between two unequal independent bit rate channels (TM and MSS). Figure 3.3-1 shows a block diagram of the basic modulator. The modulator consists of a phase amplitude equalizer (PAE), a 6 dB attenuator (for 4:1 power split), two biphase switches, a quadrature combiner, and two driver amplifiers. The PAE divides the input carrier into two paths containing phase and amplitude adjustments. The biphase switches produce 0 or 180° phase shifts, depending on the polarity of the baseband drive signal. Two driver amplifiers provide the high speed current switching to the biphase switches corresponding to the input logic state. After biphase switching, a quadrature combiner sums the two channels in a 90° relationship to produce the composite quadriphase signal.

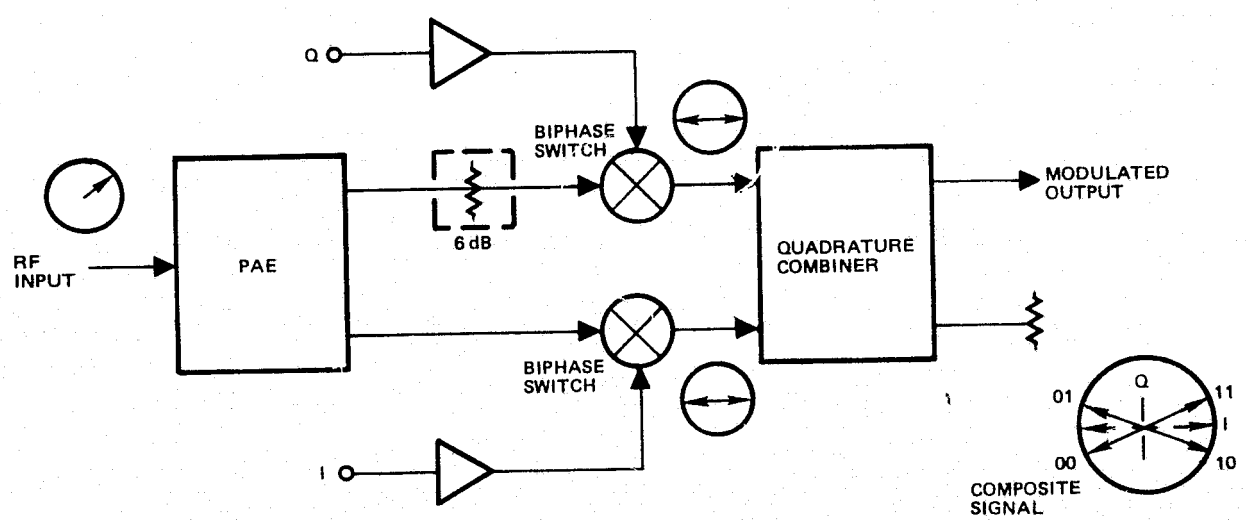

Figure 3.3-1. UQPSK Modulator

Figure 3.3-1 also shows the relative phase of the RF signal at selected locations within the modulator. Any differences in path length leading to each biphase switch are balanced by the PAE so that two signals differing in amplitude by 6 dB and phase by 0 or 180° are applied to the combiner inputs.

A basic tradeoff was made between direct and indirect modulation. Direct modulation impresses the digital information directly at the desired carrier frequency. The indirect approach involves upconversion of a previously modulated, lower frequency signal. For the TDRSS link transmitter, the choice is between direct modulation at Ku-band or upconversion from S-band (3 GHz) (Figures 3.3-2 and 3.3-3). TRW has used both approaches on qualified space programs. Figure 3.3-4 shows a Ku-band modulator developed for one of these programs. Currently, a microwave integrated circuit (MIC) version of this modulator is being developed on a TRW IR&D program (Figure 3.3-5). This unit is used in the configuration tradeoffs which follow.

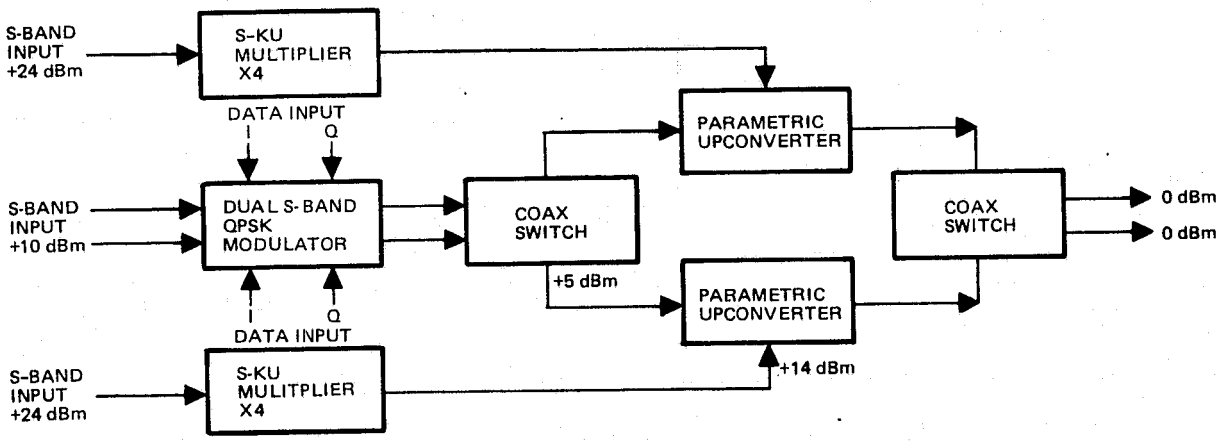

Figure 3.3-2. Indirect Approach

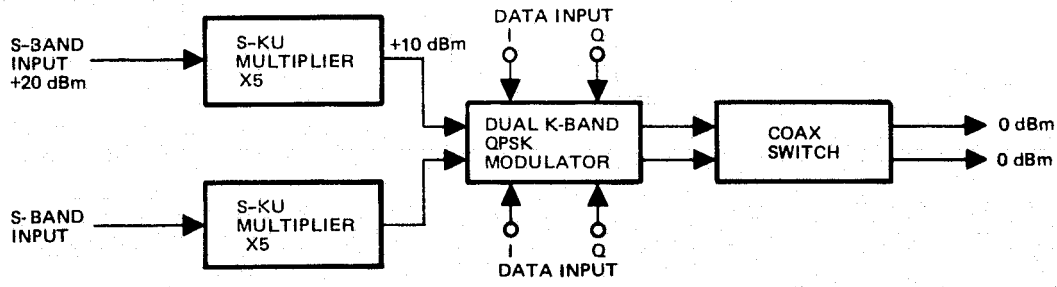

Figure 3.3-3. Direct Approach

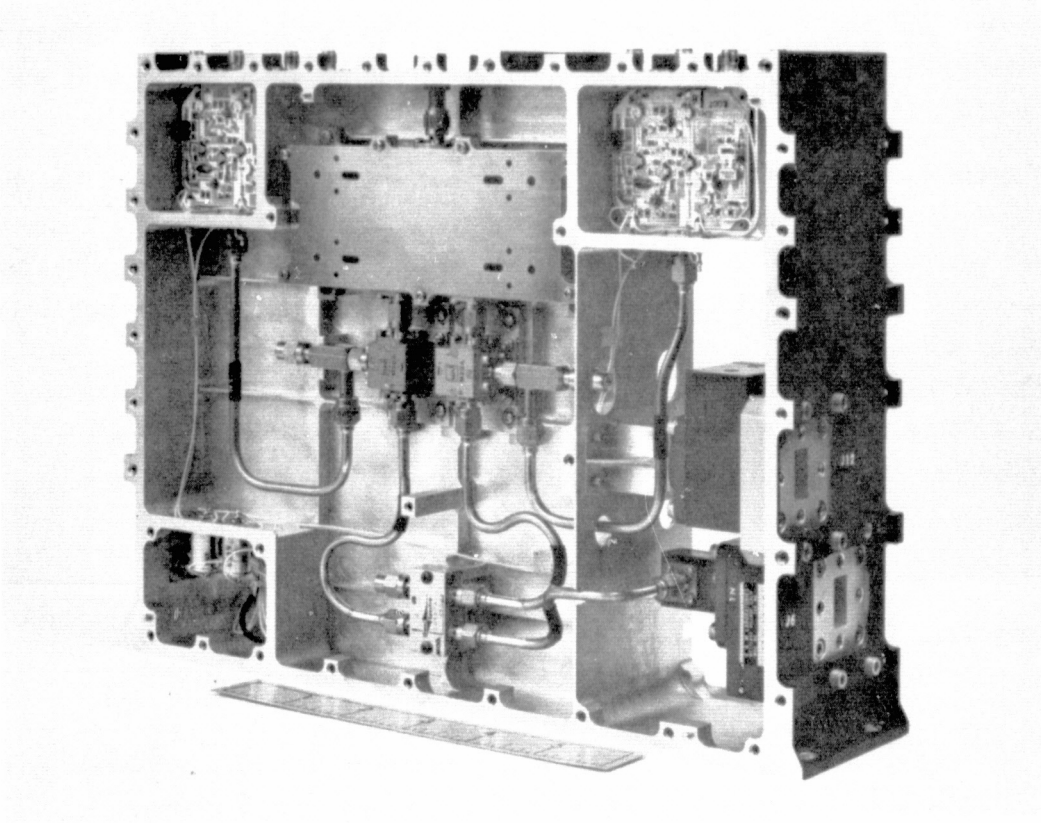

Figure 3.3-4. Ku-Band Modulator Developed for a Prior Program

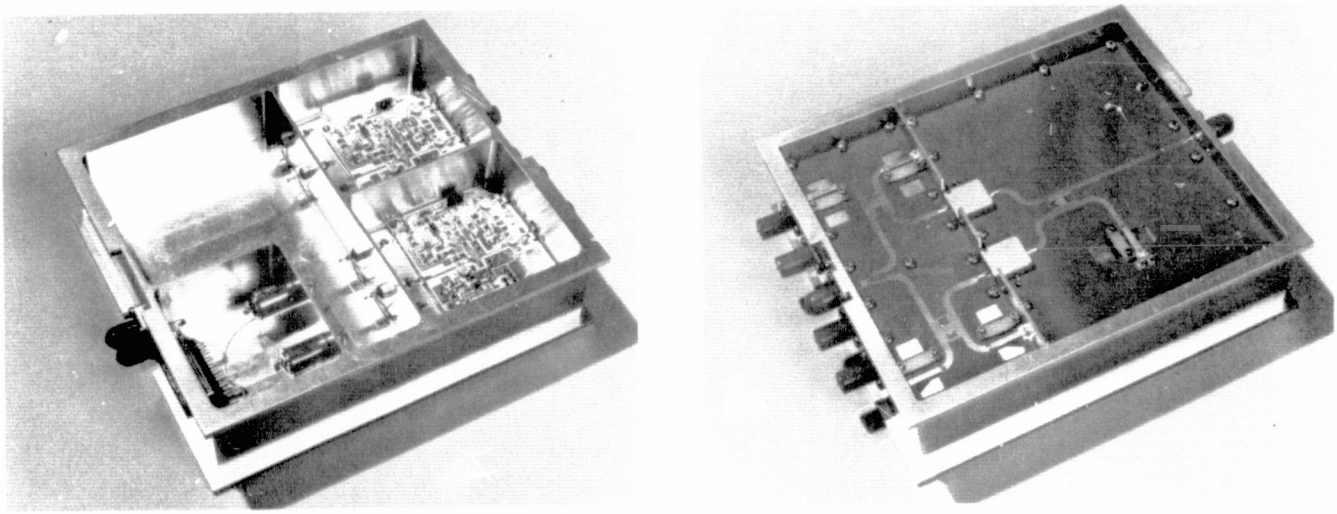

Figure 3.3-5. TRW Microwave Integrated Circuit (MIC) Version of the Above Ku-Band Modulator

A performance comparison between the two approaches is given in Table 3.3-1. The indirect transmitter/modulator system exhibits 0.3 to 0.5 dB less BER performance due to AM/PM conversion and phase distortion present in the parametric upconverter.

Table 3.3-1. Transmitter Modulator RF Performance Comparison

Parameter	Direct	Indirect
Output frequency	Ku-band	Ku-band
Output power	0 dBm	0 dBm*
Input frequency	Ku-band	S-band
Input power	+10 dBm (2 inputs)	+10 dBm (2 inputs) +24 dBm (2 inputs)
Phase balance	±2.5°	±2°
Amplitude balance	±0.25 dB	±0.15 dB
AM/PM	N/A	5°/dB
Phase linearity	N/A	±10°
Bandwidth	1000 MHz	500 MHz
Relative BER degradation	—	0.3 dB
Bit asymmetry	3%	3%

*Parametric upconverter.

Table 3.3-2 is a comparison of size, weight, and dc power consumption for each component of the two transmitter types. The TWTA's are omitted since they are common to both transmitters. The comparison shows the indirect transmitter to be larger (348 cu in. vs 194 cu in.) and heavier (7.64 lbs vs 5.42 lbs) than the direct transmitter employing the MIC modulator. The dc power consumption also favors the direct approach.

The overall frequency stability is independent of the configuration. The stability of both configurations is determined solely by the stability of the reference oscillator (see Section 3.3.2).

As a result of these tradeoffs, which are based on TRW's experience in the design and qualification of both types of QPSK transmitters, the direct modulation method is the recommended approach.

Figure 3.3-6 is a photograph of the PAE portion of the recommended modulator. The PAE is a microstrip transmission line network consisting of a power divider, two branch-line hybrid couplers, and four variable short circuits. The power divider separates the input carrier into two paths with phase and amplitude adjustment in each path provided by the variable short circuits on the branch line couplers. The signals on each output arm of the hybrid reflect from the short circuits and recombine at the isolated arm of the hybrid. A variable reflection coefficient is produced at each short circuit by moving a cutout portion of dielectric material under the microstrip transmission line. Figure 3.3-7 illustrates the fundamental concepts.

Table 3.3-2. QPSK Transmitter Weight and DC Power Comparison

Component	Direct					Indirect				
	Quantity	Size (inches)	Unit Weight (pounds)	Total Weight (pounds)	DC Power (watts)	Quantity	Size (inches)	Unit Weight (pounds)	Total Weight (pounds)	DC Power (watts)
S to Ku-band multiplier	2	7 x 2 x 1.6	0.56	1.12	0	2	7 x 2 x 1.6	0.56	1.12	0
K-band coax switch	1	1.6 x 2 x 2	0.6	0.60	0	1	1.6 x 2 x 2	0.6	0.6	0
Dual K-band QPSK modulator	1	6.5 x 5.5 x 3	3.6	3.6	1.9	—	—	—		—
Coaxial cable	3 ft	RG142	0.03	0.1	—	4 ft	RG142	0.03	0.12	0
S-band coaxial switch	—	—	—	—	—	1	1.6 x 2 x 2	0.6	1.2	0.3
S to Ku-band upconverter	—	—	—	—		2	7 x 2 x 2.5	0.6	1.2	0.3
S-band dual QPSK modulator	—	—	—	—	—	1	10.5 x 7 x 3	4	4.0	2.8
		158 cu in.		5.42 lbs	1.9 watts		348 cu in.		7.64 lbs	3.1 watts

Selected Approach

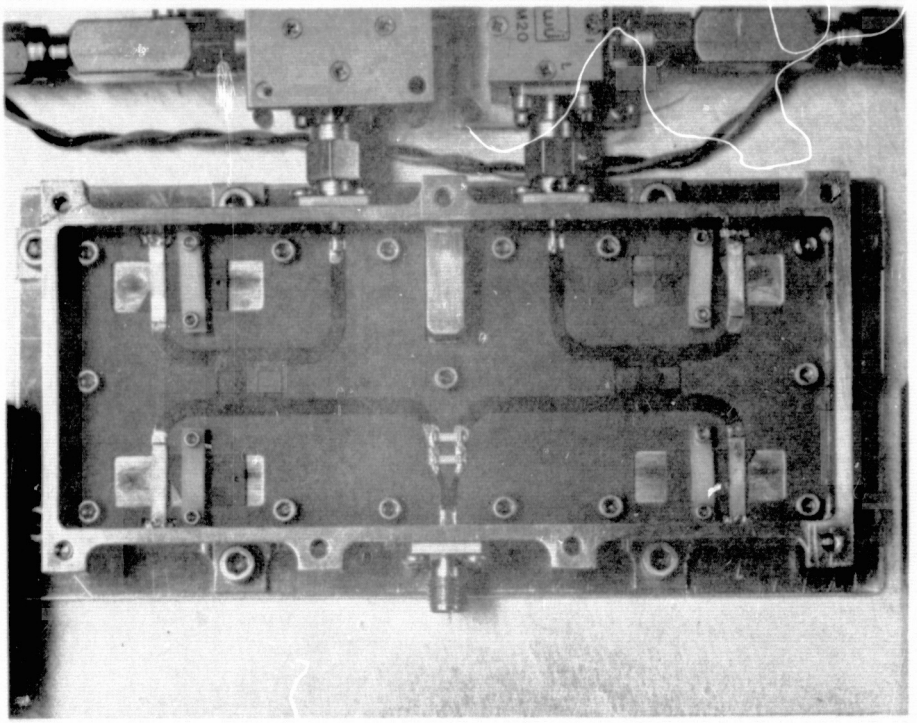

B-109

Figure 3.3-6. PAE Portion of Recommended Modulator

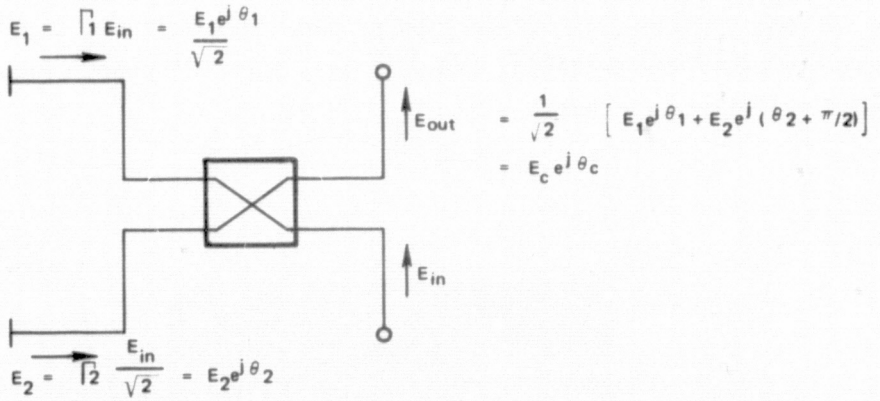

Figure 3.3-7. Power Divider Concept

Each biphase switch consists of a double balanced mixer utilizing a Schottky barrier diode quad. The design employs microstrip balum transformers and four unpackaged silicon beam lead Schottky diodes on a ceramic carrier. Each diode pair of the quad is driven by ±20 mA depending on the input logic state. The diodes exhibit a switching time of less than 500 psec. The biphase switch is available from Watkins-Johnson in a hermetically sealed flatpack housing and is space qualified. Figure 3.3-8 shows the internal construction and assembled configuration.

The driver amplifiers consist of high speed emitter coupled pairs configured with complementary transistors within a single package. The use of complementary pairs allows interstage level shifting with repect to a common reference. The use of a common reference minimizes asymmetry in the differential output since any changes in

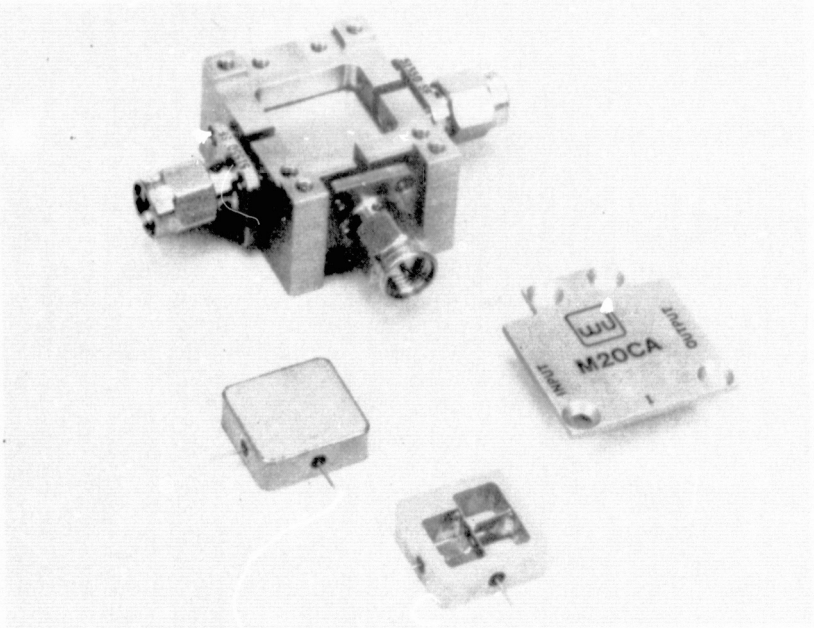

Figure 3.3-8. Double Balanced Mixer

the reference due to temperature are common to both transistors in the pair. The output stage consists of two current sources in addition to the output emitter coupled pair. Two current sources are necessary to provide ±20 mA levels to the biphase switch. This circuit has exhibited switching times of less than 400 psec. Figure 3.3-9 is a photograph of the driver circuits.

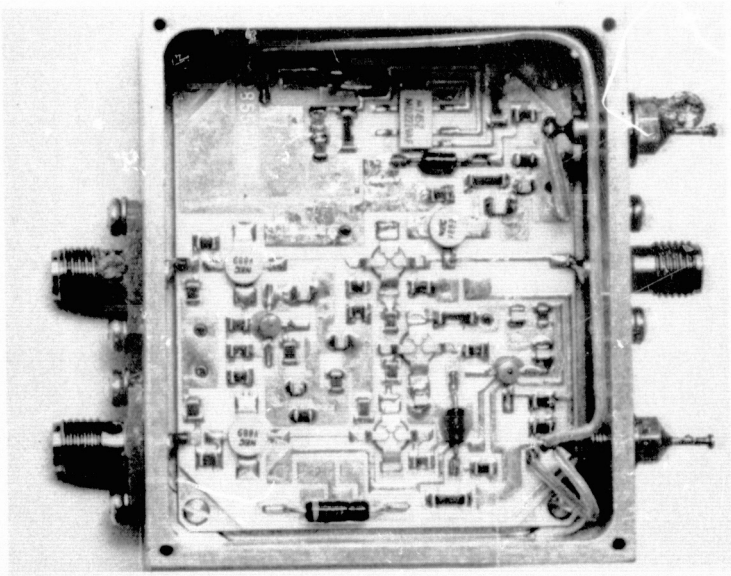

B-021

Figure 3.3-9. Driver Circuits

3.3.2 Frequency Source

The frequency source unit provides the reference frequency for both the TDRSS link and STDN/direct access transmitters as well as the tracking receiver local oscillator. Due to the remote location of much of the equipment in the RF compartment, the frequency source unit provides outputs at S-band, with final multiplication to Ku-band occurring in the RF compartment. Due to their relative simplicity and proven performance, TRW has chosen to use crystal oscillator-multiplier techniques to implement the frequency source.

The three required frequencies, 15.0085 GHz (TDRSS link transmitter), 14.70833 GHz (STDN/direct access transmitter), and 13.50765 GHz (receiver LO), are all integrally related to 75.0425 MHz, allowing a single reference oscillator to be employed. A simplified block diagram of the overall frequency generation scheme is shown in Figure 3.3-10. The recommended reference oscillator is a space-qualified oven-controlled crystal oscillator providing a stability in excess of 15×10^{-6} cumulative (-7 to +57°C) over 7 years of operation. During any 24-hour period, the stability is in excess of 4.5×10^{-8}, including the effects of orbital temperature variations. The output of the oscillator is split to provide an input to all three channels. In the TDRSS transmitter channel, the reference frequency is first multiplied by 8 in a transistor multiplier. Figure 3.3-11 shows a similar multiplier and bandpass filter built by TRW for a space program. The output, at 600.34 MHz, is again multiplied by 5 to provide a 3001.7 MHz signal. Construction of the X5 multiplier is similar to the X8 multiplier. This S-band signal is then amplified in a 3-stage amplifier, as shown in Figure 3.3-12.

The S-band high level output from the amplifier is routed up the mast through coaxial cable to the final multiplier, a X5 with a Ku-band output. This multiplier, shown in Figure 3.3-13, is a varactor diode multiplier fabricated in waveguide. An integral waveguide filter is provided for the rejection of undesired signals.

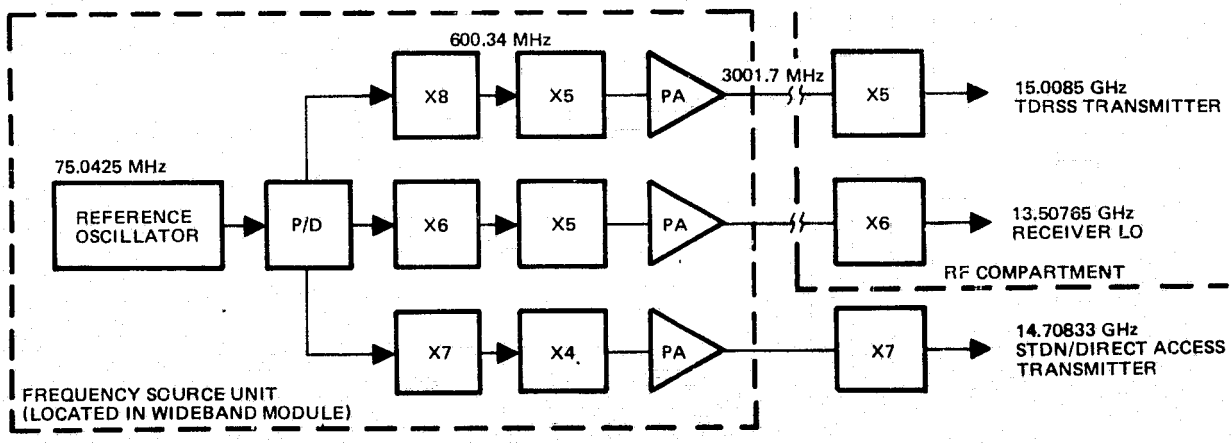

Figure 3.3-10. Frequency Generation — Simplified Block Diagram

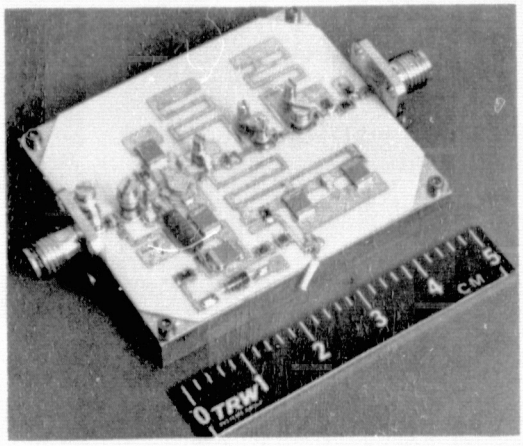

127357 6

Figure 3.3-11. Transistor Multiplier and Bandpass Filter

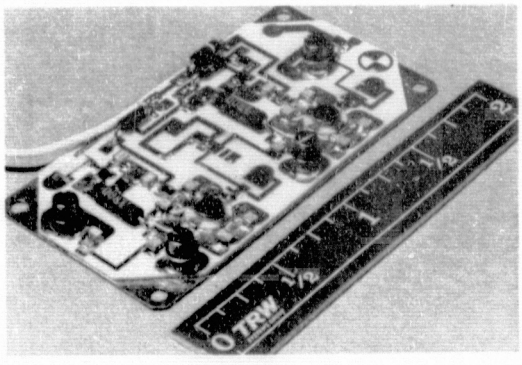

122304 5

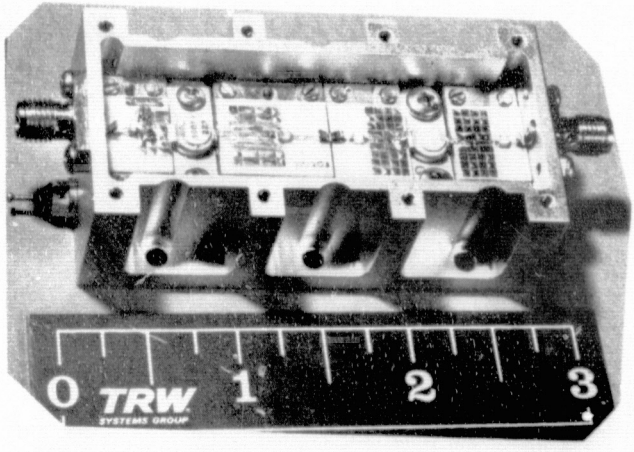

101511 3

Figure 3.3-12. Three-Stage S-Band Amplifier

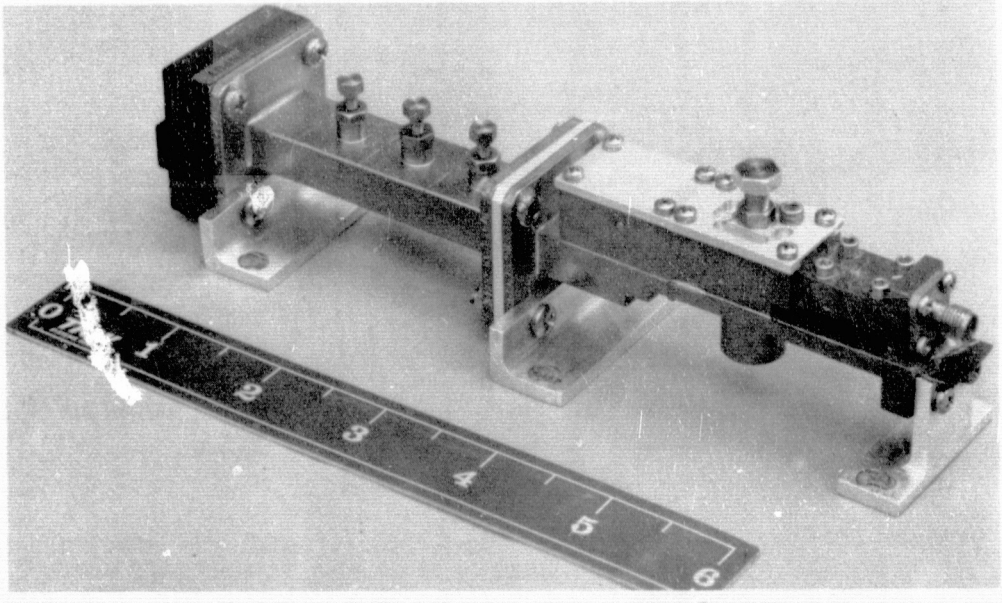

111328 4

Figure 3.3-13. Ku-Band Waveguide Multiplier

The second channel, the receiver LO, uses identical techniques to achieve the Ku-band output. Only minor changes in multiplication ratios are required to achieve the final output. The receiver LO is discussed further in Section 3.4.3. The third channel, the STDN/direct access transmitter, is again nearly identical, the major differences being the multiplication ratios, the location of the Ku-band multiplier, and a somewhat reduced cable loss to the multiplier since the STDN/direct access transmitter is collocated in the wideband module.

Each of the three channels provides similar short-term stability or phase noise performance, since the reference oscillator is the prime contributor. When multiplied to Ku-band, the recommended reference oscillator provides less than 2° of phase noise in a 100 Hz loop bandwidth.

Each channel in the frequency source is redundant as shown in the overall block diagram, Figure 3.3-14. Two reference oscillators are provided with passive coupling techniques to obtain six outputs. Passive hybrid dividers eliminate the need for relays. The primary and redundant channels are fully duplicated, with output switching provided by latching coaxial relays. The estimated power consumption of the frequency source is tabulated in Table 3.3-3.

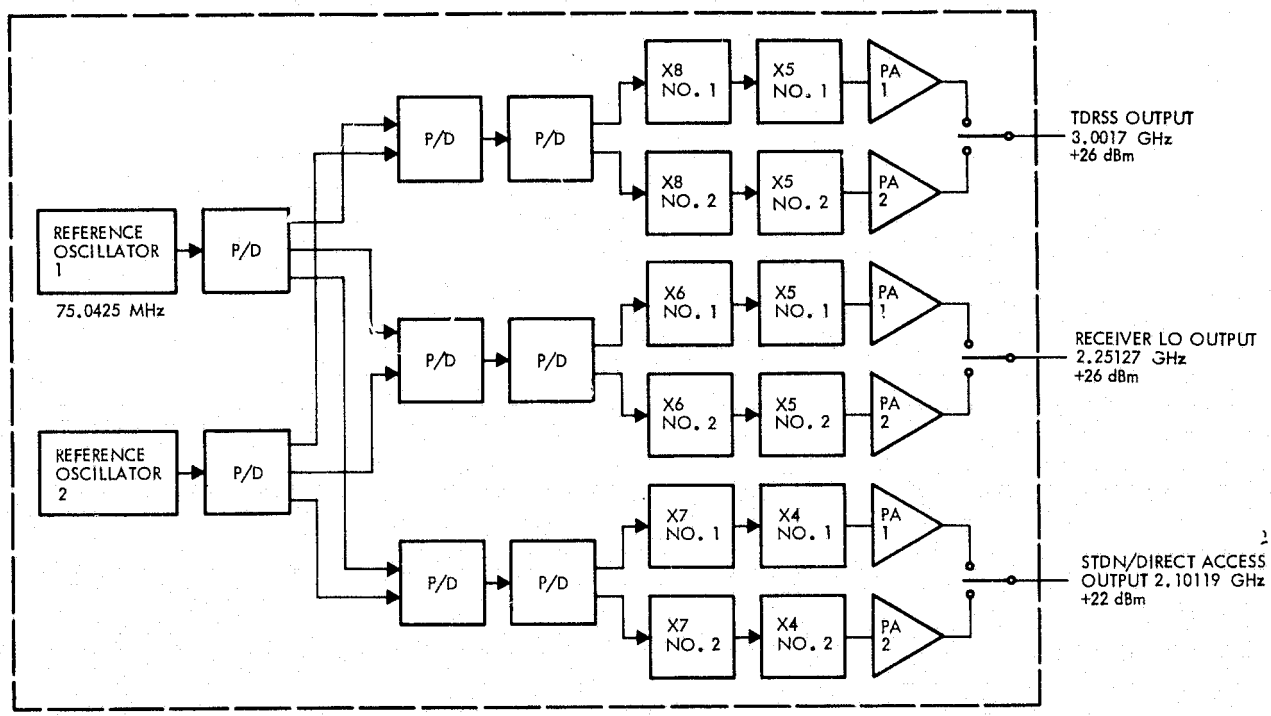

Figure 3.3-14. Frequency Source

Table 3.3-3. Frequency Source Estimated Power Consumption

	+15 V	Power
Reference oscillator*	17 mA	.25 W
TDRSS multiplier/amplifier	90 mA	1.35 W
Receiver multiplier/amplifier	90 mA	1.35 W
STDN/direct access multiplier/amplifier	50 mA	.75 W
TOTAL	247 mA	3.70 W

*Excluding heater power (1.2 W at 65°F).

Mechanically, the entire internally-redundant frequency source is packaged in a single 2.3 x 8.6 x 11-inch aluminum housing with an estimated weight of 6.5 pounds. As shown in Figure 3.3-15, the primary and redundant sections of the unit are located on opposite sides of an "H-section," with machined compartments for the substrates. Effective use of ribbon interconnects has virtually eliminated internal RF connectors, thus reducing size and enhancing reliability.

3.3.3 TWTA Tradeoffs

An output range of 15 to 20 watts was selected, primarily on the basis of TWTA availability. Currently, only three vendors have amplifiers available (or nearing availability) for space applications at Ku-band. A detailed tradeoff study was performed between the three potential sources: Hughes Electron Dynamics Division, Watkins Johnson/Thomson-CSF, and Telefunken-AEG.

The first Ku-band tube available for this type of application was the Hughes 288H. This tube has been used in programs dating back several years. The 288H was developed out of an X-band tube, also used in space programs. Due mainly to its early heritage, the tube is a relatively unsophisticated design, employing a single collector and an untapered helix. In recent years, the use of multiple collectors and tapered helices has advanced the state of tube design and improved their efficiency. Electrically, the 288H is a 16-watt tube designed for 14.3 to 15.3 GHz. The overall efficiency (including power supply) of flight models has been approximately 17%, thus requiring some 90 watts of dc power. The reliability of the tube has been suspect, due to instances of cathode poisoning and barrel outgassing leading to premature failure. Hughes has been working on this problem and has seemingly corrected it with certain changes in manufacturing.

The second TWTA is a joint effort between Watkins-Johnson and Thomson-CSF. Their device, the TH3554, is a 20-watt TWTA designed for 14.3 to 15.3 GHz. Like the Hughes tube, the TH3554 is an outgrowth of their previous space-qualified X-band tube (the

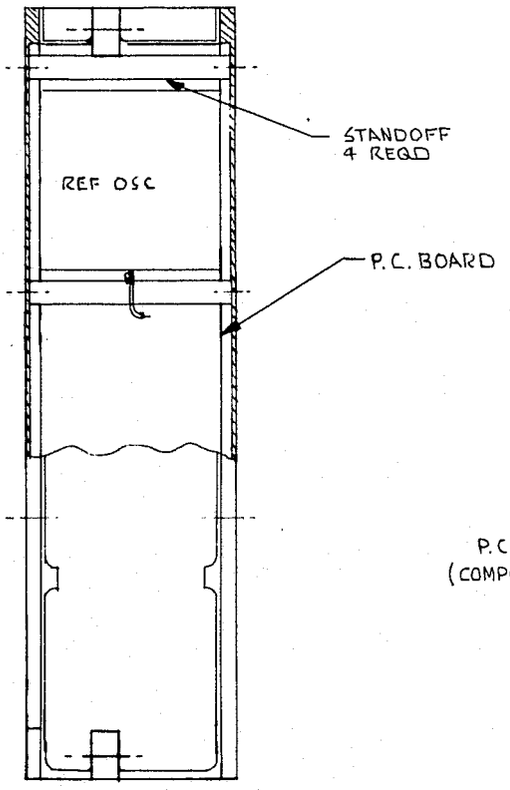

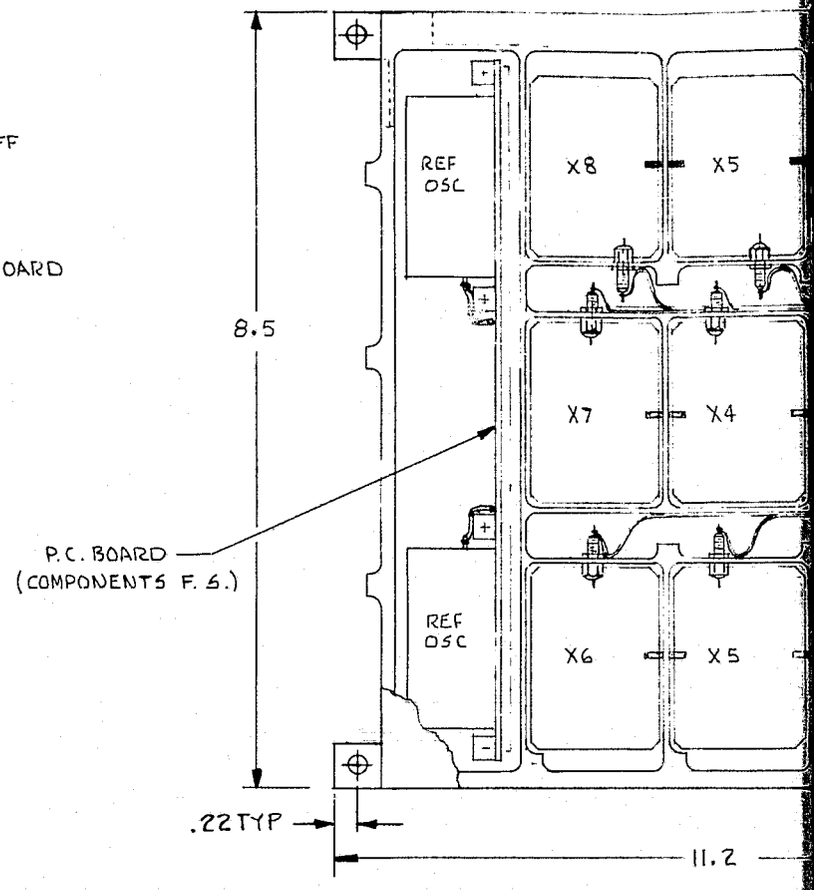

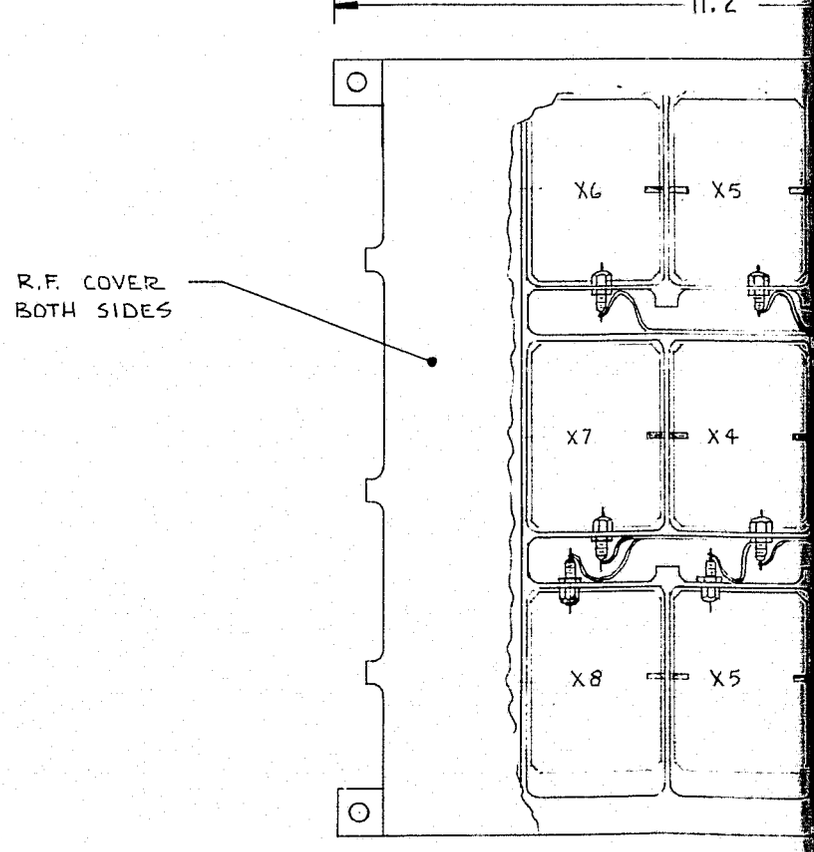

BREAKOUT FRAME)

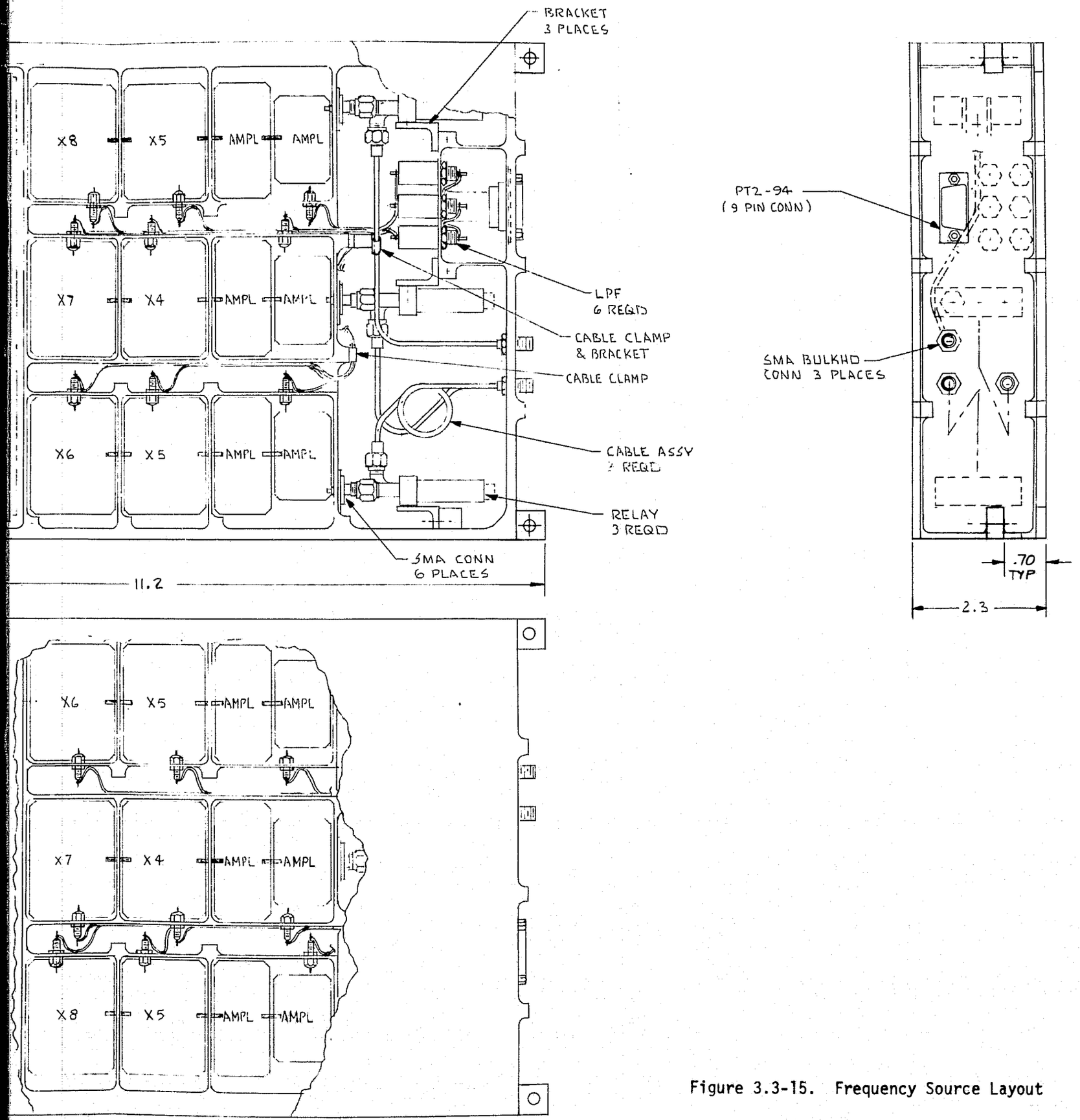

Figure 3.3-15. Frequency Source Layout

FOLDOUT FRAME 2

TH3525). The TH3525 was originally developed as part of a series of tubes for Comsat and ESA (European Space Agency). The TH3525 has been qualified for the European Orbiting Test Satellite (OTS) and the European Communication Satellite System. The TH3554 is currently in an engineering model phase, but due to its similarity to the TH3525 and the success of early tests, the TH3554 is considered a viable candidate for the LF/O application.

The Watkings-Johnson/Thomson-CSF tubes employ features not found in the Hughes tube. Much of the early development work was aimed toward increased efficiency. As a result of this work, both the TH3525 and TH3554 employ dual collector designs and multiple tapered helices. These features have allowed overall efficiencies to exceed 25% without degrading the performance characteristics. The expected dc power consumption of the TH3554 TWTA is about 75 watts and will not exceed 80 watts. This represents a typical efficiency of about 26.7%, with a minimum of 25% (including power supply).

While the TH3554 is basically a 20-watt TWTA, operation from 15 to 24 watts is feasible with only minor power supply changes. At the 15-watt level, it is estimated that the dc power consumption would only drop to about 70 watts, representing only a 5-watt savings from the 20-watt level. Modifying the existing tube to optimize the 15-watt operation would result in negligible further reduction in dc power ($\approx$2 W). At the 24-watt level, the overall dc power would approach 100 watts. Operating the tube at 24 watts is feasible without reduced reliability as the cathode emission density (600 mA/cm^2) would remain well below the accepted maximum of 800 mA/cm^2.

The third device, from Telefunken-AEG, is again a modification of a currently existing X-band tube (the TL12022). The TL12022 was developed in much the same way as was the TH3525 for ESA. The tube design is very similar to the TH3525, utilizing dual collectors and a tapered helix. Unfortunately, Telefunken has not begun development of the Ku-band version, and all information received is in the form of projections.

During the study, TRW prepared a detailed TWTA specification, and submitted it to the three vendors mentioned. Key specification parameters are summarized in Table 3.3-4. Vendor responses to this specification were all compliant for the major electrical parameters. Table 3.3-5 presents the results of major factors that TRW considered for the tradeoff. TRW has selected the Watkins-Johnson/Thomson-CSF TWTA for the recommended transmitter. This choice, in our opinion, simultaneously provides the best performance, minimum risk, and lowest overall cost.

Figure 3.3-16 shows the TH3523, a tube of very similar configuration. As previously mentioned, this tube utilizes dual collectors, permitting the electron beam to be recovered with less power dissipation and hence higher efficiency than with a single collector. The tube also utilizes helix tapering to increase efficiency by optimizing

Table 3.3-4. TWTA Specification Summary

Frequency range	14.55 to 15.2 GHz
Saturated output power	15 watts (20 watts goal)
Saturated gain	49 dB min
AM/AM conversion	≤ 0.3 dB/dB
AM/PM conversion	≤ 7°/dB
Phase nonlinearity	≤ ±10° from linear
Noise figure	≤ 30 dB
Input VSWR	≤ 2.0:1
Output VSWR	≤ 2.0:1
Spurious outputs	>40 dBc
DC power	≤ 80 watts (28 Vdc)
Weight	≤ 11 pounds, (including power supply)

Table 3.3-5. TWTA Tradeoff Factors

	HUGHES 288H	WJ/THOMSON TH3554	TELEFUNKEN TL12022 (MOD)
RF PERFORMANCE	COMPLIANT (16-WATT OUTPUT)	COMPLIANT (20-WATT OUTPUT)	COMPLIANT (20-WATT OUTPUT)
DC PERFORMANCE	92 WATTS $\eta_{TOTAL} \approx 17.4\%$ $\eta_{TUBE} \approx 22.9\%$ $\eta_{PWR\ SUP} \approx 76\%$	75 WATTS $\eta_{TOTAL} \approx 26.7\%$ $\eta_{TUBE} \approx 33.3\%$ $\eta_{PWR\ SUP} \approx 80\%$	80 WATTS $\eta_{TOTAL} \approx 25\%$ $\eta_{TUBE} \approx 35\%$ $\eta_{PWR\ SUP} \approx 75\%$
SIZE AND WEIGHT	← SIMILAR →		
STATUS	DEVELOPED AND QUALIFIED	IN DEVELOPMENT SOME TESTING COMPLETE	PROJECTED
AVAILABILITY	QUESTIONABLE, HAVE HAD PRODUCTION PROBLEMS	UNDER CONTRACT FOR DEVELOPMENT QUALIFIED FLIGHT MODELS MAY BE AVAILABLE BY LATE 77/EARLY 78	QUESTIONABLE, DEVELOPMENT IS UNCERTAIN
RELIABILITY	SUSPECT – HAVE HAD PROBLEMS	EXCELLENT HISTORY FOR PREDECESSORS (TH3525)	EXCELLENT HISTORY FOR PREDECESSORS (TL12022)
COST (SEE NOTE 1)	≈ $2.25 MILLION (SEE NOTE 2)	$1.26 TO 1.66 MILLION (SEE NOTE 3)	≈ $1.51 MILLION (SEE NOTE 4)

UNDESIRABLE FEATURES

NOTES

1. TOTAL PROCUREMENT COST INCUDING (AS APPLICABLE) NRE, QUALIFICATION AND 10 FLIGHT TWTA'S.
2. HUGHES DECLINED TO BID ON LANDSAT RFQ COST ESTIMATE BASED ON PROCUREMENT COSTS OF PREVIOUS HAC 288H TWT'S.
3. WATKINS JOHNSON/THOMSON CSF COST BASED ON QUOTES RECEIVED FOR THIS TWTA. UPPER PRICE INCLUDES QUALIFICATION, LOWER PRICE ASSUMES QUALIFICATION COMPLETE BY THE TIME FRAME OF LFO. QUALIFICATION OF TWTA BY EARLY 1978 SEEMS LIKELY UNDER OTHER PROGRAMS.
4. TELEFUNKEN ITEMIZED COSTS NOT AVAILABLE AT THIS TIME. ESTIMATE DERIVED FROM TELEFUNKEN ROM COST ($1.95 MILLION) FOR DEVELOPMENT OF TWTA AND DELIVERY OF 15 FLIGHT UNITS.

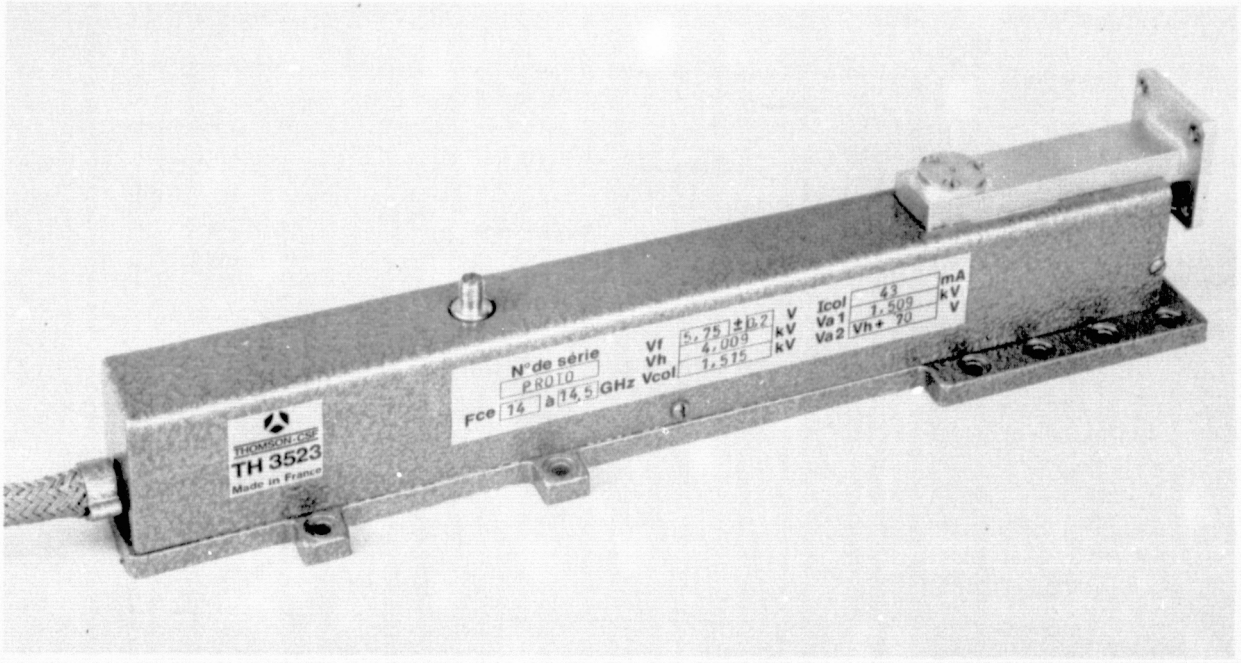

B-7486 3

Figure 3.3-16. Watkins Johnson/Thomson TH3523 TWT

the RF coupling between the RF circuit and electron beam. The helix circuit is divided into three regions separated by two attenuating sections. In the first region, the helix pitch is adjusted to maximize small signal gain. In the second section, the pitch is decreased to maintain synchronism between RF and beam phase velocities. In the third section, helix pitch is continuously tapered (decreased) to again maintain phase velocity synchronism. Focusing in the TH3554 is a standard periodic permanent magnet (PPM) arrangement. The individual magnets in the stack are typically 16 mm in diameter and 4.5 mm thick.

The tests conducted by Thomson consisted of placing a large number of diodes in operation at different elevated temperatures. A plot of the mean time to failure for each group of diodes was used to predict the time to failure at a lower, normal operating temperature. The prediction is based on Arrhenius' law

$$L = Ae^{(K/T)}$$

where

A = a constant

K = the failure rate

T = temperature in degrees Kelvin

Figure 3.3-17 shows the distribution of failure time at the elevated temperatures. Statistical analyses of these and supplemental tests on an additional 37 cathodes have shown a cathode failure rate of greater than 400,000 hours at 60% confidence (ref. 10).

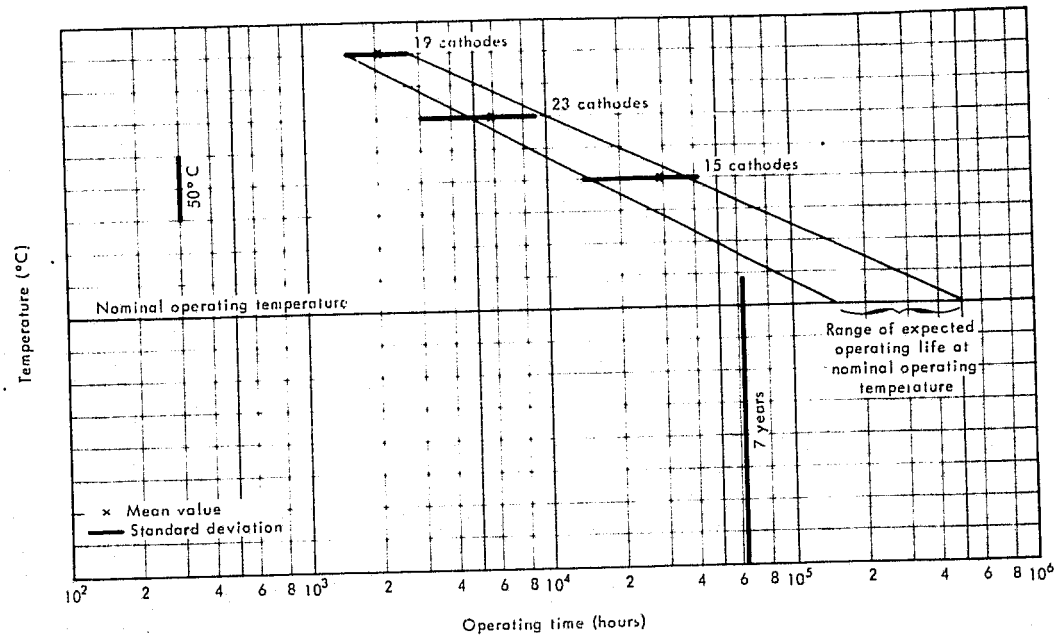

Figure 3.3-17. Results of Accelerated Life Test of Space-Tube Cathodes in Diode Mountings

In addition to the cathode tests, Thomson has placed 40 TOP 1369 TWT's on life test at normal operating temperature. This model is similar to the TH3525 discussed above. Failure criteria for RF parameters were established and periodic measurements of all critical parameters were performed. As of November 1975, no failures had been detected. Figure 3.3-18 shows a time distribution of the life test devices.

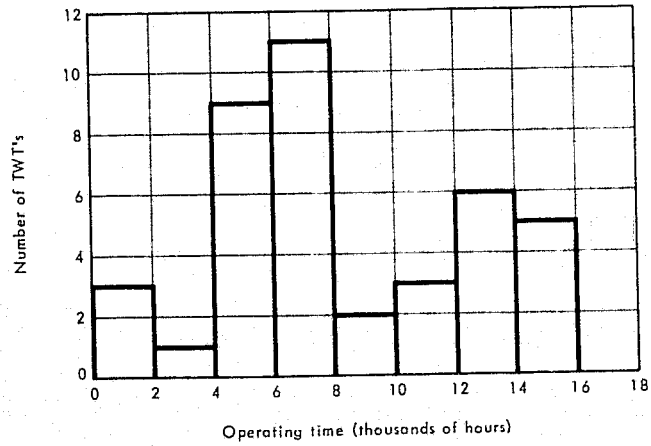

Figure 3.3-18. Time Distribution of 40 TWT's in Life Testing at Normal Operating Temperature

The Thomson-CSF claim of 250,000 hours MTTF appears to be clearly substantiated by this extensive test data.

An ancillary benefit of the dual collector design is that the tube power dissipation is nearly indpendent of the drive level, thus reducing thermal dynamic effects in the spacecraft.

The power supply for the TH3554 is based on the design of the WJ-1225 TWTA power supply developed and qualified for SAMSO (Contract F04701-74-C-0454). The majority of the design and parts are interchangeable, thus minimizing program risk. This power supply is currently being fabricated and will be part of the engineering model TWTA to be completed by December 1976.

The power supply consists of two sections: a high voltage section employing a dc to dc converter and a low voltage section employing a pulsewidth modulation-switching converter. The entire power supply is enclosed in a single package approximately 3.7 x 4.4 x 13 inches.

The most critical TWT failure mode is cathode emission falloff. The cathode design used in the TH3525 has been extensively tested. It is a tungsten matrix type operating at approximately 1000°C. Under an ESA study, a series of vacuum tube diodes was fabricated utilizing a high reliability cathode material. Results from metallurgical examinations of test samples indicate a useful life of 7 years. Test samples have accumulated 65,000 hours with no degradation.

3.3.4 Recommended Transmitter Design Summary

A block diagram of the recommended TDRSS link transmitter, including nominal gain distribution, is shown in Figure 3.3-19. Redundancy is incorporated for all active components. The 3 GHz input signal is routed along the deployable mast from the frequency source unit located in the wideband module. The relatively long interconnecting coaxial transmission line (≈ 25 feet) is terminated in an isolator to minimize VSWR between the frequency source output and transmitter input. A coaxial switch feeds the S-band signal to the input of either of two X5 multipliers. The multipliers are a standard step recovery type and exhibit a nominal 13 dB conversion loss.

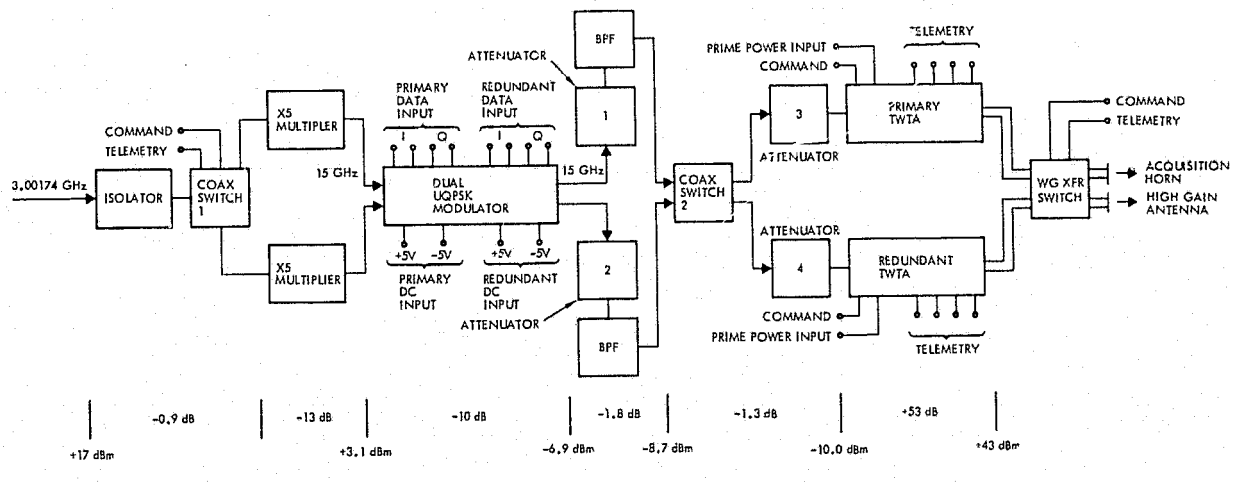

Figure 3.3-19. Recommended TDRSS Link Transmitter

The resulting 15 GHz signal is applied to the direct UQPSK modulator input. No cross-strapping is employed at the modulator input or output. Reliability analyses of similar transmitter configurations have shown that cross-strapping at either or both of these interfaces produces negligible improvement of overall transmitter reliability. Bandpass filtering ($\approx$ 240 MHz Bandwidth) is provided at the modulator output before amplification by the TWTA.

RF attenuators are shown at each modulator output and TWTA input. Previous experience has shown a wide variation from unit to unit in the nominal TWTA input power required to reach maximum saturated power. Therefore, to optimize TWTA performance, it is necessary to balance the output power of each modulator at the redundancy switch interface. The optimum input power for each TWTA is set by selecting a suitable attenuator value at each tube input (attenuators 3 and 4). A second transfer switch cross-straps the redundant TWTA outputs and provides transfer from the acquisition horn to the high gain antenna.

Table 3.3-6 summarizes transmitter performance and Table 3.3-7 summarizes the interface requirements. Tables 3.3-8 and 3.3-9 provide preliminary telemetry and command requirements.

Table 3.3-6. TDRSS Link Transmitter Performance

Input frequency	3.0017 GHz (from frequency source unit)
Nominal RF input power	+17 dBm
RF output power	+43.0 dBm
Output center frequency	15.0085 GHz
Modulation unbalance	6 dB
Data rates	120 Mbps (I channel) 15 Mbps (Q channel)
Orthogonality	±2.5°
Phase imbalance	±1.5° } For I or Q channel
Amplitude imbalance	±0.25 dB } For I or Q channel
Data transition time	800 psec
Data asymmetry contribution	3%
Phase noise contribution	0.1 degrees-rms
DC power	80 watts prime power 2.8 watts secondary power

Table 3.3-7. TDRSS Link Transmitter Electrical Interface Requirements

RF input center frequency	3.0017 GHz
RF input power	+17 dBm
Data levels (from DIU No. 2)	±0.5 V differential
DC voltage/current (secondary)	+ 5 V at 200 mA -5 V at 300 mA
DC voltage/current (primary)	28 V at 2.8 amps
Maximum source VSWR	2.0:1
Maximum load VSWR	2.0:1 (steady state) 20:1 (intermittent)

Table 3.3-8. TDRSS Transmitter Telemetry List

Monitored Parameter	Location	Level	Remarks
Switch position	Switch 1	Bilevel	Voltage supplied by secondary power supply
Switch position	Switch 2	Bilevel	
Heater voltage	Primary TWTA	Analog	
Cathode current	"	"	
Helix voltage	"	"	
Helix current	"	"	
Input current temperature	"	"	
Heater voltage	Redundant TWTA	"	
Cathode current	"	"	
Helix voltage	"	"	
Helix current	"	"	
Input current temperature	"	"	
Switch position	Waveguide switch	Bilevel	

Table 3.3-9. TDRSS Transmitter Command Requirements

Primary TWTA on	
Primary TWTA off	
Redundant TWTA on	
Redundant TWTA off	
Transfer switch 1 / Transfer switch 2	Only one command required
Transfer waveguide switch	
UQPSK modulator primary/redundant	Performed in secondary power supply

3.4 TRACKING RECEIVER DESIGN

The function of the LF/O tracking receiver is to square-law detect the 6 MHz wide PN modulated signal from the TDRSS at 13.775 GHz. It then synchronously demodulates the amplitude modulation superimposed on the signal by the autotrack comparator and modulator. The output of the synchronous demodulator provides error signals to the autotrack loop. This section discusses the tradeoffs leading to a recommended design and describes this design in detail

3.4.1 Receiver Front-End Tradeoffs

The receiver front-end downconverts the 13.775 GHz TDRSS signal to a lower frequency where amplification, filtering, and detection can be efficiently performed. The front-end consists of a downconverter and either an RF or IF preamplifier to provide RF-to-IF conversion gain. As discussed later in this section, the IF frequency selected for the recommended receiver is 267.35 MHz.

Location of the receiver front-end is in the RF compartment. This requires that the size and weight be minimized. The only RF interface between the RF compartment and the wideband module is the IF output and this can be readily carried over coaxial cable without significant loss.

The first and perhaps most critical measure of front-end performance is the noise figure. Since the front-end is the first active element in the receiver, its noise figure performance becomes the primary contributor to the overall receiver noise figure. The TDRSS link budget (Section 3.11.4) allocates a maximum noise figure of 6 dB referenced to the input of the front-end. This, of course, includes the contribution of all stages following the front-end. The effective noise figure of the two cascaded stages (Figure 3.4-1) can be computed from

$$F = F_1 + \frac{F_2 - 1}{G}$$

where

F = effective noise figure of cascade

F_1 = front-end noise figure

F_2 = total IF noise figure

G = front-end gain

This equation demonstrates a second requirement of the front-end: sufficient gain (G) to minimize the second-stage noise figure contribution. In a typical IF design, where F_2 would be on the order of 5 dB, Figure 3.4-2 presents the effective overall noise figure vs front-end gain for various values of front-end noise figure. It can be seen from Figure 3.4-2 that a minimum gain of 20 dB is required to effectively

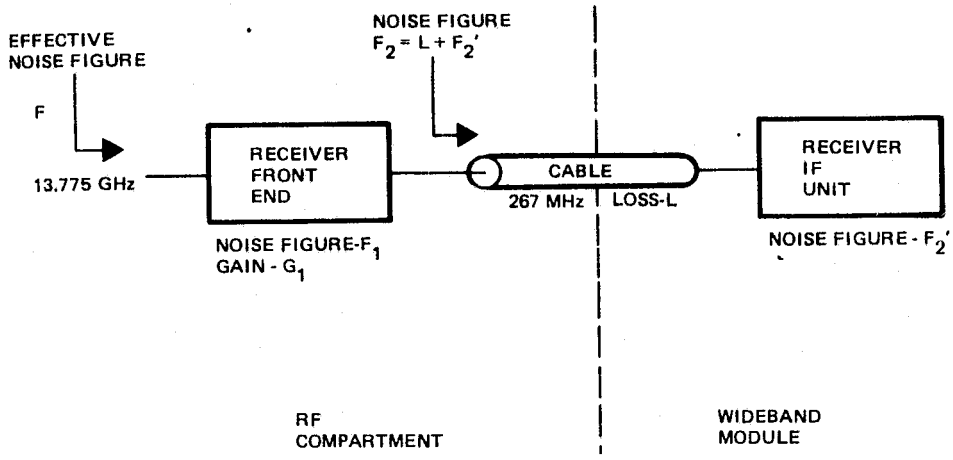

Figure 3.4-1. Receiver Noise Figure Model

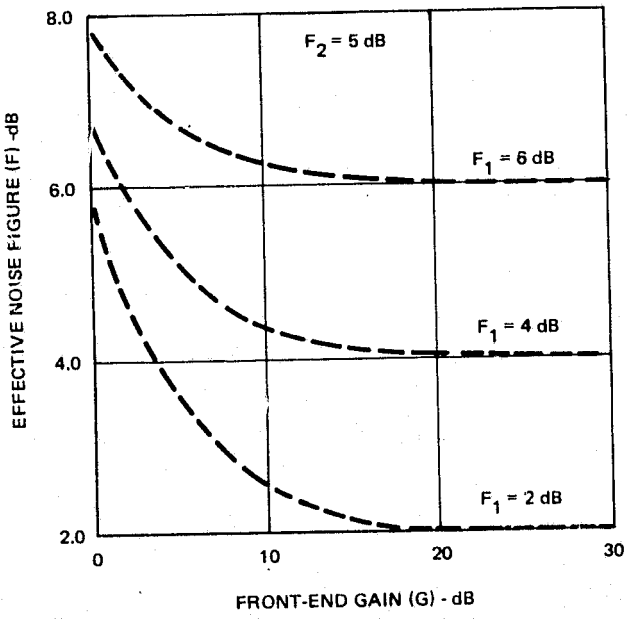

Figure 3.4-2. Effective Overall Noise Figure vs Front-End Gain

eliminate second-stage noise contributions. TRW has chosen 25 dB as the nominal front-end gain for the performance tradeoffs and recommended receiver design.

Another important aspect of the front-end design is its ability to operate at the low signal levels involved (≈ -120 dBm), with high-level transmitter leakage signals (≈ -50 dBm) simultaneously present at the input. This requirement imposes limitations on the front-end filters and dynamic range. The front-end must pass the 13.775 GHz TDRSS signal and downconvert it without being adversely affected by the 15.0085 GHz transmit signal. To avoid intermodulation distortion, the front-end should operate at least 25 dB below the 1 dB compression point. This requirement can be met by additional filtering in the front-end and by providing a front-end compression point which is well above the expected level of -25 dBm, referenced to the output of the front-end.

Several candidate front-end circuits are available. These are discussed below and compared to the requirements. The standard doubly-balanced mixer with an IF preamplifier is perhaps the simplest. Doubly-balanced mixers using Schottky-barrier diodes are routinely fabricated at Ku-band with conversion losses of approximately 7.5 dB. When combined with an input bandpass filter and low-noise IF preamplifier, overall noise figures of 9 dB are typical. With a typical IF preamplifier design, the 1 dB compression is quite high, usually 0 dBm. An attractive feature of this approach is its small size and light weight (<1 lb) even when configured in waveguide.

The second candidate studied was the image-enhanced mixer with IF preamplifier. The image-enhanced mixer is a balanced mixer using Schottky diodes not unlike those in the doubly-balanced mixer, but achieving significantly lower conversion losses and thus lower noise figures. The improved performance is obtained by providing internal reactive terminations for both the sum and different frequencies. The penalty is reduced bandwidth, compared to the doubly-balanced mixer, but several hundred MHz bandwidth is available, well in excess of the required 6 MHz.

Ku-band conversion losses of about 4 dB are typical for the image-enhanced mixer, yielding an overall noise figure of 5.5 dB when combined with the IF preamplifier. The size, weight, and electrical performance of the image-enhanced mixer/preamp are comparable to the doubly-balanced mixer, making the image-enhanced design especially attractive.

The two candidates discussed thus far have one thing in common, the lack of RF preamplification. These two approaches achieve a nominal 25 dB RF-to-IF conversion gain with IF preamplification. The amplification could, of course, be provided at RF. The simplest circuit would be a tunnel diode amplifier (TDA) followed by a doubly-balanced mixer such as the one previously considered. With the RF gain ahead of the mixer, the overall noise figure is determined primarily by the TDA, which can be as low as 5.5 dB at Ku-band. The attractive feature of this approach is again the relatively small size. The major disadvantage is lack of dynamic range. The TDA typically begins gain compression 25 dB before either of the previously discussed front-ends. While this does not preclude its use, it forces more stringent filter designs to avoid undesirable intermodulation distortion.

Recently, gallium arsenide field effect transistors (GaAs FET's) with 0.5 μ gates have become available for use at Ku-band. These devices could be used as an amplifier in place of the TDA. Noise figures in the 4 to 5 dB range are practical and at a size comparable to the previous approaches. The dynamic range of the front-end with GaAs FET's is comparable to the first two approaches. The biggest penalty with the GaAs FET's is dc power, with an estimated dc power consumption of approximately 4.5 watts as opposed to less than 1 watt for the previous three approaches.

Another area of concern for a GaAs FET front-end is qualification for space applications. One-micron GaAs FET amplifiers have been used in space, but they have not yet accumulated a large history. The 0.5 μ devices required for Ku-band applications have not yet been used in space. For this reason the GaAs FET front-end would be more costly and have a somewhat higher risk.

The fifth and final approach is an uncooled parametric amplifier (paramp) followed by the doubly-balanced mixer as before. The paramp can provide the lowest noise figure of the five approaches considered, typically between 2.5 and 3 dB. This excellent noise figure is accompanied by several penalties: about five times the weight of the previous approaches, increased complexity, increased dc power (10 watts), and a dynamic range no better than the TDA.

A tradeoff matrix of the five approaches is presented in Table 3.4-1. Conditions which are considered undesirable are shown cross-hatched.

Table 3.4-1. Receiver Front-End Tradeoffs

	DOUBLY-BALANCED MIXER WITH IF PREAMP	IMAGE-ENHANCED MIXER WITH IF PREAMP	TUNNEL DIODE AMPLIFIER PLUS MIXER	GaAs FET AMPLIFIER PLUS MIXER	UNCOOLED PARAMP PLUS MIXER
TYPICAL NOISE FIGURE	9.0 dB	5.5 dB	5.5 dB	4 TO 5 dB	2.5 TO 3 dB
RF TO IF GAIN	25 dB	25 dB	25 dB	25 dB	25 dB
1 dB COMPRESSION POINT (OUTPUT)	0 dBm	0 dBm	-25 dBm	0 dBm	-25 dBm
DC POWER	0.8W	0.8W	0.5W	4.5 W	≈10 W
RELATIVE COMPLEXITY	LOW	LOW	MEDIUM	MEDIUM	HIGH
WEIGHT	<1 LB	<1 LB	<1 LB	<1 LB	≈5 LB
SPACE QUALIFICATION STATUS	SIMILAR UNITS QUALIFIED ON MANY PROGRAMS RISK CONSIDERED LOW	SIMILAR UNITS IN QUALIFICATIONS RISK CONSIDERED LOW	SIMILAR UNITS QUALIFIED ON MANY PROGRAMS RISK CONSIDERED LOW	½ MICRON FETS HAVE NOT FLOWN - 1 MICRON DEVICES HAVE BEEN QUALIFIED SOME RISK INVOLVED	SIMILAR UNITS QUALIFIED ON PROGRAMS SOME RISK INVOLVED

SELECTED APPROACH

UNDESIRABLE CHARACTERISTICS

TRW has chosen the image-enhanced mixer for the recommended receiver. The doubly-balanced mixer was eliminated due to its inferior noise figure while the tunnel diode amplifier was eliminated due mainly to its lower dynamic range. High dc power and higher risk were the main reasons for not choosing the GaAs FET, while the parametric amplifier was eliminated because of dc power, weight, and dynamic range considerations.

During the study, TRW worked with one of several qualified vendors of image-enhanced mixers, LNR Communications, Inc., in order to arrive at an optimum design for the front-end. LNR has a long history in high reliability space programs and has recently shipped 12-GHz image-enhanced mixer preamplifiers to NASA/GSFC (Contract NAS5-19942) and to Comsat Corporation. A similar mixer is shown in Figure 3.4-3, along with a curve of its typical noise figure performance in Figure 3.4-4.

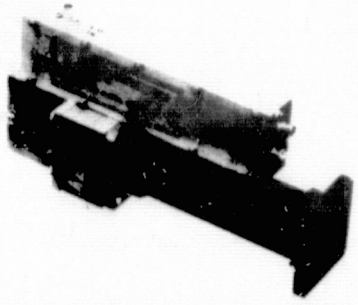

Figure 3.4-3. X-Band Image-Enhanced Mixer Preamp

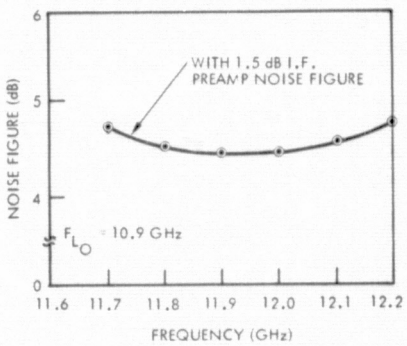

Figure 3.4-4. Typical Noise Figure Performance

The excellent performance of the image-enhanced mixer is obtained by providing optimum reactive terminations for both the sum and image frequencies. The sum frequency is terminated reactively within the balanced diode mount, while the image is reactively terminated by a waveguide filter in the RF input line. A block diagram of the receiver front-end is shown in Figure 3.4-5.

The two mixer diodes, located in a diode mount, are hermetically sealed GaAs Schottky diodes manufactured by LNR. Similar diodes have been space-qualified by LNR on previous programs. Two isolators, one on the RF input and one on the LO input, provide low VSWR terminations. The IF output from the diode mount is filtered to remove all microwave signals, then matched into the IF preamp. The IF preamp is a 3-stage, low-noise bipolar transistor design which provides a net RF to IF gain of 25 dB.

The preliminary mechanical configuration of the front-end is shown in Figure 3.4-6. The overall size is approximately 2 x 3 x 5 inches. The RF and LO are input through WR-62 waveguide flanges while the IF is output through an SMA coaxial connector.

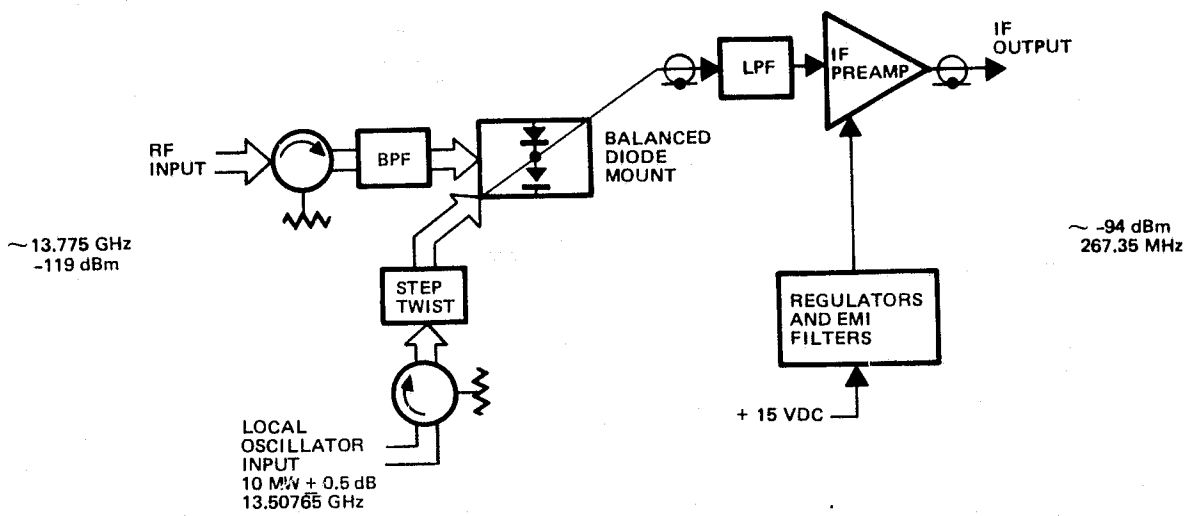

Figure 3.4-5. Receiver Front-End

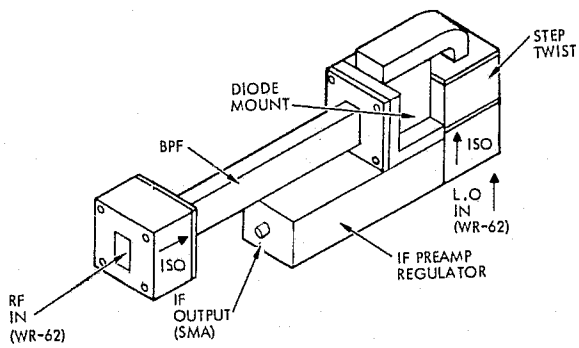

Figure 3.4-6. Receiver Front-End Mechanical Configuration

A summary of the electrical performance is given in Table 3.4-2. A complete specification for the front-end was written during the study and used as the basis for performance and cost discussions between TRW and LNR.

3.4.2 Receiver Frequency Conversion

The candidate frequency conversion processes considered were single and double-conversion. With single-conversion, the receiver front-end downconverts the Ku-band TDRSS signal to a single frequency in the range of about 200 to 500 MHz. The amplification, filtering, and detection are done entirely at this frequency. With double-conversion, the 1st IF is located somewhere in the 200 to 500 MHz region and part of the required IF filtering and gain is provided at this frequency. The 1st IF is then downconverted to a 2nd IF (<100 MHz) where the remaining gain and filtering are accomplished along with detection. Simplified block diagrams of the two approaches are shown in Figure 3.4-7.

Table 3.4-2. Electrical Performance Summary

Frequency ranges	
RF input	13,775 ± 10 MHz
Local oscillator	13,507.65 MHz
IF output	267.35 ± 10 MHz
RF input levels	-125 to -100 dBm
IF output levels	-100 to -75 dBm
Noise figure (SSB)	5.9 dB max
Gain, RF to IF (within IF passband)	25 ± 2 dB
Image rejection,	20 dB min
Local oscillator	
Power	+10 dBm
Power variation	± 1 dB max
Spurious outputs	
Within IF output range	-60 dBc max
Outside IF output range	-40 dBc max
RF input port	WR-62 cover
Input VSWR	1.2:1 max
LO input port	WR-62 cover
Input VSWR	1.2:1 max
IF output port	SMA female
Output VSWR	1.5:1
DC power	
Voltage	±15 V ±3%
Current	55 mA max
Power	0.8 watts max

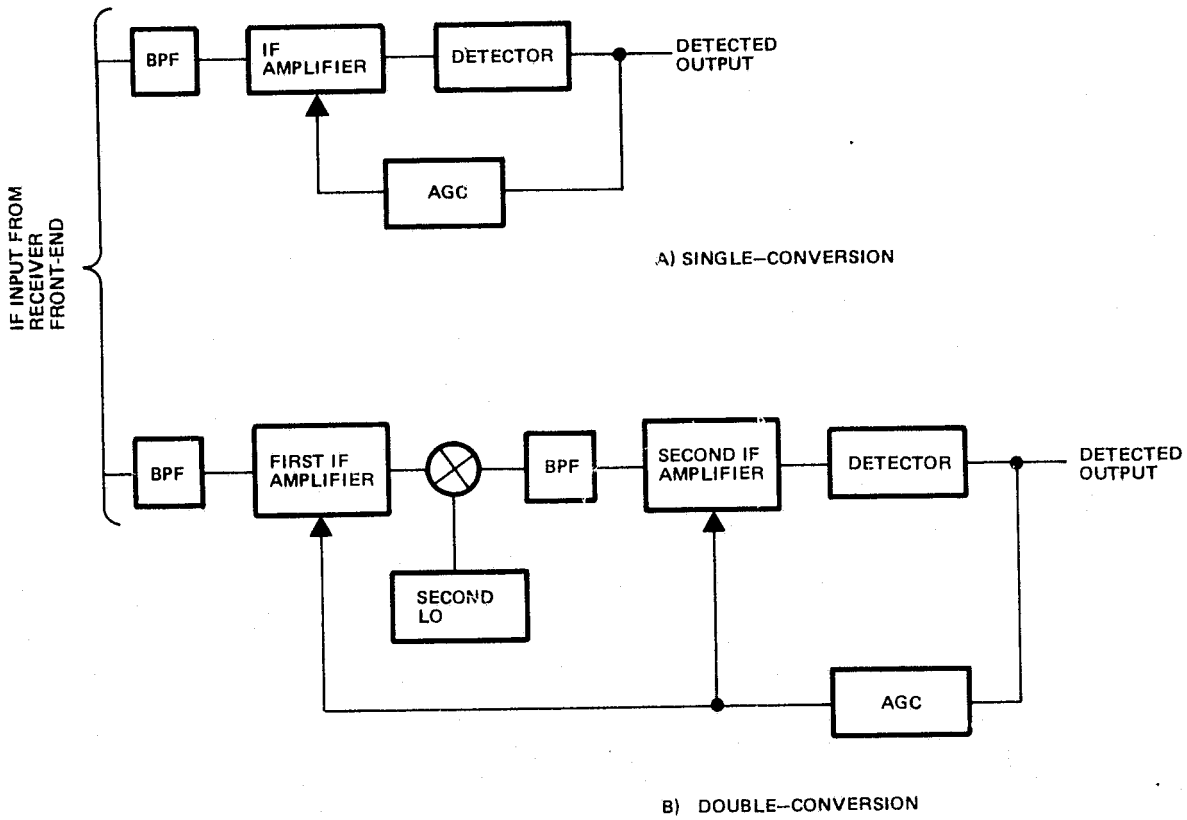

Figure 3.4-7. Candidate Conversion Schemes

Preparatory to a discussion of the tradeoffs, certain preliminaries must be addressed. For example, the 1st IF frequency must be selected and the overall IF gain estimated. The choice of the 1st IF frequency involves many parameters. Since the receiver front-end noise figure depends on the noise figure of its integral IF preamp, lower IF frequencies are favored. Figure 3.4-8 presents a typical curve of the front-end noise figure as a function of IF frequency. This favors an upper limit of about 500 MHz on the 1st IF with a preference to remain below 300 MHz. Lower IF frequencies also minimize cable losses down the mast.

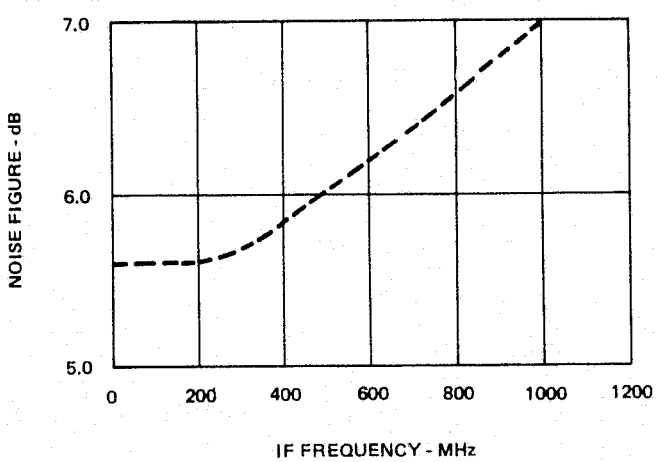

Figure 3.4-8. Estimated Front-End Noise Figure vs IF Frequency

A second consideration in selecting the IF frequency is the availability of an LO signal. The recommended LO configuration (Section 3.4.3) is a crystal oscillator/multiplier chain. To avoid duplication of costly and complex reference oscillators, it is desirable to use the same reference oscillator that the two transmitters use (75.0425 MHz). A suitable IF must then be found with a corresponding LO frequency integrally related to 75.0425 MHz. The recommended choice is an IF of 267.35 MHz and a corresponding LO frequency of 13507.65 MHz, 180 times the reference frequency. This choice is also optimum from an implementation standpoint as a multiplication of 180 is readily achieved without high order multipliers. Additionally, this frequency plan has been analyzed for spurious response and no potential problems have been identified.

In estimating the required IF gain, TRW first chose a tunnel diode as the square-law detector (Section 3.4.4). The tunnel diode detector typically requires a signal level of about -30 dBm to optimize the square-law performance. From the TDRSS link budget (Section 3.11.4) the nominal signal level into the receiver front-end is -119 dBm. With a front-end gain of 25 dB, the signal level into the receiver IF is typically -94 dBm. Assuming 10 dB of excess gain for filter losses, cable losses, and AGC operation, an overall IF amplifier gain of 74 dB is required.

A potential problem with the single-conversion configuration is that the total required IF gain (nearly 80 dB) is at a single frequency and in a single package. If adequate shielding and RF bypassing are not provided, regeneration or oscillation can occur. TRW has fabricated IF circuits with more than 80 dB of available gain without instability by compartmentizing the gain within a machined aluminum housing, exercising adequate grounding precautions, and providing sufficient decoupling of dc power lines. TRW thus feels that single-conversion is practical without sacrificing stability.

Spurious responses are a potential problem with multiple conversions, although in a fixed-tuned receiver, as this is, the problem can be overcome with proper selection of frequencies. The use of double-conversion tends to complicate IF filtering as filters for two different frequencies are required and out-of-band rejection requirements become more stringent due to the additional spurious signals that must be filtered.

When tradeoffs involving system complexity are considered, the single-conversion receiver is clearly superior. The double-conversion receiver requires an additional mixer, an additional LO chain, and additional IF gain to overcome the mixer loss (assuming a passive mixer is used).

An additional consideration is the IF filtering required to band-limit the incoming PN signal spectrum to the first null. A 4-pole overall filter response with an equal ripple bandwidth of $\approx$6 MHz is utilized for this. This response is readily achieved in either receiver configuration with helical resonators, but with reduced size and weight at 267 MHz. This again favors single-conversion as it obviates the need for filters at a lower 2nd IF.

A summary of the receiver frequency conversion tradeoffs is presented in Table 3.4-3. TRW recommends the single-conversion design. This selection allows a minimum complexity design, with minimum power consumption but with a requirement for more stringent shielding and decoupling. TRW receiver designs routinely surpass these requirements, thus establish this as a low-risk approach.

Table 3.4-3. Frequency Conversion Tradeoffs

	Single-Conversion	Double-Conversion
Complexity	Minimum	Considerable — 2nd LO, mixer, 2nd IF filters, etc.
Stability	Careful shielding and decoupling	Less critical — Gain split between two frequencies
Potential spur problems	Less	More — Must identify and/or filter
RF compartment weight	Same	Same
Development cost	Minimum	Approximately 2 times greater

Recommended Approach

3.4.3 Local Oscillator

The recommended receiver LO configuration was derived from the tradeoffs presented in Section 3.3.2 for the transmitter frequency source. The required LO frequency of 13.50765 GHz is derived by multiplying the 75.0425 MHz reference oscillator by 180. As in the case of the TDRSS link transmitter, the final multiplier stage is mounted in the RF compartment. The S-band input (2.251275 GHz) to the multiplier can be fed up the mast via coaxial cable without excessive loss.

A block diagram of the LO is shown in Figure 3.4-9. The 75.0425 MHz reference oscillator is multiplied to 450.255 MHz in a transistor X6 circuit. Bandpass filtering of the multiplier output provides rejection of the undesired products. This output is fed to a second transistor multiplier, a X5 circuit, to generate the 2.251275 GHz signal. The S-band signal is then amplified to a level of +26 dBm and fed up the mast through coaxial cable to the X6 multiplier in the RF compartment. The cable loss up the mast is estimated to be 5 dB (30 ft of RG400) leaving +21 dBm of drive to the multiplier. The X6 multiplier, fabricated in waveguide, uses a varactor diode and waveguide output filter to provide a nominal +10 dBm to the receiver front-end. Each of these multipliers and amplifiers is nearly identical to those used in the transmitter frequency source (Section 3.3.2). The principal difference are minor tuned-circuit changes.

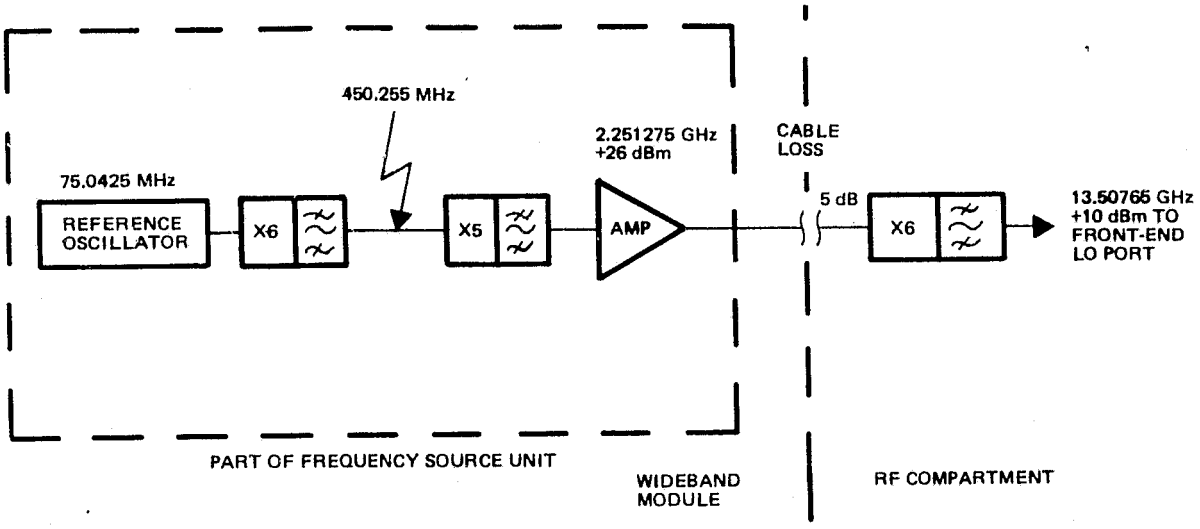

Figure 3.4-9. Receiver LO Block Diagram

Mechanically, the LO (excluding the final X6) consists of four small substrates located in the frequency source unit. Locating the LO in the frequency source unit allows minimum overall complexity since the LO shares the same reference oscillator as the two transmitters. A preliminary layout of the frequency source unit is provided in Section 3.3.4, including the LO portions.

The estimated dc power consumption of the LO is provided in Table 3.4-4.

Table 3.4-4. Local Oscillator Estimated Power Consumption

Reference oscillator	(Included in Section 3.3.2)		
X6 multiplier	+15 V	10 mA	0.15 W
X5 multiplier	+15 V	10 mA	0.15 W
S-band amplifier	+15 V	70 mA	1.05 W
X6 multiplier	—	—	—
		Total	1.35 W

3.4.4 Receiver IF Unit

The receiver IF unit (Figure 3.4-10) accepts the 267.35 MHz IF output from the receiver front-end and provides autotrack error signals as an output. A low noise hybrid IF amplifier provides 15 dB of gain to the IF signal and isolates the first bandpass filter from the loading effects of the receiver front-end and the interconnecting coaxial cable. The low noise figure of this amplifier (<2.5 dB) assures a low overall noise figure for the IF unit (<3 dB).

Two bandpass filters follow the first amplifier. Each is a 2-pole helical resonator design with a center frequency of 267.35 MHz. The composite response of the two filters is that of a 4-pole Butterworth with a 6 MHz passband. The estimated

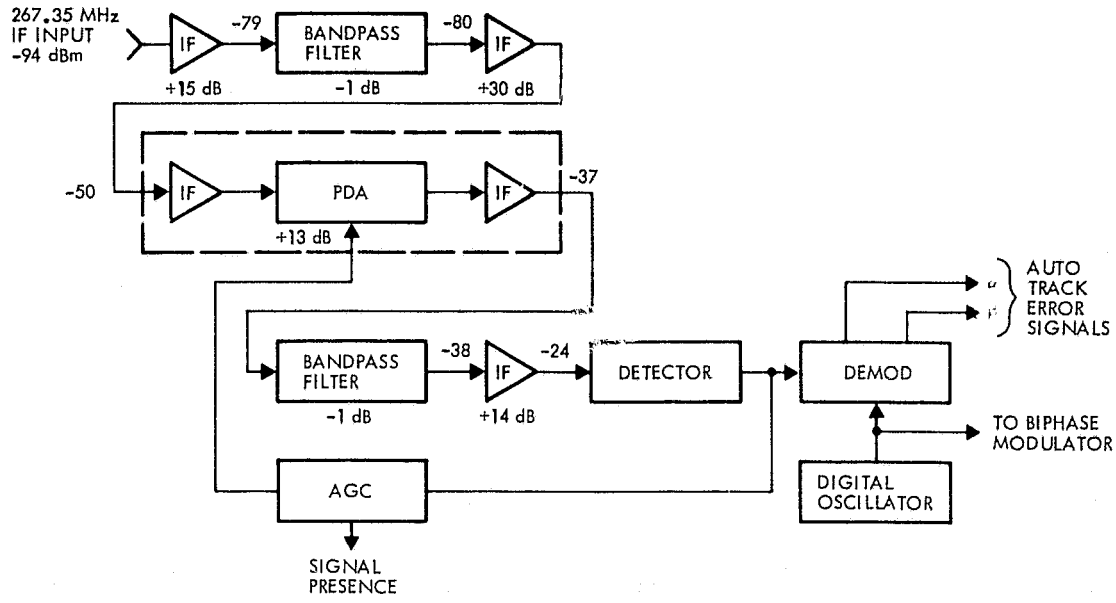

Figure 3.4-10. Receiver IF

insertion loss for each filter is 1 dB. Figure 3.4-11 is a photograph of a similar filter built for a space application. The IF filtering is accomplished at two separate points in the unit due to the relatively large amount of IF gain involved. Filtering must be provided near the beginning of the receiver IF to preclude the possibility of interference from out-of-band signals, while filtering near the detector is required to lower the out-of-band noise floor seen by the detector.

Two hybrid amplifiers follow the first bandpass filter. The first functions as a simple gain block (+20 dB). The second, built by Aertech Industries (a subsidiary of TRW), consists of two amplifier chips separated by a PIN diode attenuator (PDA). This amplifier, Figure 3.4-12, provides a 40 dB dynamic range (30 dB of gain to 10 dB of loss) making it an ideal AGC amplifier. In this application the nominal gain is approximately 13 dB, allowing the AGC to function 17 dB below the nominal levels. The PDA transfer curve is linearized with a single operational amplifier circuit, thus assuring nearly constant loop gain. The AGC amplifier is followed by the second bandpass filter and a third hybrid amplifier gain block (+14 dB). The amplifier circuits are mounted on small printed circuit cards in shielded compartments to assure stability.

A square-law detector follows the last IF amplifier. Two candidates were considered: a tunnel diode and a Schottky diode. A comparison between the two devices is presented in Table 3.4-5.

Table 3.4-5. Square-Law Detector Tradeoffs

	Tunnel Diode	Schottky Diode
Sensitivity (TSS)*	-46 dBm	-54 dBm
Dynamic range (square-law)	Up to 40 dB	Up to 50 dB
Temperature stability**	±0.5 dB	±2 dB

*Tangential signal sensitivity with 2 MHz video bandwidth.
**-65°C to +85°C.

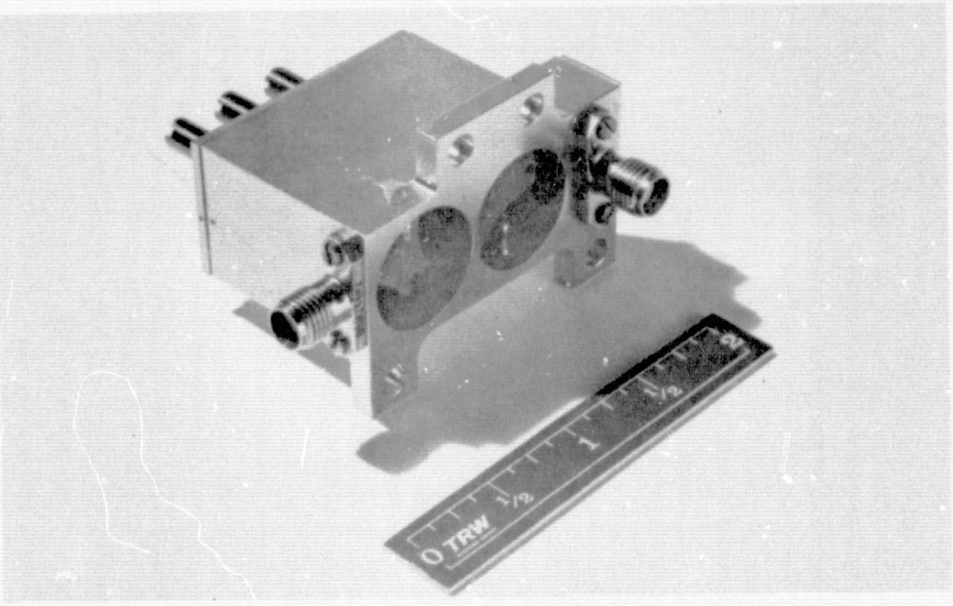

Figure 3.4-11. 2-Pole Helical Resonator Bandpass Filter

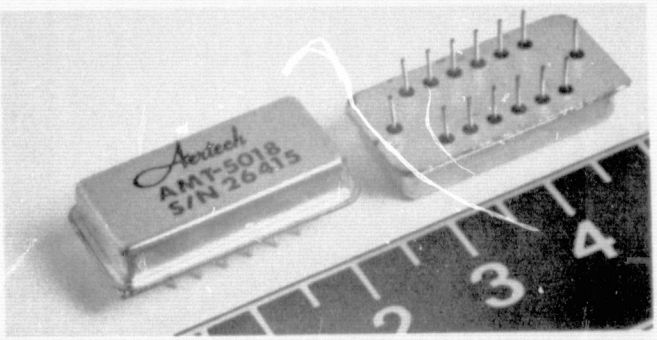

128803 6

Figure 3.4-12. AGC Amplifier

The superior temperature stability of the tunnel diode outweighs the slightly better sensitivity and dynamic range of the Schottky diode. Since the sensitivity and dynamic range of the tunnel diode is more than adequate, TRW has selected the tunnel diode detector. TRW has designed and flown similar detectors on previous programs. A typical transfer curve for a tunnel diode is shown in Figure 3.4-13. The recommended configuration provides a closed-loop IF gain of approximately 72 dB, thus setting the operating point of the detector at -24 dBm (with the expected unit input level of -94 dBm). The output of the tunnel diode detector provides AGC control and autotrack demodulator input. The AGC loop amplifies the detector output in an operational amplifier, chosen for exceptionally small drift. The AGC loop also contains an RC lowpass filter to provide a large (≈100 msec) closed loop time constant. The output of the RC filter then goes to the linearizer and PDA. An integrated circuit comparator contained in the loop provides a signal presence indicator for closed loop autotrack initialization.

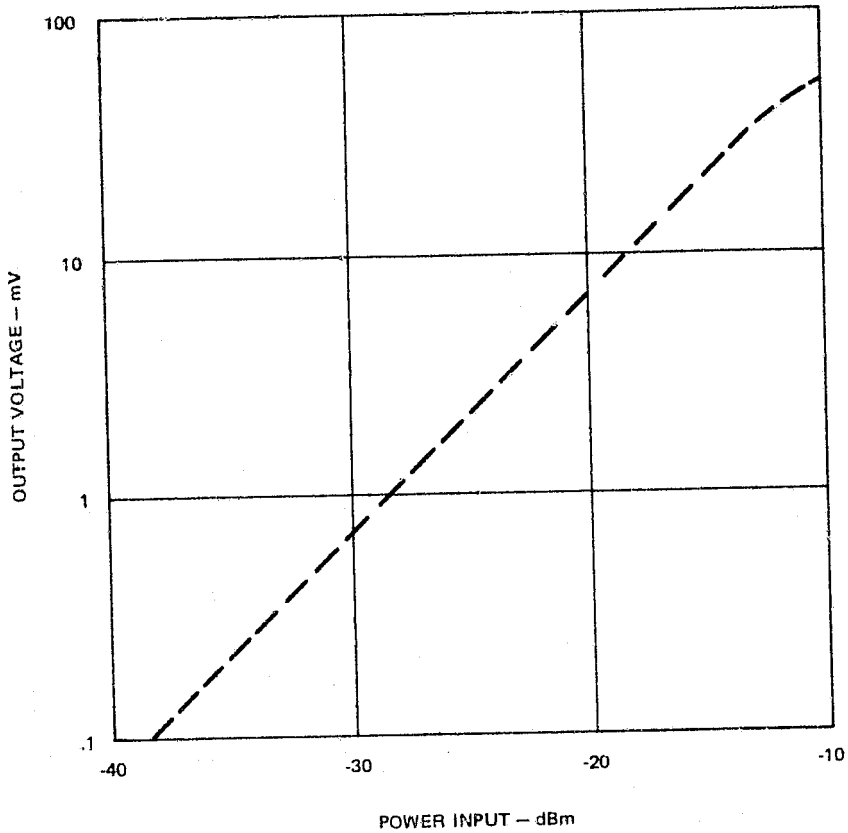

Figure 3.4-13. Typical Tunnel Diode Detector Response

The autotrack demodulator (Figure 3.4-14) demultiplexes the autotrack signal and provides autotrack error signals α and β outputs. The detector output is first amplified in an operational amplifier, then demultiplexed with FET switches by the digital

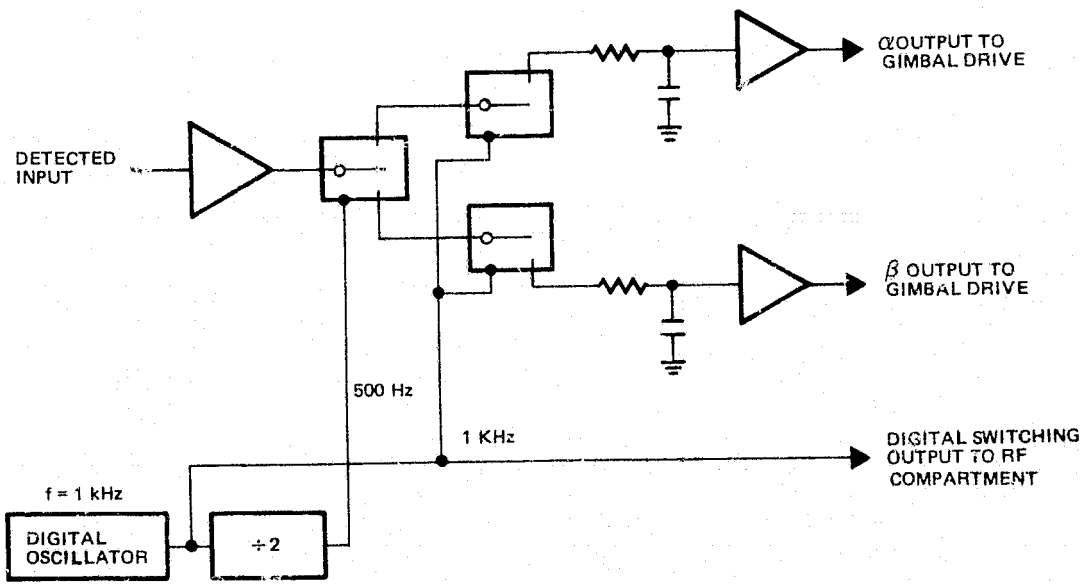

Figure 3.4-14. Autotrack Demodulator

switching signals. The switching signals are generated by a 1 kHz digital oscillator and divider. These signals interface directly with the FET switches and the 1 kHz signal is also fed up the mast to the RF compartment biphase modulator. The outputs of the FET switches are filtered in 50 Hz lowpass filters and amplified.

The complete receiver IF unit contains two identical IF strips (Section 3.4.5) to provide redundancy. Switching between the two IF strips is done with a coaxial latching relay on the IF input, and solid state switches for the outputs. DC power is switched with a latching relay. Table 3.4-6 presents the estimated power consumption for the receiver IF unit.

Table 3.4-6. Receiver IF Unit — Power Estimate

First IF amplifier	+15 V	10 mA	.15 W
Second IF amplifier	+15	23	.35
AGC IF amplifier	+12	40	.48
Third IF amplifier	+15	23	.35
AGC circuits	+15	25	.38
	-15	25	.38
Demodulator	+15	20	.30
	-15	20	.30
	+5	25	.13
Digital oscillator	+5	50	.25
Redundancy	+15	10	.15
	-15	10	.15
	+5	25	.13
Receiver IF total			3.5 watts

The entire redundant receiver IF unit is packaged in a single assembly approximately 2 x 4 x 12 inches in size. This assembly (Figure 3.4-15) is a machined aluminum housing fabricated with an "H" cross-section. One side of the center web has individual compartments containing the separate IF amplifier stages and bandpass filters. Interconnection between compartments is accomplished with ribbon leads, thus eliminating connectors. Partitioning the stages in this manner provides interstage isolation and assures circuit stability. The dc connections to each stage employ individual RFI filters, further enhancing circuit stability. The second side of the center web houses two identical printed circuit cards containing the redundant AGC and autotrack demodulator circuits. The estimated weight of the unit is 2.9 pounds.

3.4.5 Recommended Receiver Design Summary

A block diagram of the basic recommended receiver is presented in Figure 3.4-16. The TDRSS signal at 13.775 GHz is fed to the receiver front-end assembly. This assembly provides low-noise downconversion of the signal in an image-enhanced mixer followed by an IF preamplifier at the IF frequency of 267.35 MHz. LO injection at 13.50765 GHz is provided by a crystal oscillator/multiplier chain with the final multiplier, fabricated from waveguide, mounted at the antenna with the front-end. The remaining portions of the LO are mounted in the wideband module, interconnected with coaxial cable. The 267.35 MHz output of the receiver front-end is routed down the antenna mast via coaxial cable to the remaining portions of the receiver in the wideband module.

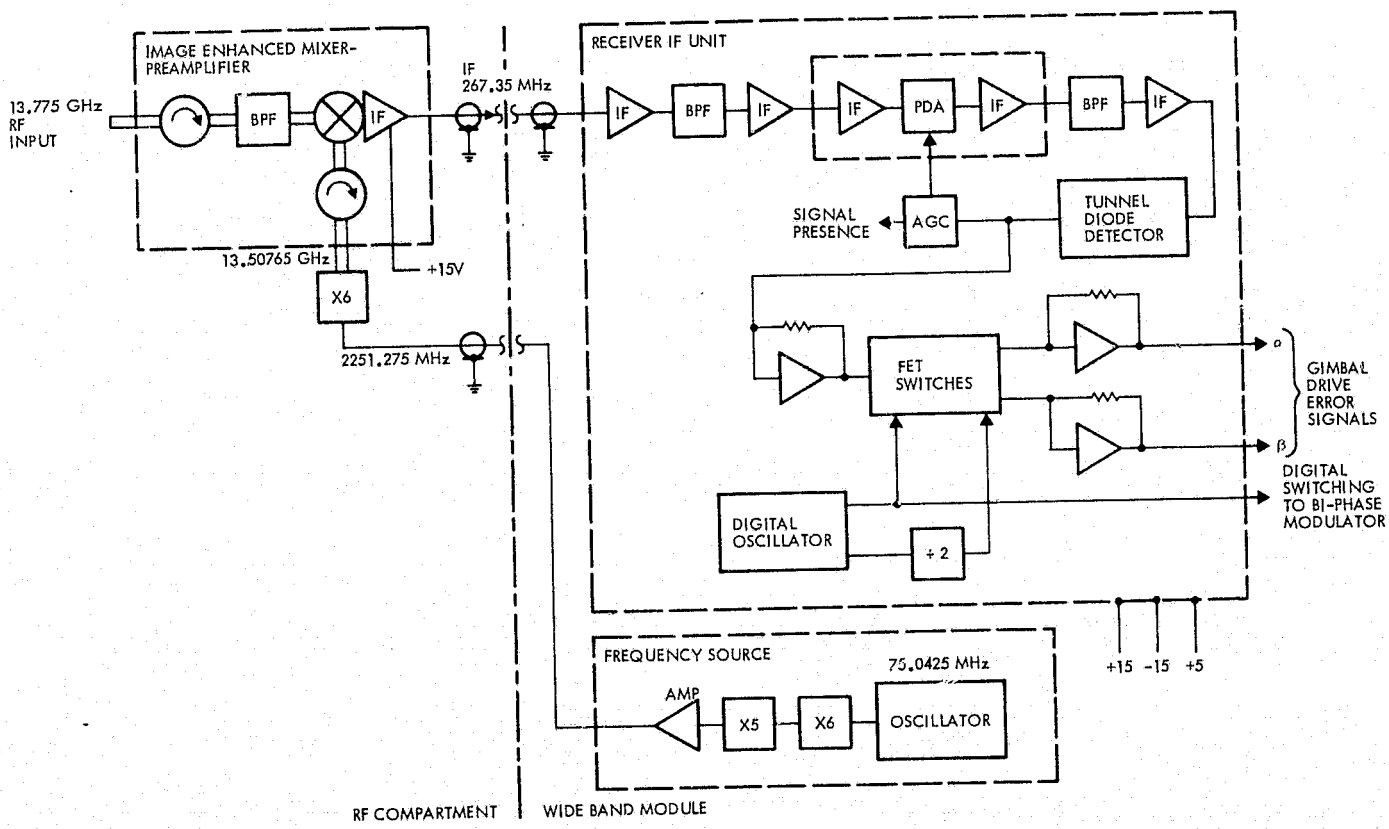

Figure 3.4-16. Tracking Receiver

The receiver IF unit contains the IF amplifiers, AGC, detector, and autotrack demodulator circuitry. It is located in the wideband module. The IF amplification and AGC functions are provided by four miniature, broadband hybrid circuit amplifiers. Two identical 2-pole helical resonator filters define the required 6 MHz bandwidth and provide out-of-band rejection of noise and undesired signals. The AGC gain control function is accomplished with a PIN diode attenuator (PDA) which is provided as a part of one of the four hybrid amplifiers. The square-law detector, which simultaneously provides an output for the AGC and the autotrack demodulator, employs a tunnel diode.

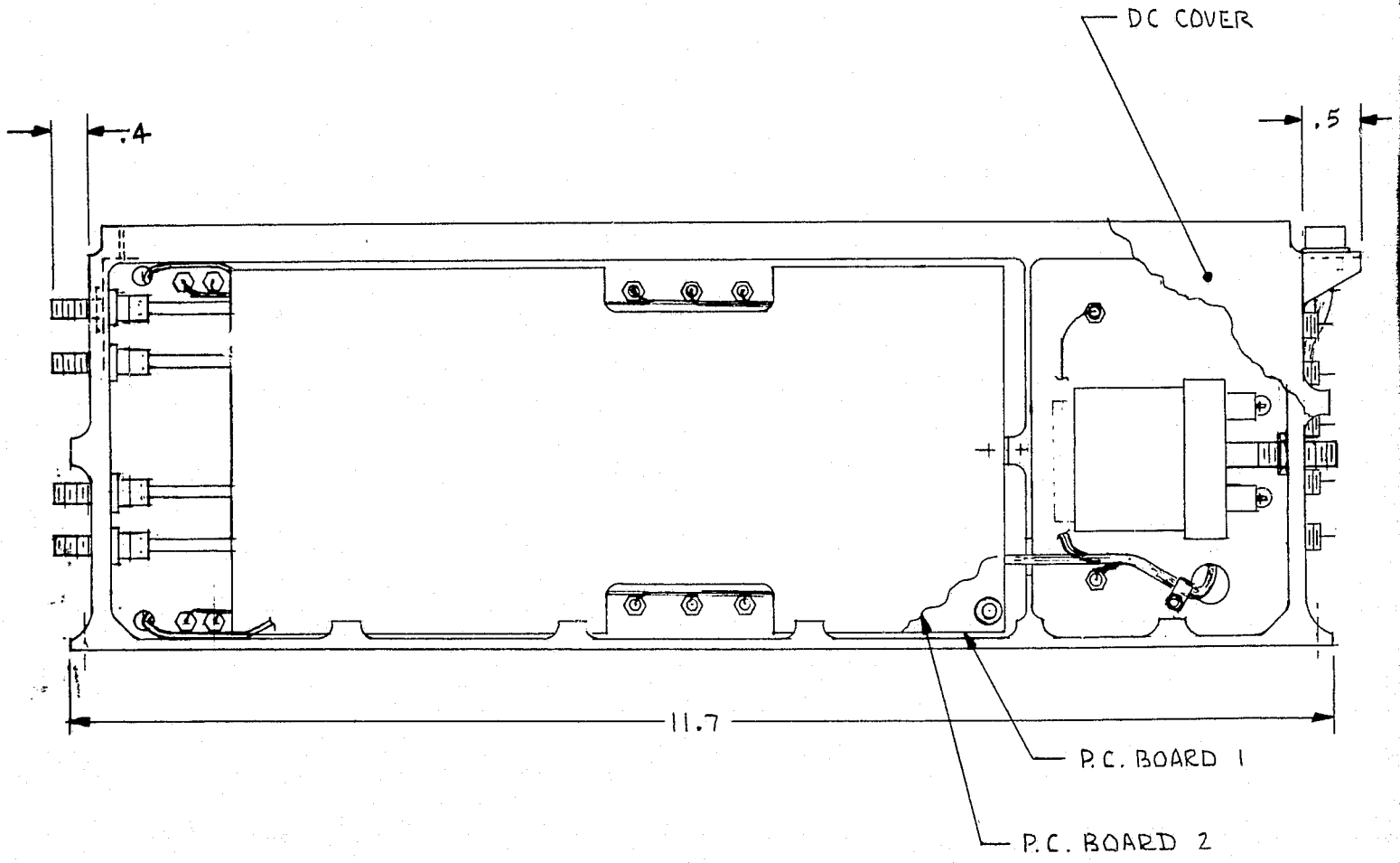

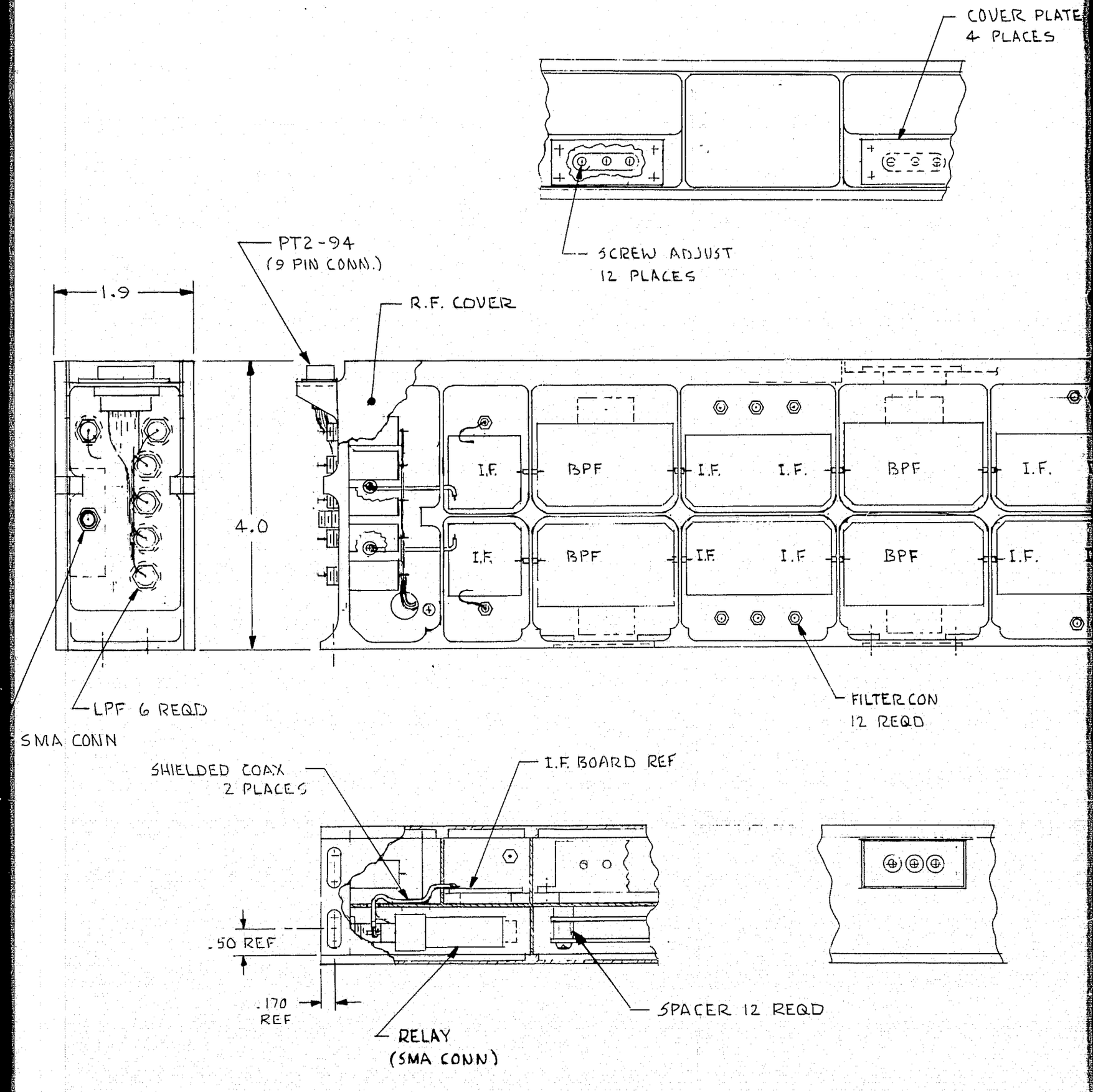

FOLDOUT FRAME 2

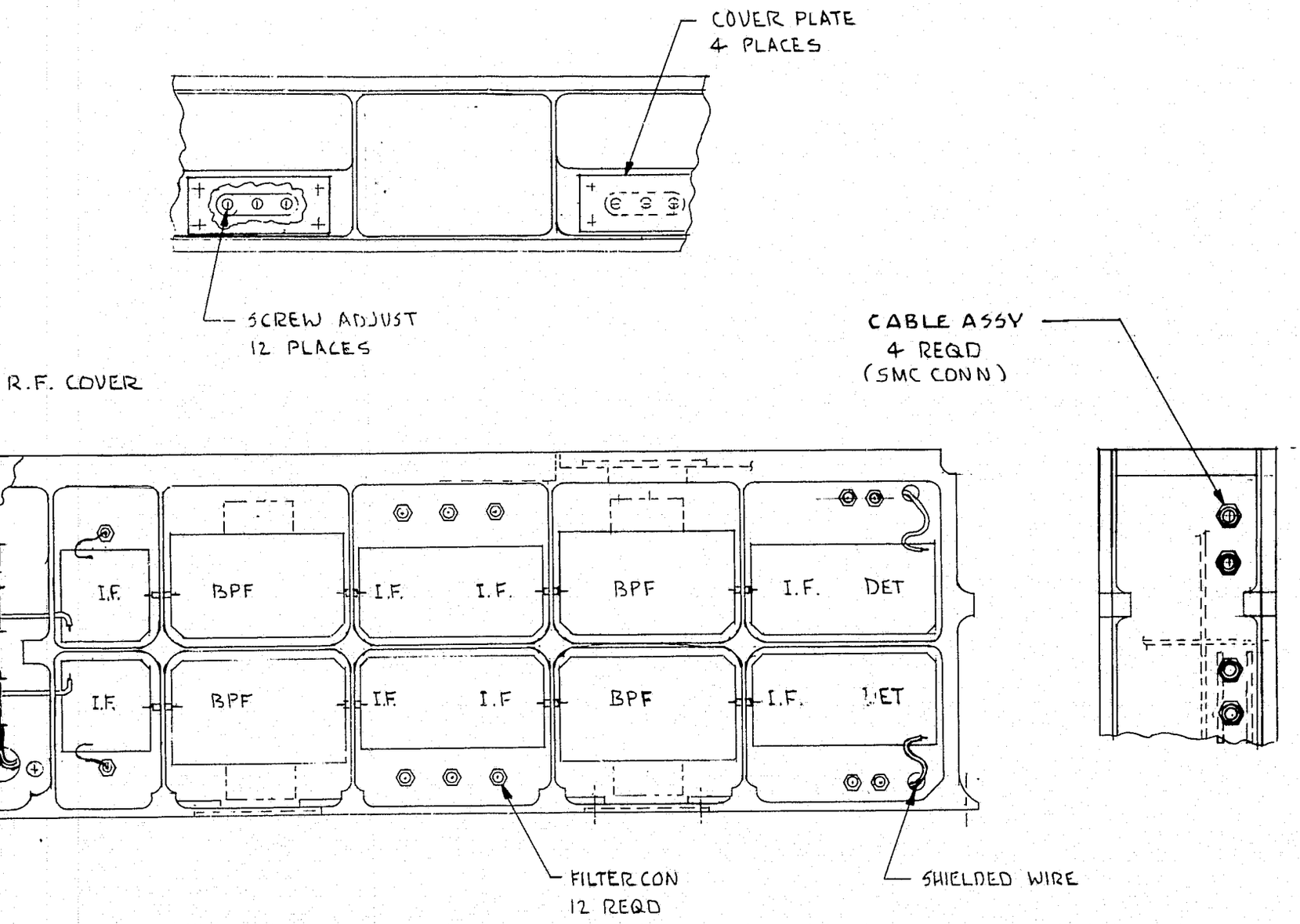

Figure 3.4-15. Receiver IF Unit Layout

The AGC circuit amplifies and filters the detector output and provides a current control to the PIN diode attenuator. An autotrack demodulator is used after the detector to extract the α and β error signals. The autotrack demodulator consists of a digital oscillator with time multiplexed outputs driving FET switches. The switch outputs, after amplification, become the autotrack error signals to the gimbal drive.

Redundancy is achieved in the RF compartment by two receiver front-ends with dedicated LO multipliers (Figure 3.4-17). RF switching is provided by a Ku-band waveguide switch on the input and coaxial switches for the multiplier input and IF output. These are space qualified latching type switches. A waveguide switch was selected for the input to minimize insertion loss (0.1 dB typical). Passive techniques for interconnecting these units using hybrid power dividers were not selected due to their inherent loss and subsequent impact on receiver noise figure and power consumption. The dc power to the front-end is switched to minimize power consumption. Switching is accomplished on command from the remote interface unit (RIU) by relay switches in each power supply lead.

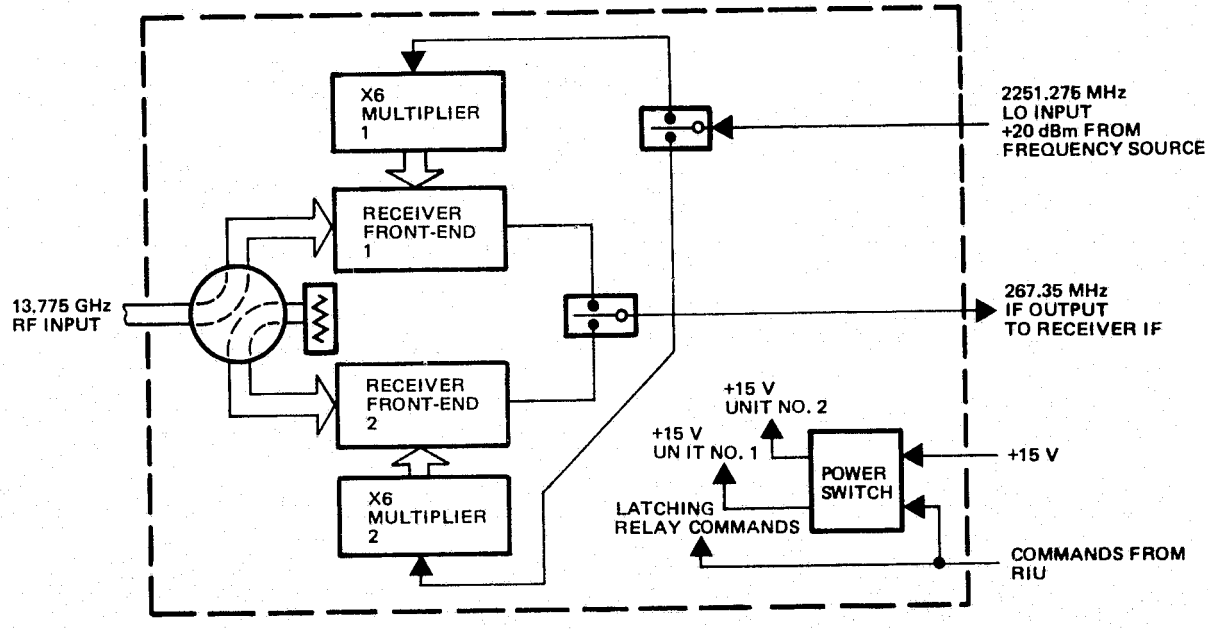

Figure 3.4-17. Receiver RF Compartment Redundancy

Two identical LO channels are provided in the frequency source (Figure 3.4-18). Output switching, at S-band, is again accomplished using relays. Distribution of the two reference oscillators between the two LO channels (and the four transmitter channels) is accomplished with hybrid power dividers. The use of passive distribution of the reference oscillators eliminates a minimum of four relays, thus reducing the size and complexity of the unit. The insertion loss of the hybrids is accounted for with slightly increased gain in each multiplier stage. DC switching of the two LO channels is accomplished with a single relay, commanded by the RIU.

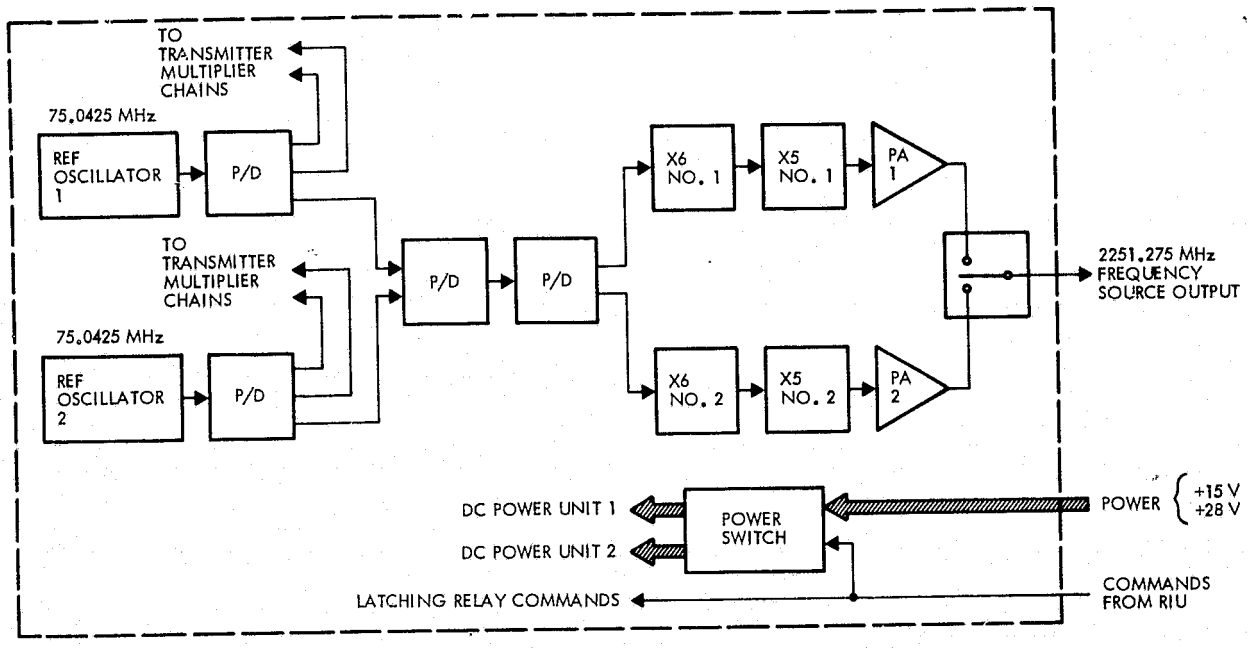

Figure 3.4-18. Receiver — Wideband Module Redundancy (Frequency Source Unit)

Redundancy in the receiver IF unit (Figure 3.4-19) is supplied by two complete receiver IF's, with selection provided by switches. The IF input is routed to the appropriate receiver IF with a coaxial relay identical to the one used in the RF compartment. Since the autotrack switching signal output is in a digital format, its switching function is accomplished with a digital integrated circuit, while switching of the tracking error signals (α, β), being analog, is done with FET switches.

The overall noise figure of the redundant tracking receiver can now be calculated from the information of this and previous sections. The circuit model of Figure 3.4-20 is used to compute the overall noise figure. The overall noise figure can be computed from

$$F = F + \sum_{n=2}^{5} \frac{F_n - 1}{\prod_{m=1}^{n} G_m}$$

where

F_n = noise figure of n^{th} stage

G_m = gain of m^{th} stage

Using the model of Figure 3.4-20, the typical and maximum noise figures are computed to be

$$F_{typ} \approx 5.6 \text{ dB}$$

$$F_{max} \approx 6.1 \text{ dB}$$

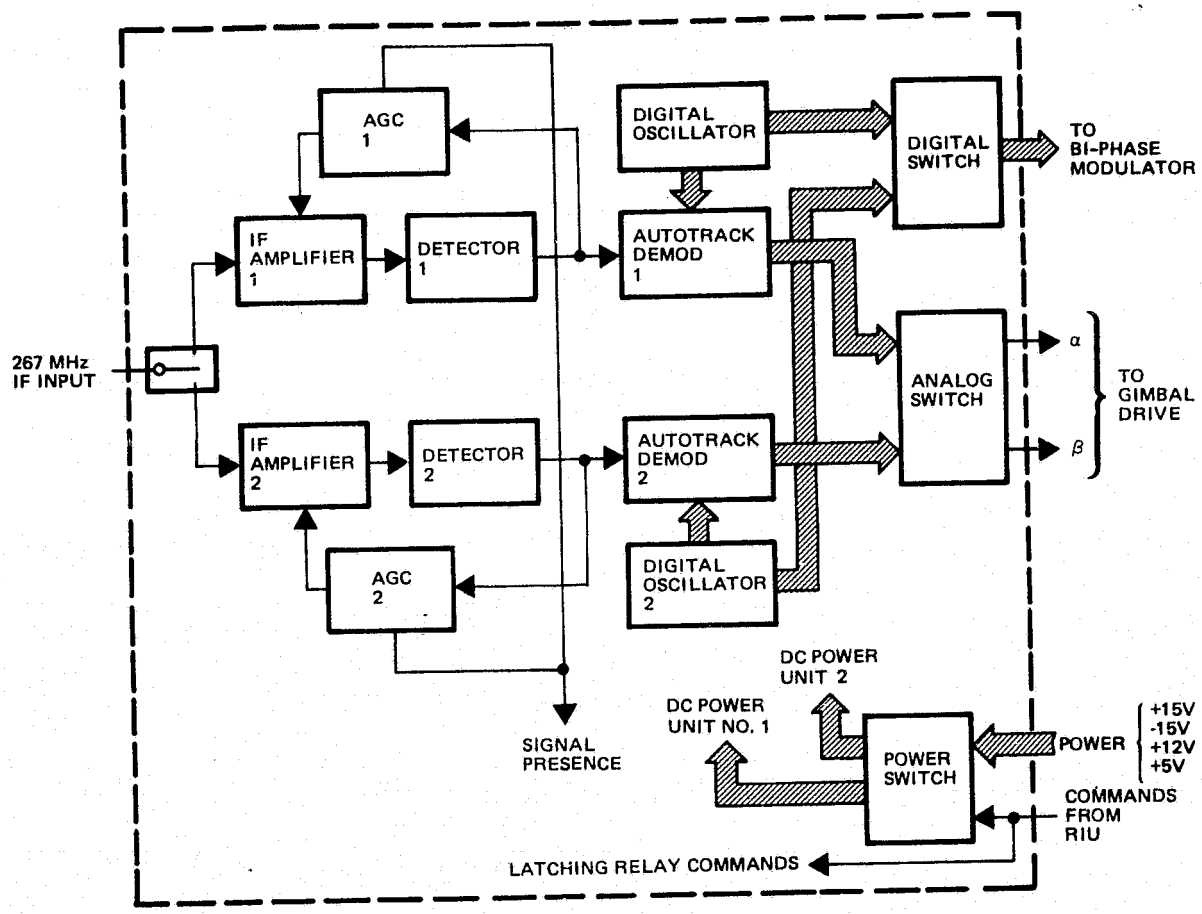

Figure 3.4-19. Receiver – Wideband Module Redundancy (Receiver IF Unit)

NOMINAL GAIN (dB)	-0.1	25.0	-0.3	-2.2	–
MINIMUM GAIN (dB)	-0.2	23.0	-0.5	-2.5	–
NOMINAL NOISE FIGURE (dB)	0.1	5.5	0.3	2.2	3.0
MAXIMUM NOISE FIGURE (dB)	0.2	5.9	0.5	2.5	4.0

Figure 3.4-20. Noise Figure Model

The rejection of spurious responses caused by 15.0085 GHz transmitter leakage is assured by the overall receiver design. The transmitter leakage (-50 dBm maximum) is rejected by a minimum of 30 dB in the image enhanced mixer. This rejection places the leakage level a minimum of 55 dB below the front-end output compression point of 0 dBm. Further rejection to out-of-band interference is provided by the two separate 2-pole IF filters.

During the evolution of the recommended receiver design, one of the goals was to minimize the dc power consumption. Table 3.4-7, summarizes the estimated total power for the receiver.

Table 3.4-7. Estimated Receiver Power Consumption

Unit	Current (amps)				Power (watts)
	+15 V	-15 V	+12 V	+5 V	
Receiver front-end	.055	--	--	--	.83
Receiver IF	.111	.055	.040	.100	3.48
Local oscillator (part of frequency source)	.090	--	--	--	1.35
Receiver total	.256	.055	.040	.150	5.66

Mechanically, the tracking receiver consists of three fundamental units: the front-end microwave components located in the RF compartment, the LO (portion of the frequency source unit) and the receiver IF located in the wideband module. The microwave components consist of the dual front-end units, the dual LO multipliers, and the relay switches for redundancy. The mounting of the individual units is shown later in the RF compartment layout (Figure 3.9-1) and the wideband module layout (Figure 5-1).

3.5 POWER CONVERTER

The power converter provides all of the regulated dc voltages needed for all of the electronics except the TWT. The unit is a high efficiency switching converter based on a Space Shuttle power converter design. The converter shown in Figure 3.5-1 features an energy-ladling buck-boost design in which the on-time of the inverter switching transistors is adjusted to maintain a constant output voltage over a wide range of load current variations. This ac control-loop approach inherently provides high input-output isolation.

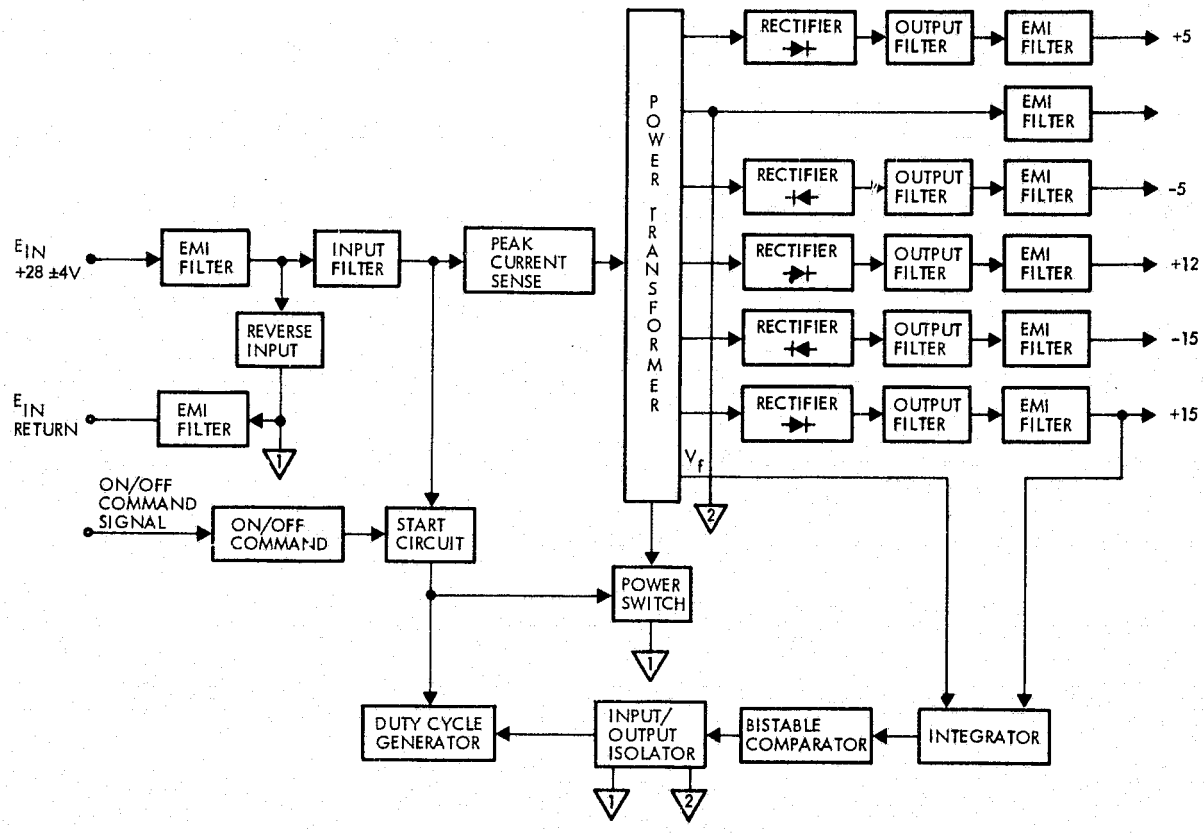

Figure 3.5-1. Power Converter

The design incorporates several key features:

- Peak current limiting. Peak collector current of the preregulator switching transistor is detected and used to terminate the on time when this current exceeds a predetermined safe level. The transistor, therefore, can never be overstressed as it would be during a momentary or accidental short circuit.

- Proportional base drive. The base drive current of the preregulator switching transistor is forced to be proportional to the collector current. This has the advantage of ensuring high efficiency under a wide range of load conditions; that is, when the load is light, less power is delivered to the base of the transistor since less power is required to maintain transistor saturation.

- ASDTIC control regulation. A control loop concept known as the "analog signal to discrete time interval converter" (ASDTIC) is used to obtain close regulation, excellent transient response, and wide bandwidth. Basically, this is a two-loop system where the average dc level is sensed, and an ac voltage proportional to the unregulated input voltage is sensed and integrated. A threshold detector converts this analog information into discrete time intervals which control the on time of the power switch. With the ac loop, the rate of change of the regulator duty cycle is not limited by the slow response of the dc loop. Wide bandwidth is obtained and high gain with stable operation is made possible.

- Overcurrent shutdown. A set of current transformers is used to detect a sustained overcurrent condition on each of the five output voltages. Should an overcurrent condition occur, a logic signal is generated and fed to the digital control processor portion of the power converter which in turn latches into an off state. The preregulator is therefore disabled until input power is removed and again applied.

- Overvoltage shutdown. The preregulator output is sensed and in the event of an overvoltage, a logic signal is generated and fed into the digital control processor which in turn latches the converter into the off state.

The converter output requirements are listed in Table 3.5-1.

Table 3.5-1. Estimated Converter Outputs

Output Voltages	+15 V	-15 V	+12 V	+5 V	-5 V
Output current (amps)	0.4	0.05	0.035	0.53	1.54
Power (watts)	6	0.75	0.42	2.7	7.7
Regulation (±%)	5	5	5	5	5
Ripple (mV p-p)	50	50	50	50	50

The power converter efficiency is approximately 75%, based on the Shuttle design. A detailed estimate of power converter output requirements is provided in Table 3.5-2. The corresponding primary bus input power is approximately 23 watts.

The power converter consists of 141 electronic component parts. Two power converters are packaged in a single housing measuring approximately 6 x 6 x 6 inches and weighing approximately 4.2 pounds. The estimated power dissipation is 5.9 watts with one converter in operation and one in standby.

Table 3.5-2. Estimated Power Converter Output Requirements

Receiver front-end	0.83 watts
Receiver IF unit	3.50
Frequency source unit	3.70
TDRSS QPSK modulator	1.90
STDN QPSK modulator	1.90
Digital interface unit No. 2	2.2
Digital interface unit No. 1	3.50
Total	17.53 watts

3.6 DIPLEXER

The diplexer is required to permit simultaneous LF/O Ku-band return link transmission to the TDRSS and forward link autotrack reception. A simplified block diagram is given in Figure 3.6-1. This section discusses the diplexer requirements and describes our recommended design.

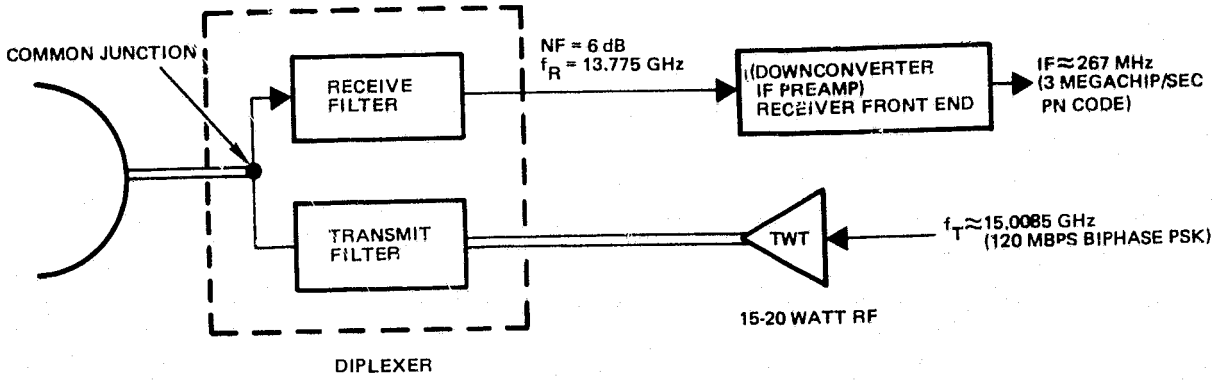

Figure 3.6-1. Ku-Band Diplexer for 6-Foot Antenna

3.6.1 Transmit Filter

Four factors must be considered in establishing the transmit filter attenuation characteristics:

- The amount of attenuation (α_1) required in the STDN/direct access band to prevent interference with this link; i.e., 23 dB at 14.768 GHz (Section 3.2.3)
- The amount of attenuation (α_2) present in the radio astronomy bands located at 16.375 GHz and 14.5 GHz (Section 3.2.4)
- The amount of attenuation (α_3) required in the receive band to prevent noise figure degradation due to regenerated spectrum sidelobes of the transmit signal
- The amount of attenuation (α_4) required in the receive band to prevent noise figure degradation due to broadband TWT noise.

The transmit filter attenuation requirements should not be excessively conservative or severe since this would result in a larger number of poles, increased passband insertion loss, and decreased EIRP for a given antenna gain and TWT power. In the event that additional filter requirements are identified at a later date, more bandpass poles can be added or an appropriate band reject filter included (as might be required for an identified out-of-band region spur or a more severe radio astonomy requirement).

Regenerated Transmit Spectrum Interference

The 120 Mbps spectrum component of the unbalanced QPSK signal is filtered prior to TWT amplification (5-pole filter, matched bandwidth of 240 MHz assumed). The TWT will regenerate, to some degree, the spectrum sidelobe structure "removed" by the input filter. The 10th low-side spectrum sidelobe falls into the autotrack receive band

(13.775 GHz ±3 MHz). Utilizing the TRW computer program previously discussed, the spectral density in the receive band is approximately 60 dB below the mainlobe spectrum density. By way of comparison, the spectrum density for a $(\sin x/x)^2$ spectrum in the 10th sidelobe region is 30 dB below the mainlobe spectrum density.

The spectrum density at the TWT output in the receive band, ϕ_R, is given by

$$\phi_R \text{ (dBW/Hz)} = (P_T - B) - S_3 = 13 - 80.8 - 60 \approx -128 \text{ dBW/Hz}$$

where

(P_T-B) = peak spectrum density of 120 Mbps biphase modulated TM signal at output of TWT (dBw/Hz)

P_T = TWT RF output power = +13 dBw (20 W)

B = bit rate bandwidth = 80.8 dB Hz (120 Mbps)

S_3 = relative amplitude of the TDRSS return link spectrum at 13.775 GHz ≈60 dB

Assuming that spectrum interference (treated as noise) should not degrade the receiver noise figure by more than 0.1 dB, the required filter lower skirt rejection (α_3) at the receive frequency is

$$\alpha_3 \text{ (dB)} = \phi_N - \phi_R - \Delta$$

where

ϕ_N = receiver noise density (NF = 6 dB) = -198 dBw/Hz

ϕ_R = spectrum density in receive band = -128 dBw/Hz

Δ = amount the attenuated transmit spectrum interference is below receiver noise density for 0.1 dB allowable noise figure degradation ≈17 dB

Therefore, α_3 = -198 - (-128) - 17 = -87 dB at 13.775 GHz.

Broadband TWT Noise

The TWT exhibits a broadband noise spectrum approximated by the TWT noise figure and gain. The output noise density (Figure 3.6-2) is

$$\Phi_o \text{ (dBW/Hz)} = KT + N + G$$

where

KT = noise density at 290°K reference = -204 dBw/Hz

N = TWT noise figure <28 dB

G = TWT small signal gain ≈60 dB

Therefore $\Phi_o \approx -204 + 28 + 60 = -116$ dBw/Hz

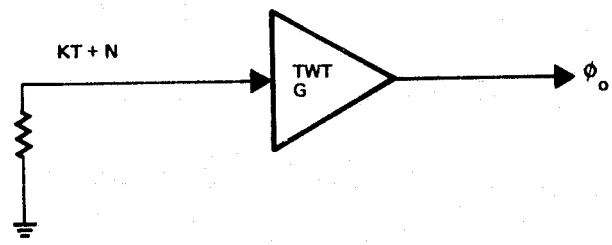

Figure 3.6-2. Output Noise Density

Assuming that the TWT noise should not degrade the receiver noise figure by more than 0.1 dB, the required transmit filter lower skirt rejection (α_4) at the receive frequency is

$$\alpha_4 \text{ (dB)} = \Phi_R - \Phi_o - \Delta$$

where

α_4 = required transmit filter attenuation, dB

Φ_R = receiver noise density (NF = 6 dB) = -198 dBw/Hz

Φ_o = TWT output noise density = -116 dBw/Hz

Δ = amount attenuated transmit noise density is below receiver noise density for 0.1 dB allowable noise figure degradation ≈17 dB

Therfore α_4 = -198 - (-116) - 17 = -99 dB at 13.775 GHz.

Selected Transmit Filter

A TE101 rectangular waveguide (WR-62) 0.01 dB ripple Chebyshev filter with five poles and a matched bandwidth of 240 MHz meets the attenuation requirements. Based on TRW design experience, an unloaded Q of 3900 is assumed. Table 3.6-1 presents a comparison of filter performance vs attenuation requirements.

3.6.2 Receive Filter

Passband insertion loss for the receive filter is not highly critical since the nominal C/N margin (≈ 10 dB) present in the tracking receiver provides good performance in terms of:

- Thermal noise induced angle jitter
- Noncoherent AGC
- Noncoherent signal presence detection.

Two factors were considered in establishing receive filter attenuation characteristics:

- The amount of attenuation, α_5, required at the transmit frequency to prevent receiver front-end overloading
- The amount of attenuation, α_6, at the image frequency (13.241 GHz).

Table 3.6-1. TDRSS Link Transmit Filter Performance

Item	Performance	Requirement
Passband center frequency	15.0085 GHz	15.0085 GHz
Passband width	240 MHz	225 MHz min
Passband insertion loss[1]		
14.8885 GHz	0.7 dB	Minimize
15.0085 GHz	0.5 dB	Minimize
15.1285 GHz	0.7 dB	Minimize
Receive frequency attenuation — 13.775 GHz	106 dB	$\alpha_3 > 87$ dB, $\alpha_4 > 99$ dB
Astronomy band attenuation — 15.375 GHz[2]	40 dB	α_2
STDN/direct access band attenuation — 14.768 GHz	26 dB	$\alpha_1 > 23$ dB[3]

[1] Includes 0.1 dB common junction loss

[2] Bounding case — requirement less severe for lower astronomy band at 14.5 GHz

[3] Includes 5 dB margin for computation uncertainties

Transmit Signal Leakage into Receiver

Direct leakage of the transmit signal power (center frequency = 15.0085 GHz) into the receiver must be sufficiently attenuated to avoid receiver desensitization due to mixer overload. For a typical receiver design, desensitization is avoided if the leakage level $P_L \approx -50$ dBm. Bandpass filters are included in the mixer and IF amplifiers so that the transmit signal leakage is subsequently attenuated to a negligible value and IF amplifier overloading is also avoided.

The required attenuation of the receive filter upper skirt at the transmit frequency is

$$\alpha_5 = P_L - P_T$$

where

α_5 = required receiver filter skirt attenuation, dB

P_L = allowable transmit power leakage into receiver = -50 dBm

P_T = TWT output power = 20 watts (43 dBm)

Therefore $\alpha_5 = -50 - 43 = -93$ dB.

Image Rejection

A receive image response will be present in a 6 MHz band, 2 x IF below the LF/O autotrack receive band. Hence the image band center is at 13.775 GHz - 2 x 0.267 =

13.241 GHz. An international and United States aeronautical radio navigation band (13.25 to 13.4 GHz, ref. 7) is located adjacent to the image band. An assessment of the possible interference environment due to these services is beyond the scope of this study. However, interference is not likely since the attenuation, α_6, at the image frequency for the selected filter, based on the transmit leakage signal criteria, is 85 dB. Further, the selected image-enhanced mixer provides an additional image rejection ratio of ≈25 dB, and the antenna sidelobe discrimination should be greater than 40 dB for ground based interference sources. The net rejection ratio is therefore 85 + 25 + 40 = 150 dB.

Selected Receive Filter

A TE101 rectangular waveguide (WR-62) 0.01 dB ripple Chebyshev filter with four poles and a matched bandwidth of 80 MHz meets the attenuation requirements. The design is identical to that of the transmit filter. Table 3.6-2 presents a comparison of filter performance vs attenuation requirements.

Table 3.6-2. TDRSS Link Receive Filter

Item	Performance	Requirement
Passband center frequency	13.775 GHz	13.775 GHz
Passband width	80 MHz	>6 MHz
Passband insertion loss* 13.775 ± 3 MHz	0.9 dB	
Transmit band attenuation 14.8885 GHz	101 dB	α_5 > 93 dB
15.1285 GHz	106 dB	
Image rejection — 13.241 GHz	85 dB	α_6**

*Includes 0.1 dB common junction loss.

**Image rejection of 25 dB provided by receiver front-end increasing total to 110 dB. Precise requirement not established.

3.6.3 Construction

Because of the benign temperature environment (Section 3.9.3), the use of graphite-epoxy or invar for temperature compensation is not required. Instead, an electroformed filter is recommended. The electroforming process is frequently utilized at TRW and yields filters with high Q's and low insertion loss. Unloaded Q's of 3900 or greater are consistently obtained at Ku-band. In addition, the precision of the electroforming process makes the filter's electrical characteristics repeatable to a high degree of accuracy.

3.7 TRACKING ANTENNA

The TDRSS link antenna provides a high gain data transmit and tracking receive capability, using right hand circular polarization, for TDRSS communication at Ku-band. The transmit frequency band is 15.0085 ±0.120 GHz and the receive tracking band is 13.775 ±0.003 GHz. A minimum antenna gain of 47 dBi is required over the transmit band and 46 dBi over the receive band. The antenna is mechanically steered on a gimbal assembly which is boom mounted.

3.7.1 Antenna Tradeoffs

Antenna Size vs Gain

Antenna gain is commonly defined as the ratio of the maximum radiation intensity in a given direction to the maximum radiation intensity produced in the same direction from a reference antenna with the same power input. If the reference is taken to be a hypothetical lossless antenna which radiates uniformly in all directions, the gain is said to be compared with that of an isotropic radiator having the same polarization. The directivity of an antenna is essentially the gain of a lossless antenna given by $G = \mu D$, where G = antenna gain, μ = antenna efficiency due to RF and VSWR losses, and D = antenna directivity.

For an array antenna, the directivity may be very high due to uniform aperture illumination but if the feed or VSWR losses are large then the actual antenna gain may be lower than an equivalent reflector antenna which has lower directivity but extremely high feed efficiency (μ). Also the beamwidth of the array is narrower than the equivalent size reflector antenna. Antenna directivity is a function of the aperture size, illumination distribution over the aperture, blockage, spillover, thermal and mechanical distortion errors, etc. These losses can be combined as the aperture efficiency of the antenna. Then we can formulate the following equation for antenna gain

$$G = \mu_L \mu_A D_A$$

where

G = antenna gain

μ_L = antenna efficiency due to RF feed and VSWR losses

μ_A = aperture efficiency

D_A = aperture directivity ($4\pi A/\lambda^2$) (where A = physical area of antenna)

An array antenna consisting of waveguide slots nominally has an aperture efficiency of 80 to 90% but may have a feed loss efficiency of 50% due to the feed complexity. A reflector antenna on the other hand may have an aperture efficiency of 60 to 70% with a feed loss efficiency of 90 to 95%.

Thus the gain of any particular antenna depends on the antenna physical aperture size, the aperture efficiency, and feed and VSWR losses. Figure 3.7-1 shows antenna gain as a function of size and aperture efficiency for relatively large aperture antennas (gains greater than 40 dBi). The figure shows that a reflector diameter of approximately 6 feet (28 square feet) provides a gain in the vicinity of 47 dBi.

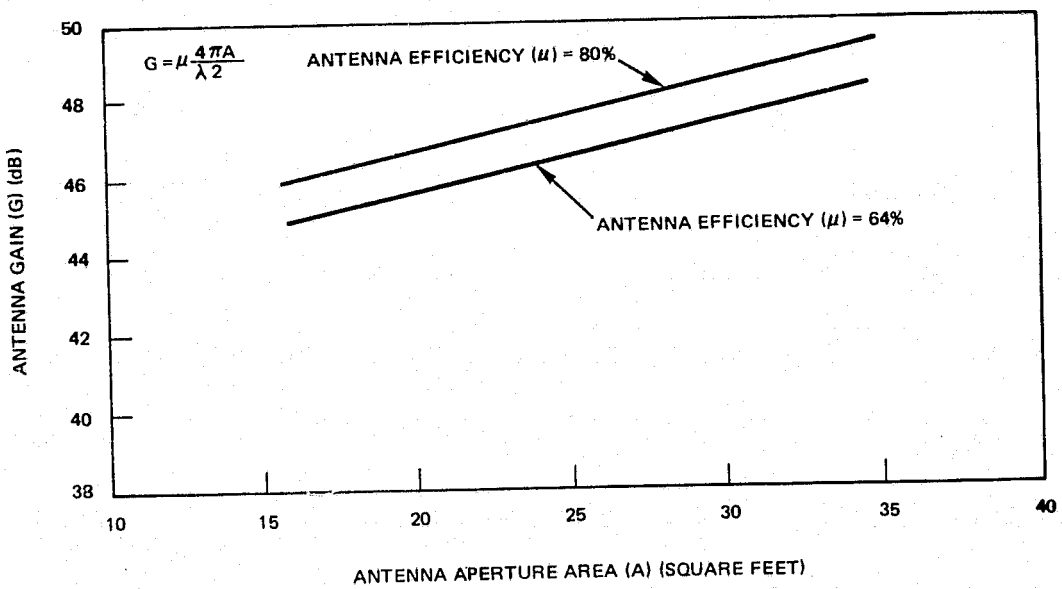

Figure 3.7-1. Antenna Size vs Gain

Radiation Patterns and Sidelobes

Maximum antenna gain from a fixed aperture size requires a uniform illumination over that aperture. For a square aperture, the first sidelobe level in the two principal planes occurs 13 dB below the main beam peak. For a circular aperture, the first sidelobe level is 17 dB below the main beam peak. If a lower sidelobe level is desired, the illumination function must be tapered over the aperture which reduces antenna gain. For any particular antenna system, a tradeoff between antenna gain and sidelobe level must be performed to determine the configuration and size of the antenna along with other possible constraints. For a shaped Cassegrain or planar array antenna, the first sidelobe level is approximately 19 dB below the main peak due to the near uniform illumination taper over the radiating aperture which provides the high antenna efficiency. If, for example, a very low first sidelobe level was desired, a sacrifice in antenna gain or an increase in antenna size would be required. Figure 3.7-2 presents a measured radiation pattern of a TRW 9-foot diameter shaped Cassegrain antenna at 15 GHz and provides the actual sidelobe response from this antenna. The sidelobe response from a 6-foot reflector operating at the same frequency would be very similar except for the slight expansion of the pattern on the degree (abscissa) scale. As shown in the above radiation pattern, the sidelobe level beyond the third sidelobe is approximately 40 dB below the main beam, whereas the far-out sidelobes are between 50 and 55 dB below the main beam. The 40 dB sidelobes result from feed horn spillover

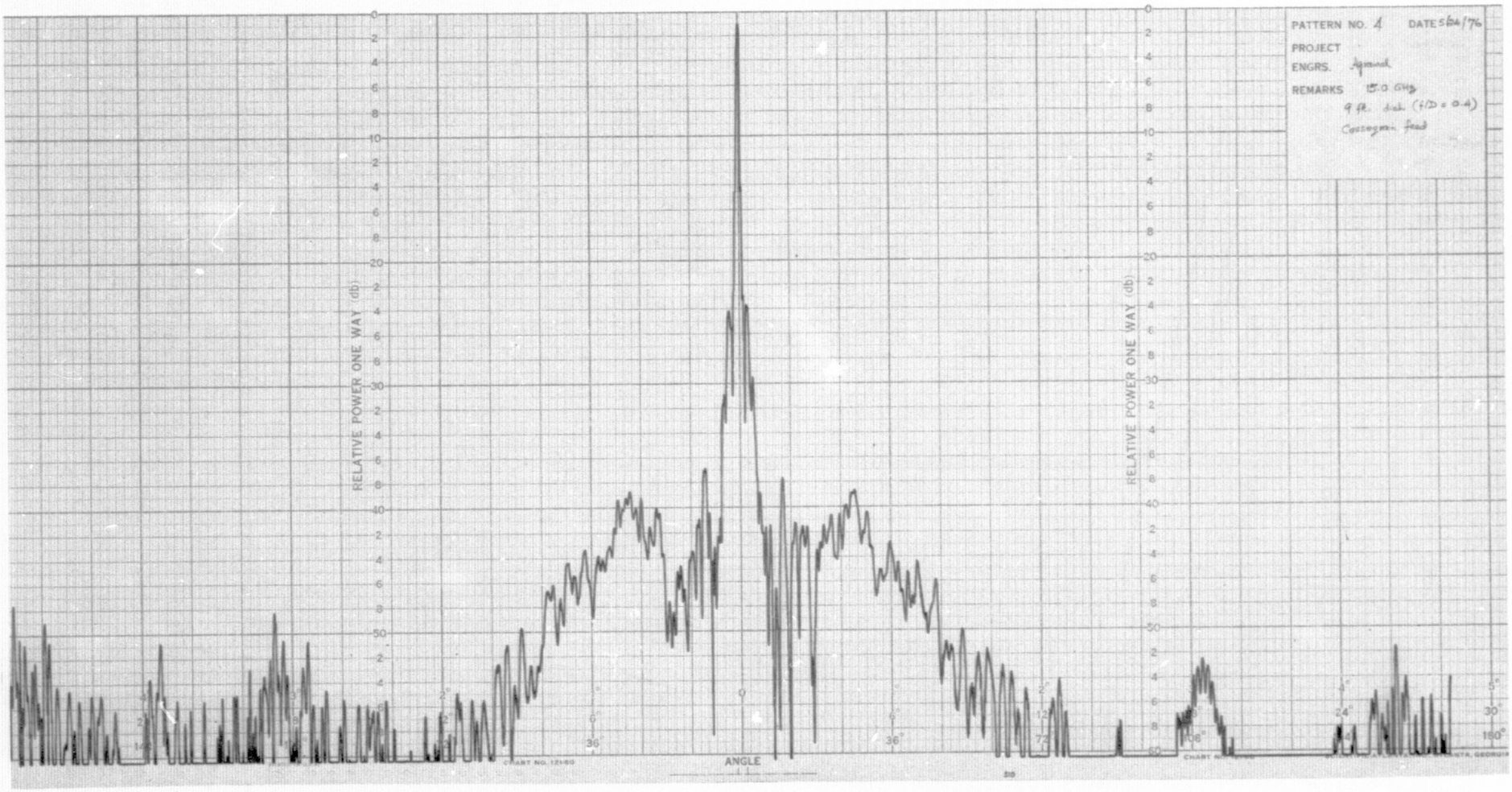

Figure 3.7-2. Measured Sidelobe Pattern Response on Antenna

beyond the edge of the subreflector and can be calculated by determining the relative gain of the spillover vs the peak gain of the main reflector. For example, a feed horn designed for a shaped Cassegrain antenna has a peak gain of approximately 18 dB. Using an illumination taper on the subreflector of 15 dB, which is typical for the shaped antenna design, the isotropic gain of the spillover energy at the edge of the subreflector is 3 dB. For a 47 dBi gain antenna, the relative sidelobe level of the spillover is 44 dB below the peak gain (47 dBi - 3 dBi = 44 dB). The far-out sidelobes (50 to 60 dB) result from blockage, edge diffraction, etc.

Planar Arrays

Consideration was given to either a planar array or reflector type antenna with respect to gain, efficiency, size, weight, complexity, and cost. At Ku-band, a waveguide slot planar array would provide the smallest aperture size for the desired gain (4.5 x 4.5 foot square).

Planar array antennas have the attractive feature of a thin form factor and high aperture efficiency. Autotracking can be obtained from the planar array by subdividing the aperture into four quadrants and feeding the outputs of each quadrant into a microwave comparator circuit. The comparator circuit consists of four magic tee's and provides the sum output along with the elevation and azimuth difference channel outputs. In this scheme, a phase sensing detector is used to compare each difference channel output with the sum channel or reference signal.

A calculation was performed of the number of slots required to fill the array to provide the transmit antenna gain (47 dBi). Assuming an aperture efficiency of 80% (typical of resonant waveguide slot arrays), the required aperture size at 15 GHz is a square, 4.5 feet on a side. Using a slot spacing of 0.7 λ (for maximum gain) requires a total number of slots approximating 8000 (2000 slots per quadrant). From this, the number of slots required for each waveguide is 45. This large number of slots greatly affects the bandwidth of the array. A general rule for array bandwidth is given by

$$B = \frac{140\ (S - 1)}{\pi\ N}$$

where

B = percent bandwidth

N = number of slots/waveguide

S = VSWR

For a maximum VSWR of 3.0:1, the bandwidth is

$$B = \frac{140\ (3 - 1)}{45\ \pi} = \frac{280}{45\ \pi} = 1.98\%$$

Obviously the quadrant array would have to be subdivided into a large number of small arrays to operate over a reasonable bandwidth. Meeting the required transmit/receive bandwidth would require each subarray to have no more than 10 slots

$$B = \frac{140\ (3 - 1)}{10\ \pi} = \frac{280}{10\ \pi} = 8.9\%$$

Because of the large number of subarrays required (approximately 200) for a common transmit/receive antenna and the complexity of the feed system, this antenna configuration presents an extremely high performance risk.

If separate transmit and receive slot arrays are used, the size of the combined apertures is larger than the equivalent reflector antenna which can be simply implemented to cover both transmit and receive frequency bands in a common feed system. Also the waveguide slot array requires a polarizer to provide the required circular polarization. The weight of the transmit and receive slot array antennas, including two polarizers, is greater than the single reflector antenna. The weight calculation assumes that both types of antennas are constructed from graphite reinforced fiberglass plastic (GFRP) and the polarizer converter is constructed from three sheets of 1 ounce copper on a 10 mil kelvar substrate. Therefore, the use of a plannar array antenna for this application has been set aside in favor of the reflector type antenna.

Reflector Type Antennas

A tradeoff between the Cassegrain and focal point fed antenna was performed. Two types of focal point fed reflector designs were considered along with the Cassegrain design:

- Center fed parabolic reflector
- Offset fed parabolic reflector
- Cassegrain relfector
- Dual-shaped Cassegrain reflector.

The center fed and offset fed reflectors require that the feed and comparator be placed at the focal point of the parabola. This configuration requires a set of waveguide transmission lines between the reflector/pedestal support structure and feed. For a tracking feed, the F/D ratio of the reflector is extremely important since the feed acts as an array with a narrower beamwidth than conventional feeds. The reflector half-angle must be relatively small, requiring F/D ratios greater than unity. Although wider beamwidth monopulse tracking feeds have been developed using dielectrically loaded waveguide, the effect of mutual coupling reduces the antenna efficiency and gain. The offset fed reflector does offer the advantage of eliminating blockage of the feed horns, comparator, and waveguide.

Maximum efficiency for a reflector type antenna is obtained when the feed energy is uniformly distributed over the reflector apeture. Since the density of the illuminating energy decreases parabolically with increasing illumination angle for all but the most exotic feeds, this condition cannot be realized with conventional parabolic reflector antennas. For example, nearly uniform reflector illumination can be achieved by designing the antenna to capture a small sector of the feed pattern, but at the expense of excessive energy being spilled beyond the edges of the reflector. Conversely, if the antenna is designed to capture most the main lobe of the feed pattern, and thus minimize feed spillover, inefficient reflector illumination results. Consequently, most all conventional reflector antenna designs are a compromise between feed spillover and aperture illumination with the typical reflector distribution being tapered so that energy at the edge is about 10 dB below that at the center. When these and other losses are considered, a well designed conventional focal point feed reflector antenna will have an operational efficiency in the neighborhood of 55 to 58%, depending on blockage.

The Cassegrain reflector antenna offers a design approach whereby both near-uniform aperture illumination and minimum feed spillover loss can be achieved with a conventional horn feed. This approach can only be used with relatively large reflector antennas (beamwidths less that 1°) due to subreflector blockage.

This high efficiency is based on the radiation pattern of the subreflector for a highly tapered illumination (low spillover). This radiation is fairly uniform over a large portion of the main reflector except near the edge, thus providing a more uniform illumination on the main reflector for a highly tapered subreflector illumination.

Dual reflector shaping of the Cassegrain antenna offers a higher efficiency design approach whereby a greater uniform illumination and minimum feed spillover loss can be achieved. It is based on a modification of the normally hyperbolic shape of the sur-reflector for the purpose of effecting a more uniform distribution of the feed energy. The central region of the subreflector is designed with a smaller radius of curvature in order to reapportion the higher density central rays to the otherwise less populated outer regions of the main reflector. Since the two reflectors operate in unison (e.g., parabola and hyperbola) to maintain a uniform phase front at the aperture plane, the main reflector must also be shaped to re-establish this condition, i.e., that all paths are equal between the feed phase center and the aperture plane (Figure 3.7-3). A further advantage of dual reflector shaping is that the subreflector/feed geometry can be designed to capture nearly all of the energy radiated from the feed since subreflector shaping corrects the inefficient illumination which would normally result. Figure 3.7-4 presents the diffraction scatter pattern for both the conventional and shaped Cassegrain subreflector.

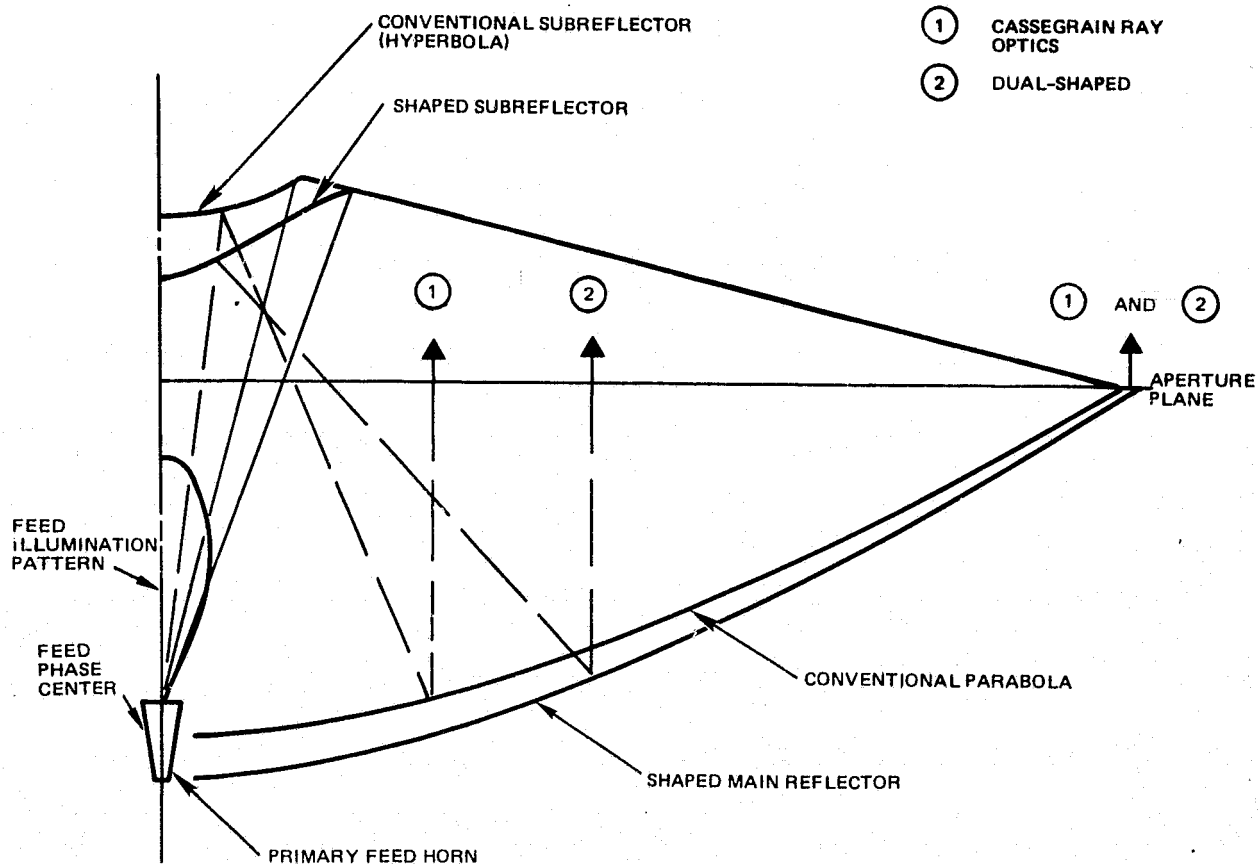

Figure 3.7-3. Geometries of Conventional Cassegrain and Dual-Shaped Reflectors

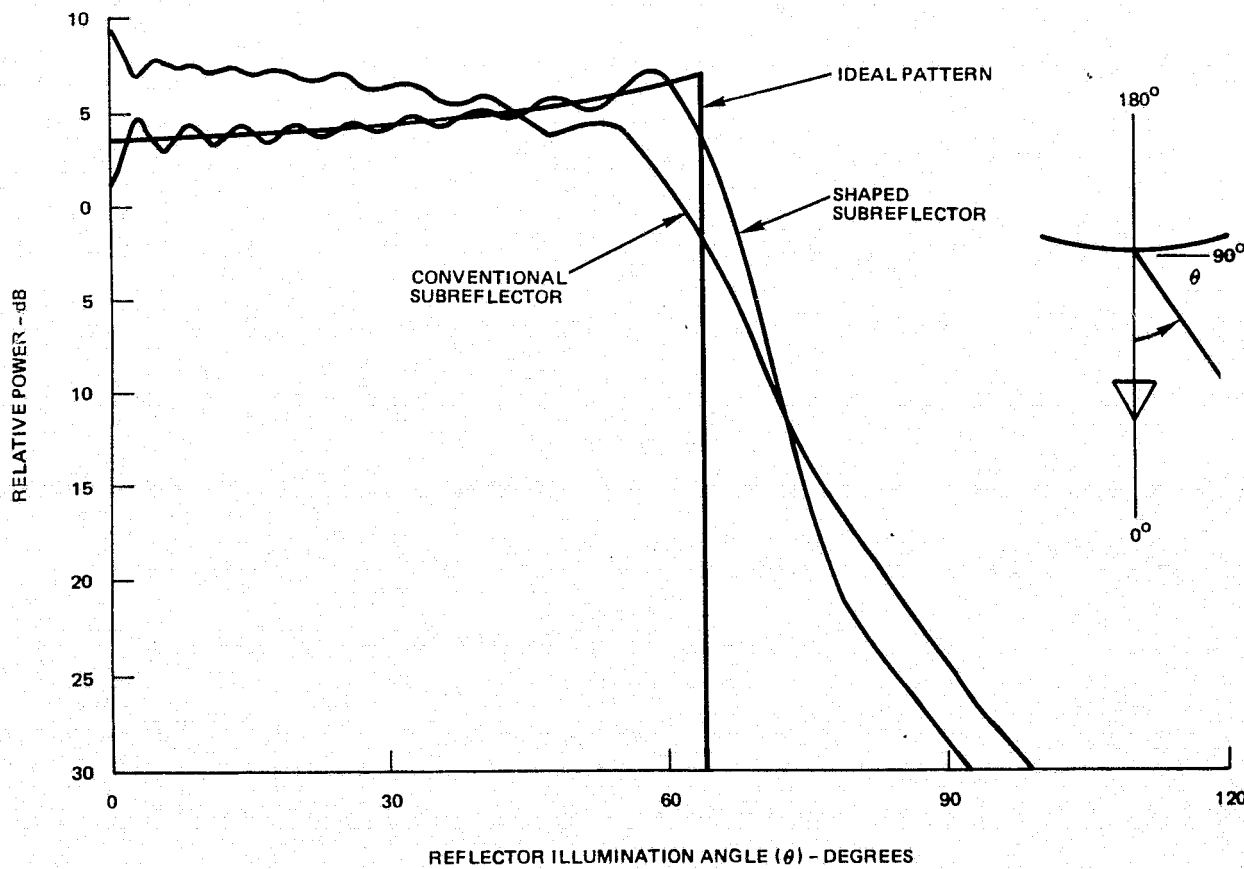

Figure 3.7-4. Shaped Subreflector Scatter Pattern

A dual reflector shaping computer model (SHAPE) based on the methods of Galindo (ref. 11) has been developed and is used for this design. Analysis of shaped antenna designs to determine the resultant performance is accomplished by calculating the secondary diffraction field. The model (CASSE) used was developed by TRW and involves a 2-dimensional vector integral representing the secondary vector field from a dual reflector antenna and is derived by integration of the induced surface currents on both the subreflector and main reflector (ref. 12).

Dual reflector shaping is in itself frequency independent. The performance improvement over the required bandwidth depends on minimizing the feed radiation pattern change over the bandwidth. The feed design is thus a dominant performance determining component.

Shaping theory allows for an endless number of design possibilities combining main reflector focal length to diameter (F/D) ratios and subreflector/feed geometries. In order to minimize the number of expensive performance calculations, the number of design possibilities and iterations were limited to a manageable few to establish performance and parametric characteristics of the recommended design (described below).

Cup turnstiles, diagonal horns, conical horns, corrugated horns, and multimode horn feeds have been developed and evaluated at TRW for use on many spacecraft. As a result of data accumulated from these many programs, corrugated conical horns have been shown to provide high efficiency performance over the largest bandwidth.

Autotrack Implementation

Closed loop autotrack capability can be achieved through various techniques such as:

- Amplitude comparison
- Phase comparison
- Conscan
- Other types of scan.

For the Cassegrain antenna design, the most practical and efficient autotrack scheme is amplitude comparison. Briefly, this consists of a multi-beam feed which is coupled to a comparator network consisting of four magic tee's. The output is three information channels giving a reference sum and communication RF signal, an α difference RF signal, and a β difference RF signal where α and β are orthogonal planes through the antenna's radiation patterns. For a five-horn feed system, an on-axis center horn designed for maximum efficiency is symmetrically surrounded by four small horns, and the output of the center horn is used directly as the reference RF signal while the other four smaller horns are combined through the comparator to provide the difference channel RF signals. This autotrack feed configuration provides maximum

main beam antenna efficiency and eliminates the comparator waveguide loss for the communication channel. Figure 3.7-5 shows a five-horn feed, three-channel autotrack configuration. Note that this configuration requires three RF receivers.

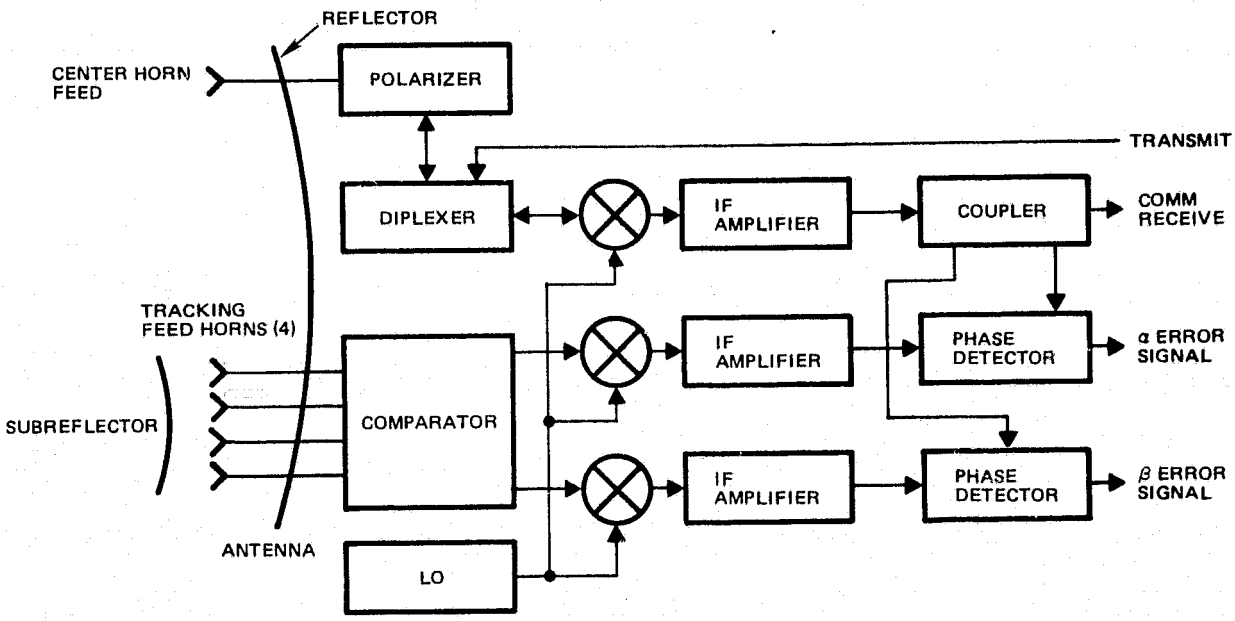

Figure 3.7-5. Five-Horn Feed/Three-Channel Autotrack

A single-channel autotrack configuration can be implemented which requires only a single RF receiver. This is accomplished by multiplexing the difference channel RF signals together and adding them to the sum or reference channel to form an amplitude modulated signal. Figure 3.7-6 shows the single-channel monopulse configuration.

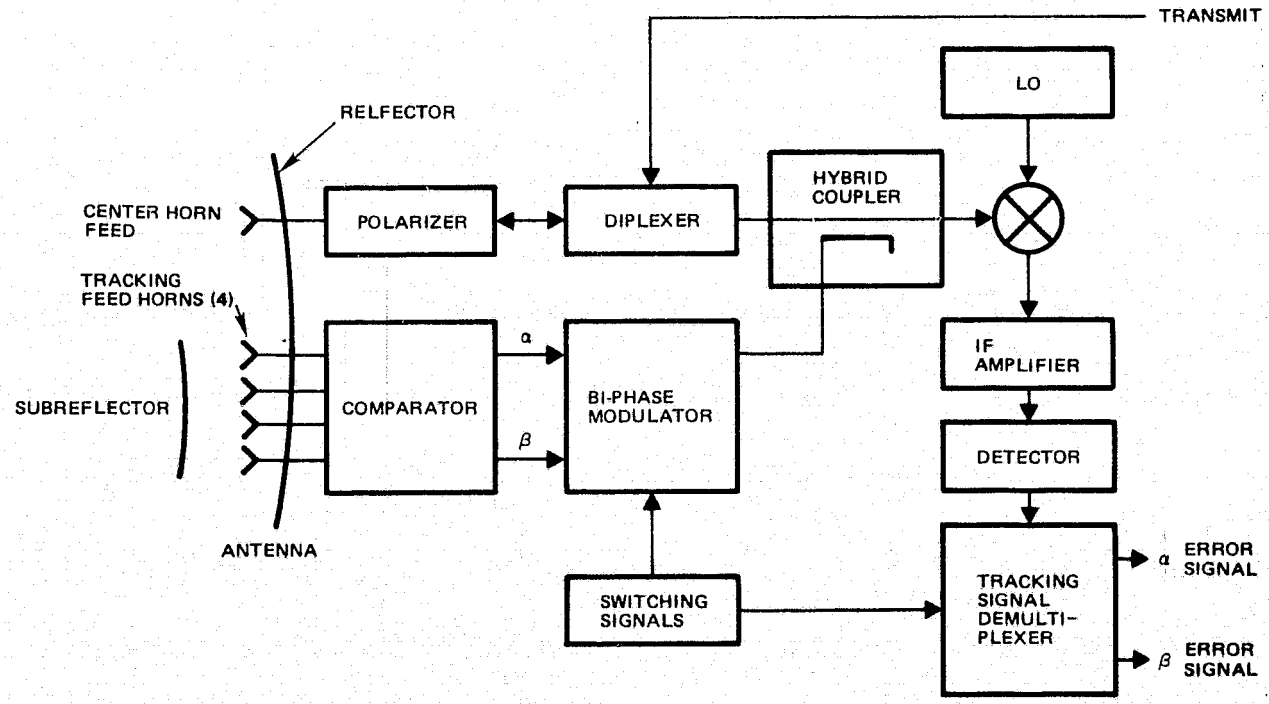

Figure 3.7-6. Five-Horn Feed/Single-Channel Autotrack

3.7.2 Recommended Antenna Description

The recommended Ku-band high gain antenna is a 6-foot diameter, shaped Cassegrain monopulse antenna operating at two frequency bands for both transmit and receive communication to the TDRSS. The feed is a five-horn autotracking design with a highly efficient broadband circularly polarized center horn which provides the communication channel along with the autotrack reference signal. A waveguide comparator consisting of four magic tee's is coupled to four symmetrically located linearly polarized horns and provides the autotrack difference channels for α and β tracking. Simultaneous transmit and receive on the communication feed horn is provided through a waveguide diplexer. Single-channel autotrack, as shown in Figure 3.7-6, is used to derive the tracking error signals. Table 3.7-1 presents a performance summary of the recommended antenna design.

Table 3.7-1. Shaped Cassegrain Antenna Performance Summary

Parameter	Transmit	Receive
Frequency	15.0085 ± 0.120 GHz	13.775 ± 0.025
Gain	47.04 dBi	46.02 dBi
Halfpower beamwidth	0.73^{o}	0.80^{o}
Polarization	RHCP	RHCP
Axial ratio	2.0 dB	2.0 dB
First sidelobe	>18 dB below peak	>18 dB below peak
Tracking error slope	N/A	0.79 V/deg/V
VSWR	<1.3	<1.3

Dual-Reflector System

The Cassegrain reflector system employs a shaped subreflector 10 inches in diameter which is focused in a 6-foot diameter parabola. Because of the use of a shaped subreflector, which provides increased antenna efficiency, the main parabolic reflector is actually a best fit parabola to meet the main reflector shaping criteria for a uniform phase distribution. By using a best fit parabola, the manufacturing is simplified without compromising antenna performance.

An analysis was performed to determine the optimum antenna geometry and subreflector diameter for maximizing antenna gain. The reflector diameter was held constant at a 72-inch diameter while the remaining parameters of the Cassegrain geometry, which optimize the peak gain at 15.0085 GHz, were varied. Figure 3.7-7 presents a sketch of the antenna geometry where the subreflector diameter (D_s), and the distance between the feed and the subreflector (L), were varied for fixed distances between the subreflector and the antenna focus (L_1).

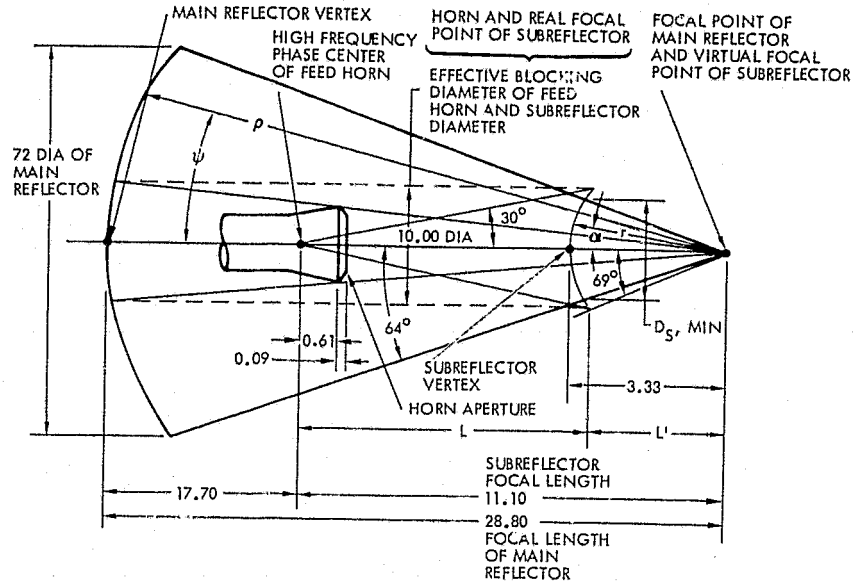

Figure 3.7-7. Cassegrain Antenna Geometry

Essentially, the task was performed by fixing two of the three unspecified parameters, while the other served to generate a curve. The value of D_s was set at an initial value of 9 inches and the gain of the antenna calculated for various values of L. The value of D_s was then increased to determine the optimum value for maximum gain. Figure 3.7-8 presents the results of the analysis and sets the value of D_s to approximately a 10-inch diameter for maximum antenna gain. For the above analysis, the subreflector half angle (θ_s) was maintained at approximately 30°. This value of subreflector half angle was selected from an evaluation of the feed horn pattern and provides a primary illumination taper of approximately 15 dB. Other subreflector half angles were studied, i.e., change of primary illumination tapers, with no increase in antenna gain. Therefore, this illumination seems optimum.

It should also be pointed out that the selected geometry provides the optimum blockage configuration where the feed blockage equals the subreflector blockage.

The final antenna geometry (Figure 3.7-9) uses a main reflector having an F/D ratio of 0.4 and a magnification factor of 2.33.

Operation of the 6-foot diameter graphite reflector at S-band, in addition to Ku-band, may be obtained through the use of a focal point S-band feed and dichroic subreflector. The dichroic subreflector is a single layer frequency selective surface which will reflect Ku-band but is transparent to S-band. Actual tests performed on a 9-foot Cassegrain reflector resulted in a reflection loss at Ku-band of 0.1 dB and transmission loss at S-band of 0.2 dB.

The 6-foot diameter reflector is a paraboloid of revolution sandwich shell with a focal length of 28.8 inches. The sandwich shell facesheets consist of four plies of celanese GH70 graphite fibers with Fiberite 934 resin as a prepreg. Each facesheet thickness is approximately 22 mils. Fiber orientation is designed to minimize weight, and thus the shell sandwich is mechanically balanced with minimum facesheet thickness.

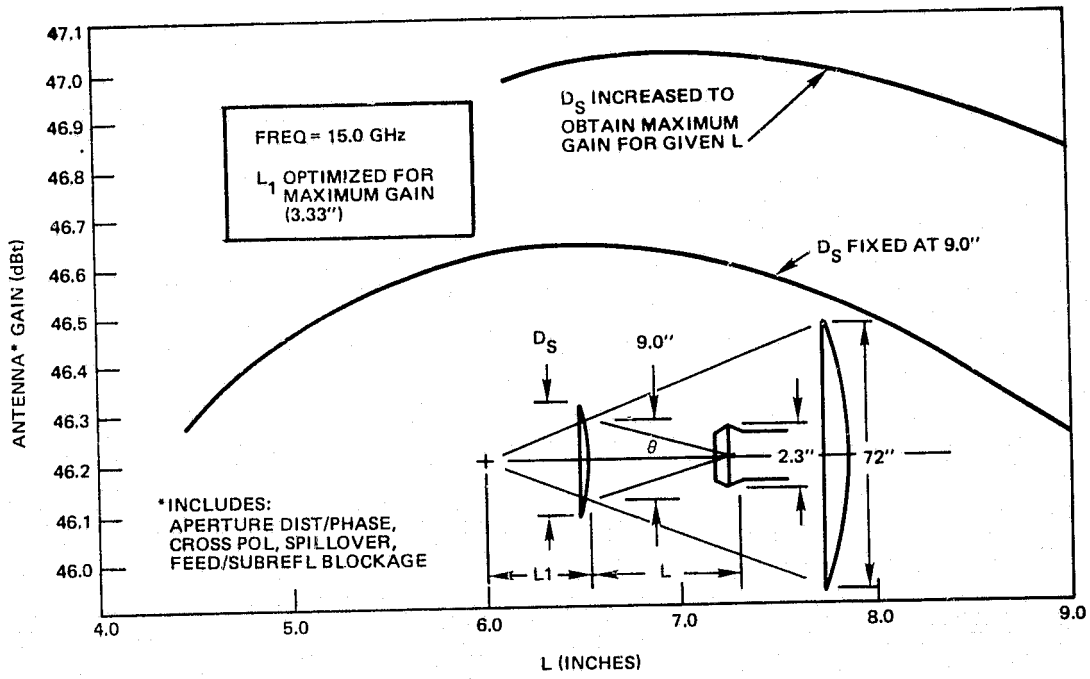

Figure 3.7-8. Gain vs Subreflector/Feed Spacing

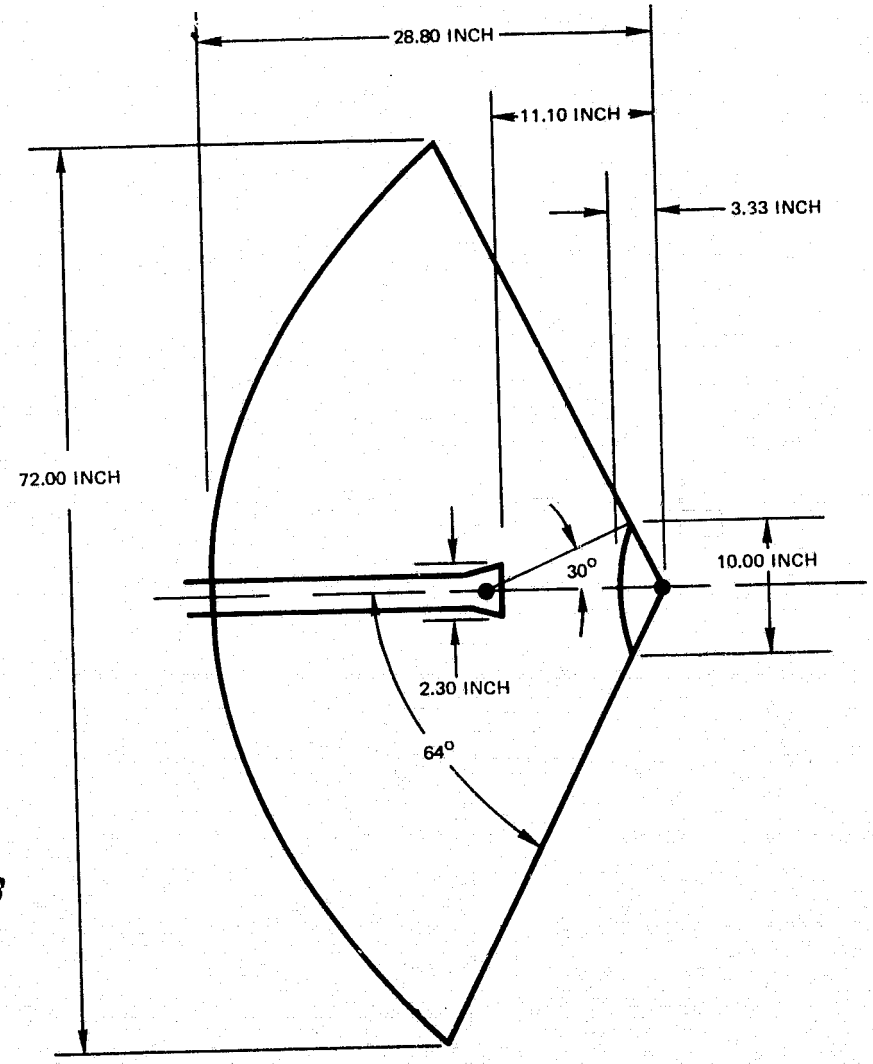

Figure 3.7-9. Recommended Shaped Cassegrain Antenna Geometry

A 0/±90/0 laminate is used in each of 12 pie-shaped segments and a circular center section to form the paraboloid of revolution. The honeycomb core is aluminum with a density of 3.1lb/ft^3. It has 0.125 inch cells and is made of 0.0007 inch foil. The core thickness is 0.5 inch. An adhesive system of FM123-4LVC epoxy is used to bond the facesheets to the core.

Vacuum deposited aluminum 4000Å thick is applied to the front face for the RF reflective surface. White paint, S13GLO, 0.005 inch thick is sprayed over the VDA for thermal control. The backside of the reflector is covered with a multilayered insulation blanket consisting of three layers of 0.25 mil aluminized Mylar with two outer layers of 0.5 mil aluminized Kapton.

A 1-inch thick Invar tube is used to form a 50-inch diameter adjustment ring which is attached to the backside of the reflector through adjustment screws which engage Invar fittings. The fittings are bonded to the reflector outer surface. The primary purpose of the ring is to permit adjustment of the reflector geometry and to retain the reflector accuracy to very close tolerances (0.003 inch rms), following its manufacture, over the thermal environment.

The subreflector consists of a spun aluminum surface and is attached directly to the reflector surface by three graphite epoxy struts (0.375 inches in diameter). The total weight of the dual reflector assembly is approximately 20 pounds.

This construction technique has been used on past flight tested antennas with excellent performance. Figure 3.7-10 presents a picture of a TRW developed flight proven GFRP Cassegrain antenna which is undergoing holography testing to accurately measure its surface. Figure 3.7-11 shows the same antenna being RF radiation pattern measured on the antenna range.

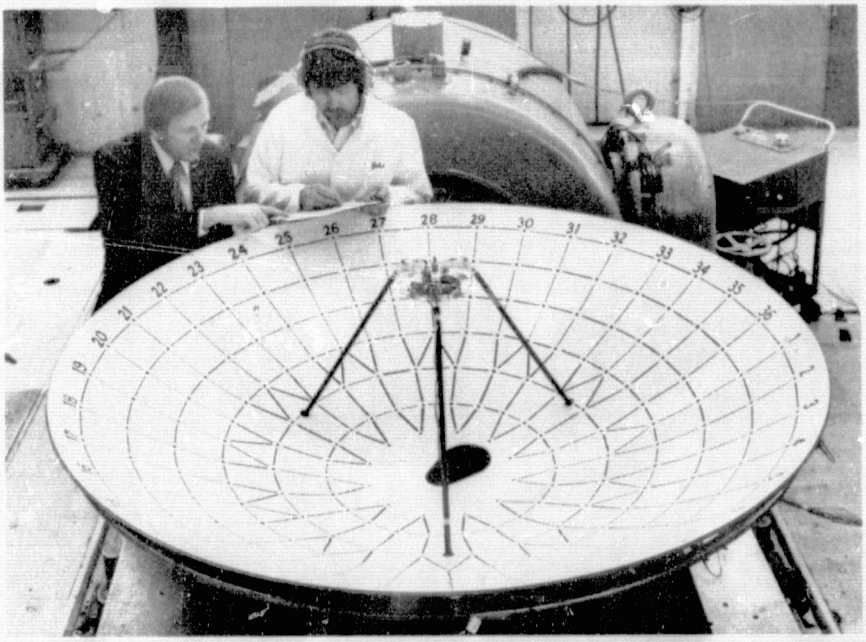

Figure 3.7-10. GRFP Cassegrain Antenna Reflector Undergoing Surface Measurements

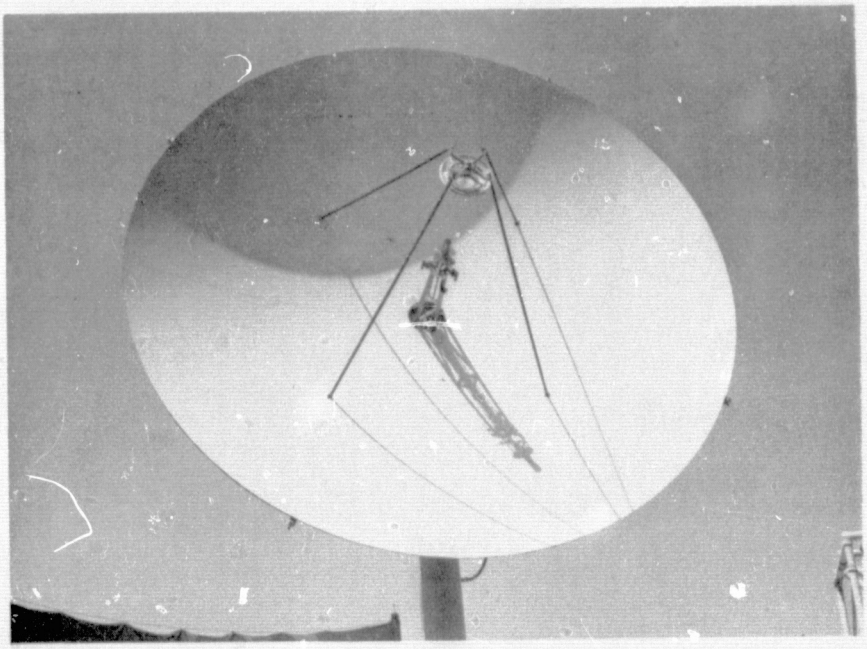

90900 1

Figure 3.7-11. 9-Foot GRFP Cassegrain Autotrack Antenna on RF Range

Using the above construction technique provides an extremely stiff antenna reflector with minimum weight and which has been test proven on various spacecraft programs.

Feed System

The Ku-band feed is a combined communications and autotracking design for a dual-shaped Cassegrain reflector system. Candidate designs are limited because of the relative wide bandwidth, 13.750 GHz to 15.121 GHz, and highly efficient feed patterns required (low sidelobes and equal E and H-plane beamwidths). The requirement for maximum antenna gain over the transmit data channel (15.0085 ± 0.120 GHz) was a key design determining factor. These requirements established the five-horn autotracking concept as the design approach over a four-horn system or a more exotic feed approach. The center horn in a five-horn feed design can be broadband and yet provide high illumination efficiencies.

The conical corrugated horn was selected as the data channel horn because of its superior RF performance over large bandwidths. The corrugated horn produces radiation patterns which are remarkably free of sidelobes and have very low radiation in the back direction over a broad band of frequencies. The horn is constructed by replacing the metallic walls of a conventional horn with corrugated surfaces operated in a cutoff condition. In addition to the low side and backlobe radiation levels, these corrugations serve to provide a radiation pattern with nearly identical E and H-plane beamwidths and coincident phase centers. Hence, the corrugated conical horn is the most nearly optimum feed for a reflector with either circular or linear polarization applications.

The low side and back radiation is obtained by eliminating the diffraction which occurs at the edge of the horn aperture, particularly in the E-plane. The corrugated surface, designed to cut off surface wave propagation, must present a negative reactance to the incident wave. To a first approximation, the surface reactance $\overline{X}_s$ is given by

$$\overline{X}_s = \frac{g}{g + t} \eta \cos (kd)$$

where

g = corrugation gap width

t = corrugation tooth width

d = slot depth

k = propagation constant ($2\pi/\lambda$)

η = free space impedance (120 π ohms)

λ = wavelength

This expression is valid provided that $t \leq g/10$ and $g \leq \lambda/10$.

An existing Ku-band corrugated horn, which has been developed on a previous spacecraft program for a Cassegrain antenna operating over a similar bandwidth and frequency, is used for the center horn. Figure 3.7-12 presents a picture of the existing corrugated horn along with a radiation pattern measured at 15.0085 GHz using a rotating linearly polarized source antenna.

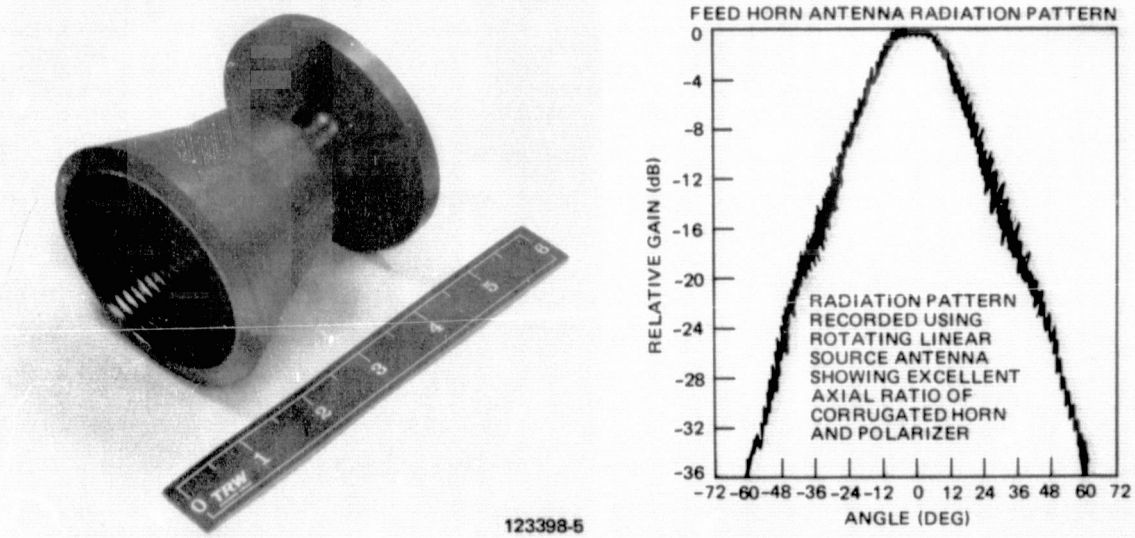

Figure 3.7-12. Ku-Band Corrugated Horn

Circular polarization is obtained in the center corrugated horn through the use of a waveguide iris type polarizer. The polarizer consists of nine symmetrical irises formed inside circular waveguide. The irises are spaced a quarter of a guide wave-

length apart and can provide extremely small axial ratios over relatively wide bandwidths. Right hand circular polarization is obtained by introducing an electric field vector at a 45° angle to the irises. The orthogonal field components of this field vector pass through the irises with unequal insertion phase. By choosing the proper relative iris dimensions, phase orthogonality is obtained and circular polarization is produced.

A polarizer of this type has been developed on the same program as the corrugated feed horn and can be used "as is." Figure 3.7-13 shows a picture of the polarizer and presents the measured axial ratio vs frequency and temperature.

POLARIZER DERIVED FROM EXISTING KU-BAND PROGRAM

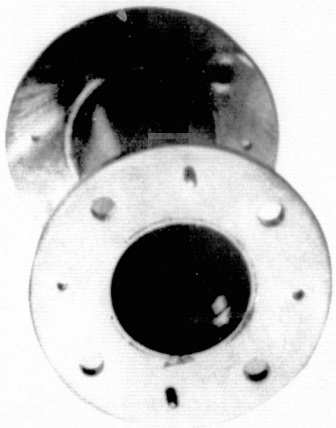

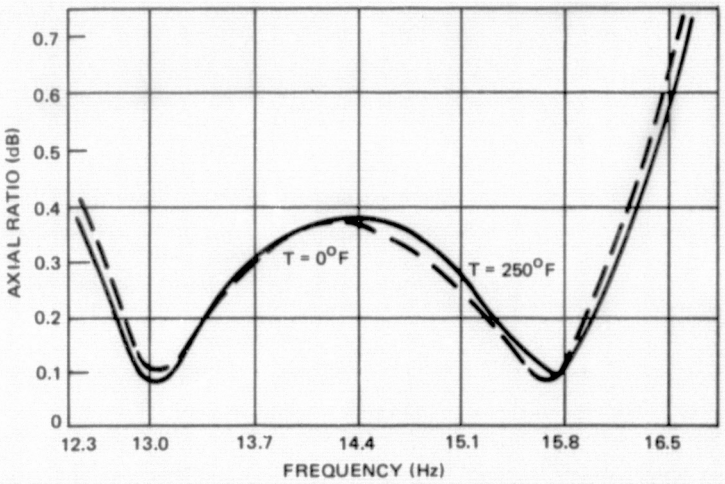

123400 5

Figure 3.7-13. Ku-Band Waveguide Iris Type Polarizer

The tracking feed selected was an 0.5-inch diameter open-ended circular waveguide. For acceptable autotrack scale factor performance, the maximum element spacing was determined to be approximately 2.7 wavelengths. To meet this requirement, the monopulse elements were required to be within the corrugated section of the center horn and installed at an angle of 6 to 10° from the axis to clear the impedance matching section of the center horn as shown in Figure 3.7-14. Although the difference elements penetrate the outer corrugations of the horn, the effect on secondary performance will be negligible. Penetration is only in four places and nearest the horn aperture where surface currents are minimum for a corrugated structure. Development tests performed on a similar design have shown this concept to be feasible. Because the pattern of the open-ended waveguide is considerably broader than required to efficiently illuminate the subreflector, there will be no significant degradation in secondary performance because of the 6° tilt. The waveguide diameter is small enough to suppress higher order modes which could cause beam amplitude and phase tilt if allowed to propagate. Similar arrangements have been developed and tested by TRW with excellent performance.

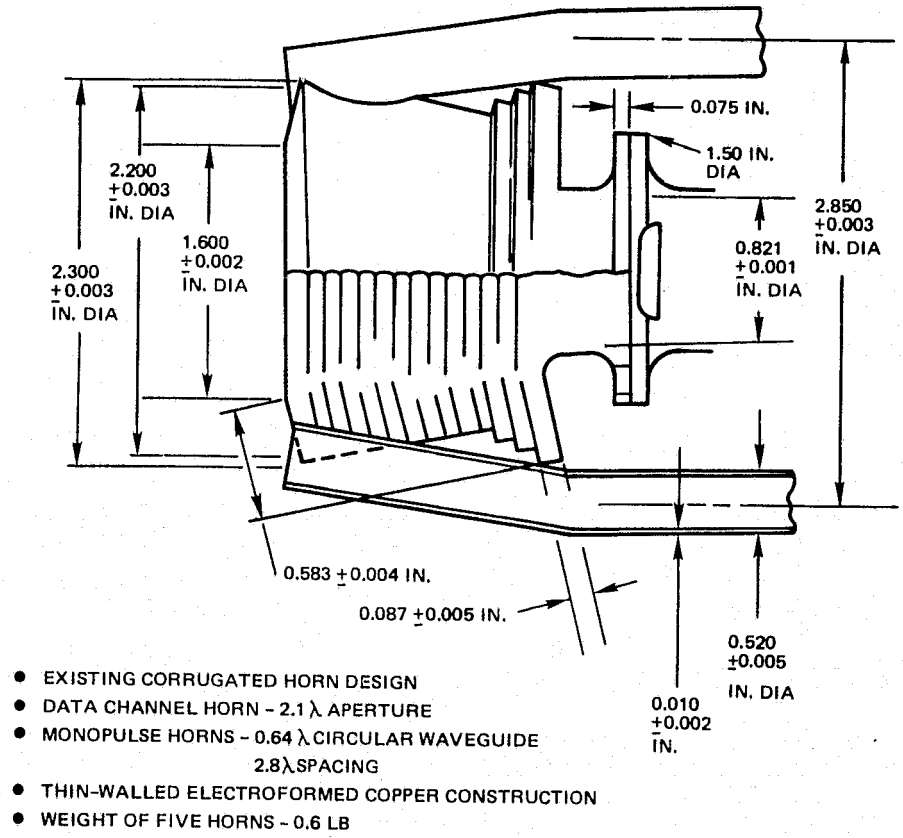

Figure 3.7-14. Autotrack Feed Design

The four monopulse horns feed the waveguide comparator located in the RF compartment where α and β tracking error signals are established. To minimize cost and weight, the four monopulse horns are not excited through polarizers and are therefore linearly polarized. This technique costs 3 dB in gain but eliminates four polarizers with no degradation in tracking performance.

The five-horn feed elements are thin walled electroformed copper designs which provide the high stiffness and design reproducibility required. The design, manufacturing techniques, and materials selected represent an approach proven by TRW on past spacecraft programs. The total weight of the feed system in less than 1.5 pounds.

Autotrack System

The comparator network combines signals from the four outside circular waveguide horns to provide the error signals to the autotrack biphase modulator. Several comparator design concepts are available; however, the magic tee approach was selected based upon its design simplicity and superior RF performance. Figure 3.7-15 shows the comparator circuitry and signal processing scheme.

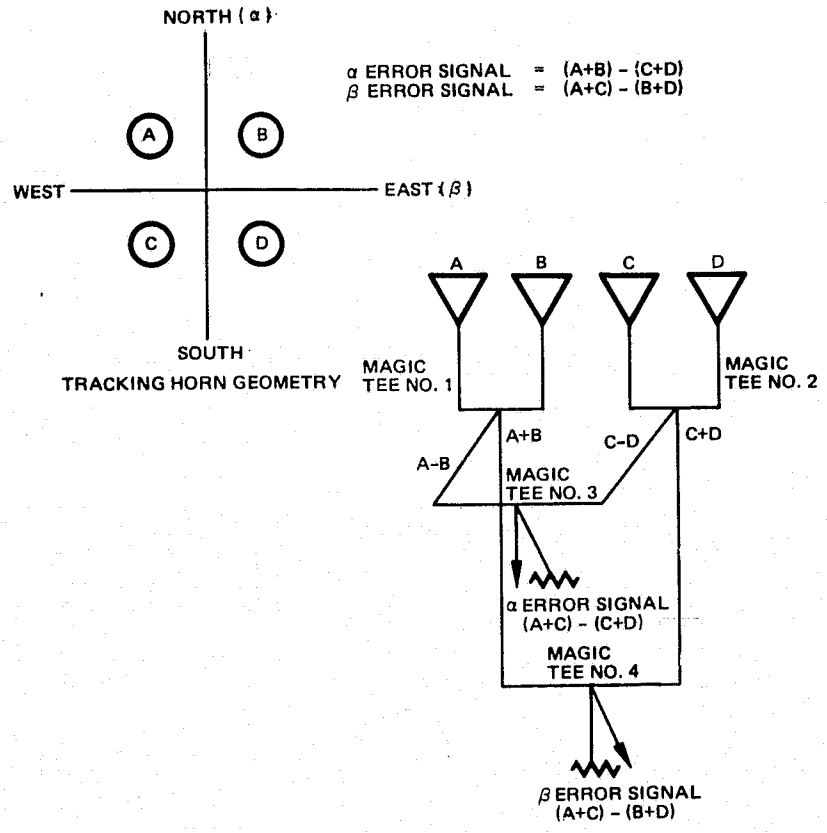

Figure 3.7-15. Autotrack Comparator

Four separate magic tees allow phase balancing to be controlled during assembly using waveguide shims. Maximum phase and amplitude unbalances of 3° and 0.25 dB, respectively, can be achieved at the output of the comparator. The unused ports of the output magic tees are terminated in matched waveguide loads.

The comparator and interconnecting waveguide will be dip brazed aluminum parts with the inside waveguide surfaces silver plated for minimum insertion loss. The comparator will be supported in the electronics compartment and will be thermally protected. Within the compartment, the length of waveguide required by the data channel is approximately the same as that required by the error channels, including comparator, and the thermal environments will therefore introduce negligible phase imbalance.

Error signals are modulated onto the received communication signals as low level, time division multiplexed, AM modulation as shown in Figure 3.7-16. This processing scheme is a single-channel monopulse system which has been used successfully on previous space programs.

Other forms of multiplexing were considered and all are about equal in performance. This system was selected on the basis of antenna alignment requirements. With the method selected, it is easy to latch the multiplexer into a fixed state and therefore obtain, for example, a steady state $+\alpha$ signal. This capability is required to allow accurate setting of autotrack phase.

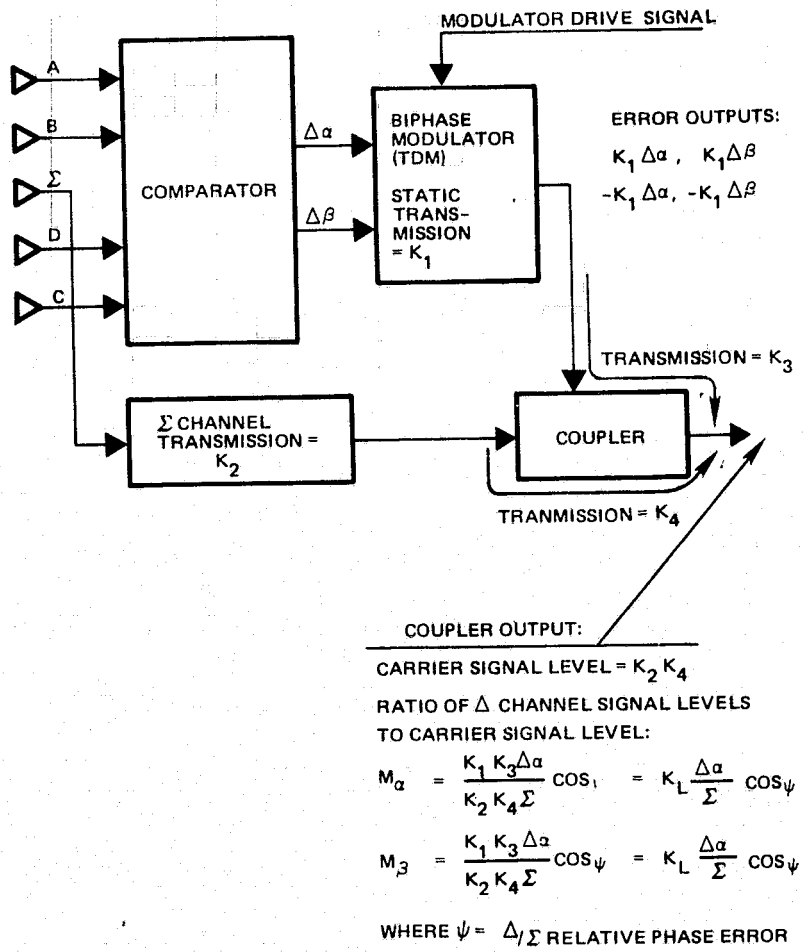

Figure 3.7-16. Autotrack Signal Modulation Scheme

A system variable is the value of the directional coupler. The true autotrack scale factor, and hence the antenna tracking loop SNR, can be increased merely by coupling more of the K_1 $\Delta\alpha$ signal into the output line. This increases the throughput loss, however, and hence reduces the G/T ratio. A -10 dB value was selected as a compromise between these competing factors. The two loss factors, K_1 and K_2, are naturally minimized in any event.

The proposed modulator/combiner block diagram is shown in Figure 3.7-17. The proposed design uses magic tees and ferrite circulator switches to modulate and time phase the error channel signals into one output. Figure 3.7-18 shows the biphase modulator outline drawing and typical dimensions.

Pre and post-comparator phase balancing is accomplished using a fixed phase adjuster which may be no more than shims to compensate for manufacturing and assembly tolerances. Final phase adjustments will be made using sum and difference phase measurements on the assembled antenna. The modulator phase variation with temperature will be less than 0.15 degree/degree F. Since the modulator is installed in the thermally controlled RF compartment, the maximum phase error contribution due to the modulator will therefore be less than 5° over the on-orbit environments.

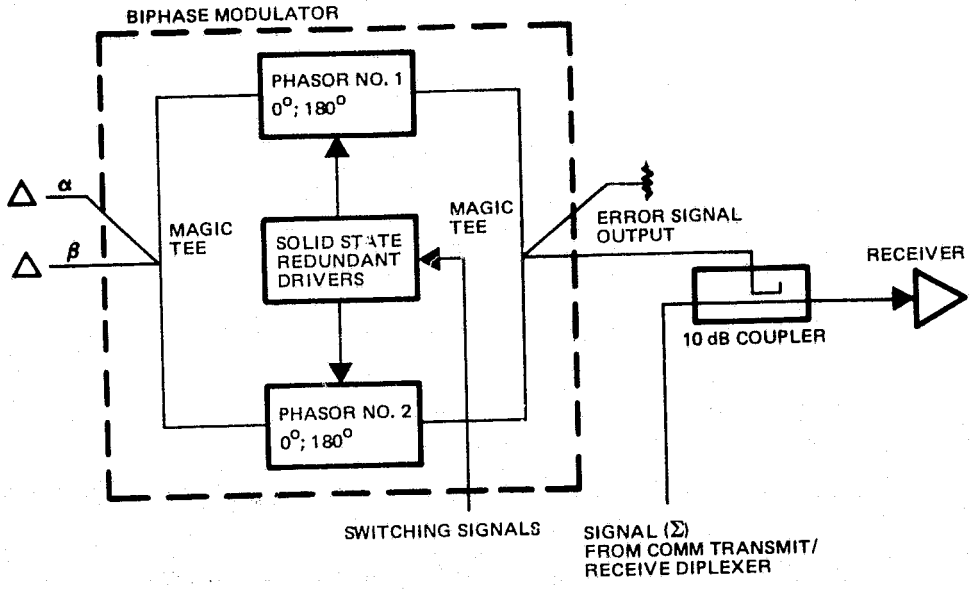

Figure 3.7-17. Autotrack Biphase Modulator

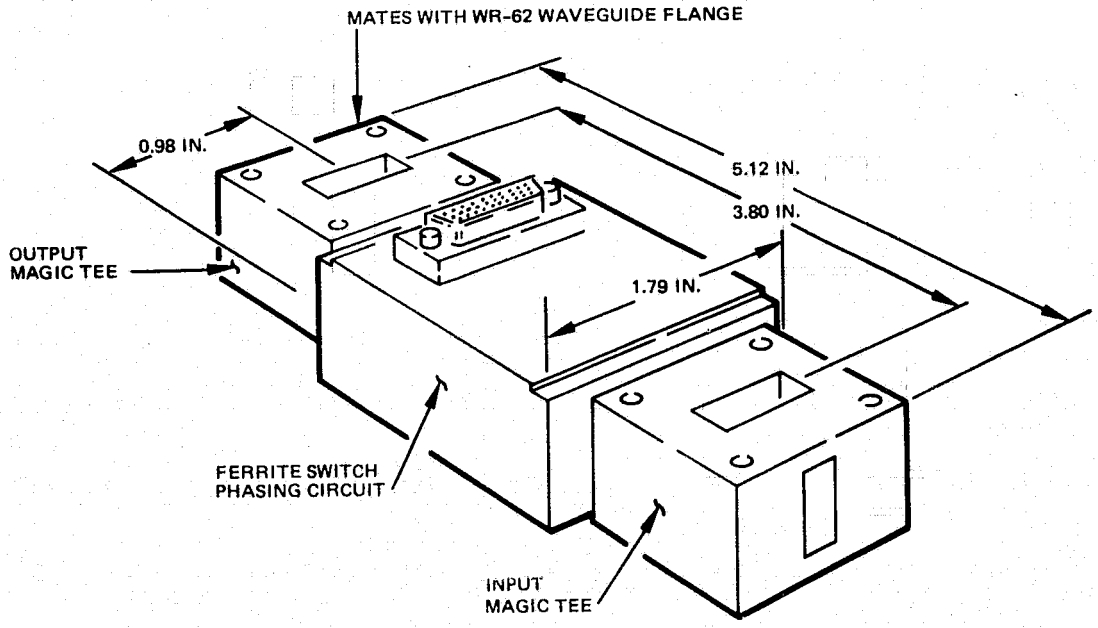

- SIMPLE LIGHTWEIGHT DESIGN
- USES DEVELOPED FERRITE SWITCHES AND REDUNDANT ELECTRONIC DRIVERS
- FERRITE SWITCHES AND DRIVER ARE QUALIFIED DESIGNS

Figure 3.7-18. Autotrack Biphase Modulator

3.7.3 Antenna Performance

Radiation pattern performance and antenna gain of the dual-shaped Cassegrain antenna were determined using the TRW-developed computer program CASSE. TRW has performed extensive design and development of Cassegrain and shaped Cassegrain monopulse antennas, and has created and verified computer programs which accurately predict antenna performance. The programs account for many antenna parameters, including feed

pattern spillover and efficiency, subreflector diffraction pattern, reflector edge diffraction, subreflector/feed blockage, and thermal distortion of the feed, subreflector, and reflector. These programs have been used to optimize the Ku-band antenna design for maximum gain, efficiency, and autotrack.

Figure 3.7-19 presents the sum patterns at 13.775 GHz and 15.0085 GHz. Figure 3.7-20 presents the sum and difference patterns of the antennas at 13.775 GHz using an expanded degree scale. The expanded scale difference pattern is superimposed on the expanded scale sum pattern such that the peak gains are relative to each other at the output of the comparator. In this way, the scale factor of the error signal relative to the communication receive signal may be calculated referenced to the comparator output. To determine the actual scale factor at the output of the 10 dB hybrid coupler, where the difference signal is modulated on the communication channel signal, one simply subtracts (in dB) the relative losses of the difference channel to the communication channel due to the biphase modulator and hybrid coupler.

The tracking error slope normalized to the communication pattern peak is 0.79 volt/deg/volt measured at the output of the comparator difference channel. This value is obtained by first normalizing the peak gain of the reference channel to 1 volt. The slope in volts per degree is then directly measured off the difference pattern at a point just off-boresight by simply determining two voltage points off-boresight of the difference pattern in volts relative to the reference pattern and dividing the difference by the angle in degrees between the two measured values.

The above tracking error slope performance of the feed and comparator depends on the precomparator phase and amplitude imbalance. It was determined that the effect on error slope is negligible if the phase imbalance is not greater than 2 electrical degrees and the amplitude imbalance is not greater than 0.25 dB. The effect of precomparator phase imbalance is to reduce the null depth, whereas the amplitude imbalance causes a null shift. A phase imbalance of 2° reduces an infinite null to -32 dB and a 0.25 dB amplitude imbalance shifts the null 0.036°.

Table 3.7-2 presents the antenna gain/loss budget for both the transmit and receive operating frequency bands (13.775 and 15.0085 GHz).

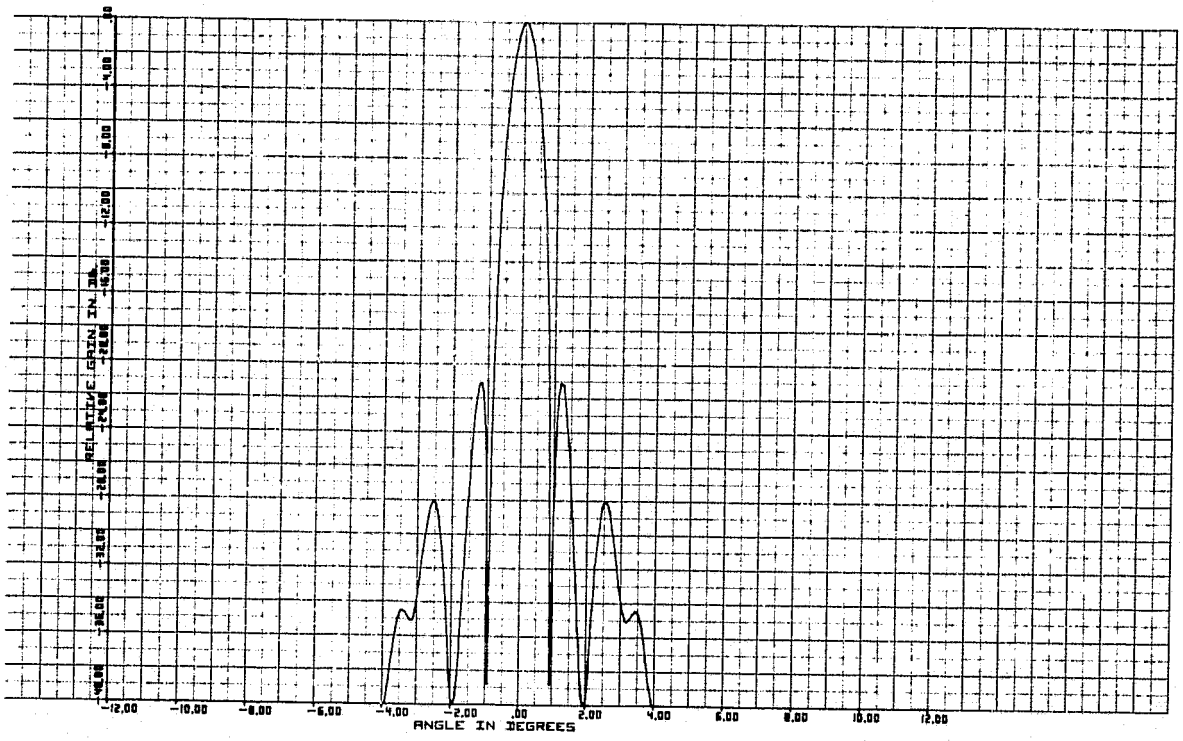

a) Transmit

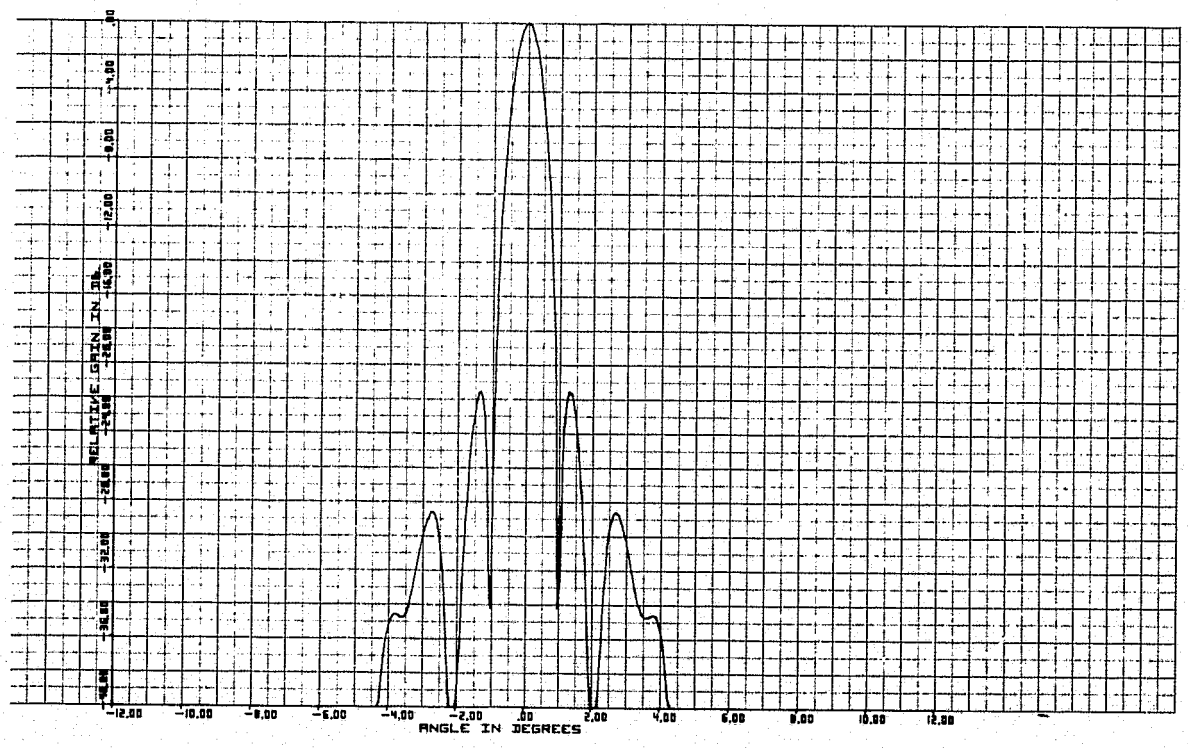

b) Receive

Figure 3.7-19. Sum Radiation Patterns of Recommended Cassegrain Antenna

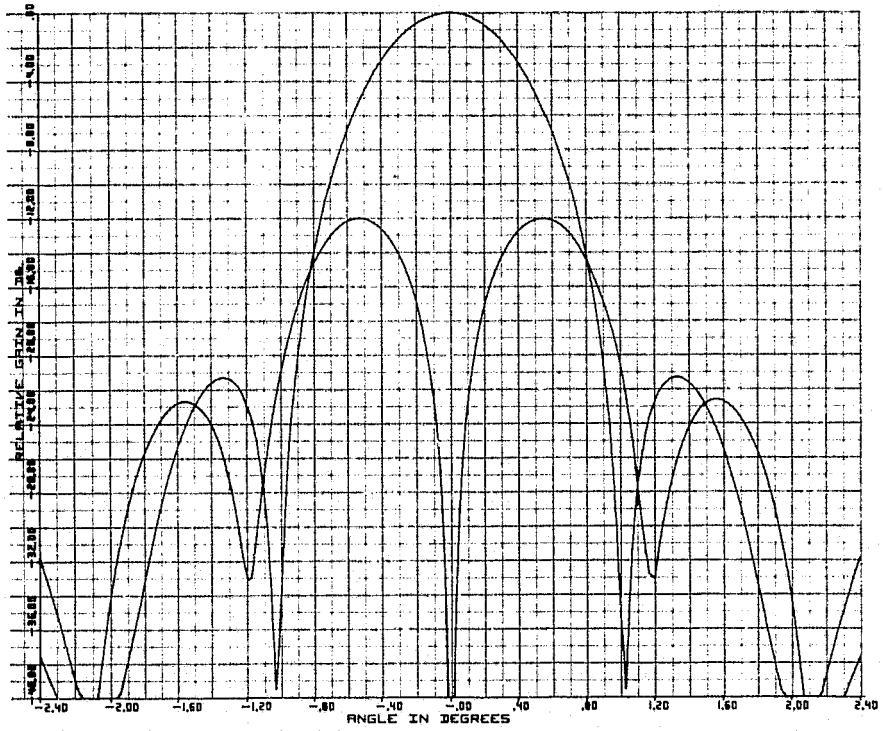

Figure 3.7-20. Expanded Scale Autotrack Sum and Difference Radiation Patterns

Table 3.7-2. Antenna Gain/Loss Budget

Parameter	Channel Transmit 15.008 GHz	Channel Receive 13.775 GHz
Uniform gain $\left(\frac{4\pi A}{\lambda^2}\right)$	49.17 dBi	48.42 dBi
Losses (dB)		
Reflector illumination	0.65	0.60
Subreflector spillover	0.29	0.65
Main reflector spillover	0.13	0.15
Cross polarization	0.03	0.03
Blockage	0.32	0.32
Surface errors (0.003 in. rms)	0.10	0.09
Subreflector and feed defocusing	0.10	0.09
Feed horn	0.15	0.13
Polarizer	0.10	0.09
Waveguide	0.20	0.18
VSWR mismatch	0.06	0.06
	2.13	2.40
Antenna gain	47.04 dBi	46.02 dBi

The sidelobe level and halfpower beamwidth of the antenna may be obtained directly from the calculated radiation pattern. Of course the calculated first and second sidelobes should be degraded by 1 to 2 dB due to such effects as structural blockage which is not part of the computer calculation. The expected near-in sidelobes of the recommended antenna are provided in Figure 3.7-21 which also provides a sidelobe peak envelope out to 8° off-boresight.

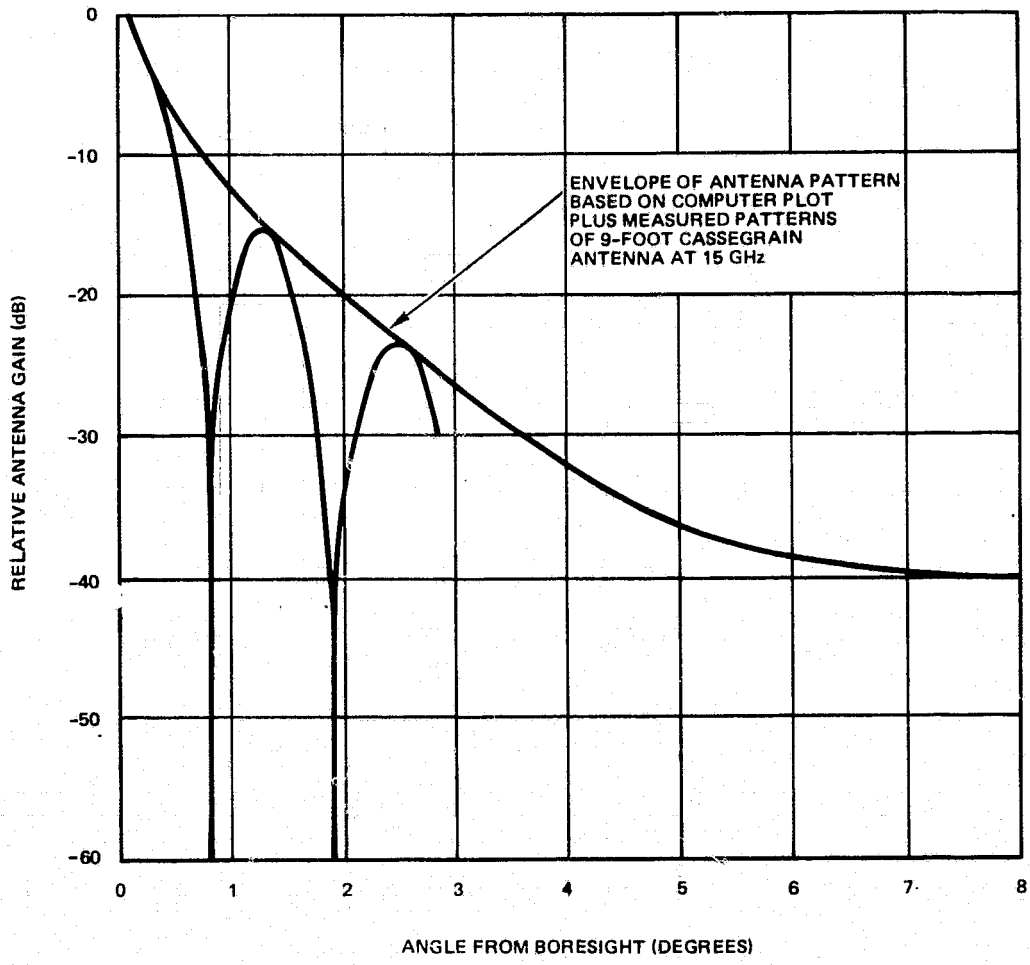

Figure 3.7-21. 6-Foot Diameter Reflector Cassegrain Antenna
Freq — 15 GHz Monopulse 5-Horn Feed
10-Inch Diameter Subreflector

3.8 ACQUISITION HORN ANTENNA

The acquisition widebeam antenna is provided for TDRSS acquisition of the LF/O Ku-band transmitted signal. The antenna design is based on providing a minimum of 33 dBW ERIP over a 12° beamwdith.

3.8.1 Description of Recommended Antenna

The recommended design (Figure 3.8-1) is a corrugated conical horn which has been developed at TRW. No tradeoffs were considered necessary for this simple and proven design. The antenna consists of a corrugated horn, a waveguide iris type polarizer (similar to the antenna polarizer), and an orthomode transducer. The corrugated horn and polarizer are obtained directly from a previous space program which operated at Ku-band. Excellent axial ratio (<2 dB) is obtained over the required 12° beamwidth.

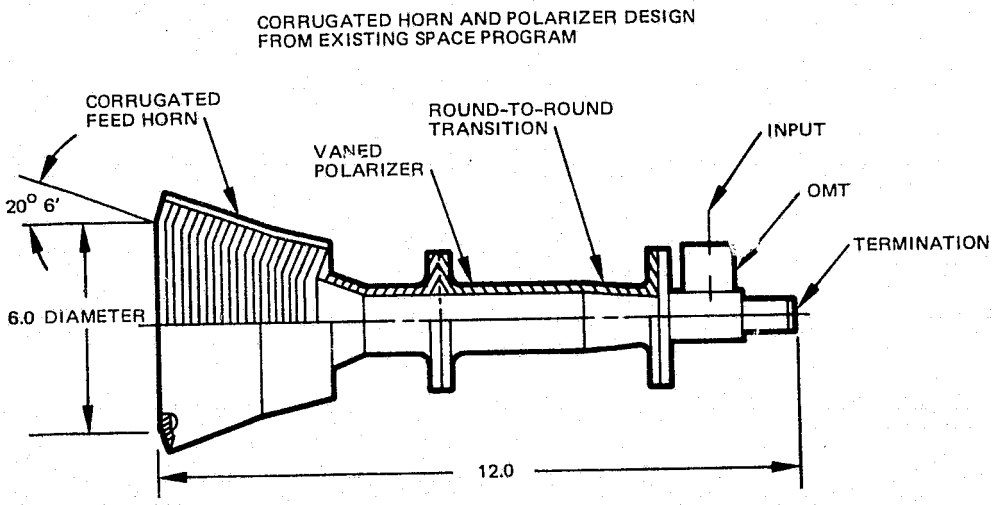

Figure 3.8-1. Ku-Band Acquisition Horn Antenna

The corrugated horn and polarizer are electroformed and immersion gold coated as separate units. A flange is provided for interfacing the units. Total weight of the horn and polarizer is approximately 2.5 pounds.

The antenna is mounted adjacent to the high gain antenna reflector using a special bracket which is attached to the reflector structure. The aperture of the horn is in the same plane as the reflector edge. This mounting position provides for boresight alignment of the two antennas to within 0.3°.

3.8.2 Acquisition Antenna Performance

The corrugated conical horn exhibits an excellent radiation pattern having essentially no sidelobes and equal E and H-plane beamwidths. This performance provides excellent axial ratio over a large percentage of the radiation pattern (greater than the halfpower beamwidth). The radiation efficiency is greater than 80%. Table 3.8-1 presents a summary of the antenna performance.

Table 3.8-1. Acquisition Horn Performance Summary

Parameter	Capability
• Frequency	15.0085 ± 0.120 GHz
• Gain	25.2 dBi
• Halfpower beamwdith	9.0°
• Polarization	RHCP
• Axial ratio	<0.5 dB on-axis <2.0 dB over 30 dBW beamwidth
• Sidelobes and backlobes	-40 dB
• Wide-narrowbeam alignment	0.3°

3.9 RF COMPARTMENT

A preliminary design is presented for the RF compartment, including mass properties and thermal design.

3.9.1 Structural Design and Layout

This compartment supports the antenna assembly and houses the associated RF equipment. The design objectives are to provide good passive thermal environments, minimum weight, minimum moments of inertia (gimbal considerations), suitable load paths for on-orbit and launch conditions, minimum cable and waveguide lengths, and easy access for inspection, service, and integration of equipment.

The area required for TWTA thermal radiation provides the starting point for sizing the compartment. This area was positioned on one side to ensure minimum reflections from the antenna or spacecraft. The remainder of the compartment surrounds the gimbal assembly. This concept provides equipment mounting surfaces near the gimbal axis, thus maintaining minimum inertia ratios. The resulting design (Figure 3.9-1) is a saddle shaped box with the upper face open for accessibility. The upper face is covered with a thermal blanket attached by velcro strips prior to launch operations.

The radiating (TWT and power supply) panel is a 0.10-inch aluminum alloy plate covered with second surface mirrors. The remainder of the compartment is fabricated with aluminum honeycomb panels with flattened and flanged edges (see AA on Figure 3.9-1). This fabrication technique was developed for the FLTSATCOM structure. An aluminum alloy frame around the top of the compartment reinforces the structure and provides a flange for attaching the thermal cover. Flexures at the upper four corners support the antenna assembly and reduce misalignment due to distortions of the compartment structure.

The saddle shape of the compartment facilitates distribution of load paths around the gimbals and provides direct attachment to the spacecraft structure for launch operation.

Table 3.9-1 is a preliminary estimate of the RF compartment weight. The honeycomb panels have the following characteristics:

Overall thickness	0.38 inches
Weight	5.3×10^{-4} lbs/in^2
Honeycomb thickness	0.36 inch
Aluminum facesheets	0.01 inch

3.9.2 Mass Properties

The weight of the RF compartment and antenna is summarized in Table 3.9-2. Reasonably firm weights have been developed for the major components. The weight growth typical during detail design is not expected.

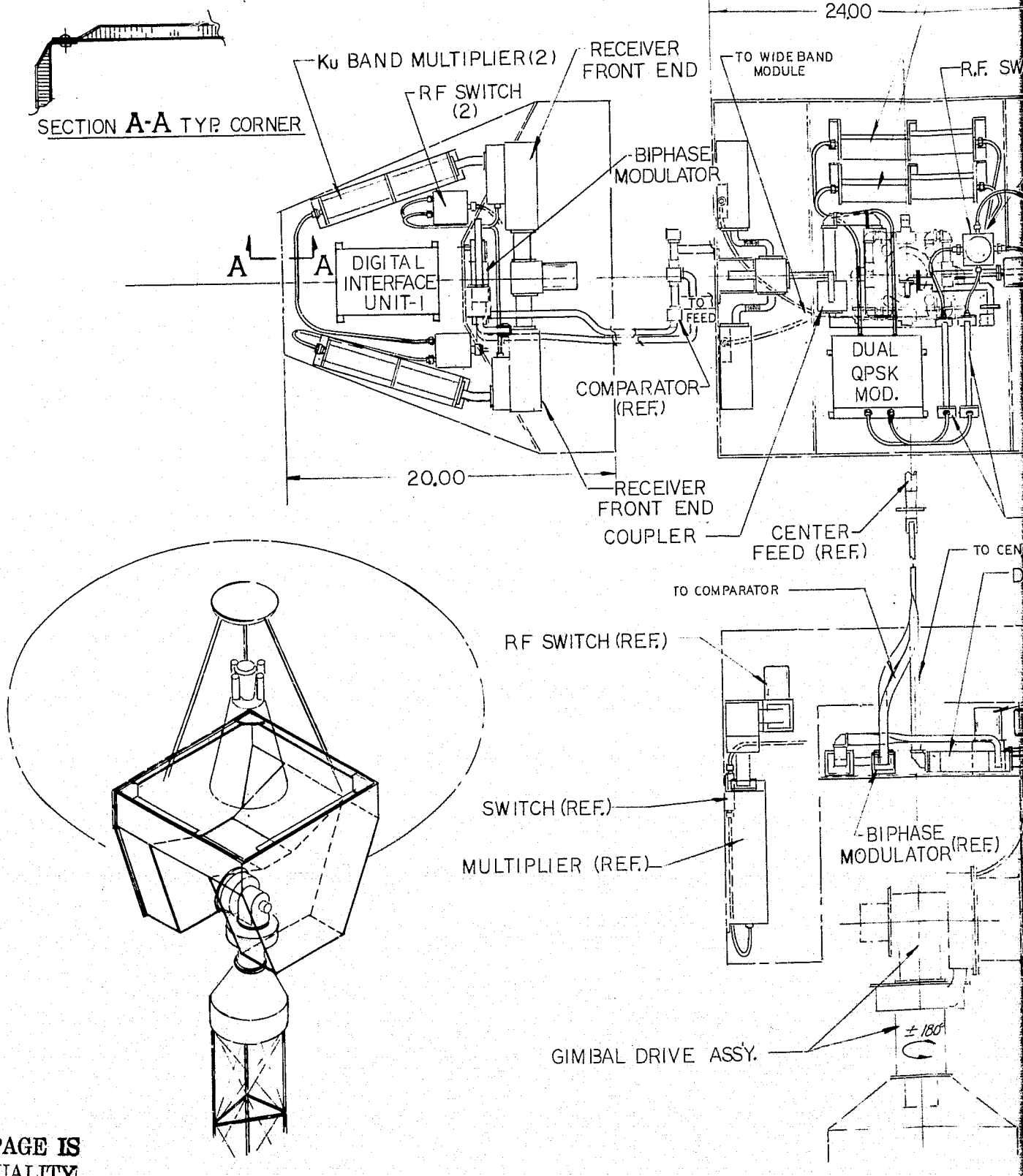

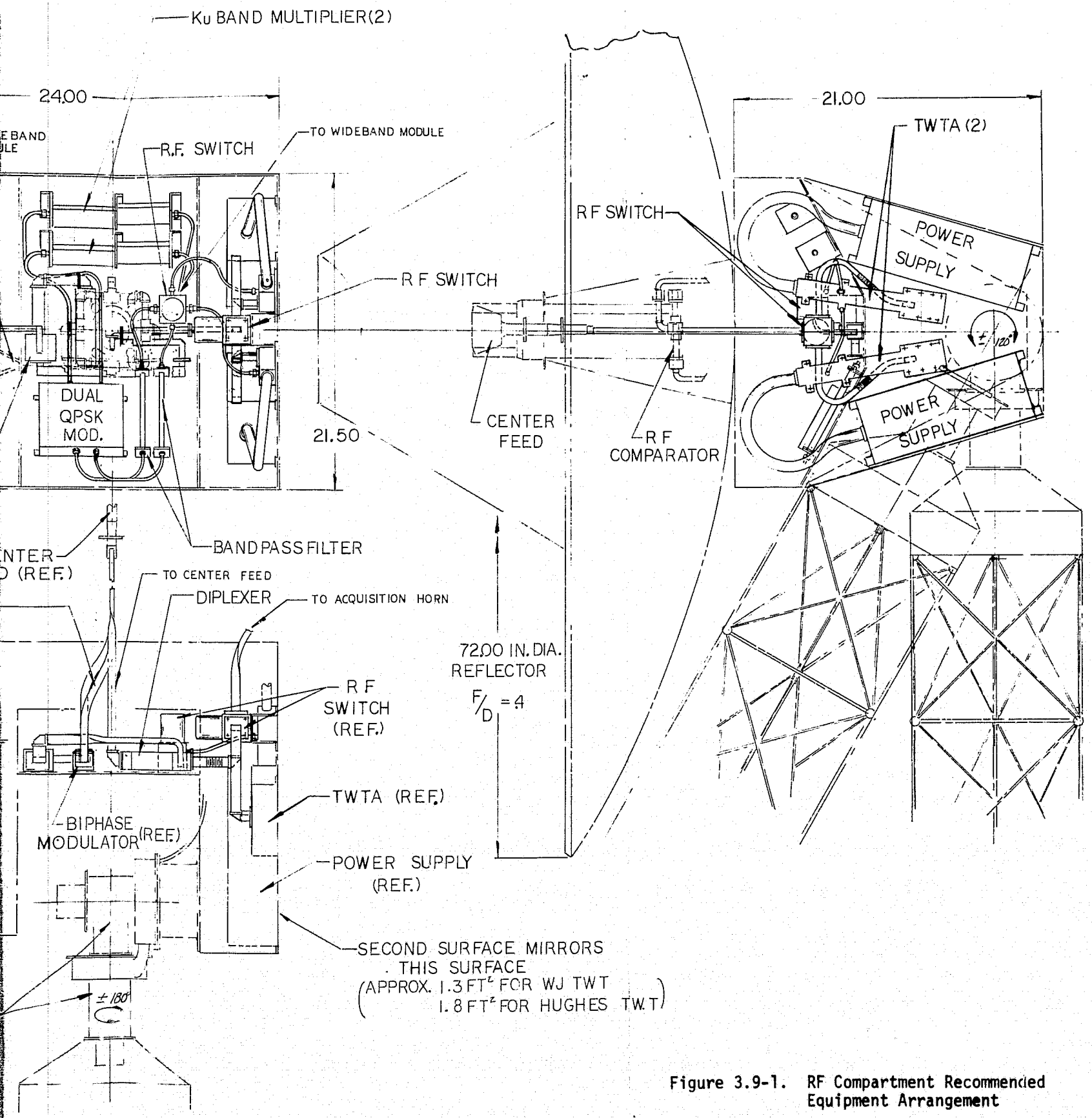

Figure 3.9-1. RF Compartment Recommended Equipment Arrangement

FOLDOUT FRAME 2

Table 3.9-1. RF Compartment Structure Weight

Item	Area (in^2)	Weight (lbs)
End panel	340	
Inner panel (2)	420	
Side panel (2)	216	
Side panel (4)	432	
Inner panel	65	
Inner panel (2)	225	
Bottom panel (2)	55	
Subtotal	1753	0.93
Second surface mirrors (335 in^2)		0.23
Doublers and inserts		2.00
Support brackets		2.00
Radiator panel (0.1" Al-368 in^2)		3.60
Margin (≈ 12%)		1.00
		9.8 lbs

Table 3.9-2. RF Compartment Weight

Component	Unit Weight (lbs)	Quantity	Weight (lbs)
Receiver front-end	1.0	2	2.0
X6 multiplier	0.6	2	1.2
QPSK modulator	3.6 (dual)	1	3.6
Ku-band multiplier	0.6	2	1.2
TWTA (power supply included)	10.7	2	21.4
Waveguide switch	1.2	2	2.4
Coaxial switch	0.25	4	1.0
Waveguide BPF	0.3	3	0.9
Digital interface unit No. 2 (internally redundant)	1.0	1	1.0
Miscellaneous (W/G, wire, etc.)	2.5	1	2.5
RF comparator	0.40	1	0.4
Biphase mod	0.50	1	0.5
RF coupler	0.20	1	0.2
Diplexer	0.6	1	0.6
RF compartment structure	9.80	1	9.8 / 48.7
Acquisition horn	2.5	1	2.5
Parabolic reflector*	15.0	1	15.0
Subreflector, struts	5.0	—	5.0
Feed components**	1.5	—	1.5 / 24.0
			Total 72.7 lbs

*Aluminum honeycomb 1/2", 4 ply GFRP facesheets, 1" invar support ring, 3' diameter.

**Feed horns, OMT polarizer.

Mass properties are based on the configuration layout of Figure 3.9-1 and the component weight of Table 3.9-2. Table 3.9-3 provides the mass properties with the antenna on the +X side. Parenthetical values show the mass properties with the compartment rotated 90° in the X-Z plane (antenna on the -Z side). Figure 3.9-2 shows the reference axis system assumed. The centerline of the gimbal drive assembly is the reference axis for the mass properties.

Table 3.9-3. RF Compartment Mass Properties

	Center of Gravity (inch)			Moment of Inertia ($lb\text{-}in^2$)			Product of Inertia ($lb\text{-}in^2$)		
	X	Y	Z	I_x	I_y	I_z	I_{xy}	I_{xz}	I_{yz}
90° rotation in X-Z plane	14.5	-3.5	0	9000	15000	17000	2600	70	20
	(0)	(-3.5)	(-14.5)	(17000)	(15000)	(9000)	(20)	(-70)	(-2600)

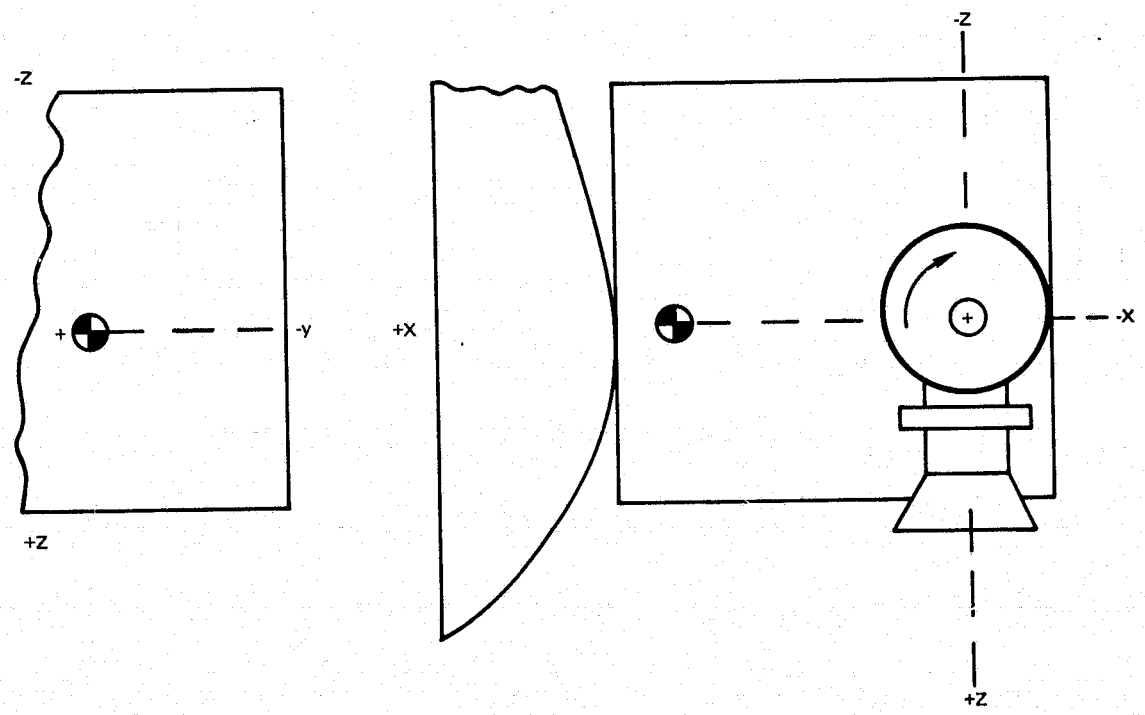

Figure 3.9-2. Reference Axis System

3.9.3 Thermal Design

The RF compartment electronic equipment is maintained at satisfactory operating temperatures at all times by simple radiators covered with low α_s/ε second-surface mirrors to reject heat dissipated by the electronics and by electrical heaters when the

equipment is off for prolonged periods. All external surfaces, except the radiator, are covered with form fitting multilayer insulation blankets. The TWTA's are mounted directly to the radiator, as shown in Figures 3.9-3 and 3.9-4, to minimize temperature differences between the TWTA and the radiator. The radiator on which the TWTA's are mounted has adequate lateral thermal conductance. A 0.1-inch thick aluminum plate is used to prevent hot spots in the TWT collector region. The heaters used during standby time can be actuated either by simple thermostats or by command.

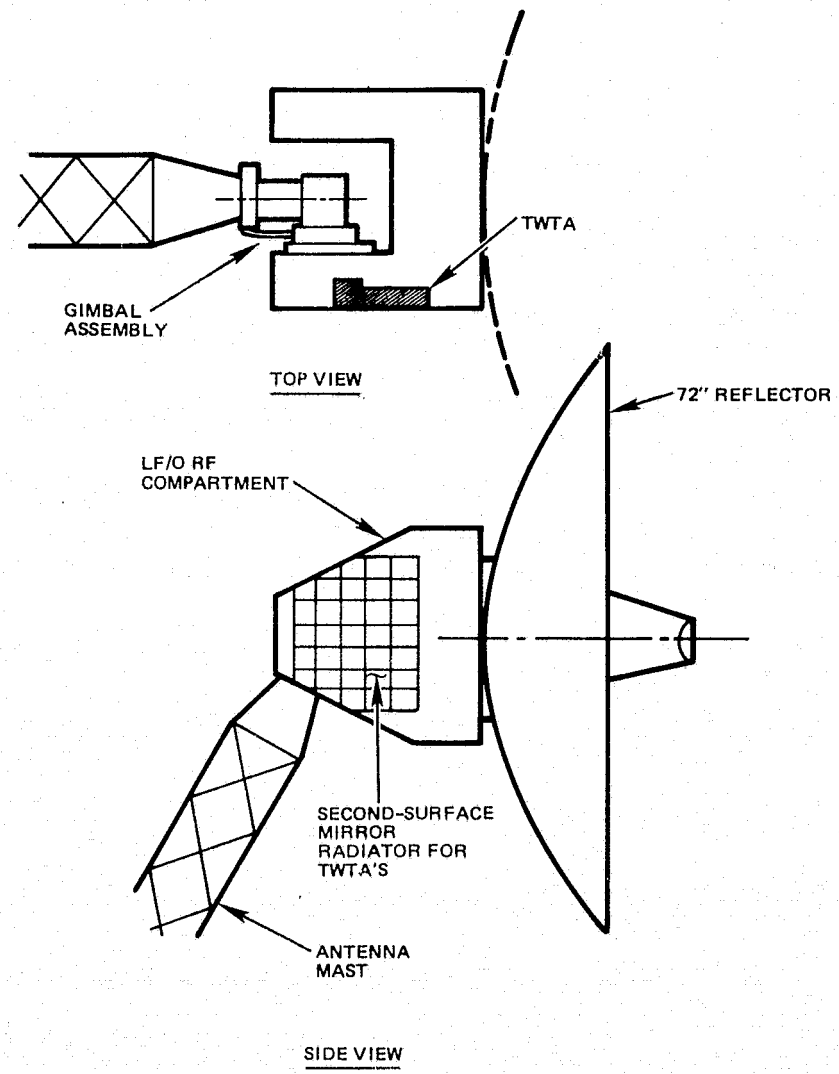

Figure 3.9-3. Configuration of LF/O RF Compartment

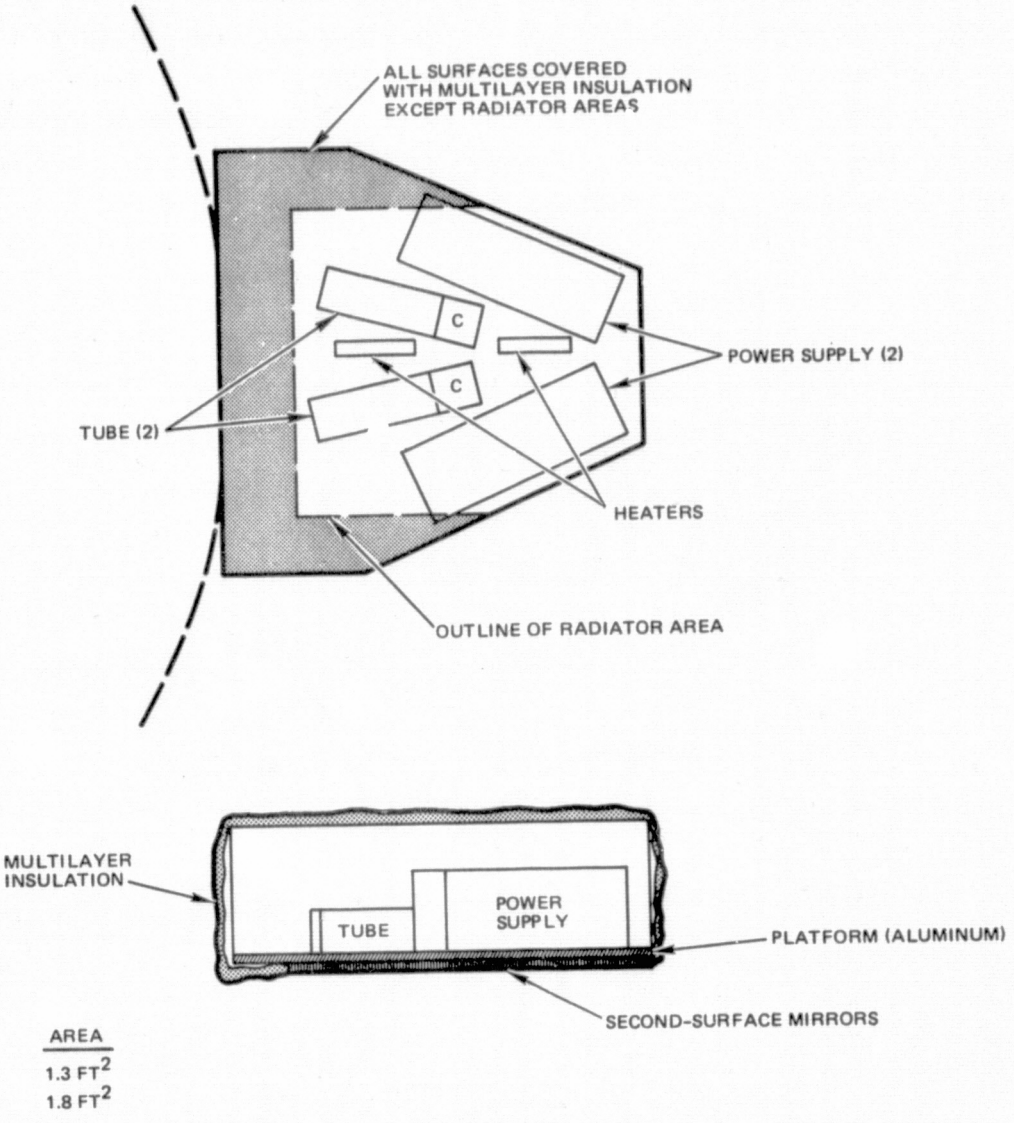

TUBE	AREA
W-J	1.3 FT^2
HAC	1.8 FT^2

Figure 3.9-4. Thermal Design of RF Compartment

TWTA Thermal Dissipation

The major heat sources are the TWTA's. The TWT's and associated power supplies are mounted on a dedicated panel containing no other components. A clear field-of-view for radiation is provided at all times.

The thermal dissipation and allowable operating temperatures are summarized in Table 3.9-4 for both the Hughes and Watkins-Johnson TWTA's.

Table 3.9-4. TWTA Heat Dissipation

Equipment	Heat Dissipation*	Allowable Operating Temperature	Qualification Temperature Range
TWTA (Watkins-Johnson)			
Tube**	40 watts	0 to 125°F	-20 to 145°F
Power supply	15 watts	0 to 125°F	-20 to 145°F
Alternate TWTA (Hughes)			
Tube***	54 watts	0 to 125°F	-20 to 145°F
Power supply	22 watts	0 to 125°F	-20 to 145°F

*The WJ TWTA provide 20 watts RF output; the Hughes TWTA provides 16 watts RF output.

**For the zero drive condition, the heat dissipation of the Watkins-Johnson tube is virtually unaffected since it is a multi-collector design.

***For the zero drive condition, the heat dissipation of the Hughes tube increases about 16 watts in the collector.

The dc power, RF power, power supply, and TWT efficiencies are given in Table 3.9-5.

Table 3.9-5. Efficiency and Power

Item	Hughes	Watkins-Johnson
DC power input	92 W	75 W
RF power output	16 W	20 W
TWT efficiency	23%	33.3%
Power supply efficiency	76%	80%
Net efficiency	17.4%	26.7%

For this evaluation, it is assumed that the equipment in the RF compartment operates 50% of every orbit, 0.83 hours of the 1.65 hour orbit period, or that it may be inactive for long periods. The 50% duty cycle establishes the radiator area, and the continuously-off mode establishes the heater power requirements. Figure 3.9-5 shows the TWT platform temperature as a function of time for the 50% duty cycle operation. With continuous operation, the TWT slightly exceeds maximum allowable temperature in about 10 hours. The maximum temperature can be reduced by increasing the TWT radiating area but this would result in increased heater power during off-times. The figure shows an extremely benign thermal environment for 50% duty cycle operation. For the other equipment panels, the expected temperature variation would be even less.

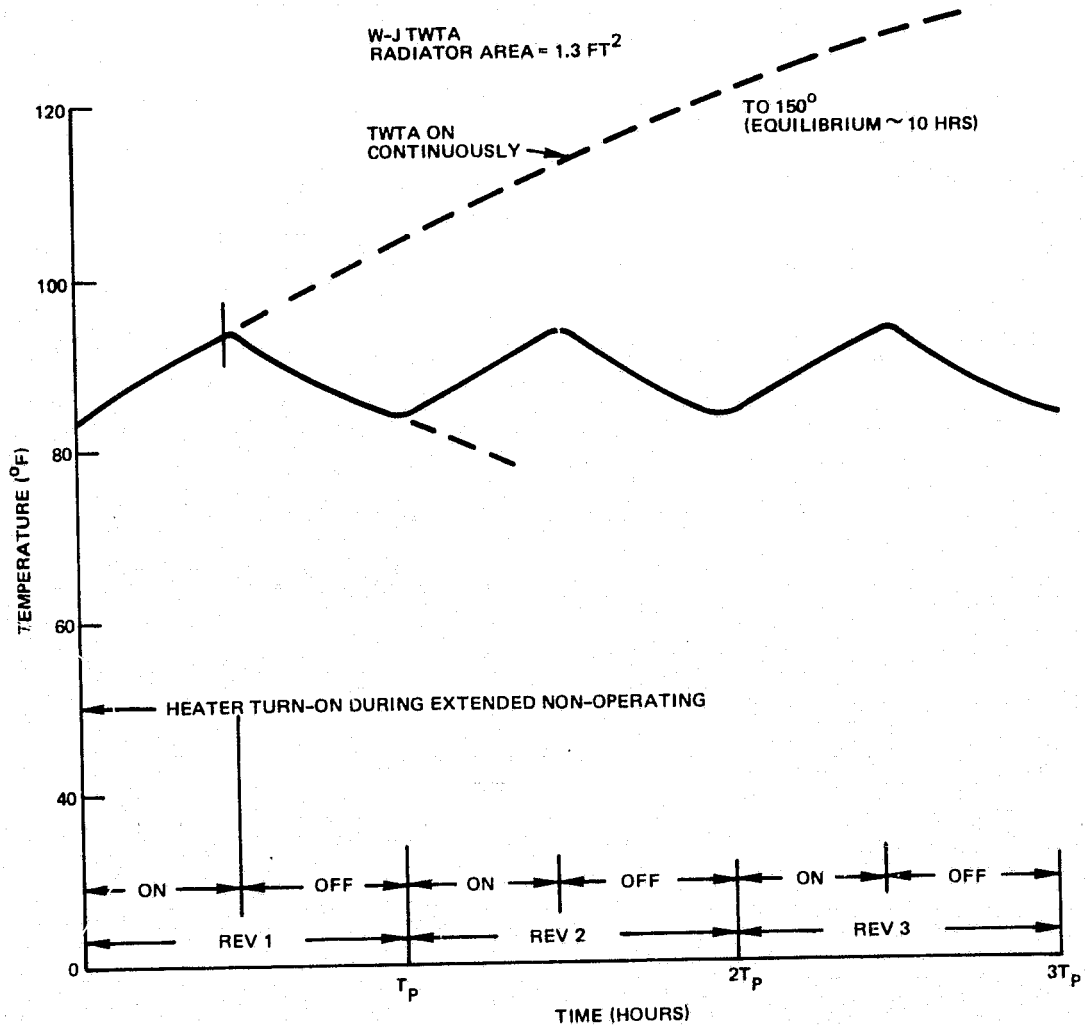

Figure 3.9-5. Temperature History of TWTA Platform for 50% Duty Cycle

The orbit for the LF/O is a low altitude (705 km) sun-synchronous orbit, with the sun between 9:15 and 11:15 when the spacecraft passes over the equator. Thus, the sun is at an angle of 11.25° to 41.25° with respect to the orbit plan, as shown in Figure 3.9-6. The +Z axis of the LF/O always points to the center of earth, and the boom for this antenna always points away from the earth. Since the antenna can be rotated ±180° in one axis and ±120° in its second axis, the external surfaces of the equipment enclosure can have almost any possible attitude with respect to the sun and earth. However, the sun exposure is limited to about 1 hour, and the eclipse lasts about 0.6 hour.

The worst-case heating during the sunlight portion of the orbit occurs when the sun is normal to the TWTA radiator, as shown in Figure 3.9-7, and the worst-case heating occurs during eclipse when the radiator faces earth. The minimum heating condition, for sizing heaters, is based on the assumption that the radiator has no external heating.

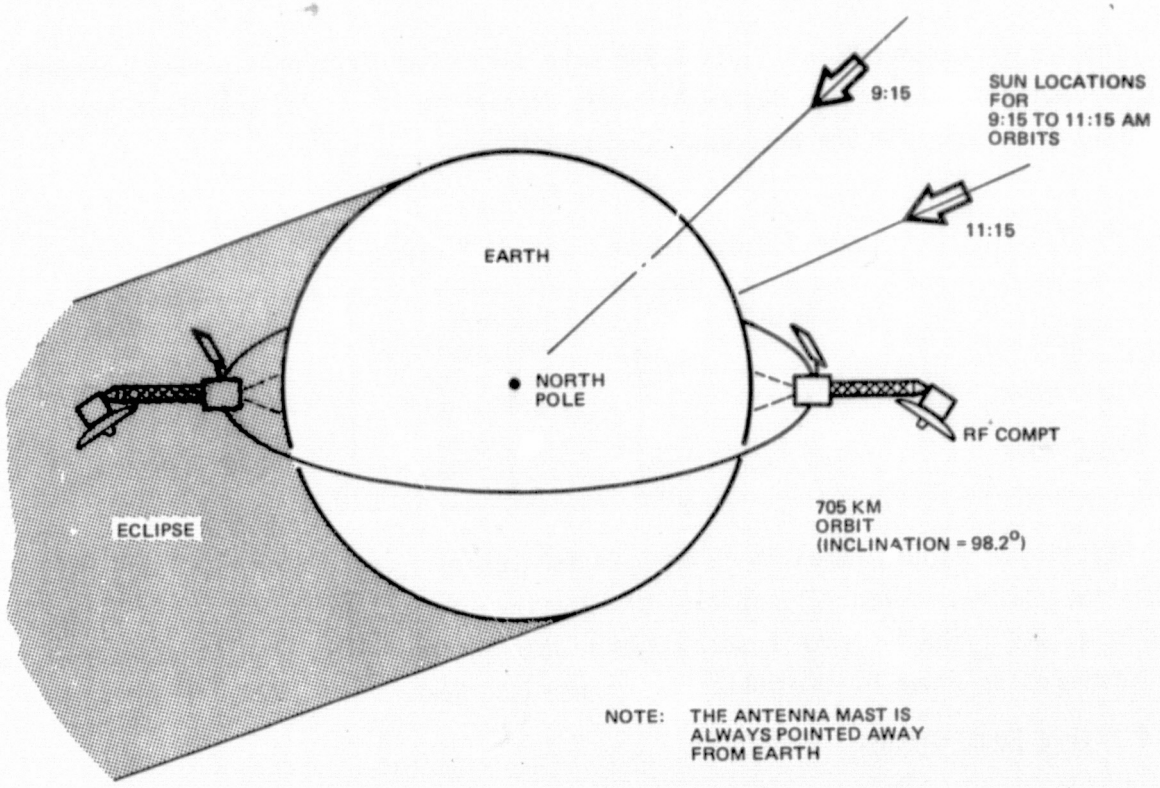

Figure 3.9-6. Definition of Orbit and Spacecraft Attitude

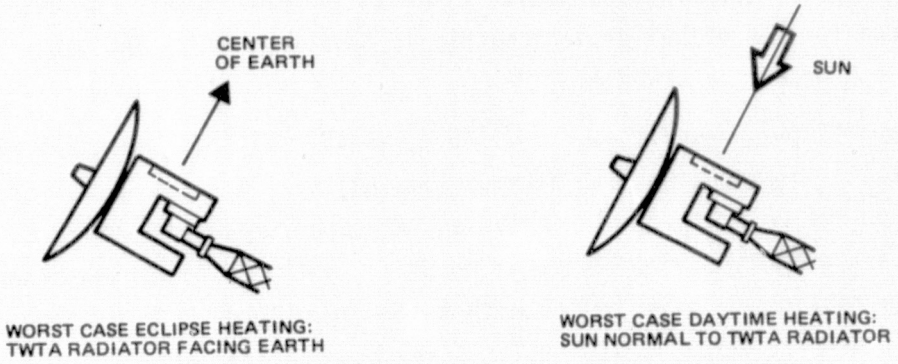

Figure 3.9-7. Definition of Worst-Case Hot External Heating Environment

Since most of the heat dissipation occurs at the collector region of the tube, the collector ends of both tubes are located near the center of the radiator panels. Thus the temperature response is the same regardless of which TWTA is active.

The TWTA panel must have substantial thickness to distribute the heat from the TWTA to the entire radiator without large temperature gradients. An optimized thickness can be determined easily once the tube manufacturer is selected and the operating duty cycle is established.

The radiator has a good view to space (view factor ≈ 0.80), and the view is never obscured by the support mast regardless of the two-axis rotations.

The design parameters of Table 3.9-6 were determined from preliminary analyses of both the Watkins-Johnson and Hughes Aircraft Company TWTA's. The standby heater power is adequate to maintain the equipment above 30°F.

Table 3.9-6. Thermal Design Parameters

Tube	Radiator Area	Platform Thickness	Standby Heater Power
W-J TWTA	1.3 ft^2	0.10 inch	19.6 watts
HAC TWTA	1.8 ft^2	0.15 inch	27 watts

Additional radiator area (0.12 to 0.24 ft^2 total) is used on other surfaces of the compartment to reject heat dissipation of the other equipment, such as multipliers, diplexers, etc. The two panels that contain this equipment can be held above 30°F during nonoperating times by thermostatically operated heaters.

3.9.4 Cable Requirements

A preliminary definition of the cable bundle required for interconnection between the RF compartment and the wideband module is given in Table 3.9-7. An estimate of the cabling required for the gimbal drive assembly is also included. The cable bundle is approximately 1.2 inches in diameter.

In the case of the power lines (28 V, +5 V, -5 V), multiple wires are utilized to provide acceptable voltage drop with maximum flexibility. A total length of 30 feet is assumed. For the 28 V line, which provides TWT power, four pair of 20 AWG wires result in a 0.4 V drop, or a power loss of about 1.2 watts. The wiring other than the RF cabling will be fine stranded copper with teflon insulation. This highly flexible type of wire is used on the FLTSATCOM solar array boom cabling and was used on the Skylab solar arrays.

Table 3.9-7. Cable Configuration

Signal	Number of Wires	Type of Wires	Diameter (inches)
Telemetry	20 wires	Single shielded 28 AWG	.093
TLM return	1 wire	Single shielded 24 AWG	.102
Coax 3 GHz		RG400*	.2
2 GHz		RG400*	.2
250 MHz		RG400*	.2
Switching oscillator	1 pair	2 cond shld 28 AWG	.124
Relay switching	6 wires	Single shielded 28 AWG	.093
Digital interface unit No. 2	2 wires	Single shielded 28 AWG	.093
Relay SW return	1 wire	Single shielded 24 AWG	.102
Power +28 V (3 amp)	4 pair	2 cond shld 20 AWG	.184
+15 V (0.05 A)	1 pair	2 cond shld 26 AWG	.134
+5 V (0.17 A)	2 pair	2 cond shld 20 AWG	.184
-5 V (0.45 A)	5 pair	2 cond shld 20 AWG	.184
Coax digital signals	4 coax	RG400*	
Gimble drive signals	10 pair	2 cond shld 28 AWG	.124
Gimble drive pwr (0.1 A)	2 pair	2 cond shld 28 AWG	.124

*RG400 Coax cable is similar to Astrolab Super-Flex cable 32000.

3.10 DIGITAL INTERFACE UNIT

Digital interface unit No. 2 (Figure 3.10-1) accepts TM and MSS data signals, and provides signal conditioning and a means for signal input mode control to the quadri-phase modulators. The unit, which is internally redundant, is located in the RF compartment.

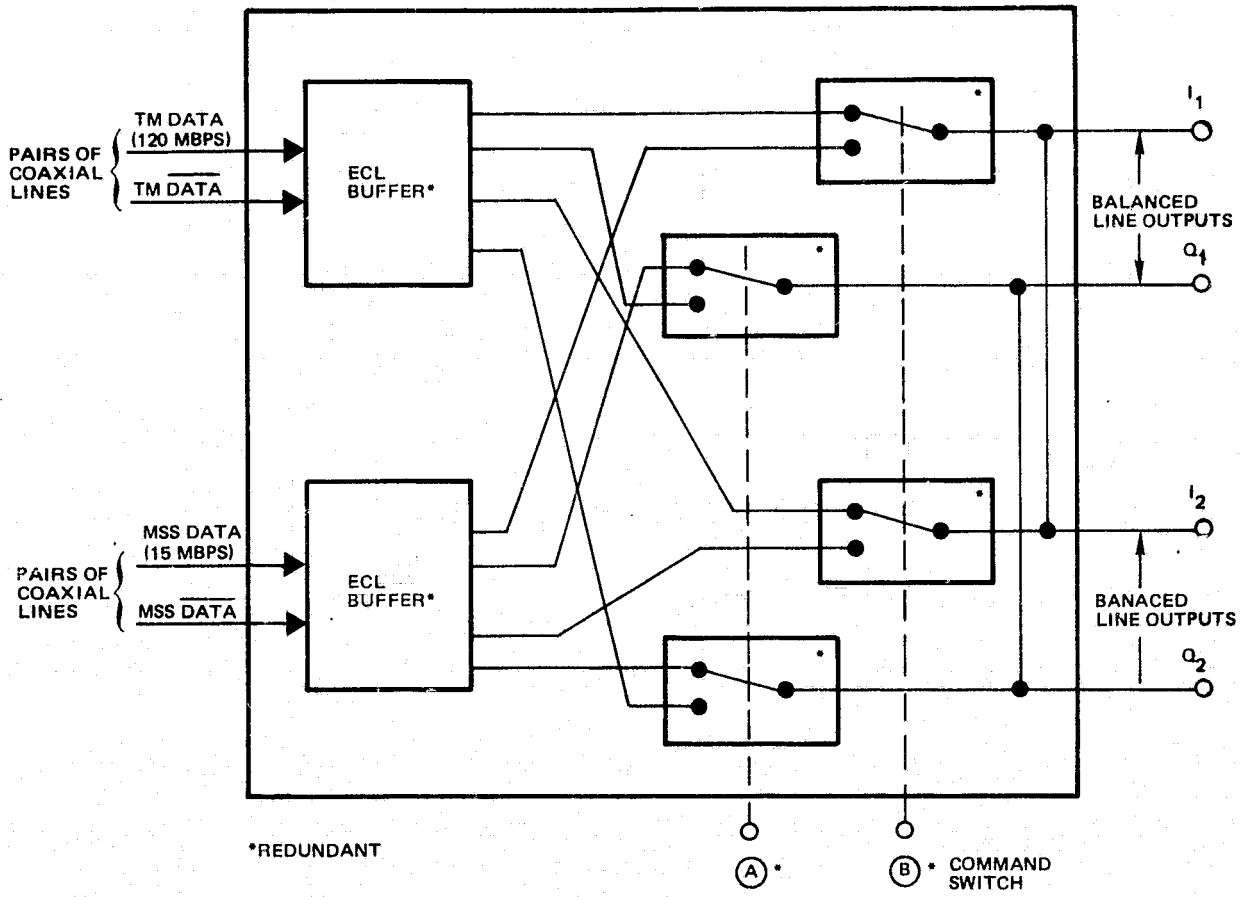

CONFIGURATION

A	B	
0	0	TM I CHANNEL, MSS Q CHANNEL (NORMAL MODE)
1	0	TM BOTH CHANNELS
0	1	MSS BOTH CHANNELS
1	1	NOT ALLOWED

Figure 3.10-1. RF Compartment Digital Interface Unit No. 2

The TM and MSS data signals are routed to the digital interface unit No. 2 from digital interface unit No. 1 located in the wideband module by two pair of coaxial cables 25 to 30 feet long. Balanced lines are used to provide noise immunity over the long cable runs and matched impedance is employed to prevent parasitic capacitance effects.

Since balanced lines are used, data and data complement ($\overline{\text{data}}$) are transmitted over each pair of coaxial cables. The data signal voltage is emitter coupled logic (ECL); i.e., logic "1" (-0.8 V) and logic "0" (-1.6 V). The 800 mV p-p data signal waveform from the wideband module should not be attenuated by more than about 2.5 dB over the coaxial cable run. Thus, a coaxial cable should be selected with no more than about 8 dB attenuation per 100 feet at 100 MHz.

The data signals received by the RF compartment digital interface unit are restored to squarewave form and ECL voltage levels by the ECL buffer receivers. Data signal input control to redundant quadriphase modulators is provided. In the normal mode of operation, the TM data signal is supplied to the redundant I channels and the MSS data signal is supplied to the redundant Q channels. Should one instrument be turned off or fail, the active instrument data signal is applied to both the I and Q channels via a ground command signal processed by the RIU as shown in Figure 3.10-1. Telemetry data, indicating the state of control, is accepted and processed by the RIU. Finally, compatible ECL balance line output signals from the digital interface unit are supplied to the RF QPSK modulators.

A digital implementation of the digital interface unit is shown in Figure 3.10-2. Board size and weight and power consumption are given in Figure 3.10-3 and Table 3.10-1, respectively. MECL logic integrated chips are used for the logic functions and resistor type integrated chips for the passive components. The board size is estimated from the number of chips employed as indicated in Figure 3.10-3.

Table 3.10-1. Digital Interface Unit No. 2 Power Consumption

Quantity	Chip	Current
4	10674	146 mA
1	10616	21 mA
2	10624	132 mA
1	10601	26 mA
1	Resistor chip	80 mA
	Total	405 mA @ -5 V
		32 mA @ +5 V
	Power	2.20 watts

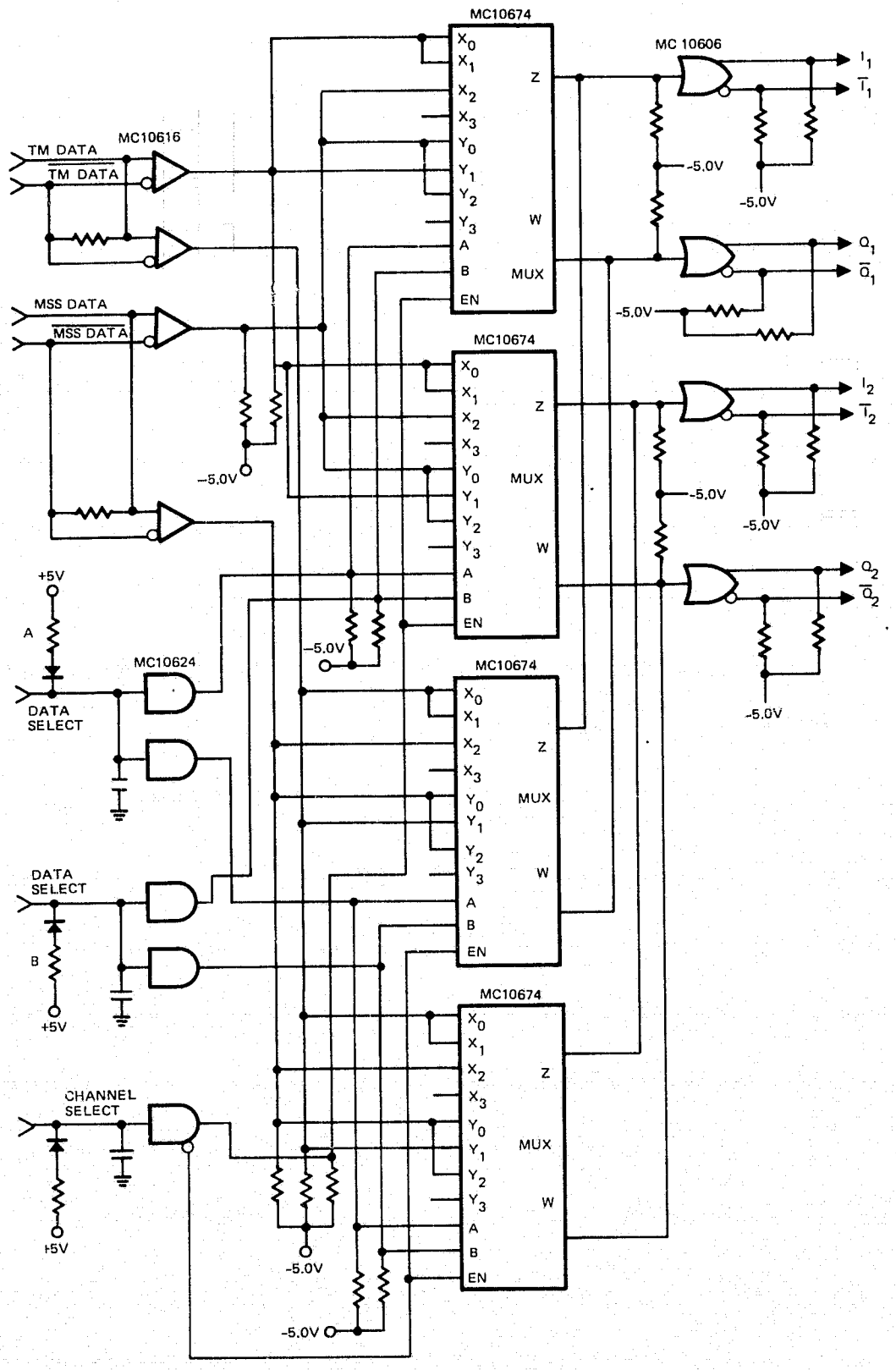

Figure 3.10-2. RF Digital Interface Logic Diagram

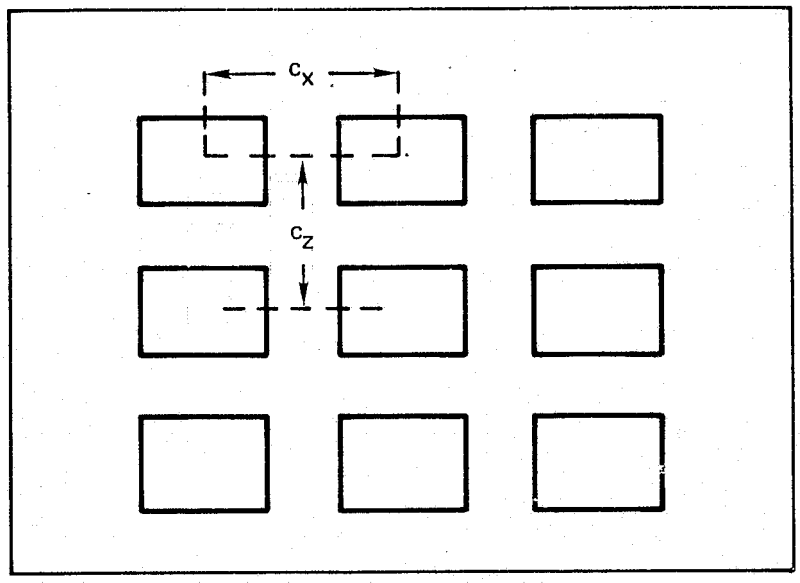

CHIP TYPE		SIZE	WT
(A)	CERAMIC PACKAGE HIGH =	0.3"	
	C_X:	0.9" x 4 = 3.6"	0.4 LB
	C_Z:	0.7" x 4 = 2.8"	
(B)	FLAT PACKAGE HIGH =	0.08"	
	C_X:	0.5(4) = 2.0"	0.3 LB
	C_Z:	0.45 (4) = 1.8"	

Figure 3.10-3. Board Size (RF Compartment)

3.11 TDRSS LINK PERFORMANCE ANALYSIS

Section 3.11.1 considers degradation in link performance when the line-of-sight between the LF/O spacecraft and the TDRSS grazes the earth. Clearly, the closer the line-of-sight can approach earth tangency (zero altitude), the smaller the LF/O-to-TDRSS coverage zone of exclusion.

Factors such as tropospheric absorbtion, refraction, earth surface multipath, and CCIR flux density restrictions were investigated and bounding altitude values established. The reflected ray(s) behaviour associated with the multipath analysis is extremely difficult to quantify precisely and the result presented may be overly conservative.

Sections 3.11.2 through 3.11.4 present the link budgets analyses for the TDRSS forward and return links.

3.11.1 Communication at Earth Grazing

Estimates of the several effects which might constitute bounds on the lowest altitude LF/O to TDRSS line-of-sight are summarized as follows:

- Tropospheric absorption — At altitudes above about 40,000 feet (12 km), the effects of precipitated water vapor are absent. The path absorption due to molecular oxygen and water vapor at 40,000 feet is about 0.23 dB. The corresponding value at 80,000 feet (24 km) is about 0.006 dB. An altitude of 40,000 (12 km) is taken as a conservative lower limit.

- Refractive beam bending — Refractive beam bending at 40,000 feet is about 0.23°. To the extent that the beam bending is deterministic, a correction could be applied to the pre-acquisition open loop pointing program to account for beam bending. The more conservative, and the recommended approach, is to choose the minimum altitude where beam bending is negligible compared to the TDRSS and LF/O spacecraft KSA beamwdiths. This would occur at about 93,000 feet (28 km) where beam bending is about 0.026°.

- Multipath — A lower limit on line-of-sight altitude due to earth surface multipath has been estimated including such factors as

  Spherical earth divergence

  Assumed surface roughness

  LF/O spacecraft antenna pattern discrimination

  TDRSS antenna pattern discrimination

  Multipath ray atmospheric absorption

  Degradation in link performance (E_b/N_o) resulting from multipath.

  A direct-to-multipath signal ratio of 30 dB has been chosen as the allowable value. This occurs at an altitude of approximately 133,333 feet (40 km) and corresponds to a link degradation of 0.25 dB or less.

- Flux density restriction — Calculations indicate that if the TDRSS guidelines are followed, a minimum height of 180 km is allowable for the LF/O spacecraft to TDRSS line-of-sight above earth. This corresponds to the LF/O mode of 15 Mbps MSS data transmission (TM transmission off).

Clear Tropospheric Absorption

The data given in Figure 7-10 of ref. 13 is used. This gives the absorption in dB/km due to water vapor and molecular oxygen as a function of altitude for the climate of Washington, D.C. The referenced figure gives data to 75,000 feet; data for higher altitudes is given in Figure 7-11 in the reference. Absorption at altitudes of 40,000 feet and above is not very climate sensitive for the Ku-band frequency region considered. The restriction to greater than 40,000 feet eliminates effects due to precipitated water vapor. For altitudes greater than 40,000 feet, the data in the referenced figure was fitted to the following expression

$$\log \alpha = -1.6 - 0.04\, h \tag{3.6}$$

where α = attenuation dB/km and h = altitude above the earth's surface in thousands of feet. To calculate the total attenuation A along the path we evaluate

$$A = \int \alpha(h)\, dx \tag{3.7}$$

From Figure 3.11-1

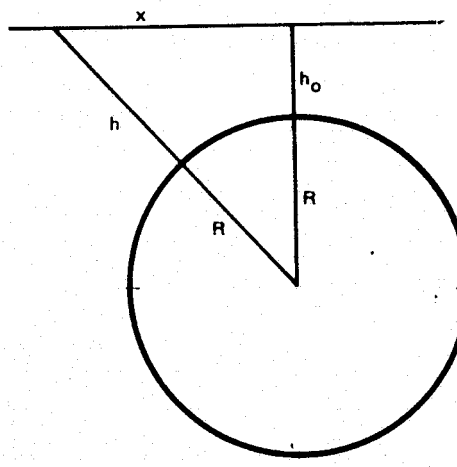

Figure 3.11-1. Signal-Earth Geometry

$$x^2 = (R + h)^2 - (R - h_o)^2$$

$$= (2R + h + h_o)\,(h - h_o)$$

and

$$2x\, dx = 2(R + h)\, dh$$

giving

$$A = 2 \int_{h_o}^{\infty} \alpha(h)\, \frac{(R + h)\, dh}{[(2R + h + h_o)\,(h - h_o)]^{\frac{1}{2}}} \tag{3.8}$$

where the integration has been extended to ∞. From (3.6)

$$\alpha(h) = e^{-(2.3)(1.6) - (2.3)(0.04)h}$$

$$= \frac{e^{-k_1 - k_2 h}}{3.28} \quad \text{dB/kilofoot} \tag{3.9}$$

with

$$k_1 = 3.68$$

$$k_2 = 0.092$$

In (3.8) the major contribution to the integral comes when $h \approx h_o$. In this range, $R + h \approx R + h_o \approx R$ since $h_o/R << 1$. Because of the exponential factor, we are justified in using the approximation

$$A \approx \frac{\sqrt{2R}}{3.28} e^{-k_1} \int_{h_o}^{\infty} \frac{e^{-k_2 h}}{\sqrt{(h - h_o)}} \, dh$$

$$A \approx \frac{\sqrt{2R}}{3.28} e^{-k_1 - k_2 h_o} \int_{o}^{\infty} \frac{e^{-k_2 y}}{\sqrt{y}} \, dy$$

$$A \approx \frac{\sqrt{2R}}{3.28} e^{-k_1 - k_2 h_o} \sqrt{\frac{\pi}{k_2}} \, .$$

and

$$A \approx 9.21 \, e^{-0.092 \, h_o} \tag{3.10}$$

For h_o = 40,000 ft (12 km) A = 0.23 dB

For h_o = 80,000 ft (24 km) A = 0.006 dB

These values depend on the data given in the cited reference. It appears that these were calculated on the basis of the Van Vleck, Weisskopf theory from radiosonde measurements of water vapor content at the various altitudes.

Refractive Beam Bending

It is desired to estimate the bending in a radio beam sent from the LF/O to the TDRSS and passing through the earth's atmosphere at a given altitude. If the atmospheric refractive index n(r) is a function of r only where r is the distance to the point of closest approach, the path of a ray will be curved and obey Snell's law for polar coordinates

$$r_1 n_1(r) \cos\theta_1 = r_2 n_2(r) \cos\theta_2 = \cdots = K \tag{3.11}$$

Figure 3.11-2 illustrates a ray passing the earth. The angle θ at a point P is shown as the angle between the ray's direction at P and the normal to a radial line from P to the earth's center. If n(r) = 1, the ray has a constant direction. Furthermore

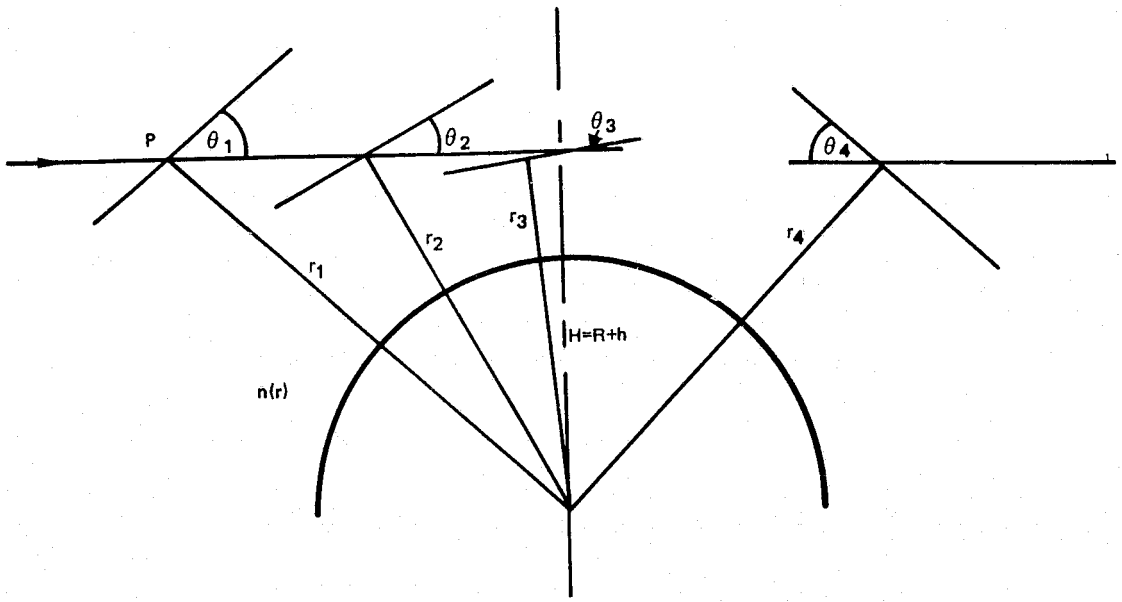

Figure 3.11-2. Refractive Effects

r cos θ = constant and the constant K is the perpendicular distance H from the earth's surface to the ray (a straight line).

In the second case, if the changes in n are gradual (compared to a wave length), a standard result for the net angular deviation τ in the direction ray when it travels from point 1 with index n, to point 2 with index n_2 (ref. 13) is

$$\tau = - \int_1^2 \frac{\cot \theta}{n} \, dn \tag{3.12}$$

From Figure 3.11-2

$$\tau = - \int \frac{K}{n(n^2r^2 - K^2)^{\frac{1}{2}}} \, dn \tag{3.13}$$

Furthermore, a relation valid at altitudes greater than 10 km between n and r is

$$n(r) = 1 + a \, e^{-b(r - R)} \tag{3.14}$$

where

$a = 2.89 \, 10^{-4}$

$b = 0.136$ (reciprocal of the scale height km^{-1})

R = earth's radius (kilometers)

We can approximately evaluate (3.12). If the ray is traveling at a great distance from earth where $n \approx 1$ so that it would pass the earth at a distance h, then $K = R + h$. Inserting this and (3.14) into (3.13) yields

$$\tau = - \int \frac{K}{[r^2 - K^2]^{\frac{1}{2}}} \frac{(-ab)\, e^{-b(r-R)}}{1 + a\, e^{-b(r-R)}}\, dr \qquad (3.15)$$

The integral from $r = \infty$ to the point of approximate closest approach to the earth is

$$\tau_o \approx ab\, e^{bR} \int_{\infty}^{K} \frac{K}{[r^2 - K^2]^{\frac{1}{2}}}\, e^{-br}\, dr \qquad (3.16)$$

The total deviation of the ray in passing the earth, starting from a great distance "to the left" (see Figure 3.11-2) to a great distance to the right, is $2\tau_o$. The transformation $r = xK$ transforms the integral into

$$\tau_o = ab\, e^{bR}\, K \int_{\infty}^{1} \frac{e^{-bKx}}{(x^2 - 1)^{\frac{1}{2}}}\, dx \qquad (3.17)$$

The integral is the modified Bessel function $K_0(bK)$ (ref. 14). Since bK is very large, an asymptotic expansion for it can be used, i.e.

$$K_0(z) = \sqrt{\frac{\pi}{2z}}\, e^{-z} \left(1 - \frac{1}{8z} + \frac{(1x9)}{2!8z^2} + \cdots\right) \qquad (3.18)$$

Finally the total deviation is

$$2\tau_o \quad 2\, abe^{bR}\, K \sqrt{\frac{\pi}{2bK}}\, e^{-bK} = 2a \sqrt{\frac{Kb\pi}{2}}\, e^{-bh} \qquad (3.19)$$

where $K = R + h$. Inserting the values of the constants, and noting $K \approx R$, we obtain

$$2\tau_o \approx 2.13 \times 10^{-2}\, e^{-0.136h} \text{ radians} \qquad (3.20)$$

where h is in kilometers. For h = 40,000 feet, $2\tau_o = 0.406 \times 10^{-2}$ radians = 0.23°. For h = 93,000 feet, $2\tau_o = 0.045 \times 10^{-2}$ radians = 0.026°.

We have assumed the beam refraction (ray bending) to be deterministic. To the extent this is true, it could be included in the loop antenna pointing program. One would not expect rapid spatial or temporal changes in the troposphere above about 100,000 feet. Daily changes due to solar heating (atmospheric tides) and seasonal changes would be expected. The impact of these on the initial pointing error is uncertain.

Because the antenna angular beamwidths involved are small (<1°), but finite, the differential ray bending for rays defining a given power contour must be considered. We have not considered this quantitatively. Since the radial dependence of the tropospheric refractive index constitutes a converging "lens," the focal length of this lens is at least 100 earth radii (ref. 15), based on the calculated bending angles. Since this is much greater than the distance of either the LF/O or even the TDRSS, any signal loss due to defocussing should be very small.

Multipath

If the transmission line-of-sight between the LF/O and the TDRSS approaches the earth's surface too closely, a strong sidelobe or a portion of the main beam will impinge on the earth's surface, and be reflected as one or more multipath signals into the TDRSS antenna. Since the user satellite is in relative motion to the reflecting surface, the multipaths produce time-dependent fading. Table 3.11-1 outlines the parameters affecting the multipath estimate (ref. 16).

Table 3.11-1. Parameters Affecting Multipath Estimate

Surface reflection coefficient (r) (smooth surfaces)	Amplitude and phase required. Different values for varying angle of incidence and for linear polarization parallel to and perpendicular to the plane of incidence. (Plane containing the electric vector and the normal to the surface.)
Reflectivity correction ($1 - e^{-\gamma}$) (rough surfaces)	A factor of $1 - e^{-\left(\frac{4\pi\,\sigma}{\lambda}\sin\theta\right)^2}$ must be applied to the smooth surface reflectivity where σ = rms surface roughness θ = grazing angle (complement of incidence angle) A surface is considered smooth if $\sigma < \frac{\lambda}{8 \sin\theta}$
Divergence factor (D)	A correction factor (≤ 1) applied to the reflectivity to account for the spherical reflecting surface of the earth.

Angles near grazing are of interest here; i.e., $\theta \ll 1$ radian.

In the most stringent case, $\lambda = 2 \times 10^{-2}$ meters (15 GHz), and for smooth surface behavior at an angle of 1°, $\sigma < 0.14$ meters. This is a rather smooth surface to expect over large areas of either terrain or ocean. For specular reflection, the smooth area would have to persist over one Fresnel zone. For an angle of 0.25°, $\sigma < 0.57$ meters defines a smooth surface. If signal absorption in the reflection process is neglected, and if only a single scattering occurs on a given signal component, the ratio of the power represented by the specular (P_s) to that of the diffuse (P_d) multipath is

$$\frac{P_s}{P_d} = \frac{1}{e^{\gamma} - 1} \text{ with } \gamma = \left(\frac{4\pi\sigma}{\lambda} \sin \theta\right)^2 \quad \text{(ref. 23)} \tag{3.21}$$

If σ is taken as 10 times the "smooth" value of 0.14 meters estimated above and $\theta = 1°$ then

$$\gamma = 2.35 \times 10^2$$

and diffuse reflection overwhelms the specular component. For $\sigma = 0.14$ m, (6 inches), $\gamma = 2.35$ and $P_s/P_d \approx 0.1$. Hence, even in this case of a postulated rather smooth surface (rms surface roughness of 0.14 m), about 90% of the reflected energy is estimated to be diffuse.

The value of P_d normalized to the incident direct power is

$$P_d = D^2 r^2 \left(1 - e^{-\gamma}\right) \text{ (ref. 16)} \tag{3.22}$$

From ref. 17, $D \approx 0.9$ and based on refs. 17 and 18, the reflectivity r for vertical and horizontal polarization achieves comparable values for angles less than 5° for Ku-band frequencies. We will assume $r = 0.5$ for the purpose of the estimate. We will further assume an rms surface roughness of 1.4 meters at a grazing angle, θ, of 1°. Then, as shown above

$$\gamma = 2.35 \times 10^2$$

and $P_d = (0.9)^2 |0.5|^2 (1 - e^{-2.35 \times 10^2}) = 0.2$ or a reduction between incident and reflected power of 7 dB.

Only a fraction of the total diffuse multipath power calculated above will be successful in entering the TDRSS receiving aperture. This fraction is difficult to estimate, as it depends on the distribution of slopes associated with the roughness scale of the reflecting surface. If the surface slopes are small, the fading tends to exhibit characteristics of specular multipath with periodic fluctuations in signal strength. In this case, the "diffuse" components are clustered around the specular direction. If the surface slopes are large, the multipath must be represented by a complex Gaussian process for the signal strength and signal phase components.

If the reflection were obtained from a smooth surface, some additional multipath rejection might be obtained due to the phase of the surface reflected component. For smooth (planar) or very symmetrical objects, the sense of circular polarization is reversed (ref. 17) upon reflection. Since the receiver is designed to accept, say, the RHCP of the direct line-of-sight transmission, the LHCP due to the multipath reflection would be rejected by an amount determined by the axial ratio of the antenna. Such polarization rejection does not seem likely in this case because of the predominantly diffuse reflection. If the grazing angle becomes smaller than about 0.1°, then the multipath could become specular even for relatively large rms roughnesses.

Antenna Beam Pattern Discrimination and Atmospheric Absorbtion on the Multipath

The previous discussion established an estimated multipath reflection attenuation (7 dB). Additional considerations are: (1) the multipath signal attenuation due to the LF/O spacecraft antenna and the TDRSS antenna pattern discrimination in the direction of the multipath signal, and (2) the atmospheric absorbtion of the incident and reflected multipath signal.

The direct ray shown in Figure 3.11-3 represents the centerline of the transmitting and receiving antenna beams. Its perigee with respect to the earth's surface is at height h_2. The multipath component represents a ray corresponding to angles ϕ_A and ϕ_B with respect to the main beam center of the antennas.

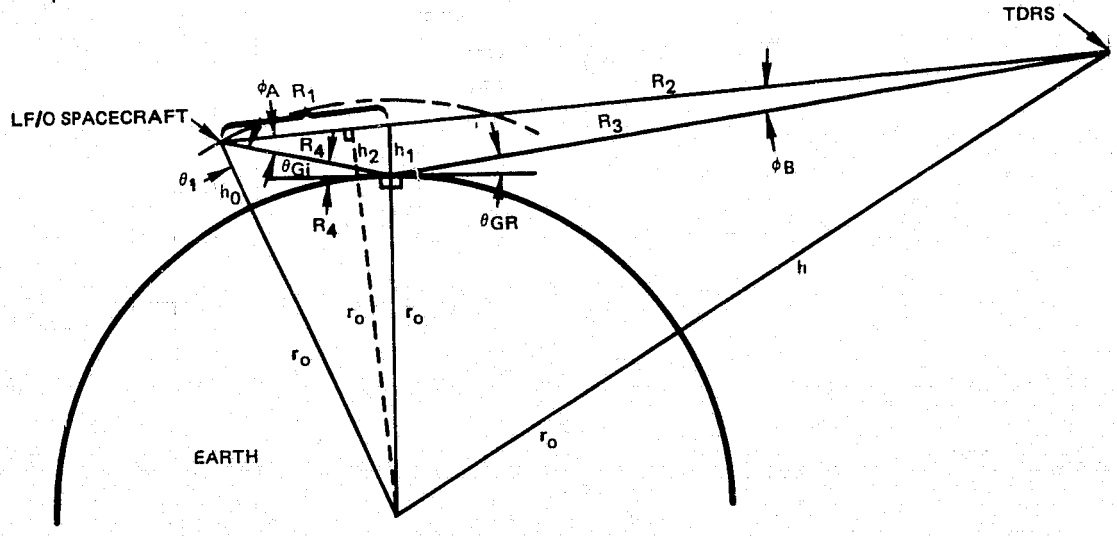

h_0 = LF/O SPACECRAFT CIRCULAR ALTITUDE (705 km)
h = TDRS SPACECRAFT CIRCULAR ALTITUDE (35,860 km)
h_1 = HEIGHT ABOVE EARTH GRAZING
h_2 = MINIMUM HEIGHT ABOVE EARTH CORRESPONDING TO h_1
θ_{Gi} = θ_{GR} = EARTH GRAZING ANGLE FOR INCIDENT AND REFLECTED RAYS
ϕ_A = ANGLE BETWEEN THE LF/O SPACECRAFT DIRECT AND MULTIPATH TRANSMITTED SIGNALS
ϕ_B = ANGLE BETWEEN THE TDRS DIRECT AND MULTIPATH RECEIVE SIGNALS

Figure 3.11-3. LF/O Spacecraft-TDRSS-Earth Geometry

The multipath-to-direct signal ratio (P_D/P_M) received by the TDRSS antenna is given by

$$\left(\frac{P_D}{P_M}\right) = X_A(dB) + X_B(dB) + L_A(dB) + L_B(DB) + 7\ dB \tag{3.23}$$

where

$X_A(dB), X_B(dB)$ = LF/O transmit and TDRSS receive antenna gains corresponding to angle ϕ_A and angle ϕ_B, respectively.

$L_A(dB), L_B(dB)$ = atmospheric absorption losses corresponding to the incident and reflected signal paths, respectively.

The 7 dB is the estimated reduction of the incident signal power following earth grazing as described earlier.

The following relationships are determined from the geometry shown in Figure 3.11-3 and the law of cosines and sines

$$\theta_o = \theta_{Gi} = \theta_{GR} \tag{3.24}$$

$$R_3 = -r_o \sin\theta_o + \sqrt{h^2 + 2h\ r_o + r_o^2 \sin^2\theta_o} \tag{3.25}$$

$$R_4 = -r_o \sin\theta_o + \sqrt{h_o^2 + 2h_o r_o + r_o^2 \sin^2\theta_o} \tag{3.26}$$

$$R_1 + R_2 = K_1 = \sqrt{R_4^2 + R_3^2 + 2R_3\ R_4 \cos(2\theta_o)} \tag{3.27}$$

$$\phi_A = \cos^{-1}\left[\frac{K_1^2 + R_4^2 - R_3^2}{2R_4\ K_1}\right] \tag{3.28}$$

$$\phi_B = \cos^{-1}\left[\frac{K_1^2 + R_3^2 - R_4^2}{2R_3\ K_1}\right] \tag{3.29}$$

$$K_2 = \frac{R_1}{R_2} = \frac{\sin\theta_B}{\sin\phi_A} \tag{3.30}$$

$$R_2 = \frac{K_1}{K_2 + 1} \tag{3.31}$$

$$h_1 = R_2 \frac{\sin\phi_B}{\cos\theta_o} \tag{3.32}$$

$$h_2 = (h_o + r_o) \sin (\phi_A + \theta_1) - r_o \tag{3.32}$$

$$\theta_1 = \cos^{-1} \left[\frac{h_o^2 + 2r_o h_o + R_4^2}{2(h_o + r_o) R_4} \right] \tag{3.34}$$

The relative reduction in the LF/O to TDRSS transmit antenna gain from peak gain (X_A) corresponding to angle ϕ_A is estimated by the antenna gain pattern envelope shown in Figure 3.7-21.

Similarly, the relative reduction in the TDRSS antenna gain from peak gain (X_B) corresponding to the reception angle ϕ_B is estimated from the curve connecting the antenna pattern peaks generated by the expression for a parabolic antenna pattern

$$P(\theta) = \frac{2J_1(X)}{X} \tag{3.35}$$

where

$X = \frac{\pi}{\lambda} \sin \theta$

d = diameter of dish (4.9 meters)

λ = signal wavelength (0.02 meter)

θ = angle off boresight

The atmospheric absorption losses L_A and L_B are determined from Hogg and Mumford (ref. 19).

The minimum height above the earth, h_2, is plotted as a function of P_D/P_M (dB) and the grazing angle ϕ_G in Figure 3.11-4. Figure 3.11-4 also shows the bounding altitudes for each propagation effect previously discussed and also shows the altitudes corresponding to flux density restrictions.

The TRW LINK simulation program was utilized to estimate the degradation in received E_b/N_o due to the addition of the multipath signal to the direct signal. The following case was simulated:

- The delayed data stream is uncorrelated with the direct data stream
- The bit transition times for the direct and multipath signals are coincident
- The RF carriers are in-phase or out-of-phase (in the quadrature case, negligible degradation occurs)
- The direct signal E_b/N_o is 15 dB (see Section 3.11.3).

The results are given in Table 3.11-2.

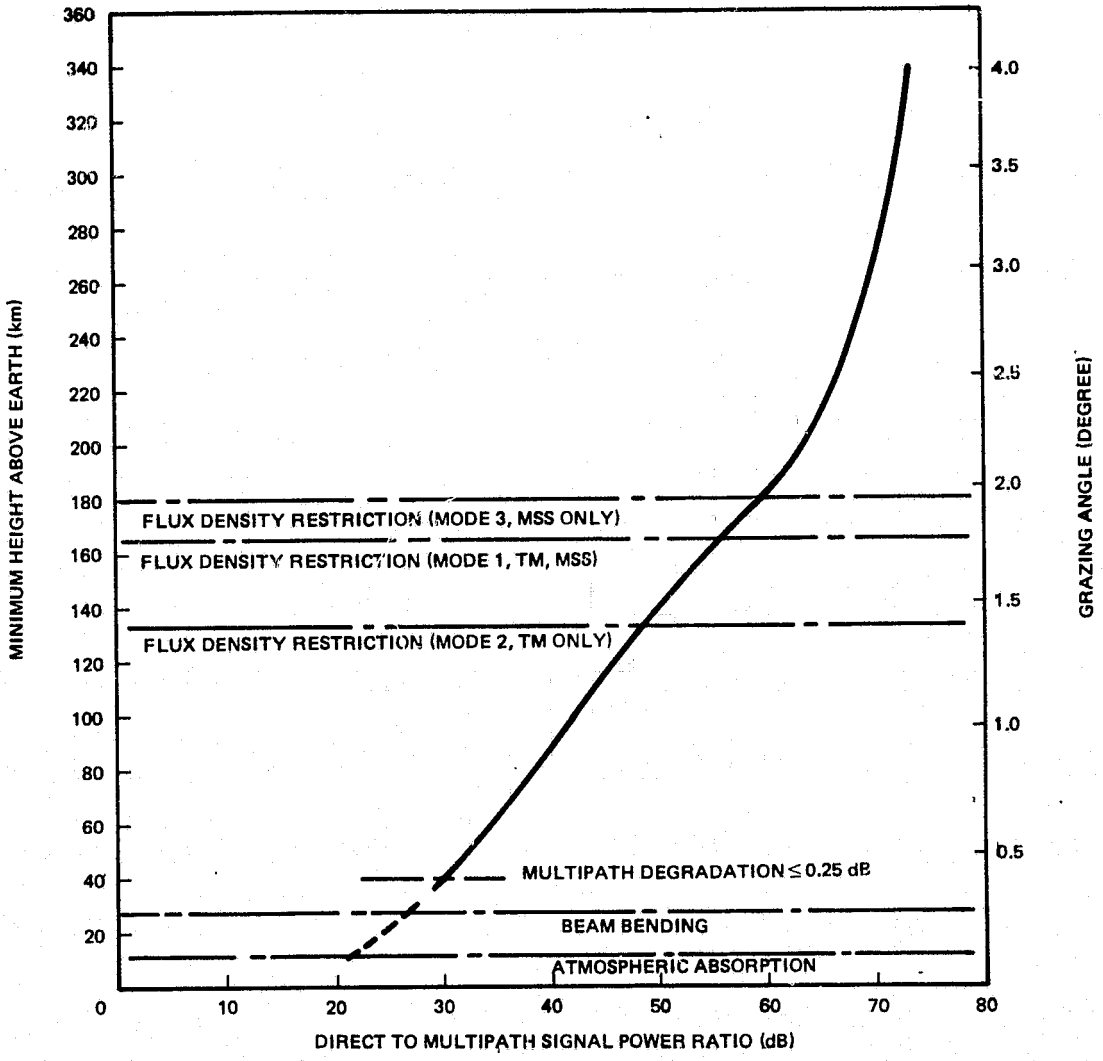

Figure 3.11-4. Minimum Earth Grazing Height for L/F/O TDRSS Ku-Band Transmission

Table 3.11-2. E_b/N_o Degradation Due to Multipath

Direct-to-Multipath Ratio (dB)	Degradation (dB)
25	0.49
30	0.25
35	0.14

Note that the "average" degradation would be less, since the bit stream transitions and RF carrier phases would be continuously shifting relative to each other with time. Further, implicit in the preceeding simulation is the assumption of specular multipath. Diffuse multipath will introduce noise perturbations in phase and amplitude of the reflected signal. An allowable value of 30 dB has been selected.

Flux Density Requirements

The power flux density requirements for TDRSS are given by (ref. 20)

$$\begin{aligned} &PFD \leq -152 \text{ dBW/m}^2\text{/4 kHz} && \text{for } \theta_{e\ell} < 5^\circ \\ &PFD \leq -152 + \frac{\theta-5}{2} \text{ dBW/m}^2\text{/4 kHz} && \text{for } 5^\circ \leq \theta_{e\ell} \leq 25^\circ \\ &PFD \leq -142 \text{ dBW/m}^2\text{/4 kHz} && \text{for } 25^\circ \leq \theta_{e\ell} \leq 90^\circ \end{aligned} \qquad (3.36$$

and the power flux density of a signal impinging on the earth is given by

$$PFD \simeq \frac{EIRP_1\ (4000)}{4\pi\ R^2\ (BR_1)} + \frac{EIRP_2\ (4000)}{4\pi\ R^2\ (BR_2)} \quad \text{for QPSK} \qquad (3.32)$$

and BR >> 4000 bps.

Forward Link

The forward link QPSK signal from the TDRSS consists of a PN modulated quadriphase signal sequenced at 3 megachips/sec. Since $EIRP_1$ and $EIRP_2$ and the corresponding BR_1 and BR_2 are equal, the PFD for the forward link is

$$PFD \approx \frac{2\ EIRP_1\ (4000)}{4\pi\ R^2\ (BR_1)} \qquad (3.38)$$

or

$$PFD \approx \frac{EIRP_T\ (4000)}{4\pi\ R^2\ (BR)} \qquad (3.39)$$

Substituting the value of $EIRP_T$ = 43.5 dBW, BR = 3 megachips/sec into (3.37) yields a PFD = -158.7 dBW/m^2/4 kHz. This meets the minimum flux density requirement so that the forward link does not determine the minimum grazing height.

Return Link

The return link design provides for three signal modes. For mode 1, TM (120 Mbps) is modulated on the I channel and MSS (15 Mbps) is modulated on the Q channel. For mode 2, TM is modulated on both the I and Q channels, and for mode 3, MSS is modulated on the I and Q channels. The I and Q channel powers are fixed at 4:1; therefore, $EIRP_1$ (I channel) is 57.8 dBW and $EIRP_2$ (Q channel) is 51.8 dBW. Table 3.11-3 summarizes the power flux density level which impinges the earth. To reduce this level, the main (peak) beam of the LF/O antenna must be restricted away from earth grazing. The restricted angle is assumed to be equal to the elevation angle. Mode 3 generates the largest flux density and thus requires the largest angle restriction of 3.85° which

Table 3.11-3. Flux Density Calculations

	Mode 1	Mode 2	Mode 3
EIRP 1 = 57.8 dBW BR1 =	120 Mbps (80.8 dB)	120 Mbps (80.8 dB)	15 Mbps (71.8 dB)
EIRP 2 = 51.8 dBW BR2 =	15 Mbps (71.8 dB)	120 Mbps (80.8 dB)	15 Mbps (71.8 dB)
$\frac{EIRP_1}{BR_1}$ (dB)	-23.0	-23.0	-14.0
$\frac{EIRP_2}{BR_2}$ (dB)	-20.0	-29.0	-20.0
$\frac{EIRP_1}{BR_1} + \frac{EIRP_2}{BR_2}$	0.015012	0.00627	0.04981
PFD ($dBW/m^2/4$ kHz)	-121.9 $\theta_e = 3.5°$	-125.9 $\theta_e = 2.75°$	-116.6 $\theta_e = 3.85°$
LF/O antenna gain relative to peak (dB)	-30.1	-26.1	-35.4
PFD ($dBW/m^2/4$ kHz)	-152.0	-152.0	-152.0
Minimum height (km)	165.8	133.8	180.1

corresponds to a point on the LF/O antenna pattern of -35.4 dB down from the main peak pattern. The height above the earth grazing point is given by

$$h_1 = R_{e\ell} \sin \theta_{e\ell} = 180.1 \text{ km} \tag{3.40}$$

where

$$R_{e\ell} = -r_o \sin \theta_{e\ell} + \sqrt{h_o^2 + 2h_o r_o^2 \sin^2 \theta_{e\ell}} = 2682.0 \text{ km} \tag{3.41}$$

h_o = LF/O circular altitude (705 km)

r_o = mean radius of the earth (6378.2 km)

For the normal case, mode 1, the restricted angle is 3.5° which corresponds to a minimum height of 165.8 km.

Conclusions

The minimum altitude for the LF/O to TDRSS line-of-sight as limited by propagation effects is estimated to be about 40 km. This is based on return link degradation due to multipath. The minimum altitide based on flux density restrictions as stated in ref. 20 is 180 km.

3.11.2 TDRSS Link Transmit and Receive Component Loss Budgets

The transmit output circuit and receive input circuit are shown in Figures 3.11-5 and 3.11-6. The loss budgets are given in Tables 3.11-4 and 3.11-5. The loss as shown are based on best estimates, not worst case values typically contained in vendor specifications. Immersion gold coated WR-62 waveguide is utilized to minimize waveguide loss.

Table 3.11-4. Transmit Loss Budget

Item	Loss (dB)
Waveguide (<1 ft)	0.05
Waveguide switch	0.10
Waveguide (<1 ft)	0.05
Diplexer (transmit filter 5-pole)	0.70
Waveguide (≈2 ft)	0.10
VSWR	0.10
	1.10 dB

Table 3.11-5. Receive Loss Budget

Item	Loss (dB)
Waveguide (≈2 ft)	0.1
Diplexer (receive filter 4-pole)	0.9
Waveguide (≈2 ft)	0.1
10 dB coupler (includes tolerance)	0.5
Waveguide (<1 ft)	0.05
Waveguide switch	0.10
VSWR loss	0.10
	1.85 dB

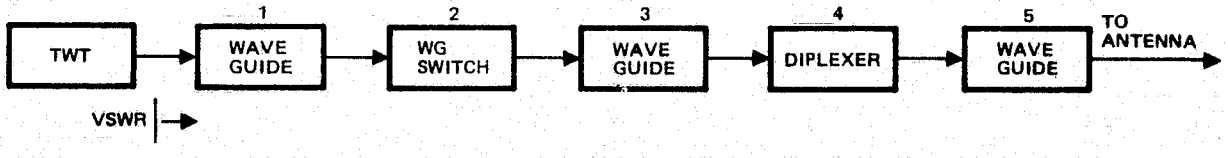

Figure 3.11-5. Transmit Output Circuit

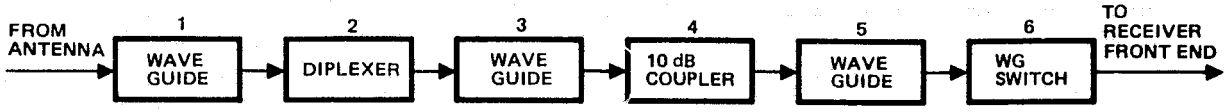

Figure 3.11-6. Receive Input Circuit

3.11.3 Transmit Link Performance

The normal communication mode for the LF/O to TDRSS Ku-band (15 MHz) return link is the transmission of TM data sequenced at 120 Mbps on the QPSK I channel and MSS data sequenced at 15 Mbps on the Q channel. The I and Q channels powers are adjusted 4:1, the maximum allowable power split. The I channel receives 80% of the transmitted EIRP and the Q channel 20%.

Additional margins of 2.4 dB for the TM and 4.5 dB for the MSS links over the 3 dB designed link performance are achieved. The link performance is based on the use of a 20-watt TWTA transmitter, a 6-foot diameter shaped-Cassegrain autotrack antenna, and the TDRSS received Ku-band return link interface parameters as summarized in Table 3.11-6.

The space loss for the LF/O to TDRSS link is based on a slant range computed for a 180 km earth grazing height as determined earlier.

3.11.4 Receive Link Performance

It was established in Section 3.1 that an antenna autotrack system is necessary to provide maximum TDRSS link transmit performance. In order to autotrack, a forward link signal from the TDRSS must be received so that autotrack signals can be modulated onto the received signal. Furthermore, the autotrack performance is a function of the receive link performance.

The TDRSS forward link signal is received with the LF/O 6-foot steerable dish antenna that is used for transmitting return link signals to the TDRSS. The receive frequency is 13.775 GHz and the link performance is computed on the basis of a LF/O to TDRSS antenna line-of-sight of 100 to 180 km above earth grazing as depicted in Figure 3.11-3.

The receive system temperature is computed in Figure 3.11-7 and the receive link performance analysis is given in Table 3.11-7. The results show that an 11 dB IF signal-to-noise ratio is realized during autotrack.

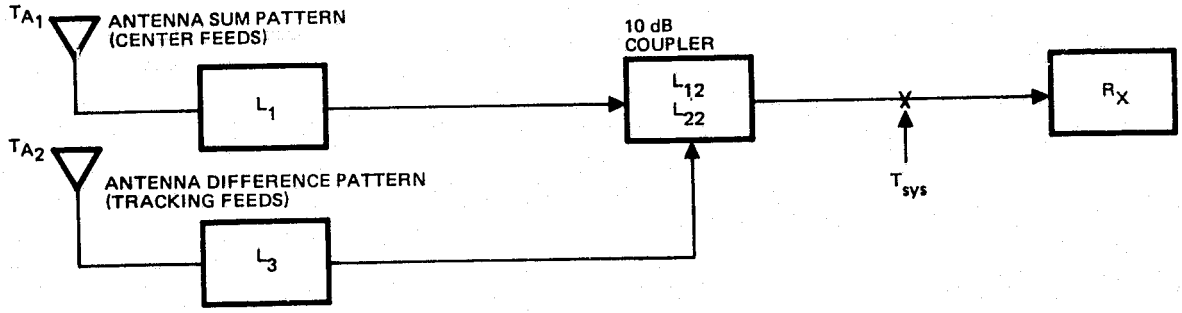

L_1

DIPLEXER	=	0.9 dB
WAVEGUIDE	=	0.2 dB
VSWR MISMATCH	=	0.1 dB
TOTAL	=	1.2 dB ⇨ 1.318

L_{12}, L_{22}

L_{12}	= 0.5 dB	⇨ 1.122
L_{22}	= 10.0 dB	⇨ 10

L_3

COMPARATOR	= 0.5 dB	⇨ 1.259
WAVEGUIDE	= 0.5 dB	

R_X (INCLUDES 0.2 dB SWITCH AND WAVEGUIDE LOSS)

NF = 6.1 dB ⇨ 4.074

$$T_{sys} = \frac{T_{A_1}}{L_1 L_{12}} + \frac{(L_1 - 1)}{L_1 L_{12}} T_o + \frac{(L_{12} - 1)}{L_{12}} T_o + \frac{T_{A_2}}{L_3 L_{22}} + \frac{(L_3 - 1)}{L_3 L_{22}} T_o + (F-1)T_o$$

$T_{A_1} = T_{A_2} = T_o = 290^\circ K$

$T_{sys} = 1210.5^\circ K$

$N_o = kT_{sys} = -197.8$ dBw/Hz

Figure 3.11-7. Receive System Noise Temperature

Table 3.11-6. TDRSS Ku-Band Return Link Performance

Parameter	Value	Notes
S/C xmit pwr	12.0 dBW	20 watt transmitter (80% for TM, 20% for MSS)
S/C ant gain	47.0 dBi	6-foot parabolic dish
S/C line loss	1.1 dB	See Table 3.11-4
S/C pointing loss	0.1 dB	Autotrack analysis
TDRSS EIRP	57.8 dBW	
Space loss	208.9 dB	100 to 180 km earth grazing height
Polarization loss	0.5 dB	TDRSS User's Guide, May 1975
TDRSS pointing loss	0.5 dB	TDRSS User's Guide, May 1975
TDRSS antenna gain	52.6 dBi	TDRSS User's Guide, May 1975
Power at antenna output port	- 99.5 dBW	
System temperature	893°K	Referred to antenna output terminals, TDRSS User's Guide, May 1975
TDRSS noise spectral density	-199.1 dBW/Hz	TDRSS User's Guide, May 1975
Received signal power-to-noise spectral density ratio	99.6 dB/Hz	
TDRSS transponder loss	2.0 dB	TDRSS User's Guide, May 1975
Demodulation loss	1.5 dB	TDRSS User's Guide, May 1975
Designed system margin	3.0 dB	TDRSS User's Guide, May 1975
Required energy-to-noise spectral density for 10^{-5} BER	9.9 dB	ΔPSK
Achievable data rate	83.2 dB	120 Mbps channel
Data rate	80.8 dB	120 Mbps
Additional margin	2.4 dB	120 Mbps channel
EIRP of 15 Mbps channel	51.8 dBW	Use 20% of 20 watts
Acheivable data rate	77.2 dB	15 Mbps channel
Data rate	71.8 dB	15 Mbps
Additional margin	5.4 dB	15 Mbps channel

Table 3.11-7. TDRSS KSA Forward Link Calculation

Parameter	Value	Notes
TDRSS antenna gain	52.0 dB	TDRSS User's Guide, Rev. 2
TDRSS RF transmit loss	-2.0 dB	TDRSS User's Guide, Rev. 2
TDRSS transmit power	-3.0 dBW	TDRSS User's Guide, Rev. 2
Transmitted EIRP	47.0 dBW	S + N
TDRSS transponder loss	-1.0 dB	TDRSS User's Guide, Rev. 2
Peak signal EIRP	46.0 dBW	
TDRSS pointing loss	-0.5 dB	TDRSS User's Guide, Rev. 2
Signal EIRP	45.5 dBW	
Space loss	-208.2 dB	100 to 180 km earth grazing
LF/O antenna gain	46.0 dBi	6-foot parabolic antenna
LF/O antenna pointing loss	0.1 dB	Calculated (Table 3.1-3)
LF/O receive loss	1.7 dB	Diplexer = 0.9 dB Waveguide = 0.2 dB Coupler = 0.5 dB VSWR MM = 0.1 dB
Polarization loss	0.5 dB	TDRSS User's Guide, Rev. 2
Power received at preamp input	-119.0 dBW	
System temperature referred to receiver input	1210.5°K	Figure 3.11-7, receiver noise figure of 6.1 dB includes waveguide and WG switch losses = 0.2 dB
$K T_{sys}$	-197.8 dBW/Hz	
C/N_o	78.8 dB/Hz	
$C/N_o B_{IF}$	11.0	BW = 6 MHz (67.8 dB)

An overall block diagram description of the STDN/direct access transmitter is given in Figure 4.0-1. All active components of the subsystem are redundant, as shown. RF interconnections prior to the TWTA's are coaxial cable. All TWTA output connections are immersion gold coated WR62 waveguide.

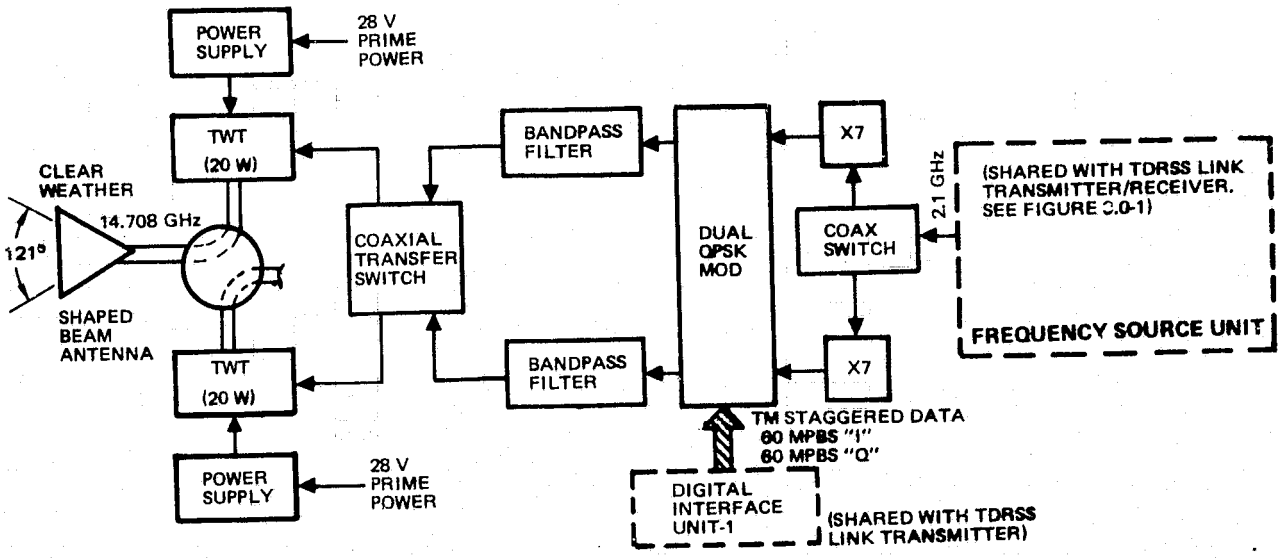

Figure 4.0-1. STDN/Direct Access Link

The transmitter is entirely contained in the mission-unique wideband module along with a portion of the TDRSS link autotrack receiver and shared components (frequency source unit, digital interface unit No. 1, power converter, and RIU). The shaped beam antenna mounts directly to or closely adjacent to the "bottom" (earth facing side) of the module. The TWTA's are mounted to the side panel which is never exposed to the sun (+Y) for effective heat radiation.

The STDN/direct access link operates at a center frequency of 14.708 GHz in a 120 MHz band (main spectrum lobe) utilizing balanced and staggered QPSK modulation. The use of a band separated from the TDRSS 15 GHz return link band prevents TDRSS link antenna sidelobes from causing interference in the STDN/direct access ground stations. The specific frequency of 14.708 GHz was chosen to permit a simple implementation in the frequency source unit. The use of staggered (offset) QPSK modulation minimizes out-of-band spectrum sidelobe regeneration due to limiter action in the TWTA, thus minimizing or eliminating the need for TWTA output filtering with a consequent output circuit loss decrease on the order of 0.5 dB or more.

The shaped beam antenna provides excellent low elevation angle ground coverage for the 120 Mbps TM data link. Receive elevation angles of 14° and 22° for clear conditions and for 4 mm/hr rain conditions are achieved with a 3 dB performance margin at 10^{-5} BER.

The following sections discuss the detail performance analyses and tradeoff studies that were performed in arriving at the recommended design, and provide detailed descriptions of the recommended hardware.

4.1 STDN/DIRECT ACCESS LINK OUTPUT FILTER REQUIREMENTS

In the case of the TDRSS link, an output filter was found necessary for a number of reasons:

- The transmitter operates simultaneously with an autotrack receiver via a common antenna
- The TM and MSS streams are combined in an unbalanced QPSK modulator – this precludes use of a staggered QPSK modulator which would minimize spectrum sidelobe regeneration, but which would require time multiplexing of the TM and MSS data (see Section 3.2 tradeoffs)
- Spectrum sidelobe attenuation is required to prevent interference with the STDN/direct access link
- Spectrum sidelobe attenuation is needed to prevent radio astronomy interference.

In the case of the STDN/direct access link, the above items (except possibly the last) do not apply because:

- The transmitter is not diplexed with a receive function
- A single TM data stream is transmitted, hence staggered QPSK modulation may be used to minimize out-of-band spectrum sidelobes
- Clearly the STDN/direct access link does not intefere with the TDRSS link. However, there remains the possibility of radio astronomy interference which is examined below.

4.1.1 Interference with Radio Astronomy Band

The recommended frequency plan (Figure 3.2-20) places the STDN/direct access link at a center frequency of 14.708 GHz. Spectrum sidelobes of the signal will lie in the adjacent radio astronomy band located at 14.485 to 14.495 GHz. To minimize spectrum regeneration of spectrum sidelobes in the TWT transmitter, it is recommended that offset or staggered QPSK (SQPSK) modulation be utilized.

A TRW computer simulation program was utilized to determine the expected level of spectrum density in the radio astronomy band region for the case of SQPSK modulation. A 5-pole Chebycheff filter with a matched bandwidth of 120 MHz at the TWT input was assumed. This bandwidth corresponds to the spectrum main lobe bandwidth for the 120 Mbps TM data stream feeding a balanced SQPSK modulator. The results of the simulation are summarized in Figure 4.1-1. The peak spectrum density, ϕ_D, is

$$\phi_D(\text{dB}) = \text{ERP} - \text{B}/2 = -66.8 \text{ dBW/Hz}$$

where

ERP = nadir ERP = 11.0 dBW

B/2 = 77.8 dB-Hz (120 Mbps/2)

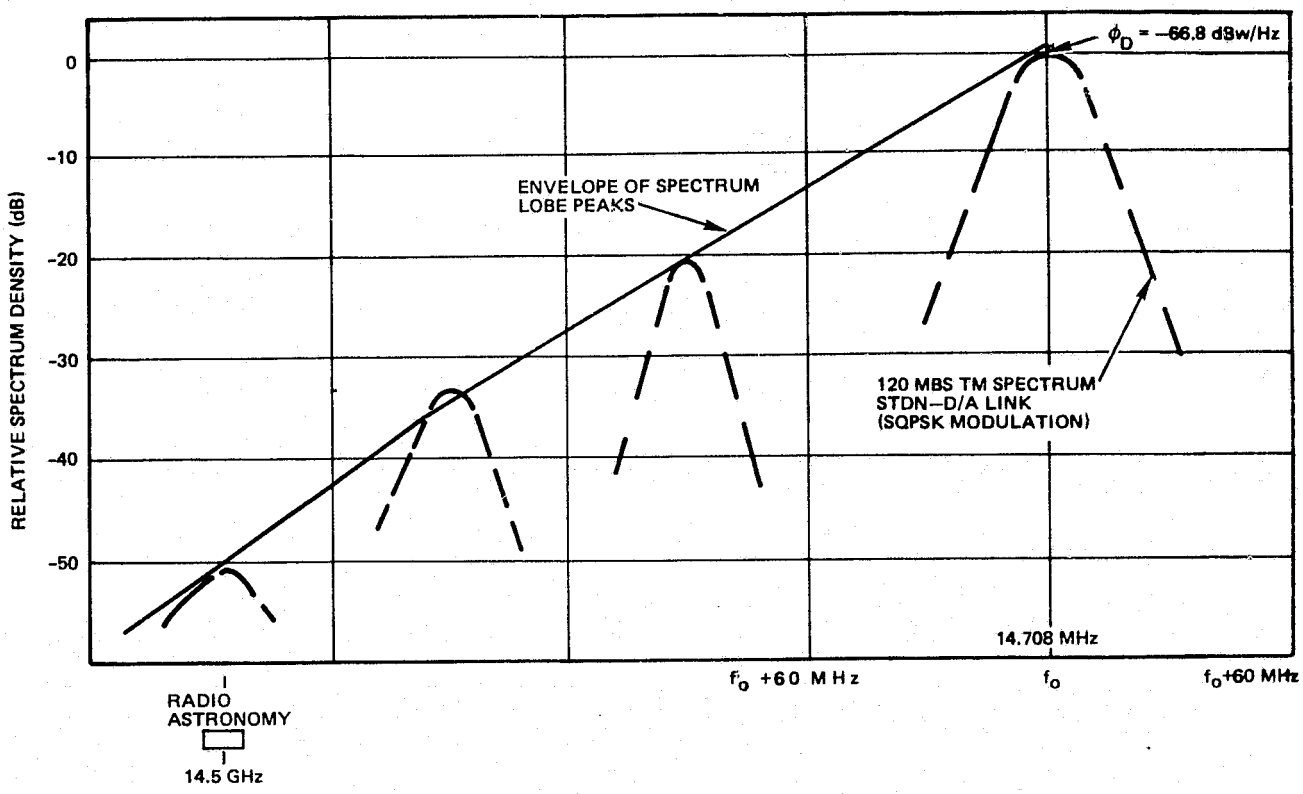

Figure 4.1-1. STDN/Direct Access Link Spectrum

The approximate level of interference (for continuous interfering signal) from the STDN/direct access link into the 14.5 GHz radio astonomy band without TWT output filter attenuation is given by

$$\phi_i(\text{dB}) \approx \phi_D - S_4 - 10 \log (4\pi R^2)$$

where

ϕ_i = interferring signal at the radio telescope (dBW/m^2/Hz)

ϕ_D = STDN/direct access link peak spectrum density ≈ -67 dBW-Hz

S_4 = relative amplitude of spectrum at 14.5 GHz ≈ 51 dB (Figure 4.1-1)

R = nadir range = 705 km

Hence

$$\phi_i(\text{dB}) \approx -67 - 51 - 128 = -246 \text{ dBW/m}^2\text{/Hz} \quad .$$

The above level, ϕ_i, is well below the allowable level of -219 dBW/m^2/Hz given in the current CCIR document (ref. 8) for interference relative to an isotropic receive antenna, but exceeds the level which results when (as currently defined) the allowable interference level is reduced an amount equal to the radio telescope main beam gain.

However, as discussed in Section 3.2.4 and summarized below, it is our conclusion that interference is not a problem:

- Revised interference criteria are being recommended which refer only to the isotropic receive level
- The interference is not continuous but consists of a short noise-like "pulse" as the LF/O traverses the radio telescope beam
- It would be simple to add bandstop filtering at the transmitter output if an interference situation were identified.

4.1.2 Other Requirements

No requirements for transmitter output filtering have been identified at this time. Possibly electromagnetic interference (EMI) specifications or CCIR requirements do exist which would require some form of additional filtering. Further, there is always a possibility of a self-compatibility problem that has not yet been identified. However, it is recommended that an output filter not be utilized until explicit requirements are established.

4.2 TRANSMITTER DESIGN

The STDN/direct access transmitter, located in the wideband module, shares many design characteristics with the TDRSS link transmitter described in Section 3.3. It employs staggered QPSK (SQPSK) modulation at a carrier frequency of 14.70833 GHz.

4.2.1 Transmitter Configuration Tradeoffs

Generation of the SQPSK signal for the STDN/direct access link involves the same tradeoffs discussed for the TDRSS link transmitter. The only difference is the absence of an attenuator in the QPSK modulator. Section 3.3.1 can be referenced for the detailed configuration tradeoffs.

The MIC Ku-band modulator recommended in Section 3.3.1 for the 15.0085 GHz TDRSS link can be used without modification (except for the attenuator) for the STDN/direct access link.

4.2.2 Frequency Source

The recommended frequency source configuration is a result of the same tradeoffs presented for the TDRSS link. The required frequency of 14.70833 GHz is derived by multiplying the 75.0425 MHz reference oscillator by 196 (Figure 4.2-1).

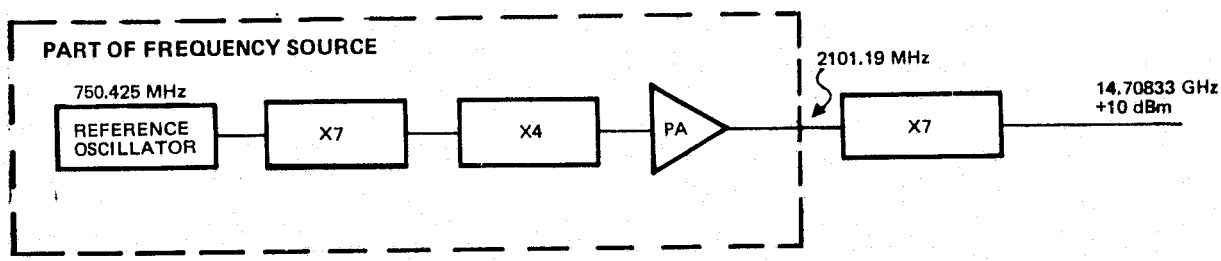

Figure 4.2-1. STDN-D/A — Frequency Generation Block Diagram

Multiplication to 2101.19 MHz is accomplished within the frequency source unit. This signal is then multiplied to the final Ku-band frequency by a varactor diode X7 circuit nearly identical to the multiplier shown in Figure 3.3-13. The circuits used in the frequency source unit are described in detail in Section 3.3.2.

4.2.3 TWTA

The identical TWT selected for the TDRSS link is used for the STDN/direct access link. The TWT bandwidth is adequate to cover both bands. A detailed description of the TWT and the tradeoffs involved in its choice are given in Section 3.3.3.

4.2.4 Recommended Transmitter Design

A block diagram of the completely redundant transmitter is shown in Figure 4.2-2. The STDN/direct access frequency is generated from a 75.0425 MHz reference frequency

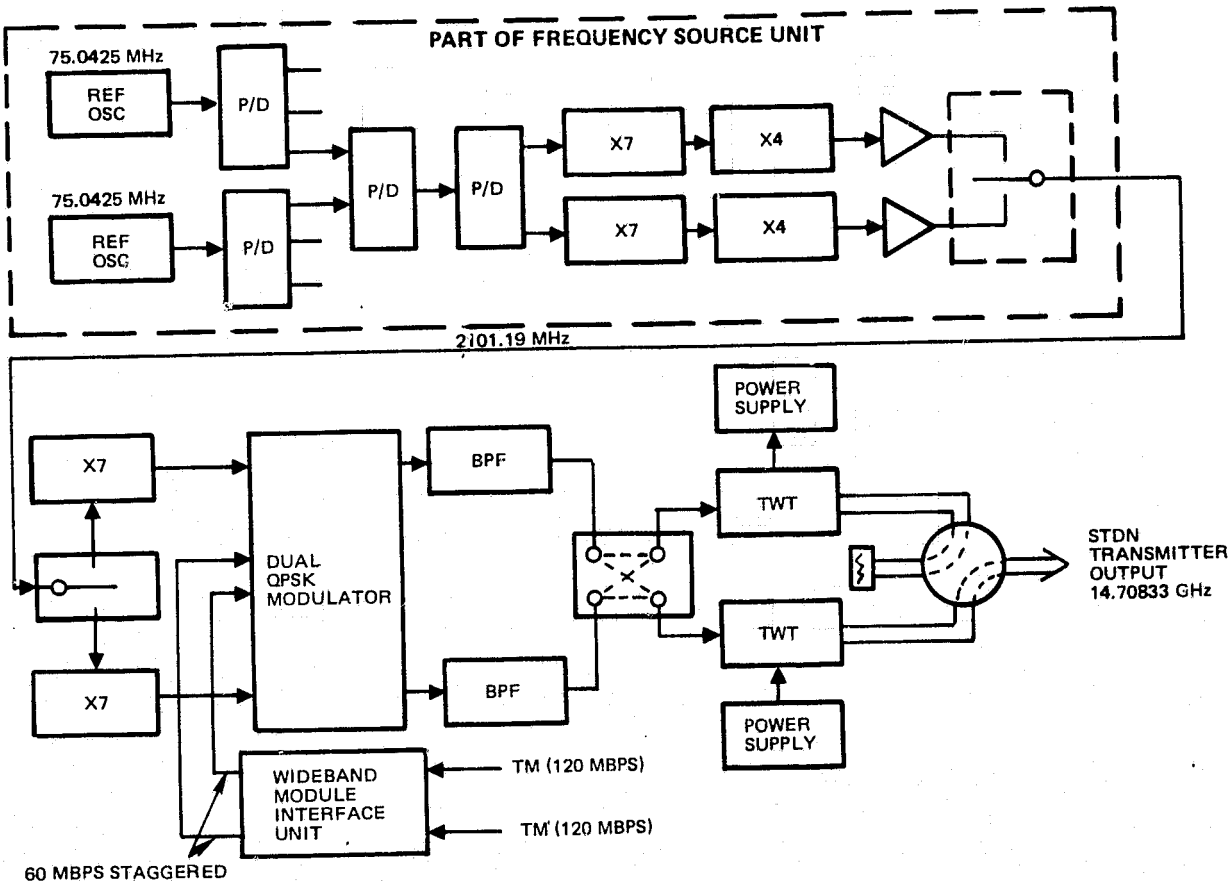

Figure 4.2-2. STDN-D/A Transmitter — Block Diagram

common to all of the Ku-band equipment. The redundant reference oscillators are multiplied to 2101.19 MHz with redundant multipliers as part of the frequency source unit. The output of the frequency source unit is multiplied with redundant multipliers to an output at the desired 14.70833 GHz. The two multiplier outputs are fed to the dual-QPSK modulator. The modulator accepts two staggered 60 Mbps data streams from digital interface unit No. 1. A 120 MHz bandpass filter at the modulator output filters the signal spectrum to the first nulls.

The outputs are then coupled through a coaxial transfer switch to the redundant TWTA's. The output of the TWTA's are cross-strapped with a waveguide transfer switch.

The entire STDN/direct access transmitter is mounted in the wideband module (Figure 5.0-1). All RF interconnections up to the TWT input are made with coaxial cables. All RF connections between the TWTA output to the shaped beam antenna are made with WR-62 waveguide.

4.3 INTERFACE UNITS

Two interface units are located in the wideband module. The remote interface unit (RIU) (an integral part of the communication and data handling module (C&DH) standard telemetry and command components (STACC) central unit (CU)) provides communication with the CU in which commands to the subsystems are processed and telemetry data from the subsystems are conditioned (refs. 21, 22). Two RIU units are utilized to provide redundancy.

The wideband compartment digital interface unit No. 1 shown functionally in Figure 4.3-1 conditions the signals provided by the TM and MSS instruments and distributes them to the STDN/direct access modulators located in the wideband module and to digital interface unit No. 2 located in the RF compartment.

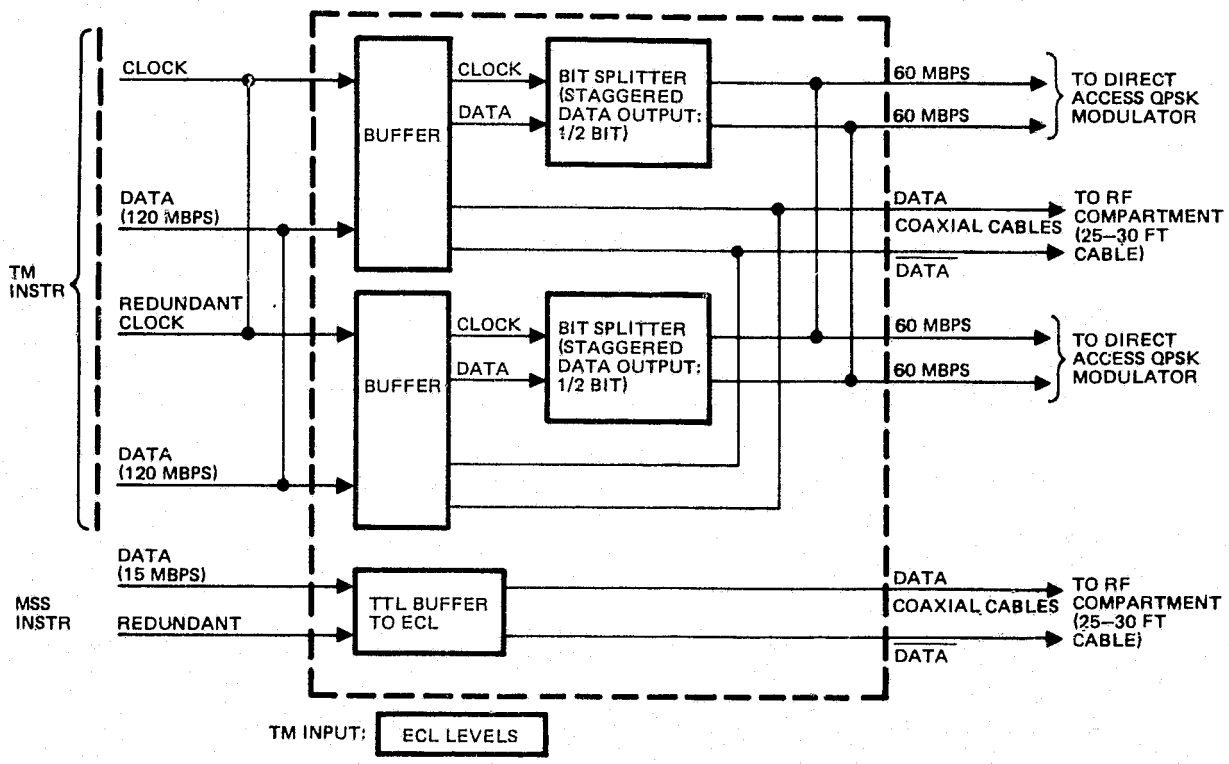

Figure 4.3-1. Digital Interface Unit No. 1 Block Diagram

The TM instrument is assumed to provide redundant emitter coupled logic (ECL) balance line data and clock inputs. The MSS instrument is assumed to provide a redundant signal TTL input.

The TM data signals are routed to a redundant interface buffer where clock and data signals are fed to redundant bit-splitters. TM data is also routed to the TDRSS transmitter in the RF compartment via coaxial cables. The bit-splitter generates two data streams containing alternate bits of the original signal, sequences them at one-half the original 120 Mbps rate, and staggers the two data stream relative to one

another by one-half a bit period as shown in Figure 4.3-2. It is assumed that no signal is received from the TM instrument redundant input as long as the normal input side is active. This assumption allows the output cross-stripping arrangement shown in Figure 4.3-1.

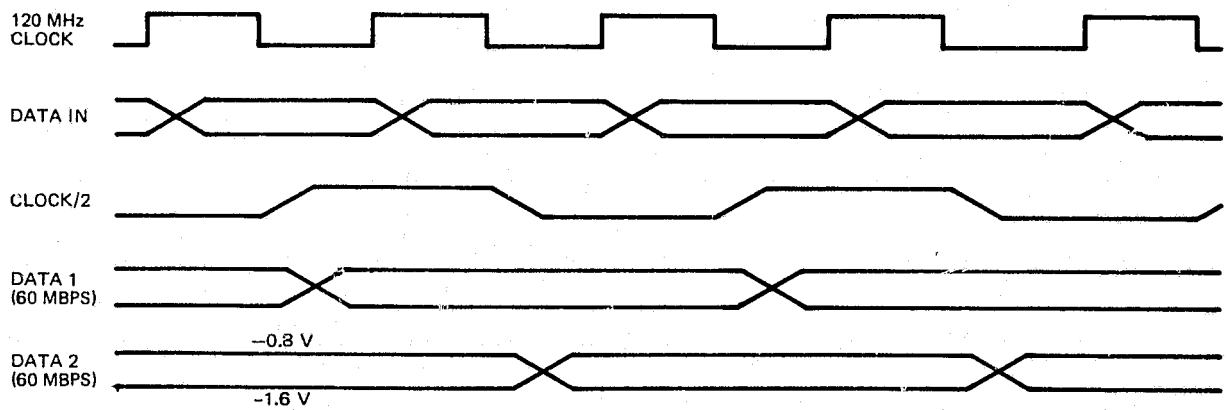

Figure 4.3-2. Bit Splitter Timing Diagram

The MSS input data TTL levels are converted in the MSS buffer to ECL levels in addition to providing balanced line driver outputs for routing to interface unit No. 2.

In summary, the interface unit provides balance line staggered 60 Mbps data signals to the STDN/direct access Ku-band transmitter and balanced line TM and MSS signal inputs via pairs of coaxial cables to the Ku-band TDRSS link transmitter.

The digital implementation of Figure 4.3-1 is presented in Figure 4.3-3 and the physical characteristics in Figure 4.3-4 and Table 4.3-1. Logic functions are performed by MECL integrated circuit chips and passive components are provided by resistor integrated circuit chips. The circuit board size is estimated by the 13 integrated chips required to implement the interface unit.

Table 4.3-1. Digital Interface Unit No. 1 Power Consumption

Quantity	Chip	Current (mA)
2	10616	42
3	10631	145
2	10624	66
2	10602	52
3	Resistor chips	330
1	10601	26
		661 mA @ -5 V
		32 mA @ +5 V
	Power	3.5 W

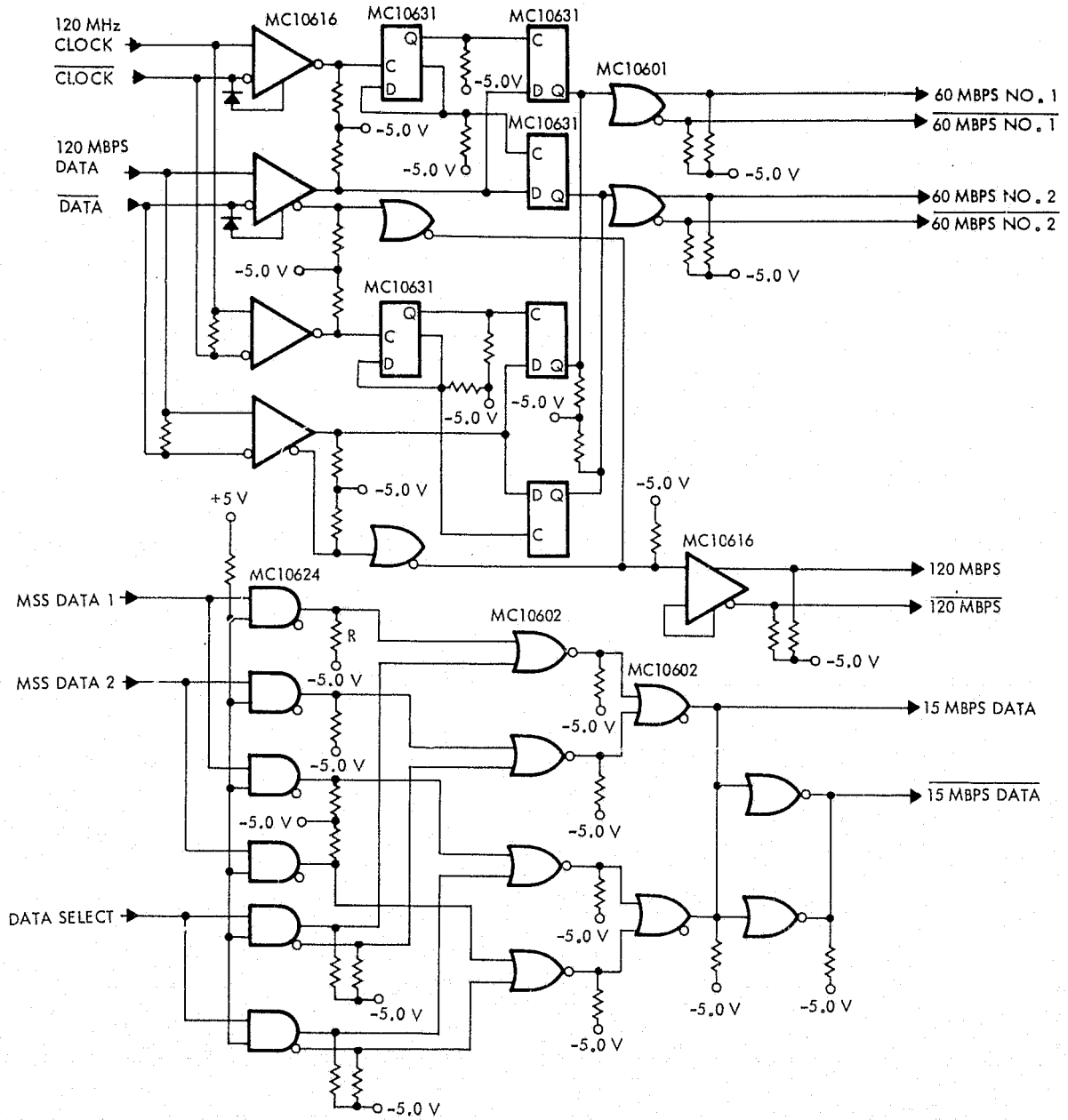

Figure 4.3-3. Digital Interface Unit No. 1 Logic Diagram

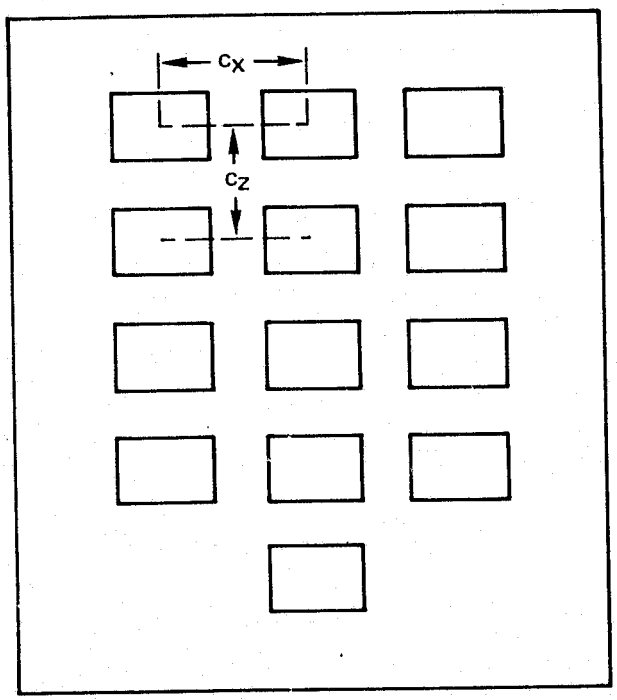

CHIP TYPE			SIZE	WT
A CERAMIC PACKAGE HEIGHT		=	0.3-IN.	0.6 LB
	C_X: 0.9-IN. x 4	=	3.6-IN.	
	C_Z: 0.7-IN. x 6	=	4.2-IN.	
B FLAT PACKAGE HEIGHT		=	0.18-IN.	0.5 LB
	C_X: 0.5(4)	=	2.0-IN.	
	C_Z: 0.45(6)	=	2.7-IN.	

Figure 4.3-4. Board Size (Wideband Module)

4.4 SHAPED BEAM ANTENNA

The LF/O is in a low altitude (705 km) circular orbit. A shaped antenna pattern is therefore required to maximize ground coverage for STDN/direct access stations. This section determines the ideal antenna pattern and recommends an antenna implementation which best approximates this pattern.

4.4.1 Requirement Analysis

Several factors impact the determination of the required antenna gain pattern: the variation of inverse R^2 (range) loss with elevation angle, the variation of oxygen and water vapor absorption with elevation angle, the variation in signal attenuation and sky temperature with elevation angle for rain and clouds conditions, and the available spacecraft transmitter power. These factors were investigated and used to determine the minimum antenna gain pattern requirement.

The following ground rules are assumed:

Direct-link operation	14.708 GHz
Spacecraft circular orbit	705 km
Interface with STDN/direct access users	
— Antenna gain	59 dBi (30 foot; 0.2 dB pointing loss
— System noise temperature	200°K (zenith)
Spacecraft transmitter power	20 watts
Rain conditions	4 mm/hr
TM data rate	120 Mbps
System margin at 10^{-5} BER	3 dB
Ground system demodulation losses	3 dB

4.4.2 Link Analysis

The link budget given in Table 4.4-1 is used to establish a reference design point for the required antenna gain distribution. An elevation angle of 30° was arbitrarily chosen, and a link margin of 3 dB plus estimated adverse tolerance was assumed.

Weather Model

The atmospheric effect under clear sky conditions for Ku-band frequencies is found to be small at large elevations angles but more significant at lower elevation angles. In the presence of rain, however, the atmospheric effects at Ku-band become increasingly significant at any elevation angle since the communication links are

Table 4.4-1. Ku-Band Direct Access/STDN Link Performance

Parameter	Nominal Value	Adverse Tolerance	Notes
S/C xmit power	13.0 dBW	0.0	20 watts
S/C line loss	0.4 dB	0.2 dB	Waveguide and switch
S/C antenna gain	1.5 dBi	0.2 dB	51.2° from S/C nadir
S/C EIRP	14.1 dBW		
Space loss	177.7 dB	0.0	S/C circular orbit = 705 km, slant range at 30° elevation equals 1245 km
Absorption	0.4 dB	0.1 dB	See Figure 4.4-1, tolerance assumed
Rain attenuation	1.5 dB	0.0	4 mm/hr (see Figure 4.4-4)
Polarization loss	0.5 dB	0.0	
STDN antenna gain	59.0 dBi	0.0	NASA supplied: 30-foot
Antenna pointing loss	0.2 dB	0.0	NASA supplied
Received signal power at antenna port	-107.2 dBW	0.3 dB	RSS tolerances
System temperature referenced to antenna port	207°K	10°K	T_{sys} = 200°K at zenith +7° for 30° elevation (see Figure 4.4-2)*
Total system noise spectral density referenced to antenna port	-205.4 dBW/Hz	0.3 dB	
Degradation due to rain induced increased sky temperature	1.4 dB	0.0	ΔT_{sky} = 80° (see Figure 4.4-5)
Received signal-to-noise spectral density ratio	96.8 dB-Hz	0.4 dB	RSS tolerance
Data rate	80.8 dB	0.0	120 Mbps
Received energy-to-noise spectral density ratio	16.0 dB		
Required energy-to-noise spectral density ratio for 10^{-5} BER	12.6 dB	0.0	Theoretical CPSK = 9.6 dB +3.0 dB hardware degradation
System margin	3.4 dB	0.4 dB	RSS tolerance
System margin less adverse tolerance	3.0 dB		

*7° Relative to zenith temperature.

degraded by the absorption and scattering of the signal by the rain and the associated clouds. Furthermore, the signal attenuation caused by the rain and clouds results in an increased sky temperature which increases the effective system temperature of the communication receiver system. The total effect constitutes a degradation in the communication link performance margin.

The atmospheric effects for clear and rainy weather are given in terms of signal attenuation and increased sky temperature for different elevation angles.

Clear Weather

Measured and analytical oxygen and water vapor absorption data for signals operating at different frequencies and taken at different elevation angles is reported by Hogg and Mumford and Benoit (refs. 19, 23). Furthermore, the Hogg and Mumford paper contains measured data of sky noise temperatures due to oxygen and water vapor for different frequencies and elevation angles. The data for summer conditions is shown in Figures 4.4-1 and 4.4-2.

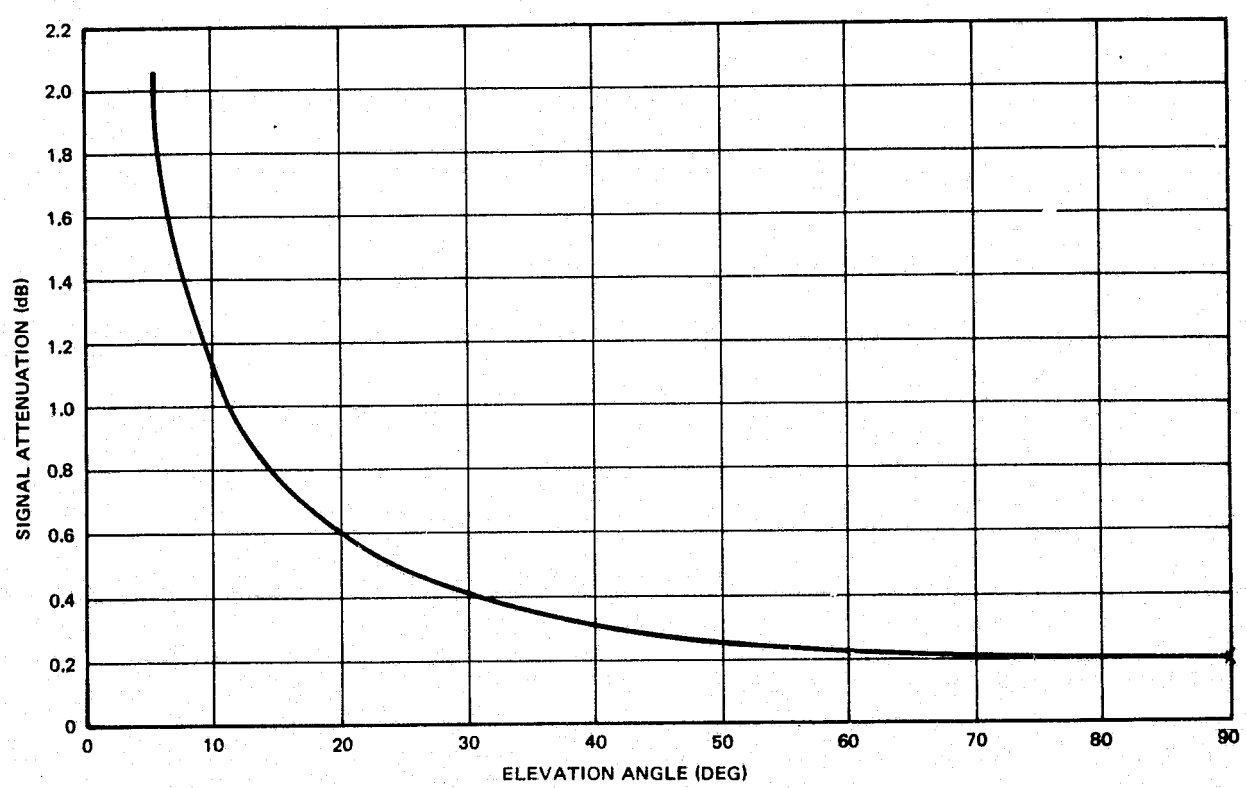

Figure 4.4-1. Atmospheric Attenuation Due to Oxygen and Water Vapor Absorption (Summer Conditions)

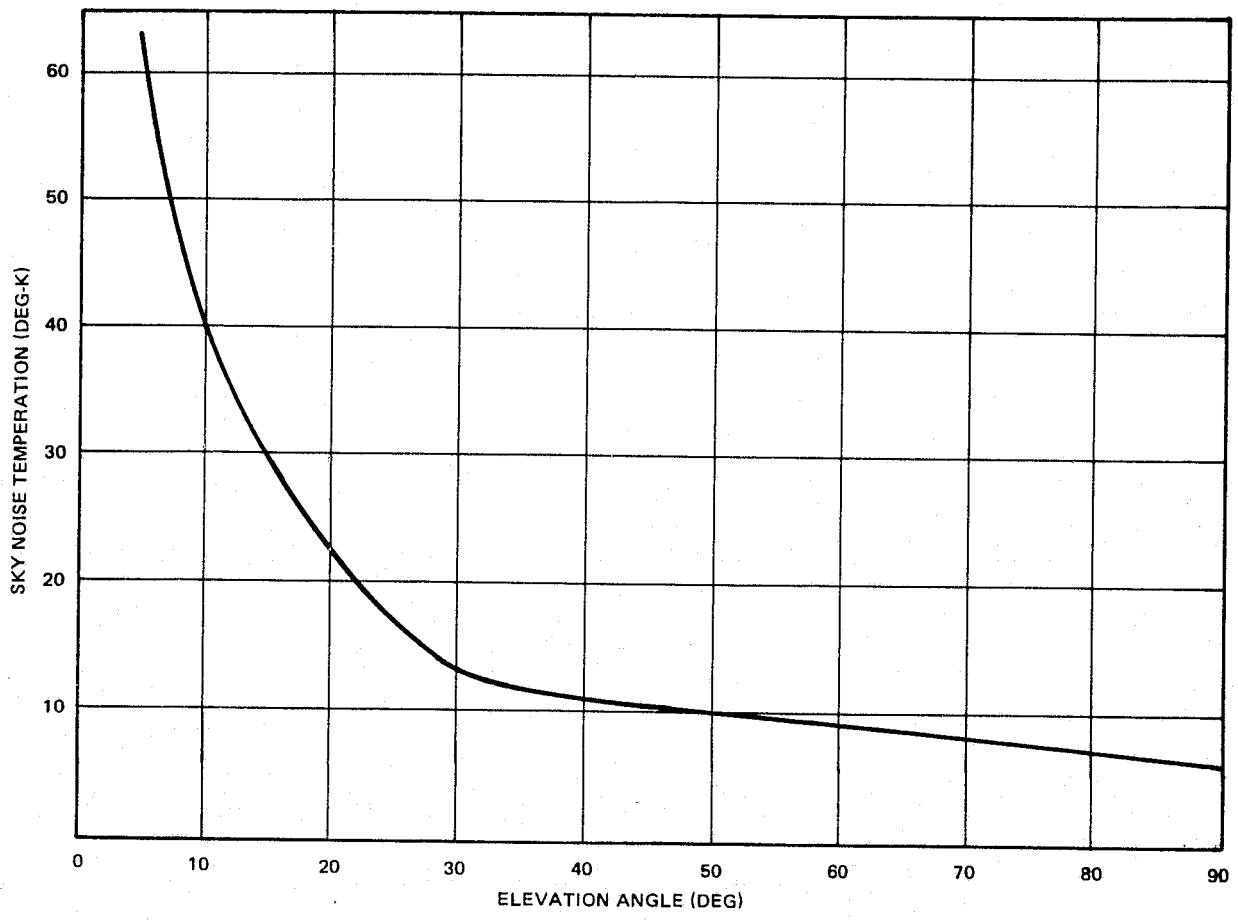

Figure 4.4-2. Sky Noise Temperation (Summer Conditions)

Rain Model

The amount of space-to-ground link degradation is directly related to the size and intensity of the rainstorm and the path of signal propagation through the rain and clouds. The horizontal size of the rain cell(s) is reported by James (ref. 24) to be a function of the rain intensity, i.e.,

$$H(km) = 41.3 - 23.6 \log_{10} P = 27.1 \text{ km} \qquad (4.1)$$

for P = 4 mm/hr. The signal path length from the satellite to ground is a function of the ground system antenna elevation angle and satellite orbital altitude.

A model atmosphere for temperature regions has been developed by Holzer. His model is considered appropriate for the rain intensity (4 mm/hr) stipulated in the design ground rules. Holzer's model (ref. 25) is modified slightly by more current cloud data reported by Altshuler, Falcone, and Wulfsberg (ref. 26). The atmospheric model shown in Figure 4.4-3 consists of a 2.5 km vertical precipitation layer and two cloud layers containing different water vapor densities. The lower cloud layer extends from 2.5 km (the cloud base) to 3.0 km (the melting level) and the upper cloud layer from 3 to 6 km. Both cloud layers are reported to have relatively unlimited horizontal extent.

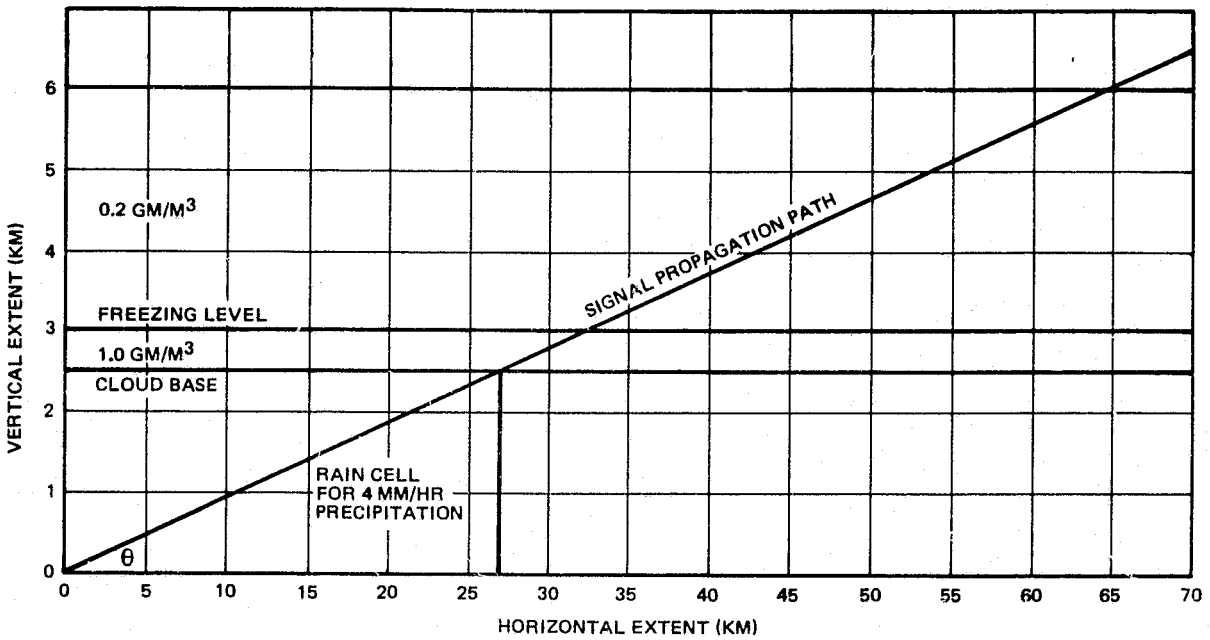

Figure 4.4-3. Model Atmosphere for Temperate Regions

The water vapor density in the lower cloud layer is reported by Altshulter, et al., (ref. 26) to range between 1 and 4 gm/m^2 and to range between 0.1 and 0.5 gm/m^3 above the freezing layer. It is reasonable to assume that the cloud water densities vary with rain intensities and, for 4 mm/hr, water vapor densities of 1 gm/m^3 and 0.2 gm/m^3 are used for the lower and upper cloud layers, respectively.

The atmospheric model represents a single rain cell and associated cloud layers and is used to determine the signal path lengths through the rain and clouds and to calculate the cloud signal attenuation.

The attenuation per path length of microwave (millimeter wave) energy due to rain was reported by Ippolito (ref. 27) (and many others) to depend in a very complex manner on rain drop size distribution and rain intensity. An empirical expression proposed by Gunn and East (ref. 15 of Ippolito's report) relates the attenuation per path length to rainfall rate or intensity as

$$A_p(\text{dB/km}) = a[P(\text{mm/hr})]^b \qquad (4.2)$$

where a = 0.04 and b = 1.17 for ≈14.7 GHz frequency. For P - 4 mm/hr

$$A_p = 0.2025 \text{ dB/km} \qquad (4.3)$$

The cloud attenuation model reported by Holzer and others is given by

$$A_c = k\rho \text{ (dB/km)} \qquad (4.4)$$

where

k = cloud coefficient (function of frequency)
= 0.21 dB/km/gm/m^3 for 14.7 GHz

ρ = liquid water content (gm/m^3)

Since there are two cloud layer with different water vapor densities

$$A_c = k\rho_1 + k\rho_2 \tag{4.5}$$

where

ρ_1 = 1 gm/m^3

ρ_2 = 0.2 gm/m^3

The total signal attenuation is determined from (4.3) and (4.5), i.e.,

$$\begin{aligned} A_T &= A_p + A_c \text{ (dB)} \\ &= 0.2025\ h_o + 0.21\ h_1 + 0.042\ h_2 \end{aligned} \tag{4.6}$$

where

h_o = propagation path length through the precipitation layer

h_1 = propagation path length through lower cloud layer

h_2 = propagation path length through upper cloud layer

The signal propagation path is determined from Figure 4.4-3. Note that the horizontal extent for the precipitation layer given by (4.1) is 27.1 km and the cloud layers are assumed to have relatively unlimited horizontal extent. Furthermore, it is assumed that the ground station is located at the rain cell boundary which gives the worst case conditions. The elevation angle which corresponds to the maximum propagation path length through the rain cell precipitation layer is given by $\theta = \tan^{-1}[v/h] = 5.27°$, where v is the vertical height of the rain cell precipitation layer and h is the corresponding horizontal extent.

The propagation path length through the precipitation layer for elevation angles greater than $\theta = 5.27°$ is given by

$$h_o = \frac{V_1}{\sin\theta} \tag{4.7}$$

where V_1 = 2.5 km and θ is the elevation angle.

The propagation path lengths through the cloud layers are given by

$$h_1 = \frac{V_2}{\sin \theta} \tag{4.8}$$

$$h_2 = \frac{V_3}{\sin \theta} \tag{4.9}$$

where V_2 = 0.5 km and V_3 = 3 km.

The total signal attenuation is determined from (4.6), (4.7), (4.8), and (4.9), i.e.,

$$A_T = \frac{0.73725}{\sin \theta} \tag{4.10}$$

A plot of rain and cloud attenuation vs elevation angle is given in Figure 4.4-4.

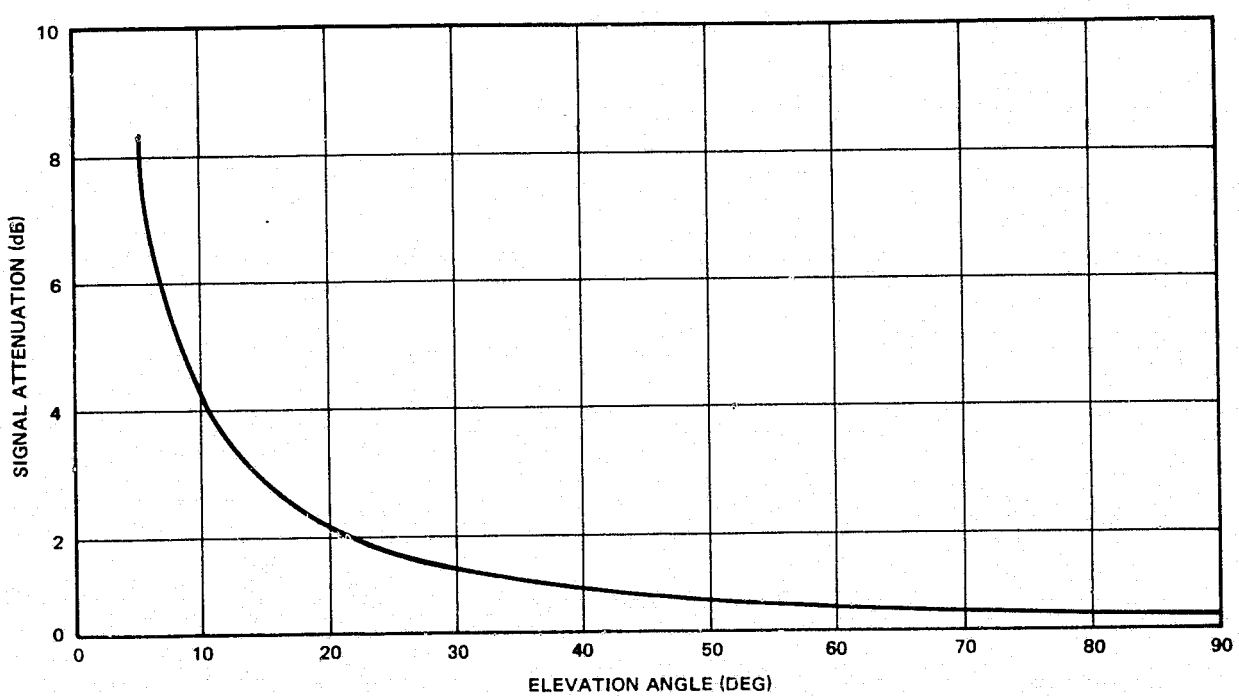

Figure 4.4-4. Signal Attenuation Due to 4 mm/hr Rain and Clouds

The increase in sky temperature due to rain and clouds has been found to be a function of the signal attention (ref. 28). The relation is reported to be given by

$$\Delta T_{sky} = \frac{L-1}{L} \; T_m \tag{4.11}$$

where

L = total signal attenuation $\left(10^{L(dB)/10}\right)$

T_m = mean absorption or rain temperature

The mean temperature is reported to be independent of frequency and is approximately 273°K. The rain and cloud induced increase in sky temperature as a function of elevation angle is determined from (4.11) and Figure 4.4-4. A plot of increase in sky temperature vs elevation angle is given in Figure 4.4-5.

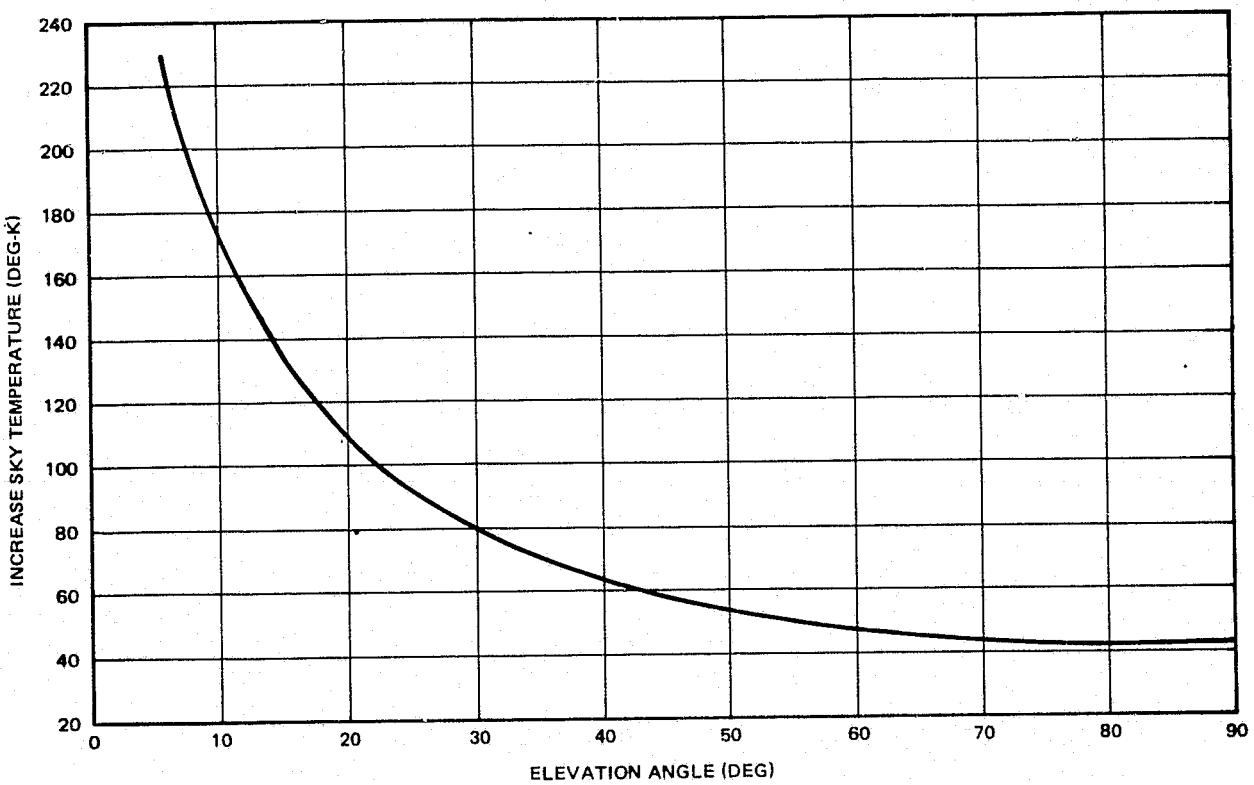

Figure 4.4-5. Increase in Sky Temperature Due to 4 mm/hr Rain and Clouds

Minimum Spacecraft Antenna Gain Pattern Requirement

The minimum spacecraft antenna gain pattern requirement are functions of the signal R^2 (range) loss, oxygen and water vapor absorption, rain and cloud attenuation, and the increased rain and cloud induced sky temperatures. The atmospheric losses which are a function of elevation angle have been determined earlier. The R^2 loss is given by

$$L(R^2) = \left(\frac{4\pi fR}{c}\right)^2 \qquad (4.12)$$

where

$$R = -r_o \sin\theta + \sqrt{h_o^2 + 2\, r_o h_o + r_o^2 \sin^2\theta} \qquad (4.13)$$

R = slant range (Figure 4.4-6)

f = transmitted frequency = 14.7 GHz

c = speed of light $\simeq 3 \times 10^8$ meters/sec

h_o = circular orbit altitude = 705 km

r_o = mean radius of earth (6378.2 km)

θ = elevation angle

R^2 loss is plotted in Figure 4.4-7.

The spacecraft antenna gain distribution shown in Figure 4.4-8 is determined from Figures 4.4-1, 4.4-2, 4.4-4, 4.4-5, 4.4-7, and Table 4.4-1 for clear weather and for rain and cloud weather conditions. The minimum spacecraft antenna gain distribution is given as a function of the ground antenna system elevation angle and the spacecraft nadir angle ϕ which is related to the elevation angle as shown in Figure 4.4-6.

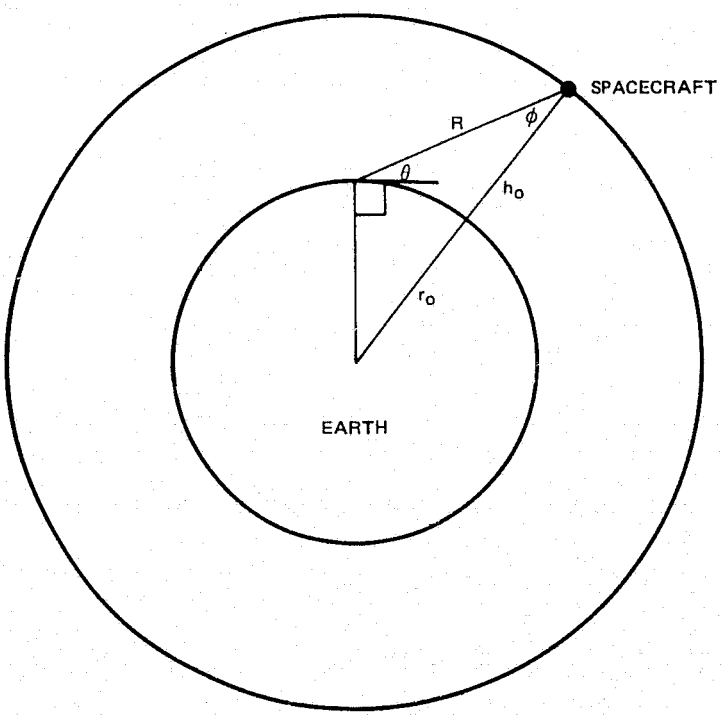

$$R = -r_o \sin\theta + \sqrt{h_o^2 + 2r_o h_o + r_o^2 \sin^2\theta}$$

$$\phi = \sin^{-1}\left\{\frac{r_o}{r_o + h_o} \sin\,(\theta + 90)\right\}$$

h_o = 705 km (CIRCULAR ORBIT ALTITUDE)

r_o = 6378.2 km (MEAN RADIUS)

Figure 4.4-6. Spacecraft — Earth Geometry

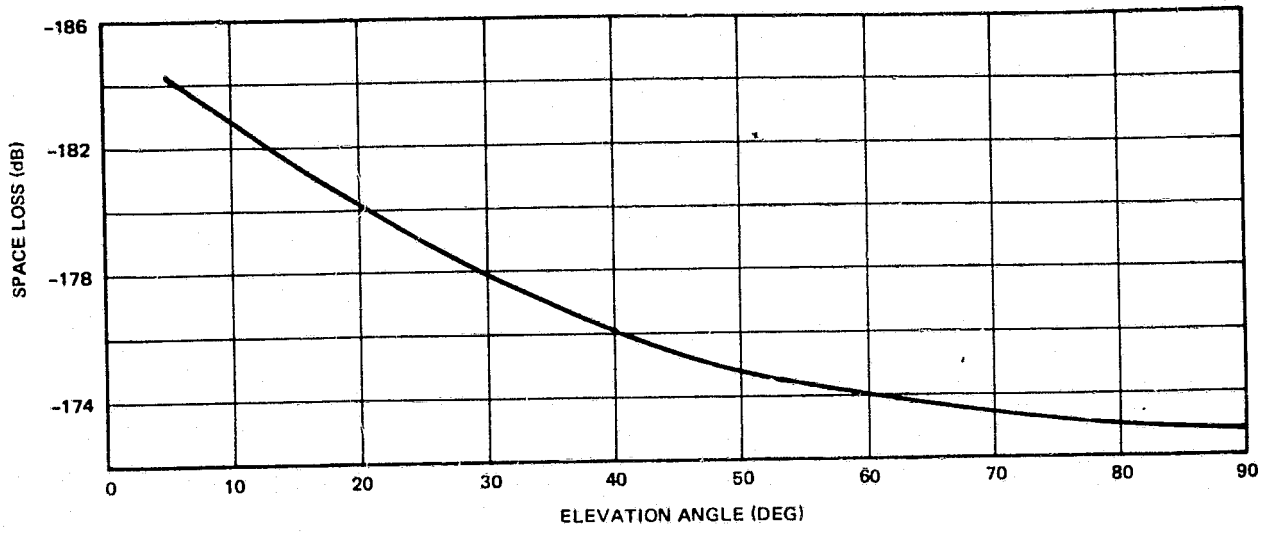

Figure 4.4-7. Space Loss for 705 km Circular Orbit

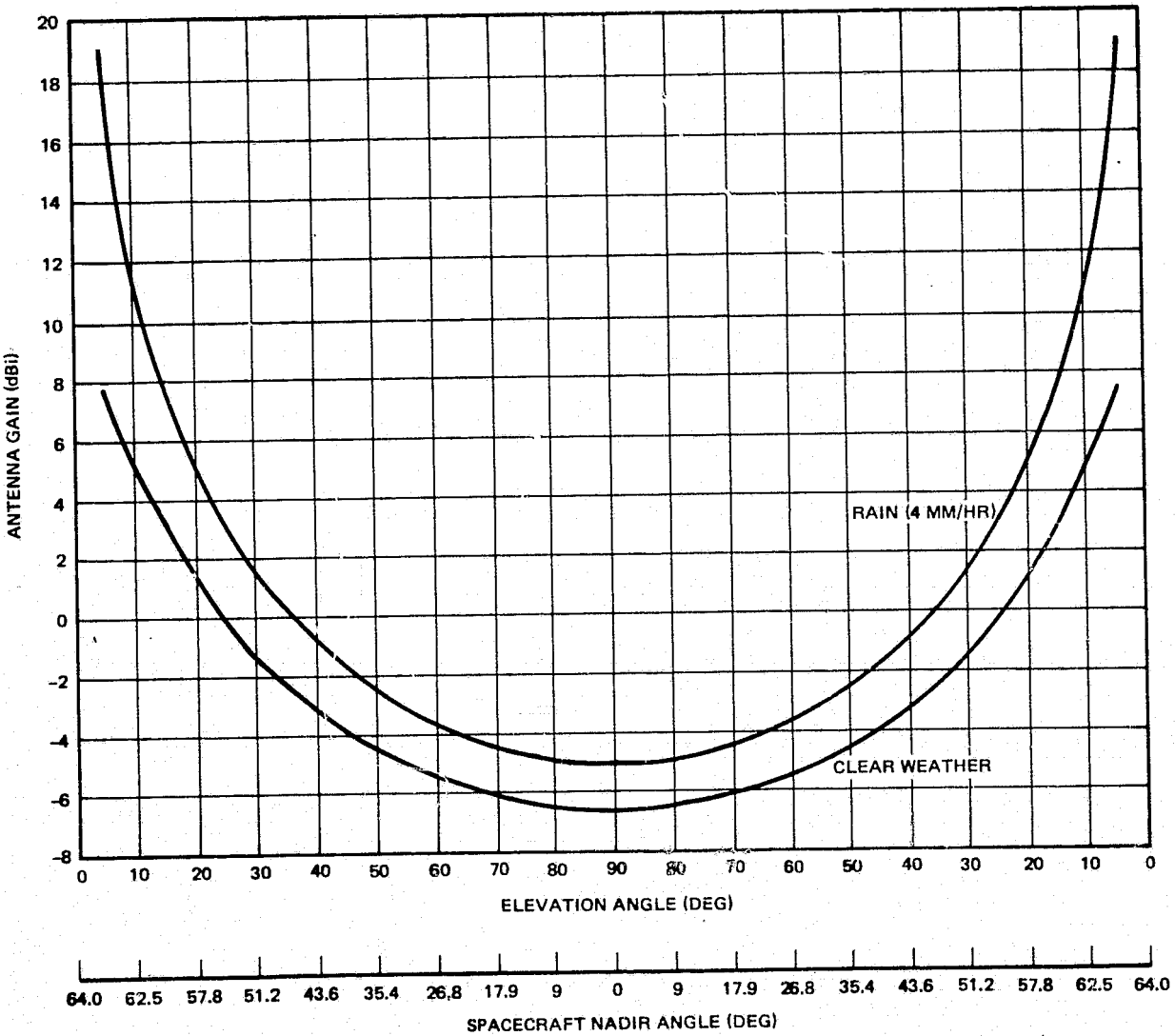

Figure 4.4-8. Minimum Spacecraft Earth Coverage Gain Distribution for the Ku-Band STDN/Direct Access (3 dB Margin Above 0.4 dB Adverse for 10^{-5} BER)

The spacecraft antenna gain pattern represents the minimum antenna gain which provides 3 dB performance margin above adverse tolerance for 10^{-5} BER.

4.4.3 Tradeoffs and Design Implementation

Antenna design concepts were analyzed to determine how to obtain optimum earth coverage from a low altitude spacecraft. The optimum antenna design would provide gain which is inversely proportional to the path loss between the spacecraft and any particular point on earth and which does not radiate beyond the edge of earth. Since the peak gain of the antenna's pattern would occur at edge of earth (maximum path loss), a very sharp pattern cutoff is required to minimize spillover outside the earth's coverage cone (> ±60°).

A colinear array of four equally fed turnstile antenna elements, which was experimentally tested for a similar past program, would provide the proper radiator pattern shaping but exhibited a large amount of spillover (peak gain of 4 dBi at ±60°). It was determined that a relatively large aperture antenna would be required to provide the fast radiation pattern cutoff (minimum spillover). A large array of elements was considered but would have considerable feed loss and complexity for providing the proper aperture phase and amplitude distribution. A reflector type antenna having a high amplitude illumination taper along with the required phase illumination through shaping techniques would provide the optimum radiator pattern and gain and has been selected as the recommended design.

The recommended antenna is a center fed, shaped reflector having the desired contour to provide near optimum coverage. To eliminate spillover loss, a tapered illumination of 17 dB is distributed symmetrically on the reflector by the feed horn. This highly tapered illumination requires the reflector diameter to be relatively large (approximately 23 wavelengths) to obtain the maximum peak gain.

Figure 4.4-9 presents a sketch of the recommended shaped beam antenna. The reflector consists of a shaped hyperboloid fed from a defocussed feed horn. The resulting radiation pattern provides ample gain margin above the requirement model contour over a wide range of elevation angles as shown in Figure 4.4-10. The feed (Figure 4.4-11) is scaled from a previous Ka-band antenna development program and provides the desired illumination with negligible blockage.

The mounting location of the antenna should permit the antenna axis to coincide with the earth's nadir. To eliminate possible shadowing of the antenna's radiation pattern, spacecraft obstacles should not be in view of the antenna look angles. This look angle can be approximated by a cone whose included angle is 120° centered about the antenna axis.

A weight estimate for the antenna assembly is given in Table 4.4-2.

Table 4.4-2. Shaped Beam Antenna Weight

Item	Weight (lbs)
Honeycomb reflector	1.0
Feed	0.7
Feed support	0.5
Mounting bracket	0.8
	Total 3.0 lbs

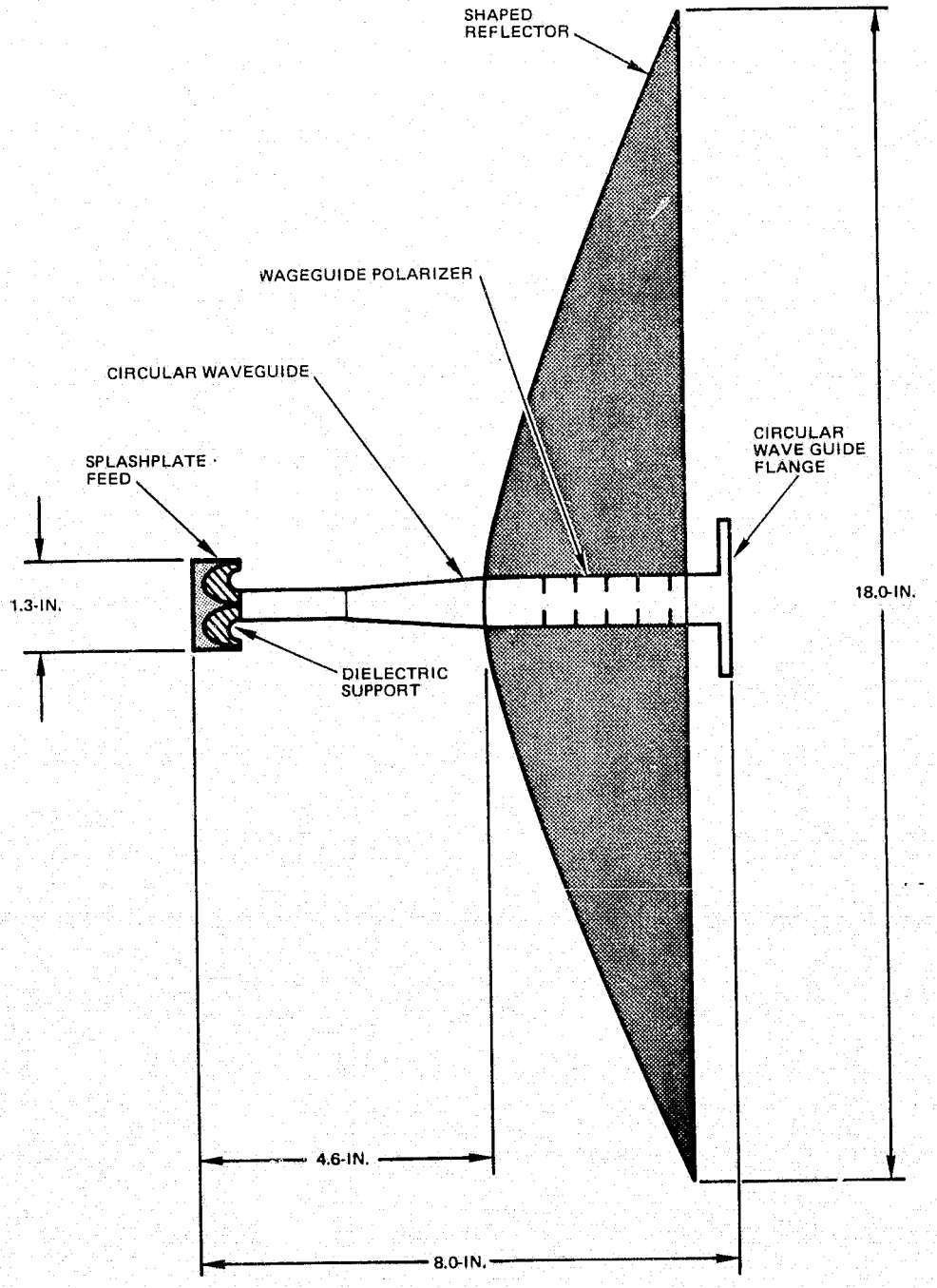

Figure 4.4-9. Recommended Shaped Beam Antenna

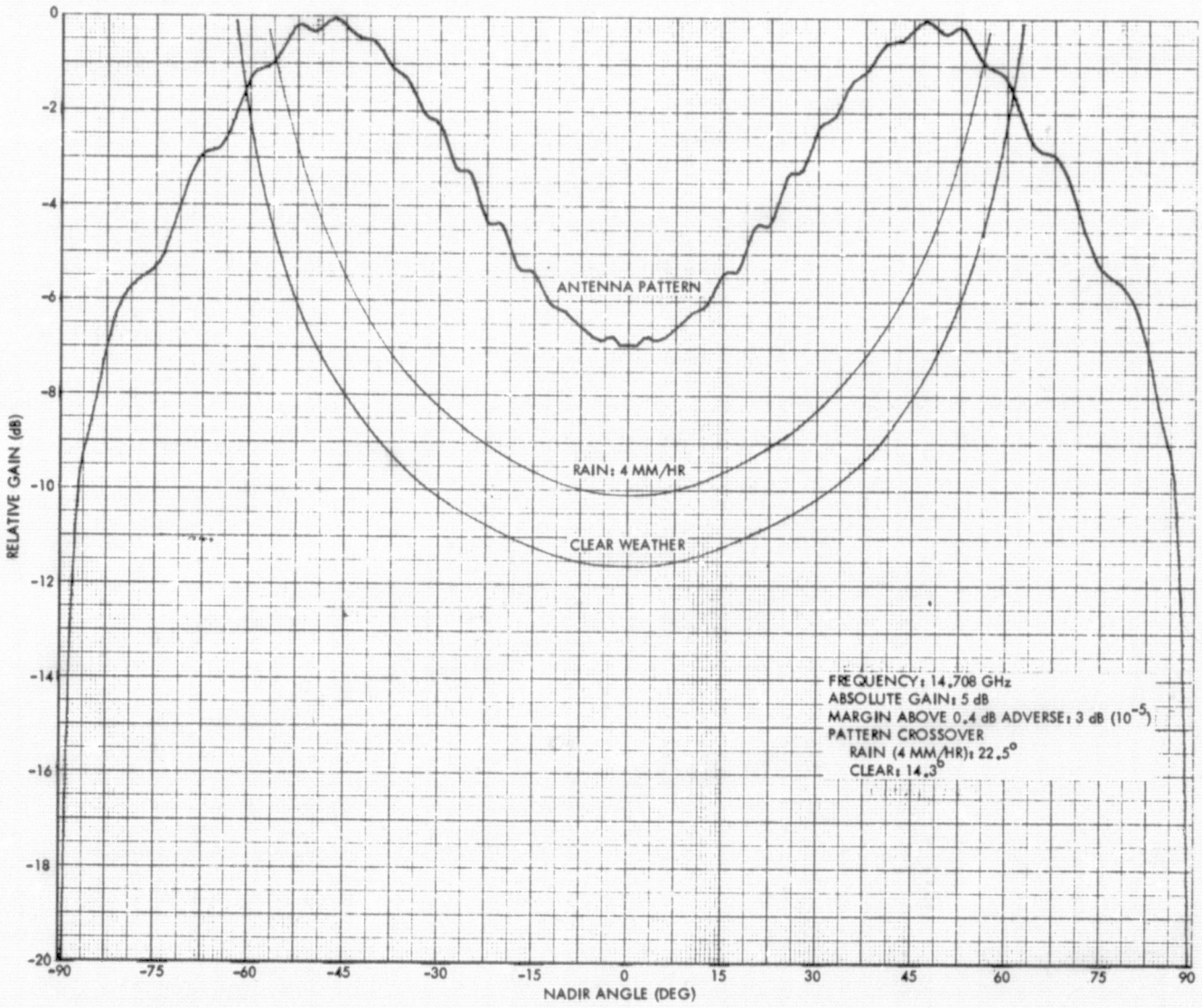

Figure 4.4-10. Computer Plotted Radiation Pattern of Recommended Design

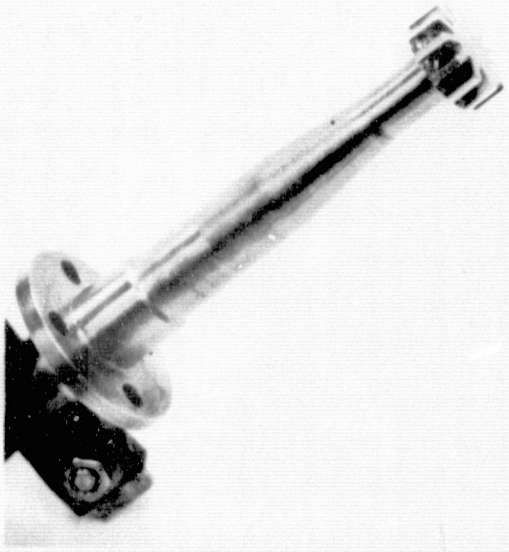

Figure 4.4-11. Shaped Beam Antenna Feed

4.5 STDN/DIRECT ACCESS LINK PERFORMANCE ANALYSIS

The Ku-band STDN/direct access link transmits QPSK-modulated TM data. Two 60 Mbps staggered data streams are utilized to minimize spectrum regeneration. The STDN/direct access frequency is 14.7 GHz to minimize interference with the TDRSS link operating at 15 GHz.

4.5.1 STDN/Direct Access Link Transmit Loss Budget

The transmit output circuit is given in Figure 4.5-1 and the loss budget in Table 4.5-1. These losses are based on a best estimate of expected losses, not worst case values. Immersion gold coated WR-62 waveguide is utilized for loss minimization.

Table 4.5-1. Transmit Loss Budget

Item	Loss (dB)
Waveguide (<1 ft)	0.05
Waveguide switch	0.10
Waveguide (≈2 ft)	0.10
VSWR	0.10
	0.35 dB

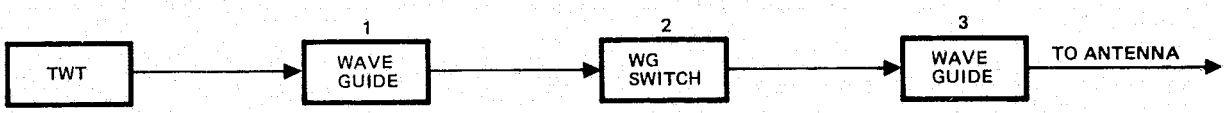

Figure 4.5-1. Transmit Output Circuit

4.5.2 Transmit Link Performance

The Ku-band STDN/direct access performance margin above a 0.4 dB rss adverse tolerance is shown in Figure 4.5-2 as a function of elevation angle. The margins are achieved with a LF/O spacecraft 20-watt TWTA, transmit losses of 0.4 dB, a shaped-beam Ku-band antenna, and a ground station G/T of 36.0 dB/°K at zenith for a Ku-band 30-foot antenna and uncooled parametric amplifier. The performance curve was obtained from the difference in the theoretical design pattern and the required calculated patterns contained in Figure 4.4-10.

The recommended 3 dB margin above 0.4 dB RSS adverse tolerance correspond to elevation angles of 22.5° and 14.3°, respectively, for rain and clear weather conditions. Note that for 0 dB margin, clear weather, the coverage extends to 10° elevation angles.

The results in Figure 4.5-2 are general enough to determine the minimum receive elevation angles for other performance margins.

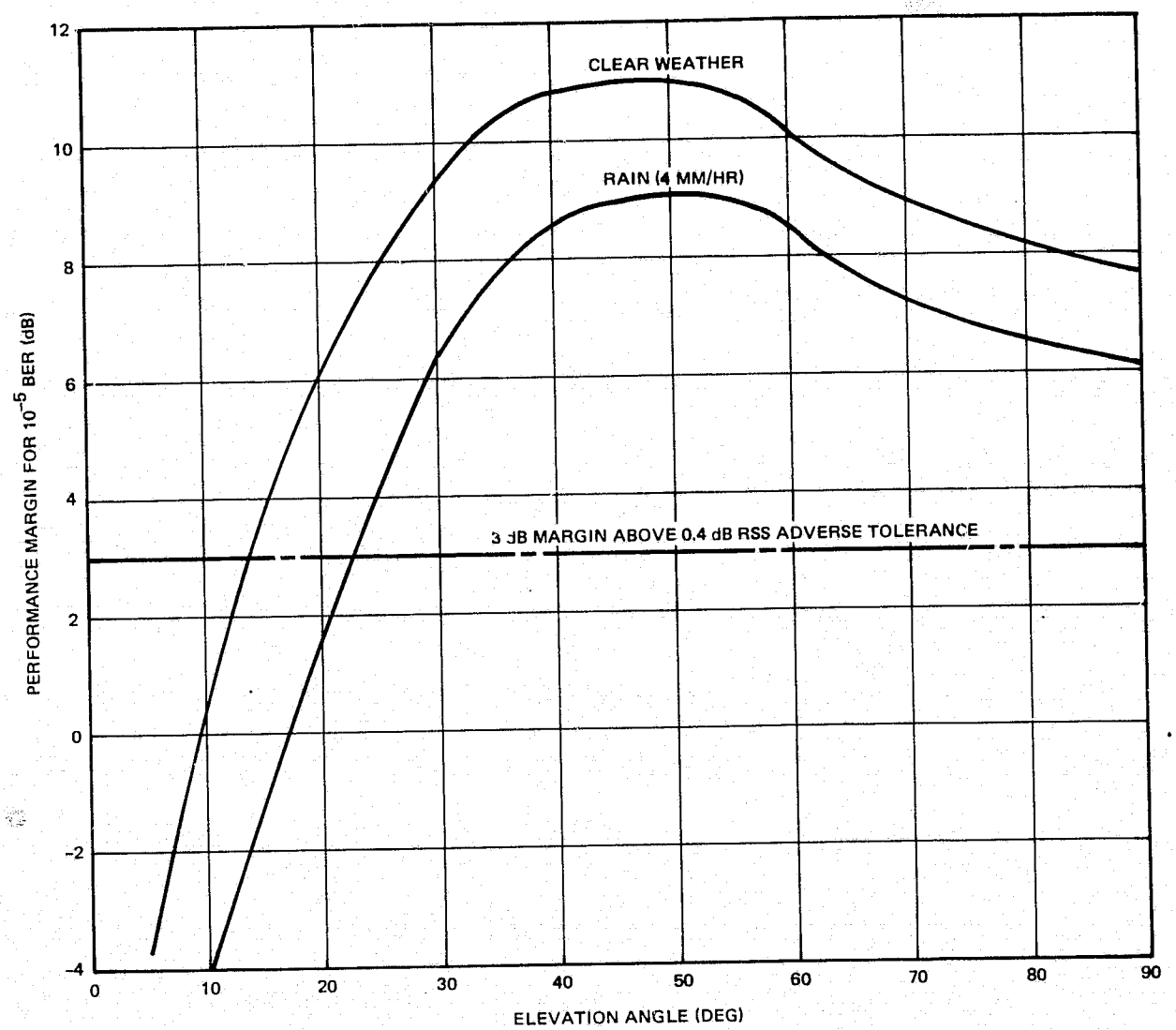

Figure 4.5-2. Ku-Band STDN/Direct Access Performance

5. WIDEBAND MODULE LAYOUT

A preliminary equipment arrangement (Figure 5-1) for the wideband modules was established to determine feasibility within the envelope constraints defined by GSFC. The envelope given is a rectangular box, 12 x 18 x 42 inches, of which 12 x 18 x 24 inches are available for the Ku-band equipment. Panel 3 (12 x 18 inches) is exposed to outer space and points away from the sun. Panel 4 (18 x 24 inches) is also exposed to outer space, but is partially shadowed by the antenna and is exposed to sunshine only a few minutes each day.

The TWTA's are mounted to the cold space end (panel 3) and the power supply and power converter are mountedto the adjoining partially exposed panel 4. Second surface mirrors are utilized on the TWT panel. The remaining equipment is placed to favor minimum bend radius for cables and waveguides and to minimize cable and waveguide lengths within the allowed envelope.

The weight of the Ku-band components, the associated power converter, and redundant remote interface units (RIU) are summarized in Table 5-1. The weight of the wideband module structure and the S-band equipment are not included.

Table 5-1. Wideband Module Equipment Weight

Component	Unit Weight (lbs)	Quantity	Weight (lbs)
Receiver IF unit	2.9	1	2.9
Frequency source unit	6.5	1	6.5
Digital interface unit No. 1	1.5	1	1.5
Power converter	4.2	1	4.2
Waveguide switch	1.2	1	1.2
Coax transfer switch	0.3	2	0.6
X7 multiplier	1.1	2	2.2
QPSK modulator	3.6	1	3.6
Waveguide bandpass filter	0.3	2	0.6
TWTA	10.7	2	21.4
RIU	3.0	2	6.0
Misc (W/G, wire, etc.)	2.5	—	2.5
Shaped beam antenna		1	3.0
		Total	56.2 lbs

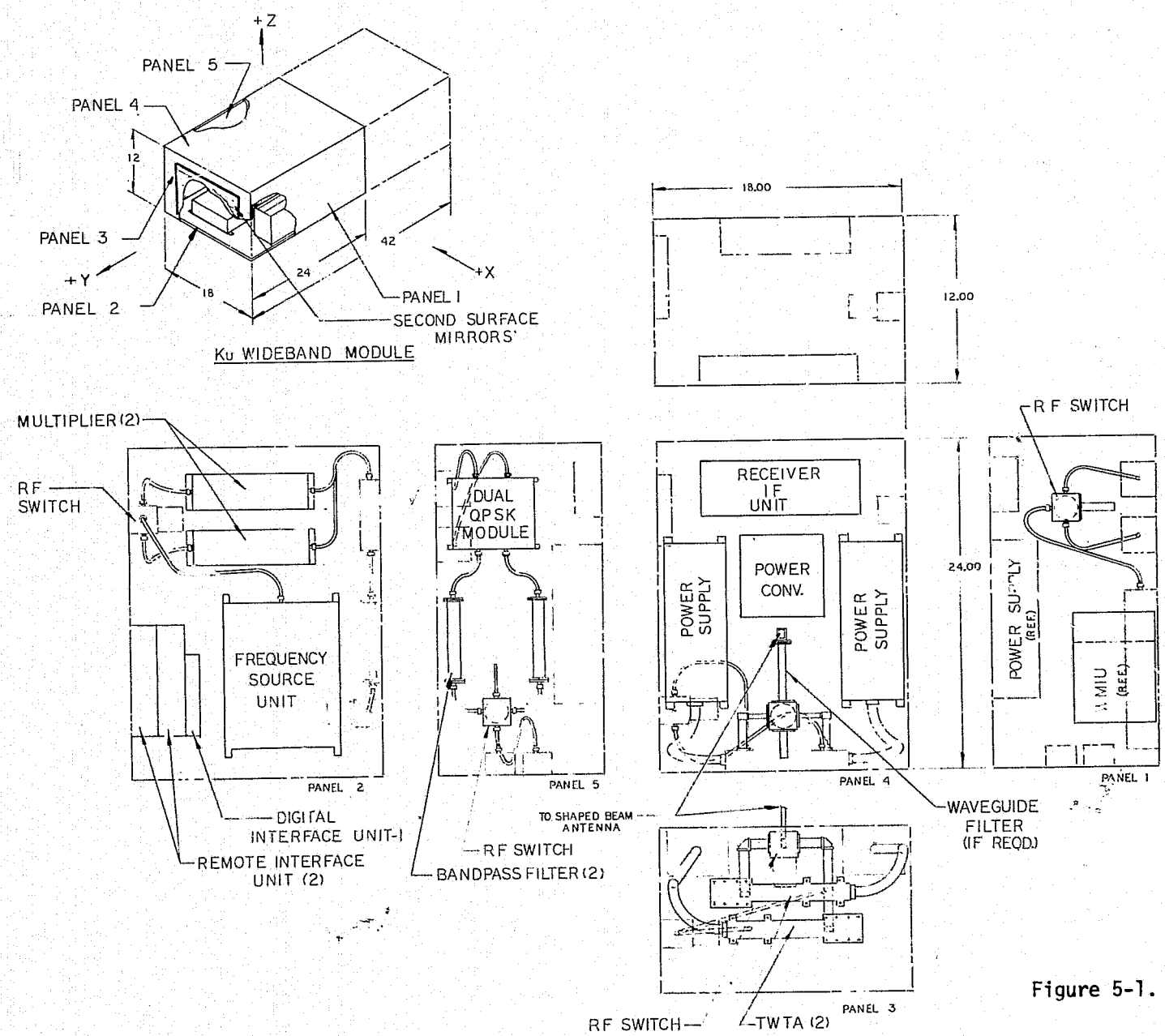

Figure 5-1. Equipment Layout in Wideband Module

6. NEW TECHNOLOGY

A careful review of the recommended configuration and design implementation for the TDRSS link Ku-band transmitter, tracking receiver, the STDN/direct access transmitter, and the associated antennas indicates that no new technology is required. Moreover, the recommended communications system is considered a low-risk implementation.

7. ROM COST ESTIMATE

The organization of work for a major program such as the Landsat Follow-on communication system is defined through a work breakdown structure (WBS). At TRW the WBS is the common framework for planning, measuring, reporting, and controlling program cost and schedule performance. It accounts for all items in the contract statement of work and provides for the integration of subcontractor effort. The WBS also permits matching tasks to functional (performing) organizations. Each task, e.g., electrical design, product design, etc., which is defined within the lower levels of the WBS is supported by a task description, job number, schedule, budget, and responsible performing organization. Labor hours are estimated for each task and these hourly estimates are converted to dollars via labor categories and the direct labor and overhead rates applicable to the contract period of performance.

A WBS at a summary level has been prepared for the LF/O communication system and is shown in Figure 7-1. A comparison of the WBS to the TDRSS system block diagram (Figure 3.0-1) shows that hardware is partitioned to spacecraft location, system function, and stand-alone electrical and mechanical interfaces. Examples of stand-alone units or shop replaceable units (SRU) are the frequency source and the receiver IF shown in Figure 3.0-1. These entities or units later become the basis for contractual negotiation by way of "unit" specifications.

The WBS also serves to produce a cost collection framework whereby recorded costs can be data banked as a basis for estimating the costs of future space program equipment, such as Landsat Follow-on. A specific example of this is the estimated development cost for the LF/O frequency source, which has been extracted from the historical cost data base. These recorded costs were modified to reflect only the new design effort needed for LF/O. Design costs, where the hardware is identical to existing equipment, have not been included.

The LF/O recommended hardware is within the state-of-the-art and is similar to existing, developed TRW hardware. Table 7-1 is a development status list of the major modules or components within shop replaceable (SRU) functional blocks. The listing includes the manufacturer, program source where the equipment is derived from existing designs, and the principal modifications required for the LF/O application. Also shown are the components which require some breadboard circuit development to finalize the electrical design.

When the WBS has been completed in detail, it will be possible to collect and summarize costs in greater detail. For the LF/O study, this summary has been made at the line replaceable unit (LRU) or major subsystem level, i.e., at the RF compartment and wideband module levels. Table 7-2 shows the cost summary for this WBS level. The costs are also included on the summary WBS of Figure 7-1. The costs indicated are

Table 7-1. Equipment Development Status

Equipment	Source/Derivation	Principal Modifications	Breadboard Development Requirement	Comment
High gain antenna reflector	TRW program	Increase diameter Change F/D ratio	No	Existing mechanical design approach is proven for space use
Feed horns/polarizer	TRW program	Modify size for required performance	Yes	
Comparator	TRW/New	N/A	Yes	
Earth coverage antenna	TRW/New	N/A	Yes	Scale feed from existing design
Biphase modulator/coupler	Electromagnetic Sciences/New	N/A	Yes	
Diplexer	TRW program	Scale to exact frequencies	Yes	
Acquisition horn antenna	TRW program	Scale	No	Existing size is small; available gain is therefore low
Receiver front end/down-converter	LNR/Air Force program	Freq scale from 12 GHz	Yes	Several vendors have demonstrated required performance
Waveguide transfer switch	Transco/TRW program	None	No	
S to Ku-band multiplier (X6)	TRW program	Retune to new center frequency	No	Original design has 5% bandwidth
Receiver/IF module	TRW/Shuttle S-band program	Modified packaging	No	Shuttle 2nd IF design is almost directly utilizable. Shuttle SCTE IF includes other hardware
Demodulator	TRW program	Detector modifications	Yes	
Frequency source reference oscillators	FEI*/Defense Support program, etc.	Cut crystal for LF/O frequency	No	Verify aging on engineering models
Frequency multipliers	TRW various programs, e.g., FLTSATCOM	Modify X6 (UHF to S-band) to X8	Yes	All other electrical designs are identical to a developed frequency source
Power converter	TRW/Shuttle S-band program	Add over & under voltage protection & short circuit protection	No	Designs are mature including modifications intended
TDRSS link transmitter				
TWTA (inc. pwr. supply)	Watkins-Johnson/ TRW sponsored	None	No	TWTA now in development
Waveguide transfer switch	Transco program	None	No	Identical to that utilized for receiver front end
Coaxial transfer switch	Transco program	None	No	
Unbalanced QPSK modulator	TRW IR&D program	Minor	No	Nearly identical to balanced QPSK modulator
Digital interface unit	TRW/New	N/A	Yes	Breadboarding limited to low confidence circuits
S to Ku-band multiplier (X5)	TRW program	Retuning	Yes	
Bandpass filter	TRW program	Minor retuning	No	
STDN link transmitter				
TWTA (inc. pwr. supply)	Watkins-Johnson/ TRW-sponsored	None	No	Identical to TDRSS link TWTA
Waveguide transfer switch	Transco program	None	No	
Coaxial transfer switch	Transco program	None	No	
Balanced QPSK modulator	TRW IR&D program	None	No	
Digital interface unit	TRW/New	N/A	Yes	Breadboarding limited to low confidence circuits
S to Ku-band multiplier (X7)	TRW program	None	No	Identical to existing design
Bandpass filter	TRW program	Freq scale from 15 GHz	Yes	

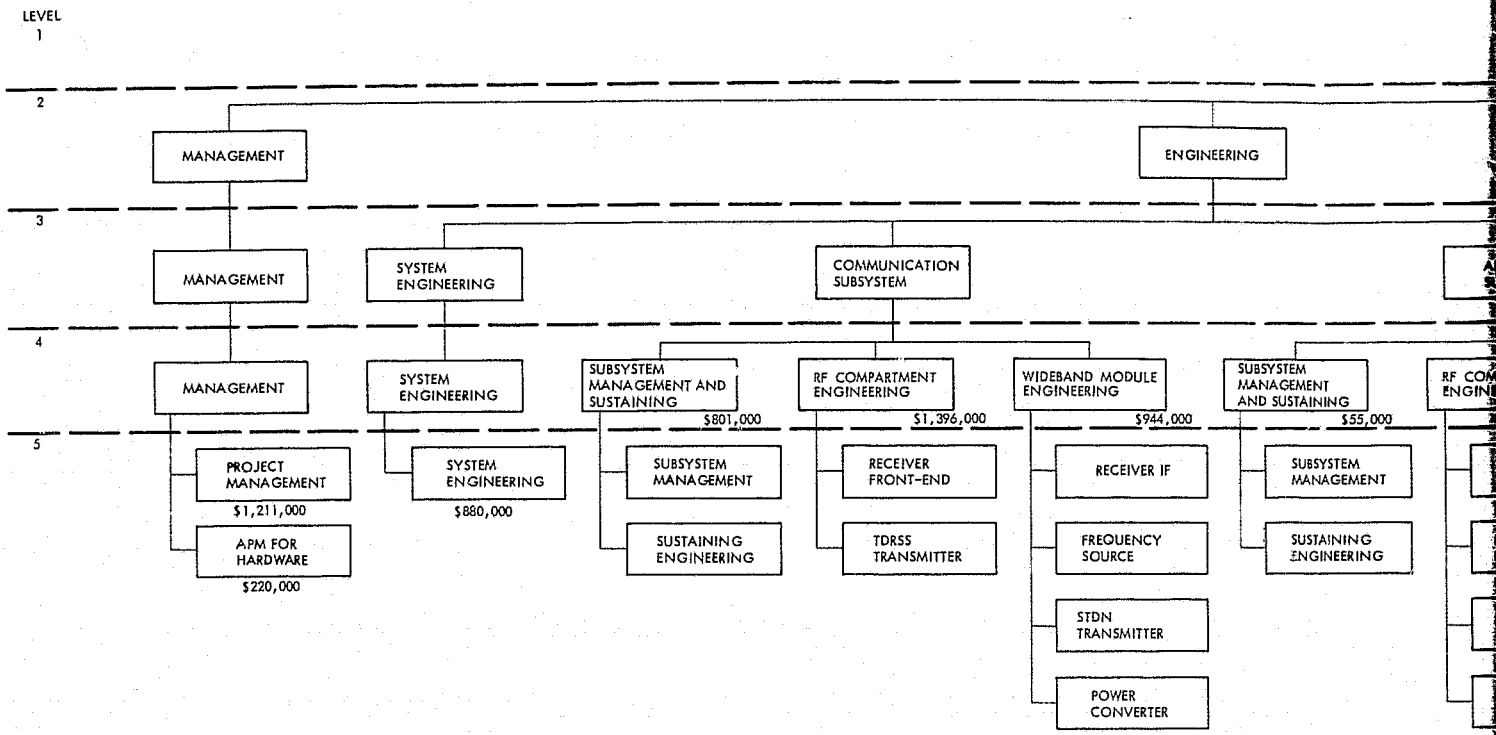

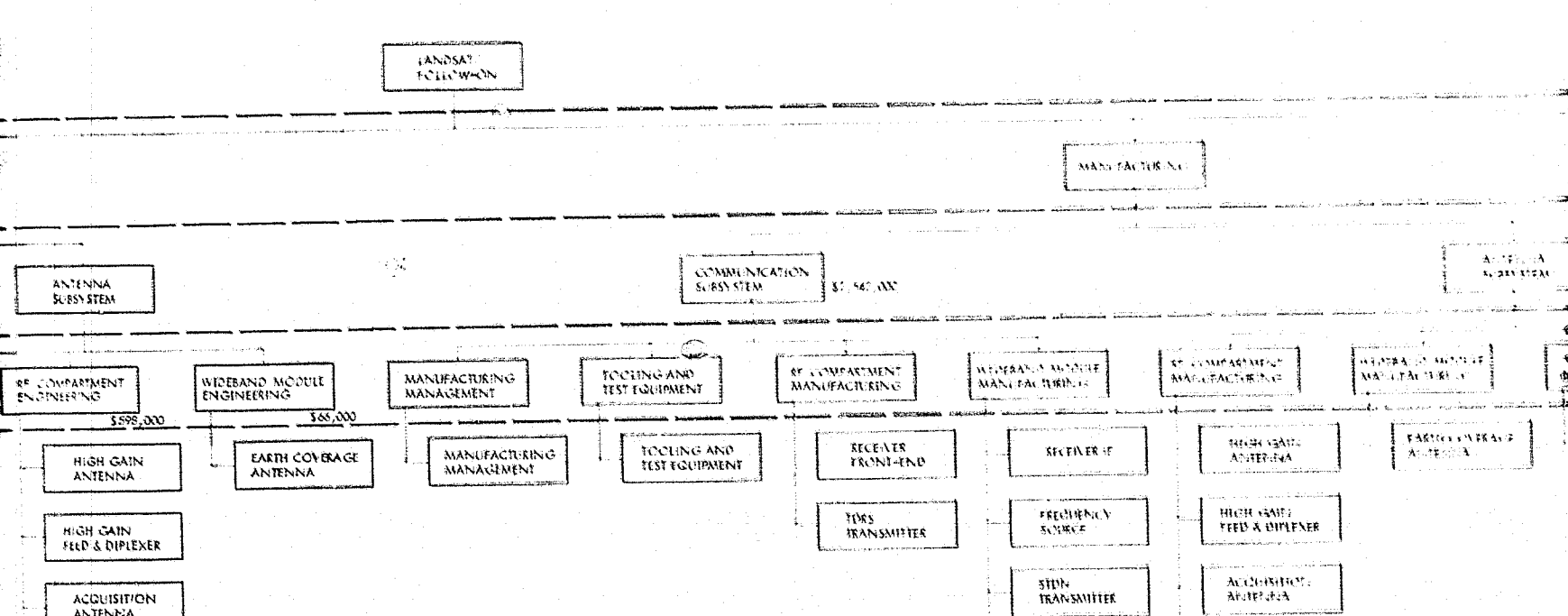

FOLDOUT FRAME 2

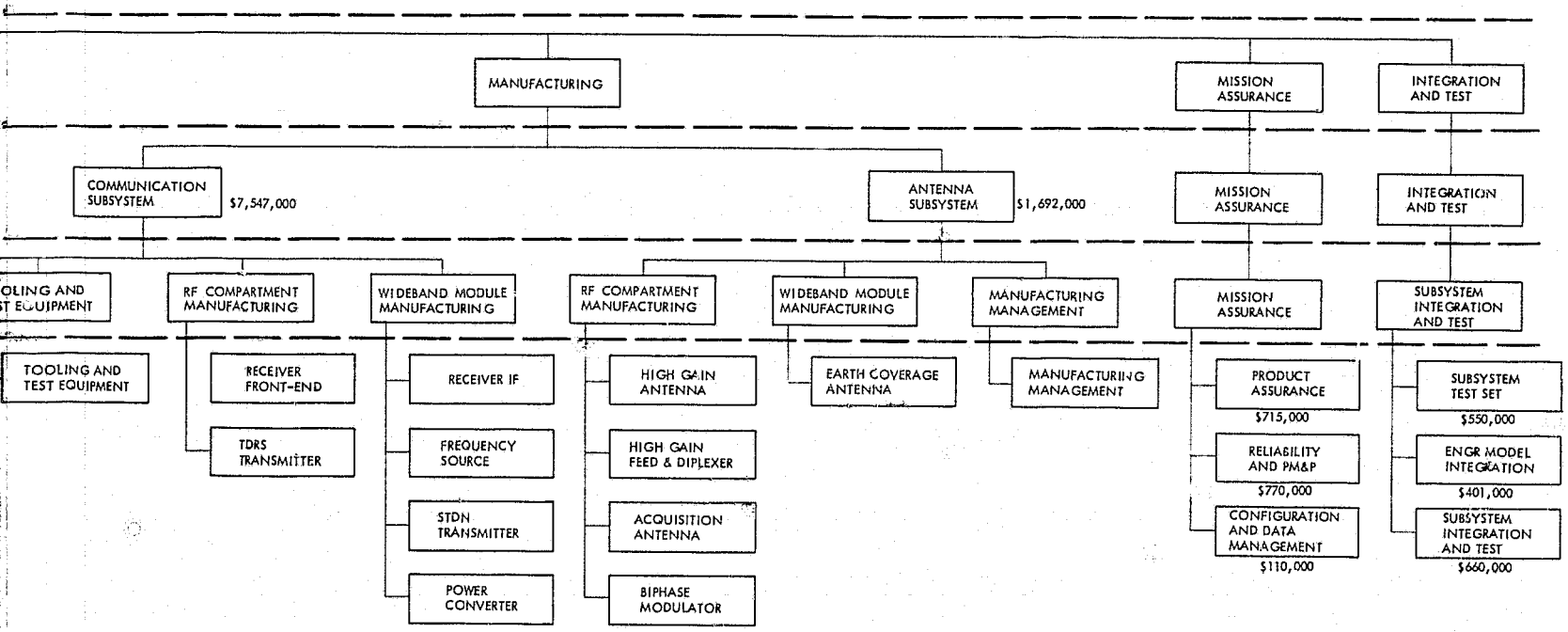

Figure 7-1. Work Breakdown Structure

representative of averages from TRW's historical data bank. The information presented is intended for budgetary and planning purposes.

The price summary of Table 7-2 is in general self-explanatory. The costs for the deliverable test set have been identified separately and include purchased capital equipment which may more economically be purchased directly by NASA. "Price" is 10% above cost.

Design, recurring, and integration costs have been separated for the RF compartment and wideband module. Prorations for typical project operations such as program office, systems engineering, etc., have been included within the subsystem integration task so that costs associated with that activity can be isolated from line replaceable unit development costs in the event that NASA might contract independently for development and systems integration.

Figure 7-2 is the development schedule associated with the ROM cost estimates. Start of development is keyed to the conceptual design review at which time requirements have been reviewed and allocated to the shop replaceable unit and subassembly levels. Breadboard circuit development of new designs is completed by the preliminary design review. Packaging design of the mature circuits would also progress in parallel during this period.

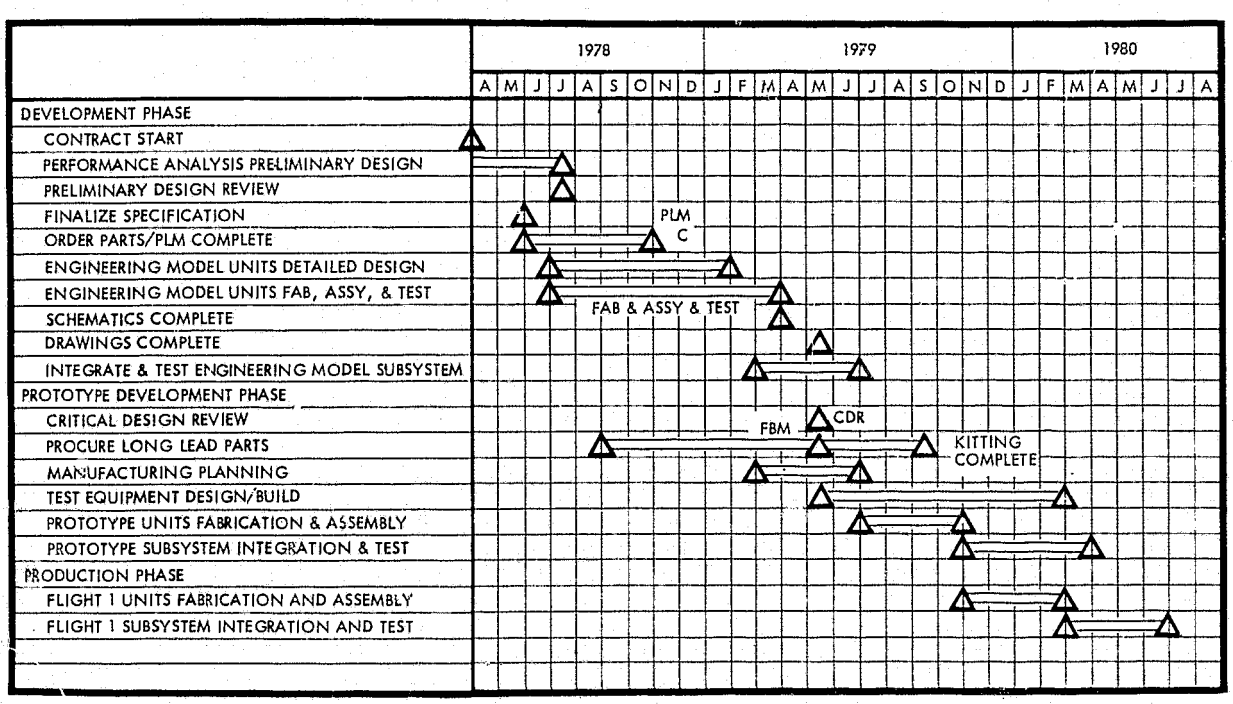

Figure 7-2. Development Schedule

Table 7-2. Landsat Follow-On Communication Subsystem Price Summary

WBS Cost Categories	RF Compartment ($,000)			Wideband Module ($,000)			Other	Total
	Non-Rec	Rec	Sub-Total	Non-Rec	Rec	Sub-Total		
Project management	431	295	726	289	154	443	42	1,211
APM for hardware	55	44	99	99	44	99	22	220
Systems engineering	528		528	352		352		880
Reliability & PM&P	370	77	447	246	62	308	15	770
Product assurance	343	72	415	229	57	286	14	715
CADM (data management)	66		66	44		44		110
Deliverable subsystem test set							550	550
EM integration	241		241	160		160		401
Subsystem integration & test							660	660
Communication subsystem								
Engineering			1,396			944		2,340
Design	1,394			944				
Manufacturing			3,747			3,800		7,547
Engineering models	556			504				
Proto refurb		142			350			
Proto & flight hardware		1,854			2,348			
Tooling & test equipment		1,195			598			
Management & sustaining	54	426	480	36	285	321		801
Antenna subsystem								
Engineering			598			66		664
Design	598			66				
Manufacturing			1,550			142		1,692
Engineering models	542			51				
Proto refurb		6			4			
Proto & flight hardware		1,002			87			
Management & sustaining	55		55					55
Total								18,616

Specific ground rules for the ROM cost were developed to assure that all engineering estimates were made within a common framework. The detailed list of these basic assumptions follows:

COSTING GROUND RULES FOR LF/O STUDY ROM

General

The LF/O program is divided into three phases:

Phase 1. Design engineering: both electrical and mechanical.

Phase 2. Product verification: Both engineering model and prototype model fabrication, assembly, and test. The prototype will be tested to levels approximately 10% above acceptance levels and is to receive any refurbishment required to restore it to flight status.

Phase 3. Production: Fab, assembly, and test of flight equipment.

Specific Ground Rules Utilized

- For the LF/O pricing activity, July 1976 direct labor and overhead rates were utilized.
- Breadboards were estimated in only those areas which were considered to have sufficient design risk to warrant a "first-cut" development.
- The engineering model is to be fabricated and assembled to controlled drawings by Manufacturing and tested by Engineering to informal test procedures.
- In general there will be no qualification models. In specific cases where the risk necessitates a qual model, it will not be a deliverable end item.
- Engineering model hardware must be of high quality since they will be subjected to acceptance level environmental and electrical tests on a "unit" or "black box" level.
- Engineering is responsible for any special test equipment required for breadboard and engineering model test.
- All management and administrative costs are included in the estimated project office costs.
- Breadboard housings, if any, are simple and not fabricated to released (controlled) drawings.
- A subsystem integration test set (deliverable) has been priced into the integration and test task.
- It is assumed that the contract start is April 1978. Program duration is to be approximately 18 to 27 months (27 months has been assumed for study purposes).

8. REFERENCES

1. Proposal to NASA, "Telecommunicator Service via a Tracking and Data Relay Satellite System, Phase II, IMplementation and Operations," Part 2, Vol. 4, 15 January 1976.

2. X-700-75-140, "Low Cost Modular Spacecraft Description," GSFC Document, May 1975.

3. STDN No. 101.2, "Tracking and Data Relay Satellite System (TDRSS) Users' Guide, Revision 2," GSFC Document, May 1975.

4. 13900-6012-R0-01, "PPCS System Design and Analysis," TRW Technical Report, 1 July 1972.

5. "K-Band Satellite Communication SET AN/ASC-( )," Volume I: TRW Proposal No. 23631, 11 September 1972.

6. D.D. Carpenter, "Performance Analysis for LANDSAT Autotrack System," TRW No. 76-7130.32-02, 17 April 1976.

7. "Radio Frequency Allocations for Space and Satellite Requirements," Mission and Data Directorate, 15 June 1973, Goddard Space Flight Center, Greenbelt, Maryland, p. 20.

8. CCIR, XIIIth, Plenary Assembly, Geneva, 1974, Volume II, Space Research and Radio Astonomy, published by the International Telecommunication Union, Geneva, 1975, Report 224-3, Annex I, Tables I and II.

9. "The 100-Meter Radio Telescope at Effelsberg," Proceedings of IEEE, September 1973, Special Issue on Radio Astronomy.

10. Thomson-CSF publication NTH6073, "Life and Reliability of Thomson-CSF X-Band Satellite-Transponder Traveling Wave Tubes," November 1975.

11. V. Galindo, "Design of Dual Reflector Antennas with Arbitrary Phase and Amplitude Distributions," IEEE Transactions on Antennas and Propagation, 12 April 1964.

12. W.C. Wong, TRW computer program CASSE.

13. B.R. Bean and E.J. Dutton, "Radio Meteorology," NBS Monograph 92, 1966.

14. M. Abramowitz and I.A. Stegun, "Handbook of Mathematical Functions," NBS-AMS 55, 1965.

15. R.C. Rudduck and C.H. Walter, "Luneberg Lenses for Space Communication," IRE Transactions on Space Electronics and Telemetry, 9, 31 (1972).

16. P.A. Bello, "Aeronautical Channel Characterization," IEEE Transactions on Communication, 21 548 (1973)

17. P. David and J. Voge, Propagation of Waves, Pergamon Press, 1969.

18. D.E. Kerr, Propagation of Short Radio Waves, McGraw-Hill 1947, MIT Radlab Series Vol. 13.

19. Hogg and Mumford, "The Effective Noise Temperature of the Sky," Microwave Journal, March 1960.

20. "Performance Specification for Telecommunications Services via the Tracking and Data Relay-Satellite System," S-805-1, Goddard Space Flight Center, June 1976.

21. Multimission Modular Spacecraft (MMS) Communications and Data Handling Subsystem Specification, Goddard Space Flight Center S-700-15 (Preliminary).

22. GSFC Specification: Standard Telemetry and Command Components (STACC): Remote Interface Unit (RIU) and Expander Unit (EU), GSFC-S-714-11, March 1976.

23. Benoit, "Signal Attenuation Due to Neutral Oxygen and Water Vapour, Rain and Clouds," Microwave Journal, November 1968.

24. James, "The Effect of the Weather in Eastern England on the Performance of X-Band Ground Radars," Technical Notes, No. 655, Royal Radar Establishment.

25. Holzer, "Atmospheric Attenuation in Satellite Communications," Microwave Journal, March 1965.

26. Altshuler, Falcone, and Wulfsberg, "Atmospheric Effects on Propagation at Millimeter Wavelengths," IEEE Spectrum, July 1968.

27. Ippolito, "ATS-V Millimeter Wave Experiment Data Report, Oct-Dec 1969," GSFC X-733-70-123, March 1970.

28. Ippolito, "ATS-V Millimeter Wave Experiment Data Report, Jan-Aug 1970," GSFC X-751-70-369, October 1970.